Politecnico di Milano

DEPARTMENT OF ENERGY

Doctoral Program in Energy and Nuclear Science and Technology

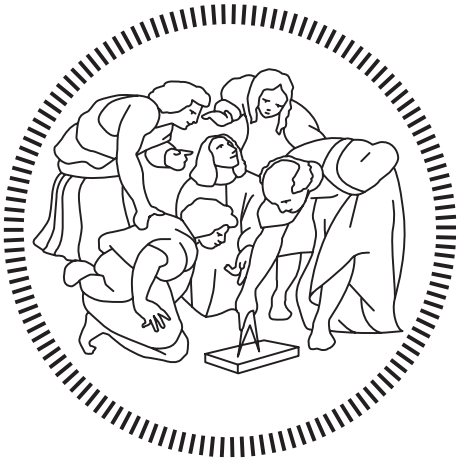

Flexible Biomass-to-X plants for resilient renewable energy system

Doctoral Dissertation of:

Alessandro Poluzzi

Supervisor:

Prof. Matteo C. Romano

Co-Supervisor:

Prof. Giulio Guandalini

The Chair of the Doctoral Program:

Prof. Vincenzo Dossena

2022 – XXXIV cycle

Executive summary

In a carbon constrained economy with the objective of reaching net zero CO_2 emissions, biomass represents a scarce resource. Therefore, it is fundamental to make the best use of the biogenic carbon according to market and societal needs, and to sustainability criteria (IEA, 2017; Camia et al., 2018). In the past decades, the relatively low value of carbon compared to energy was such that biomass has been mostly used for heat and power generation through combustion, with unrestricted emission of CO_2. This is likely to change in the next decades if the commitment of governments and the regulations in limiting the CO_2 concentration in the atmosphere is confirmed, that will lead to an increase of the biogenic carbon value. Also, the rise of solar and wind power generation will likely cause a reduction of the average electricity prices and an increased value of the services to improve the resiliency of the electric energy system through energy storage and flexible power generation. In this context, understanding the best use of biomass depending on the regional energy mix (Patrizio et al., 2021) and on the market and regulatory conditions is a strategic issue for industry and policymakers. The possible uses of biomass include the combustion to generate electricity and/or heat, and the conversion into a high value product (e.g. carbon-based products, bio-hydrogen, biochar).

When final synthetic products are considered, biomass-to-X systems may produce either carbon-based products or hydrogen, which can be used in a wide range of sectors, from industry to transport. A large fraction of chemicals are carbon-based products, where the carbon has a fossil origin. Bioenergy offers a solution to "defossilize" the chemical sector by substituting fossil carbon with biogenic carbon (Gabrielli et al., 2020). As regards the transport sector, liquid biofuels represent a valuable option for the decarbonization of heavy-duty road and off-road vehicles, shipping, and aviation due to the significant challenges in the electrification of these sectors. Biofuels are also suitable for reducing CO_2 emissions from light duty vehicles in the transition to electric and hydrogen-based mobility. In the coming decades, an increased share of advanced biofuels from low-risk ILUC (indirect land use change) feedstocks is expected and required by regulations (European Commission, 2021, 2022). Increasing the economic competitiveness of advanced biofuels is key for their wide deployment. The current estimated costs of advanced biofuels lie in the range of 17-44 €/GJ for biomass-based production and of 13-29 €/GJ for waste-based production, while the fossil fuel production cost varies between 8 and 14 €/GJ (Brown et al., 2020).

This research work focuses on plants for the conversion of second-generation biomass into liquid products and hydrogen via gasification-based pathways shown in Figure ES 1:

a. biomass-to-X, with emission of the excess CO_2 (BtX);
b. power & biomass-to-X, with reduced CO_2 emission and increased productivity thanks to green hydrogen addition by means of water electrolysis (PBtX);
c. biomass-to-X, with capture and storage of the excess CO_2 (BtX CCS).

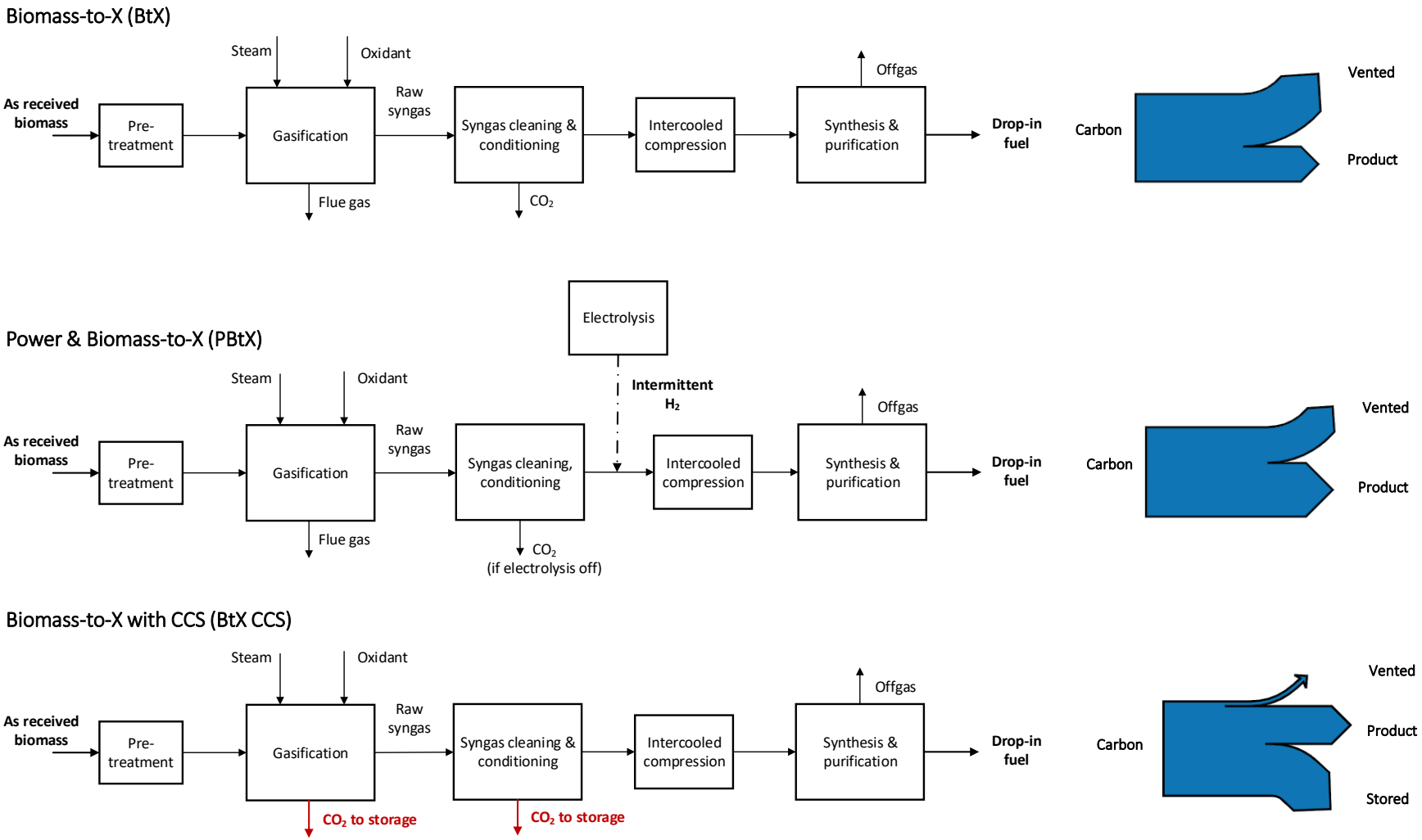

Figure ES 1 – Biomass conversion pathways via gasification and corresponding qualitative destination of the carbon

.The thesis investigates different types of fluidised bed-based gasification technologies, i.e. direct, indirect and sorption-enhanced gasification, and different final products, i.e. methanol and hydrogen

All the investigated plants combine the same fundamental conversion steps, namely biomass drying, gasification, syngas purification, conditioning and compression, and final product synthesis and purification.

Three gasification technologies have been considered:

- In the *direct gasification*-based plant, the gasification process is thermally sustained through the partial oxidation of biomass by means of oxygen either from air separation unit (ASU) or as by-product from water electrolysis. Most of the inlet carbon remains in the nitrogen-free syngas as CO, CO_2 and CH_4, while a minor part is extracted from the fluidized bed as unconverted char.
- In the *indirect gasification*-based plants, a solid heat carrier material (i.e. olivine) circulates between a higher temperature combustor and a lower temperature gasifier to provide the heat required for biomass gasification. The heat is generated from the combustion with air of the unconverted char, that flows from the gasifier to the combustor, and of additional biomass.
- In the *sorption-enhanced gasification*-based plants, CaO-rich solids are used as bed material and circulate between the gasifier and the combustor. In addition to behaving as a heat carrier as in the indirect gasification process, the circulating solids absorb CO_2 through the carbonation reaction ($CaO + CO_2 \leftrightarrow CaCO_3$). The produced $CaCO_3$ is calcined into CaO and CO_2 in the combustor by means of the combustion of the unconverted char flowing from the gasifier to the combustor and of additional biomass, if needed. Solids circulation is tuned to achieve a target CO_2 uptake, which is controlled by the equilibrium of the carbonation reaction. Therefore, by increasing the solids circulation rate, the gasifier temperature increases and the CO_2 separation reduces. In this way, it is possible to control the CO_2 content in the produced syngas.

The aforementioned gasification processes produce a nitrogen-free syngas, which contains a significant amount of tar and methane. A catalytic auto-thermal reformer (ATR) unit is included downstream the gasifier and a high temperature filtration unit, to convert methane and tar into useful reactants for the synthesis (i.e. CO and H_2). Oxygen is produced either with an ASU or is delivered as by-product of water electrolysis. In such a case, an oxygen storage system is foreseen in order to store the intermittent oxygen production from the electrolyser.

The reformed syngas must be further conditioned, purified and compressed to be fed to the downstream final product synthesis. The main syngas chemical components should be in proper proportions to have a high conversion of the feed gas into the final product. This proportion is defined as the syngas module $M = (H_2 - CO_2)/(CO + CO_2)$, which has a specific value depending on the final product. In order to produce a tailored syngas for the downstream final product synthesis, the syngas conditioning section in direct and indirect gasification-based plants includes different processes such as water-gas shift (WGS), which allows to further shift the syngas composition towards hydrogen, and CO_2 capture, which allows to remove the excess carbon from the syngas. The sorption-enhanced gasification-

based plant does not need a further syngas conditioning, because the syngas composition may be tuned within the gasifier.

Syngas purification includes the removal of undesirable compounds, such as sulphur, chlorine and alkali, that would poison the downstream catalytic reactors. To this end a water scrubber, H_2S absorption by liquid Redox LO-CAT process (Echt et al., 2017) and adsorption with activated carbon are included in the plant.

The syngas needs to be compressed by means of one or more intercooled compressors, depending on the plant configuration, in order to reach the target pressure of the final product synthesis and purification (i.e. 90 bar for methanol production plants and 30 bar for hydrogen production plants).

Final product synthesis and purification allow to provide the product with the required purity specification. In methanol production plants, a conventional methanol synthesis technology is adopted, based on a boiling water reactor (BWR) where the syngas flows through tubes filled with catalyst and surrounded by boiling water at 238°C. Since the per-pass methanol yield is limited by thermodynamic equilibrium, most of the unconverted reactants are recycled back to the reactor. The crude methanol is cooled down to 40°C, separated from the light gases in a flash unit and then throttled to about 2 bar before purification. The purification section includes distillation columns aimed at stripping off the light gases from the crude methanol and at separating water from methanol, to reach the target purity of 99.85%$_{wt}$. In hydrogen-production plants, hydrogen is produced in a pressure swing adsorption (PSA) system with a purity higher than 99.9%$_{vol}$.

Off-gas from methanol synthesis and purification, and PSA unit contains light gases, whose heating value is exploited for electricity and/or steam production, depending on the plant configuration. Steam cycle/loop is included in order to recover the heat from the different sections and to produce electricity and/or steam for internal consumption.

The presence and the location within the plant of the aforementioned process steps may change depending on the gasification technology and on the final product, therefore a case-specific description of the investigated plants is provided in the next sections.

Biomass gasification for advanced biofuel production is not commercially deployed at significant scale yet. However, the single process units (i.e. conventional gasifiers, ASU, cleaning technologies, WGS reactors, CO_2 removal, etc.) are commercially adopted in plants for the production of chemicals (hydrogen, methanol, ammonia, etc.) from fossil fuel gasification/reforming. Sorption-enhanced gasification is the less mature process, which was tested in the Guessing demo plant at TRL7 and has been object of demonstration for flexible operation at TRL5 in the H2020 FLEDGED project.

Biomass composition is characterized by different carbon-to-hydrogen ratio than the final biogenic product. Therefore, in “conventional” BtX systems, the excess carbon is removed as CO_2 to be subsequently vented to the atmosphere. PBtX and BtX CCS plants allow to valorise the excess biogenic carbon by using it for different purposes. In the PBtX pathway, the plant is integrated with a water electrolysis unit which generates hydrogen to be combined with the carbon-rich syngas from biomass gasification. The potential benefit of such a concept is to increase the utilization of the biogenic carbon in the biomass, enhancing the production of high value bio-product for a given size and cost of the biomass supply chain, pre-treatment and gasification equipment. Moreover, PBtX systems can potentially provide services to the electric grid through power-to-X energy storage. The BtX CCS pathway includes the capture of the CO_2 during the conversion of the biomass into the

final product. As a consequence, the carbon which is captured from the air during the biomass growth can be stored underground resulting in a negative emission process. When hydrogen is the final product, all the biogenic carbon contained in the feedstock can be potentially captured. Given the current situation, the penetration in the market of these alternatives mainly depends on economic and environmental factors. The PBtX route is feasible only with a high penetration of non-programmable renewable energy sources (RES), while the BtX CCS pathway requires either a relatively high carbon tax or a reward for CO_2 removal from the atmosphere. If the product of BtX systems is hydrogen, a sufficiently developed hydrogen market is necessary.

Bioenergy plants integrated into the broader energy system may be required to cope with the intermittency of renewable energy sources, that lead to variable price of electricity on hourly time-scales and may lead to variable carbon-based products and hydrogen prices on daily–monthly time scales depending on the flexibility of the market demand and on the cost of storage. Therefore, the expected time-dependent relative value of power, carbon-based products, hydrogen, and sequestered CO_2 may lead to economic benefits for bioenergy plants integrated with electrolysis units increasing carbon utilization and product yield during low electricity price periods (power and biomass-to-X plants) and for bioenergy plants which deliver a high value final product while capturing and sequestering the CO_2 thus producing negative emission (biomass-to-X plants with CCS) (see Figure ES 2). Additional value may be obtained from operating biomass-to-X plants flexibly, e.g. modifying the electric power consumption, the destination of the biogenic carbon or the type of bio-product over time, following the market and regulatory conditions.

Figure ES 2 – IRR and operation revenue maps for biomass-to-methanol (BtM), power and biomass-to-methanol (PBtM), biomass-to-power (BtP) and biomass-to-hydrogen (BtH) plants with and without CCS. Lines identify the boundary of the regions of the most profitable options for different values of electricity, CO_2, methanol, and hydrogen (Poluzzi et al., 2021).

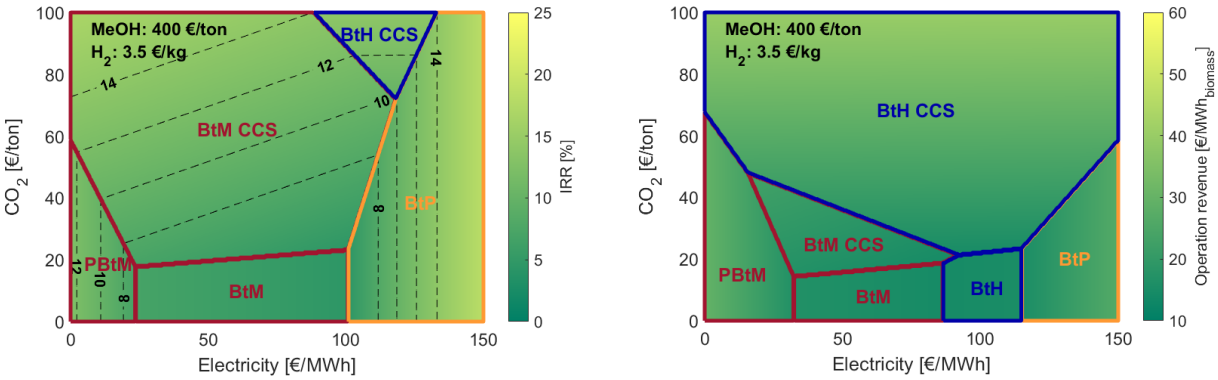

In-depth review of the recent scientific literature allowed to highlight the following research gaps:

- none of the assessed recent papers on PBtX systems investigates the design of the process units of plants conceived to operate flexibly. The economic performance of the plants are computed by fixing the electricity price and assuming that the electrolysis system operates continuously, at the same capacity factor of the biomass conversion process. The effect on the capital and

operating costs of plants conceived to operate flexibly is currently unexplored in the open literature.

- The expected capacity factor of the electrolysis system of a PBtX plant is closely linked with the expected electricity price curve, which will depend on factors such as the geographic location, the type of renewable energy sources, their penetration in the regional grid and the willingness to pay of other potential users of electricity connected to the grid. Therefore, to understand the potential of PBtX plants and the value of their flexibility for the energy system, the integrated modelling of plants connected to electric grids of the future should be pursued.
- In future carbon-constrained world, the best bioenergy conversion pathway (e.g. electricity, H_2, methanol, etc.) will depend on the relative value/price of the products and of CO_2, that vary over time with different time scales. Multi-product plants able to operate flexibly to produce the good with the highest added value are not investigated in the scientific literature and are worth exploring from a techno-economic perspective.

The present research work aims at filling the aforementioned research gaps and discusses the techno-economic analysis of the following plants:

- Power and biomass-to-methanol plants (PBtM). For this class of plants, a first analysis explores the optimal equipment design and plant operating criteria, while a second analysis compares plants based on different gasification technologies.
- Biomass-to-methanol (BtM) and biomass-to-hydrogen (BtH_2) plants with CCS. For this class of plants, multi-product plants operating flexibly to produce the good (methanol or hydrogen) that generates the highest revenues are investigated.

Methods

The research work is based on modelling and on the development of techno-economic analysis of different plant configurations. The technical part which includes heat and mass balances is performed with the process simulator Aspen Plus®.

Direct and indirect gasification heat and mass balances are calculated with a lumped parameter model. Gasification process parameters and assumptions needed to define the syngas composition at the gasifier outlet (i.e. the advancement of the WGS reaction in the gasifier, the content of CH_4 and higher hydrocarbons, and the char conversion) are calibrated to reproduce the syngas composition from the Varkaus plant (Palonen, 2012) and from GoBiGas plant (Thunman et al., 2018), for the DG- and IG-based plants respectively. The sorption enhanced gasifier (object of demonstration at TRL5 in the H2020 FLEDGED project) is modelled with a 0D model which is validated against i) 3D simulation results performed by Lappeenranta University of Technology, ii) experimental data collected in University of Stuttgart pilot plant, iii) values from the review paper (Fuchs et al., 2020).

The methanol synthesis is modelled by adopting the rigorous model for plug flow reactors. The SRK equation of state is chosen to compute the thermodynamic properties since it is suited for the high temperature and pressure conditions within the reactor. The kinetic model proposed by Bussche and Froment (1996) is used in the analysis. The methanol synthesis reactor presents fixed design criteria which are among others the tube length and diameter (i.e. 6 m and 0.04 m, respectively), the reactor pressure (i.e. 90 bar), the temperature of the boiling water (i.e. 238°C) and the catalyst-related specifications. Moreover, the number of the tubes inside the reactor depends on the selected gas hourly space velocity (GHSV), referred to the volume of the reactor tubes. In this work, the plants are designed with a GHSV of 5000 h^{-1} and a recycle ratio (RR, defined as the molar flow rate of the recycle stream divided by the molar flow rate of the fresh syngas) of 5. The output composition of the raw methanol in Aspen Plus® is validated with the results provided by a 2D heterogeneous single tube model coupled with a 1D description of the catalyst pellet, implemented in gPROMS®. The more accurate gPROMS® model is also used to analyse the catalyst temperature which must be controlled in order to prevent excessive temperature hot-spot that may lead to catalyst deactivation.

In methanol production plants, the purification section is performed with a rate-based approach, to take into account the mass transfer occurring on each tray. The employed thermodynamic method is based on the Non-Random-Two-Liquid (NRTL) model (Renon and Prausnitz, 1968). In hydrogen production plants, the PSA unit is modelled as a black-box with 90% of hydrogen separation efficiency (Stöcker et al., 1998).

The heat recovery and thermal integration design of the investigated plants is case-specific. In power and biomass-to-methanol plants, the excess heat available is efficiently converted into electrical power by means of a heat recovery steam cycle which is modelled with a systematic optimization-synthesis method proposed by Elsido et al. (2020, 2021).

When CCS equipment (i.e. MDEA and mainly MEA scrubbing unit) is integrated with BtX plants, the high heat demand for CO_2 capture does not leave heat available for power generation or does not make it economically competitive to produce very small electric power output. Therefore, the investigated BtX CCS plants only adopt steam/water loops to transfer heat from waste heat sources to the heat users.

The off-gas of the methanol synthesis and purification process, and of the PSA for hydrogen purification are used to produce either electricity and steam with an internal combustion engine (ICE) or steam with a boiler, depending on the heat demand of plant configuration.

Among the key performance indicator used in this work, the potential carbon efficiency proposed by Poluzzi et al. (2020) is also applied in order to track the effect on the achievable carbon efficiency of processes that entail not only carbon separation, but also involve oxygen, water or hydrogen addition.

The economic analysis is performed by adopting the Levelized Cost approach. In the Capex estimation, the purchase equipment delivered is increased to the fixed capital investment (FCI) by using the Lang factors. The summation of FCI and working capital (WC) provides the total capital investment (TCI). The capital cost estimates derives from in-house estimation in the framework of the FLEDGED project (Poluzzi et al., 2022a, 2022b) and from scientific literature. All the costs reported in this work refer to the year 2019. In order to compute the Opex, the following costs are determined: utilities, maintenance and repairs, operating supplies, operating labour, laboratory costs, local taxes, insurance, and catalyst. A summary of the key parameters which are used in the analysis is reported in Table ES 1.

Table ES 1 - Parameters and assumptions for the evaluation of the LCOF.

Economic parameters	**Value**
Discount rate, %	10
Lifetime, y	20
Capital Charge Factor, %	11.75
Availability, h/year	7884
Electrolyser capacity factor, %	80
Variable Opex	
Biomass feedstock cost, €/t	45.72
Yearly average electricity price, €/MWh	38.49
Average electricity price, €/MWh (enhanced operation) [1]	34.30
Average electricity price, €/MWh (baseline operation) [1]	55.26
CO_2 transport and injection/storage costs [2], $/t	15.0
Fixed Opex	
Maintenance and repairs, % FCI	5
Operating supplies, % FCI	0.5
Operating labor, % Opex	10
Laboratory costs, % Opex	2.5
Local taxes, % FCI	1
Insurances, % FCI	1
Catalyst cost, €/kg	18.12
Catalyst lifetime, y	4

[1] If the electrolyser is included in the process for flexible PBtM plants.

[2] If CCS is included in the analysis.

The flexible PBtM plants, which are analysed in this work, operate in the two different modes: baseline operation (without hydrogen injection) and enhanced operation (with hydrogen injection). With the aim of assessing the economic competitivity and the profitability of such plants, it is necessary to identify the number of hours of operation in baseline and enhanced operating modes and the corresponding electricity prices. The

fraction of the total operating hours in baseline and enhanced operation may be estimated with the 'Willingness to Pay' (WTP) methodology proposed by van Leeuwen and Mulder (2018). The 'short-term WTP' expresses the breakeven electricity price that makes economically profitable to activate the electrolyser and operate in enhanced mode. Under such conditions, the revenues from the additional methanol production compensate the additional operational costs (electricity and water).

The procedure is graphically illustrated in Figure ES 3. The cumulative price duration curve (green) is generated by ranking all the hourly prices of the 2019 day-ahead market of West Denmark (DK1) in ascending order. A certain point of the curve indicates how long during the year the price has been equal or lower than a certain value. The ascending (red) and descending (blue) average price curves are obtained by averaging the values of the cumulative curve starting from the lowest price and from the highest price, respectively. Therefore, the yearly average electricity price can be read on the right end of the red curve and on the left end of the blue curve. For example, if a methanol selling price of 450 €/t is assumed, a short term WTP of 46.5 €/MWh can be calculated accordingly. By comparing this value with the cumulative electricity price curve, the number of operating hours in enhanced operation can be estimated to be the 76.3%. For that electrolyser capacity factor, the value on the ascending average electricity price curve identifies the average electricity price in enhanced operating mode (33.7 €/MWh in this example) and the value on the descending average electricity price curve identifies the average electricity price in baseline operating mode (53.9 €/MWh).

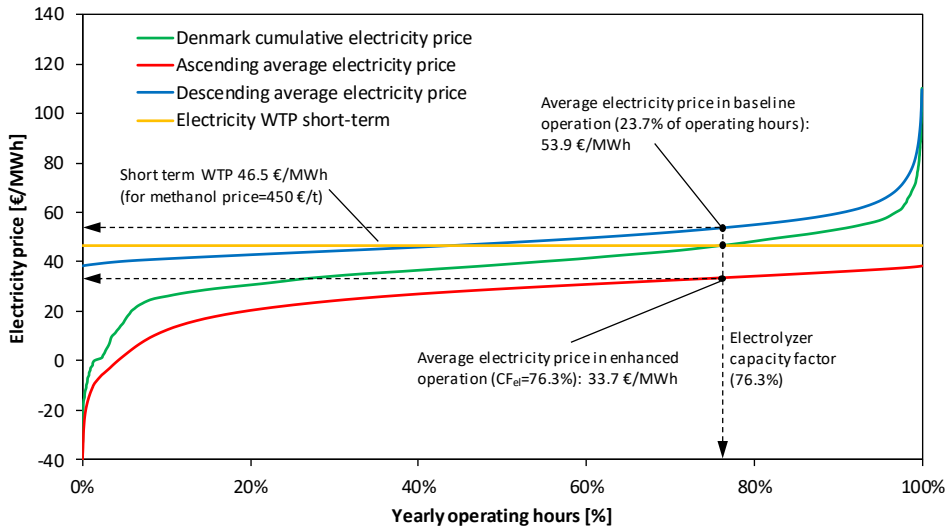

Figure ES 3 - Willingness to Pay approach with 2019 Denmark day-ahead market price curves. Breakeven points and resulting operating hours and electricity prices are shown for a methanol price of 450 €/t.

The electrolyser capacity factor is deeply influenced by the shape of the cumulative electricity price duration curve which depends on different factors such as the location, the penetration of renewable energy sources (RES), the type of RES technology, the price of the fuel and the technology of fossil fuel power plants and the type of final user (Afman et al., 2017; Seel et al., 2018; Ruhnau, 2020; Sorknæs et al., 2020). The general expected tendency is that by increasing the penetration of intermittent RES, the average electricity prices tend to reduce but the peak prices and the cost of grid balancing tend to increase. For the

aforementioned reasons, a modified cumulative electricity price curve is added to the discussion (see Figure ES 4).

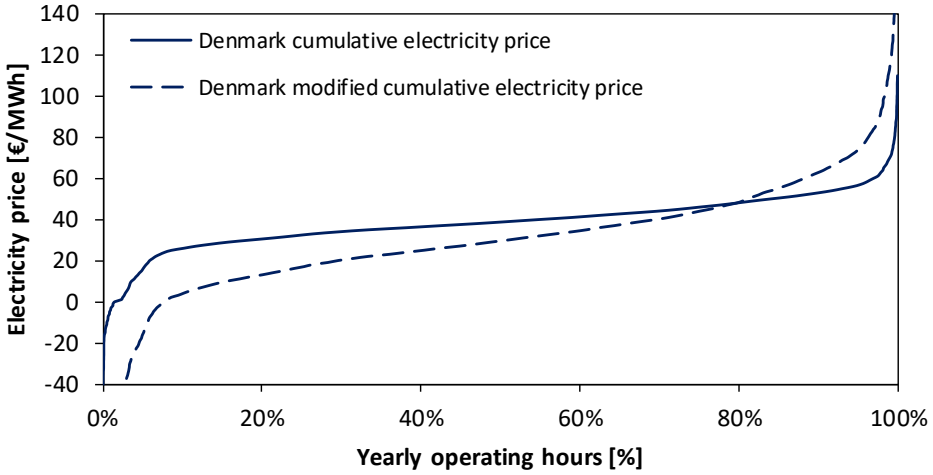

Figure ES 4 – Denmark cumulative electricity price and modified Denmark cumulative electricity price.

Power and biomass-to-methanol plants

Unit operations in power and biomass-to-methanol plants must be designed to manage the intermittent addition of hydrogen, since the electrolyser is turned on only when the electricity price is lower than the short-term 'willingness to pay'. Therefore, two main operating points are assessed, namely: (i) baseline operation (i.e. without hydrogen addition) and (ii) enhanced operation (i.e. with hydrogen addition).

The techno-economic analysis of PBtM plants is developed through the following steps:

- definition of the criteria for optimal equipment sizing and plant operating criteria for flexibly operated plants (Poluzzi et al., 2022a);
- comparison of plants based on different gasification technologies (Poluzzi et al., 2022b).

In the first part of the analysis, the SEG technology is considered (see block diagram in Figure ES 10). The flexible operation of the sorption-enhanced gasification unit involves the production of syngas with a module close to 2 in baseline operation and lower than 1 in enhanced operation. The module is controlled by increasing the sorbent circulation rate which causes an increase of the gasification temperature from 714°C in baseline operation to 772°C in enhanced operation (see Figure ES 5). The latter condition leads to zero CO_2 absorption in the gasifier due to thermodynamic limitation of the carbonation reaction ($CaO + CO_2 \leftrightarrow CaCO_3$). In this way, the syngas retains the maximum amount of carbon (i.e. all the carbon except the unconverted char in the gasifier), which allows accepting and converting the maximum amount of hydrogen from electrolysis. In baseline operation the syngas has the target composition (M=2) for the downstream synthesis, while in enhanced operation the target module is reached after hydrogen addition from the electrolyser upstream the methanol synthesis.

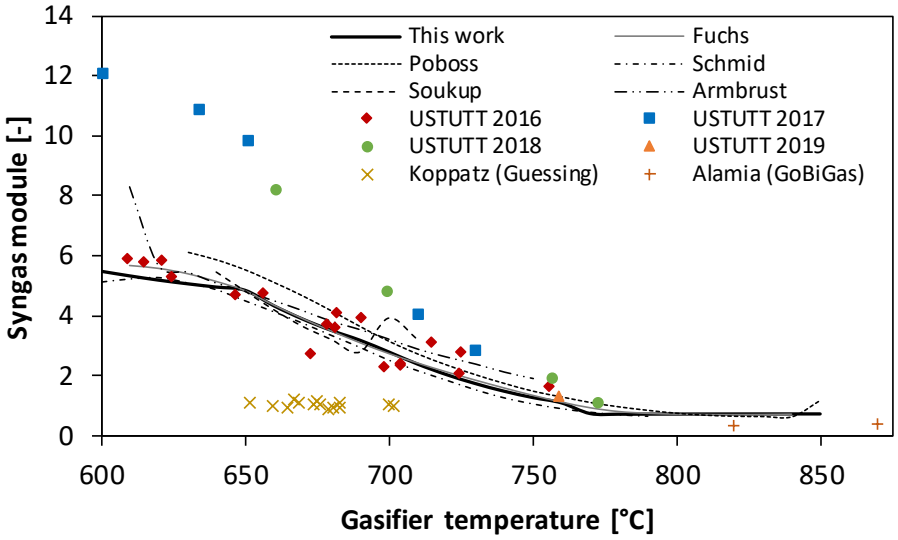

Figure ES 5 - Syngas module as a function of the gasifier temperature from the 0D model of this work (thick solid line), compared with the data from literature (Pröll and Hofbauer, 2008a; Koppatz et al., 2009; Armbrust et al., 2014; Poboß, 2016; Alamia et al., 2017; Schmid et al., 2017; Fuchs et al., 2020) *and with experimental campaigns conducted in the FLEDGED H2020 project at the University of Stuttgart (USTUTT)* (Hafner et al., 2018, 2021; Hafner and Schmid, 2020).

The flexibility requirement also affects the methanol synthesis unit, which is fed with a fresh syngas with a similar composition between the operating modes (CO/CO_2: baseline 0.90 vs. enhanced 0.86), however with a 60% higher mass flow rate in enhanced operation compared to baseline. Therefore, two different methanol synthesis reactor designs are proposed: enhanced reactor design (ERD) (i.e. larger reactor designed on the feed flow rate when hydrogen is added to the system, resulting in a reactor with 7580 tubes) and baseline reactor design (BRD) (i.e. smaller reactor designed on the feed flow rate without hydrogen addition, resulting in a reactor with 4704 tubes). The design condition is characterized by a gas hourly space velocity (GHSV) of 5000 h^{-1} and recycle ratio of 5. In off-design, the recycled molar flow rate is kept constant fixed by blower design. The ERD is overall more efficient with a methanol yield of 97.9% in baseline operation and 96.3% in enhanced operation, compared to 95.4% and 89.1% of the BRD. In all cases, the maximum temperature is well below the critical temperature limit of 300°C reported in literature for the CZA catalyst.

The methanol purification island includes stabilizing and concentration columns which are designed: i) to manage different operating mass flow rates (+ 54.7 ÷ 61.9% in enhanced operation) and to avoid flooding, ii) to guarantee the final product purity specification (99.85%$_{wt.}$) in both the operating conditions.

A minimum capacity factor for the electrolysis unit of 18.6% is required to produce O_2 without external import or back-up ASU.

The heat recovery steam cycle performance depends on high temperature availability and steam exports of the different cases. Regarding the cogenerative ICE, the lower is the recycle ratio in methanol synthesis, the higher is the off-gas flow rate, the higher is the electricity production.

The resulting biomass-to-methanol efficiency of the overall plant is higher in enhanced operation than in baseline operation for both ERD and BRD configurations (see Table ES 2). The ERD configuration is more efficient than the BRD because of a more efficient methanol synthesis section. The biomass-to-methanol efficiency is 68.8% vs. 63.8% in enhanced operation for ERD and BRD cases respectively and 62.0% vs. 60.4% in baseline operation. The gap in biomass-to-methanol efficiency between the two operating modes is lower in BRD configuration because the enhanced operation shows the lowest efficiency of the methanol synthesis section. The increase of carbon efficiency made possible by hydrogen addition is significant, especially with the ERD design, where it increases from 40.3% in baseline operation to 64.4% in enhanced operation mode.

The effect of hydrogen injection in boosting methanol production is higher in the ERD configuration than BRD and involves higher hydrogen-to-fuel (84.2% vs. 71.4%) and power-to-fuel efficiencies (57.5% vs. 52.3%). The net electricity balance is mainly influenced by the electrolysis consumption in enhanced operation.

Table ES 2 - General performance of SEG-based power and biomass-to-methanol plant.

Performance indexes	**ERD, baseline operation**	**ERD, enhanced operation**	**BRD, baseline operation**	**BRD, enhanced operation**
Biomass-to-methanol efficiency (LHV basis),%	62.00	68.78	60.37	63.75
Carbon efficiency, %	40.34	64.40	39.27	59.67
Methanol production enhancement, %	-	59.63	-	51.93
Power-to-methanol efficiency, $MW_{LHV,M}/MW_{el}$	-	57.48	-	52.27
Hydrogen-to-methanol efficiency, $MW_{LHV,M}/MW_{LHV,H2}$	-	84.21	-	71.44
Net electric output, MW	-2.86	-67.24	2.03	-58.01

The economic analysis is performed in a differential way which means that the costs of the PBtM plants are compared with the costs of a reference Biomass-to-Methanol (BtM) plant, whose main differences are the absence of the electrolysis system and the presence of an ASU to produce oxygen for the reformer. In the economic analysis, the 2019 Denmark day-ahead market electricity price curve is considered and a capacity factor of 80% in enhanced operation is assumed (see Table ES 1). The assumed specific cost for the electrolysis system is 700 €/kW_{el} which is consistent with the current alkaline technology and with the future cost estimations of PEM technology (Bertuccioli et al., 2014; International Energy Agency, 2019). In Figure ES 6, the levelized cost of the e-fuel (LCOe-F) breakdown is reported. The main contribution is associated to the purchase of electricity, whose share is about 48% and 56% in BRD and ERD plants, respectively. The share of the electrolyser capital cost is about 20% in both cases. The fixed Opex share is in the range 22-24%, with BRD as upper bound. Other costs, resulting from the net contribution of the avoided ASU and the other capital investments, contribute by about 9% in BRD and 3% in ERD plants. The advantage in capital cost of BRD plant (small methanol reactor) is more than compensated by the higher power island cost (to recover more waste heat from off-gas combustion). Overall, it can be concluded that designs aimed at high power-to-methanol conversion efficiencies (i.e. the ERD design in this case study) should be preferred due to the high cost of hydrogen production compared to the cost associated to oversizing the equipment for fuel synthesis (LCOe-F BRD 37.76 vs. ERD 30.80 €/GJ).

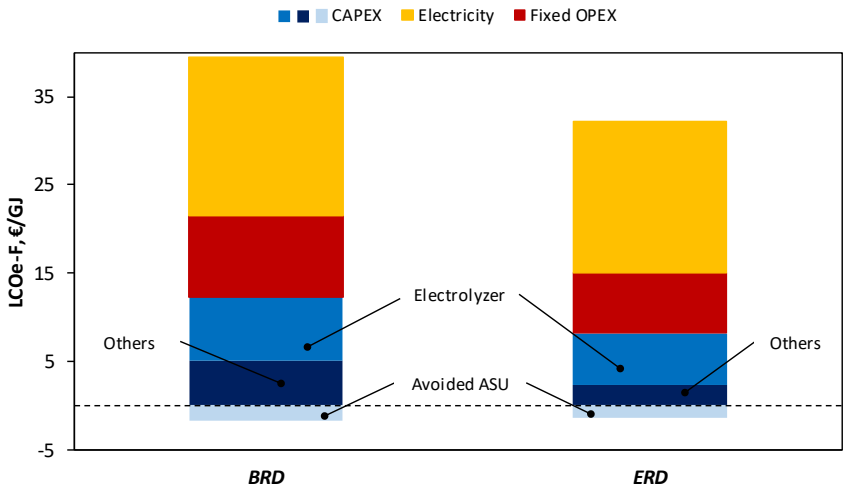

Figure ES 6 - LCOe-F breakdown for the BRD and ERD cases.

By following the aforementioned WTP approach, once the number of hours of operation in the two operating modes and the corresponding average electricity prices are identified for a certain methanol selling price, the profitability of the PBtM plant investment can be evaluated by computing the Internal Rate of Return (IRR). In Figure ES 7, the IRR is reported as a function of the methanol selling price for an electrolyser investment cost of 400 €/ kW_{el} (potential cost in favorable long-term scenarios (Blanco et al., 2018)). The functions are derived from the 2019 Denmark electricity price curve and from the modified curve. The solid lines refer to the flexible PBtM plant, where the increase of the methanol selling price involves an increase of the electrolyser capacity factor, with the method described previously. The dashed lines refer to inflexible plants, with 100% capacity factor of the electrolysis system, purchasing the electricity at the yearly average electricity price of the current price curve (38.5 €/MWh) and of the modified curve (30.4 €/MWh). The IRR value of 10% defines the region above which the PBtM plants is considered profitable with respect to the reference BtM plant. The curves which derive from the current Danish electricity prices ('current' curve) display profitable investment compared to the BtM route at methanol selling prices higher than about 525 €/t. The curves derived from the modified data show profitable investment compared with the reference option at significantly lower methanol selling prices. This is due to the lower average electricity price of the modified curve with respect to the Denmark one. For both the cases, it can be observed that the solid line is always above the dashed line, meaning that flexible operation of the electrolyser always leads to a more profitable investment than an inflexible plant. However, with the current electricity price curve, the solid and dashed lines are very close for a wide range of methanol prices, indicating a little advantage of flexible operation. On the contrary, with the modified electricity price curve, the flexible PBtM plant becomes significantly more profitable than the inflexible PBtM plant.

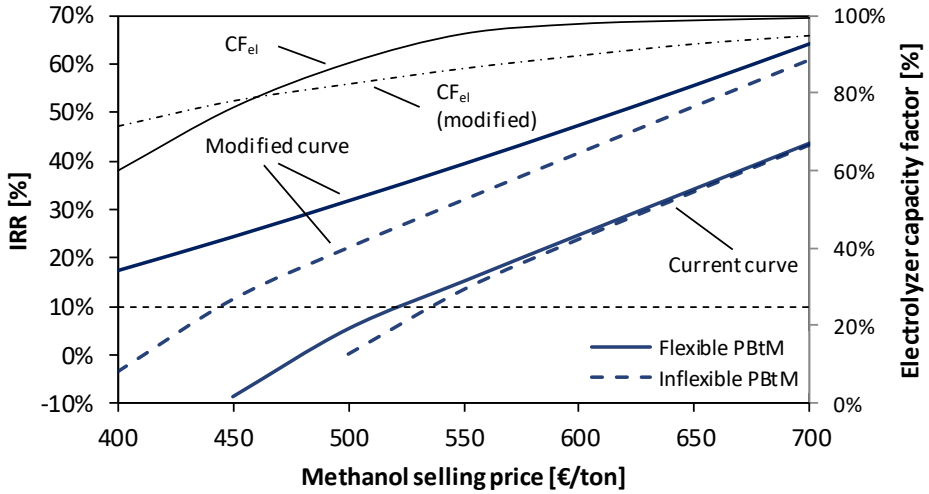

Figure ES 7 – IRR as a function of the methanol selling price for an electrolyser investment cost of 400 €/kW. Curves are derived from the two electricity price curves shown in Figure ES 4.

The main conclusions of this study are the following:

i. the enhanced reactor design has to be preferred over the baseline reactor design because of the higher relative cost of hydrogen from electrolysis compared to the capital cost of oversizing the methanol synthesis unit;

ii. high capacity factors of the electrolyser are needed in order to provide cost competitive e-Methanol to the market and to pay back the high capital cost of the electrolysis unit;

iii. the attractiveness of operating this kind of plants in a flexible way may increase significantly in future scenarios with very high penetration of intermittent renewables, leading to low average electricity prices, but also longer periods of high peak prices.

The second part of the analysis on power and biomass-to methanol plants illustrates a techno-economic comparative analysis of three flexible PBtM plants based on different gasification technologies, namely direct gasification (DG), indirect gasification (IG) and sorption-enhanced gasification (SEG) (see block diagrams in Figure ES 8, Figure ES 9, Figure ES 10).

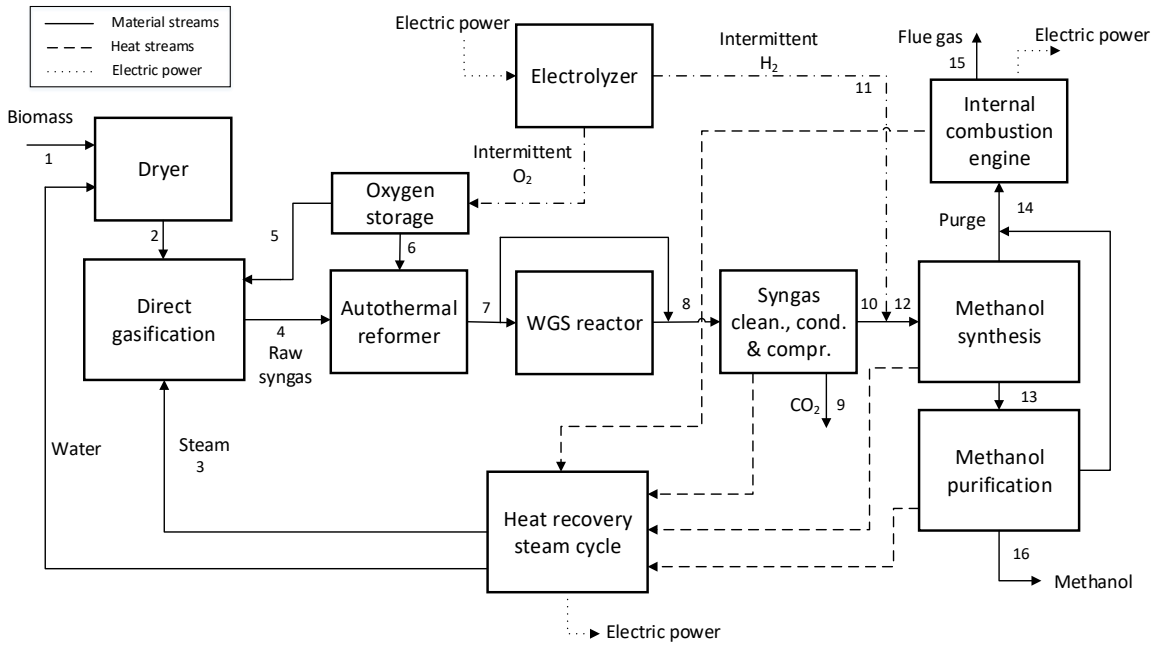

Figure ES 8 - Block diagram of the DG-based power & biomass-to-methanol plant

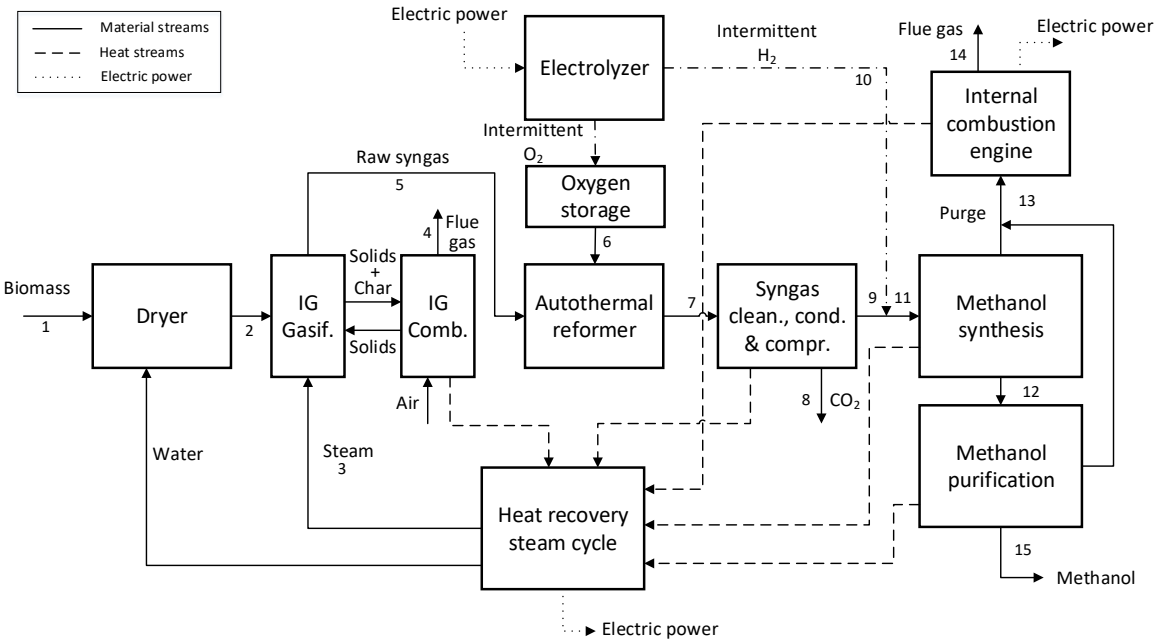

Figure ES 9 - Block diagram of the IG-based power & biomass-to-methanol plant

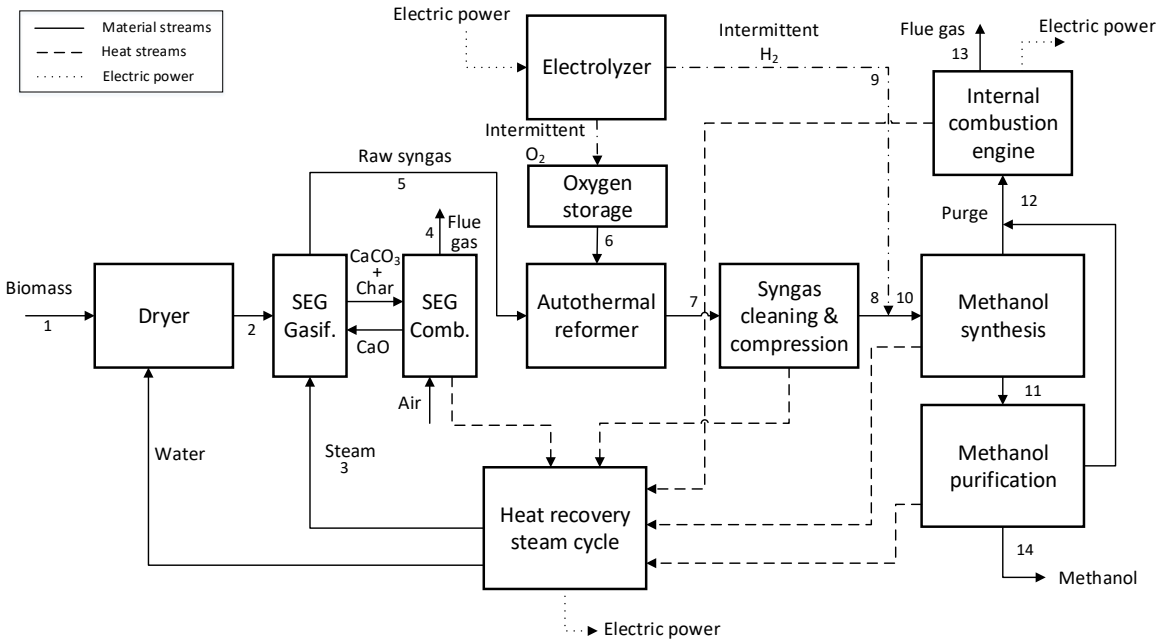

Figure ES 10 - Block diagram of the SEG-based power & biomass-to-methanol plant

Different gasification technologies need different design and operating strategies to manage operational flexibility. The SEG-based plant design and flexible operation is the same as previously described with the ERD case.

Differently from the SEG unit, the DG and the IG options produce a syngas with the same characteristics in both baseline and enhanced operation. Therefore, the control criteria for the plant operation with intermittent hydrogen addition are applied in the conditioning section (CO_2 removal and WGS reactor, required), which is necessary, in this case, to reach the target module upstream the methanol synthesis. In the DG configuration, the syngas module is controlled by adjusting the amount of syngas which bypasses the WGS reactor in baseline operation and by bypassing the WGS reactor and the CO_2 removal unit in enhanced operation. In the IG-based plant, the CO_2 removal unit is bypassed in enhanced operation. In both the options in baseline operation, the 90% of the CO_2 contained in the syngas is separated.

In DG- and IG-based plants, the composition of the fresh syngas shows a major variation between baseline and enhanced operating mode as a consequence of the different conditioning units (CO/CO_2: DG baseline 6.74 vs. enhanced 1.21; IG baseline 14.04 vs. enhanced 1.40). Moreover, the fresh syngas mass flow rate is about 135% higher in enhanced operation compared to baseline, in DG-based plants, and about 75% higher in enhanced operation compared to baseline, in IG-based plants. As previously discussed, it is economically preferable to size the methanol reactor on the enhanced operation condition, rather than on the baseline operation. The design condition is characterized by GHSV of 5000 h^{-1} and RR of 5. Differently from the off-design condition of the SEG case, the recycled molar flow rate of the DG- and IG-based plants is controlled in order to reach 99% of overall methanol yield.

Since both the flowrate and the composition of the DG- and IG-based plants vary significantly between baseline and enhanced operation, in the concentration column a recycle of the product streams rich in methanol and in water is adopted in baseline operation.

The minimum capacity factor of the electrolyser which is required to produce the needed oxygen without external import or back-up ASU is 15.1%, 18.6% and 41% for IG, SEG and DG-based plant, respectively. Due to the high oxygen demand in the gasifier, the DG-based plant obtains a great advantage by being operated between a minimum load to satisfy the oxygen demand at high electricity prices and a maximum load to maximize methanol production at low electricity prices. This allows to avoid large oxygen storages with significant benefits for Capex and safety issues.

As previously described, an optimized heat recovery steam cycle and a cogenerative ICE are used for heat recovery purposes.

The technical results are reported in Table ES 3. In enhanced operation, the DG-based plant holds the highest overall biomass-to-methanol efficiency of the series (73.3%), followed by the IG case (71.0%) and the SEG-based plant (68.8%). The resulting biomass-to-methanol efficiencies of the overall plant are higher in enhanced operation than in baseline operation for all the configurations. The carbon efficiencies of all the plants in the series show modest differences in baseline operation. The rise of carbon efficiency achievable by hydrogen enrichment is significant, especially with the DG-based plant which retains most of the carbon in the syngas, and where carbon efficiency increases from 42.6% in baseline operation to 90.5% in enhanced operation mode. The higher margin in hydrogen addition for the DG-based plant allows the methanol production to increase by 112.3% in enhanced operation, while in the IG and SEG cases, hydrogen addition boosts the methanol output by 57.3% and 59.6% respectively. As to the hydrogen-to-fuel efficiency, the SEG-based plant shows the highest value of 84.2%, followed by the DG case with 82.2% and by the IG one with 81.1%. The different efficiencies reflect the different CO/CO_2 ratio of the feed to the methanol synthesis loop. The power-to-fuel efficiency does not follow the same trend of the hydrogen-to-fuel efficiency. This is because the power-to-fuel efficiency also depends on the effect of the modified operating conditions on the heat recovery steam cycle and on the consumption of auxiliaries, leading to variation of the steam generated, the utility consumptions and ultimately to the electric balance, that are not only linked univocally to the consumption of the electrolysis system. The calculated power-to-fuel efficiency ranges from 56.5% of the IG case to 58.5% of the DG plant, confirming the values reported in the literature for PBtX plants based low temperature electrolysis systems.

Table ES 3 - General performance of the Power & Biomass-to-Methanol plants.

Performance indexes	**DG BO**	**DG EO**	**IG BO**	**IG EO**	**SEG BO**	**SEG EO**
Biomass-to-methanol efficiency (LHV basis),%	65.48	73.35	66.24	70.97	62.00	68.78
Carbon efficiency, %	42.63	90.46	43.13	67.79	40.34	64.40
Methanol production enhancement, %	-	112.30	-	57.29	-	59.63
Power-to-methanol efficiency, $MW_{LHV,M}/MW_{el}$	-	58.48	-	56.54	-	57.48
Hydrogen-to-methanol efficiency,	-	82.15	-	81.07	-	84.21
Net electric consumption, MW	4.06	129.89	2.35	69.49	2.86	67.24

The economic analysis is performed with the previously reported assumptions (see Table ES 1). The DG-based plant is characterized by the highest fixed capital investment (FCI) and total capital investment (TCI) of the series, because it has the largest electrolysis system and the largest oxygen storage. When the storage is not installed (DGns-based plant), the FCI and the TCI decrease by 11%. The SEG-based plant exhibits the lowest FCI and TCI

of the series thanks to process intensification. When FCI is referred to the methanol production in enhanced operation (i.e. the prevalent operating mode), the DG-based plants show the lowest specific costs of the series, as the highest absolute FCI are compensated by the highest methanol productivity. The O&M costs follow the same trend as the TCI. The DG and DGns cases feature the highest purchased electricity cost, as they incorporate the largest electrolysis systems and the highest production of hydrogen. Among these two, the DGns plant shows the highest purchased electricity expenditure, since the electrolysis unit is turned on for all the operating hours of the plant. The DGns configuration also shows the lowest LCOF of the series, thanks to the highest methanol production. The SEG-based plant is characterized by a slightly lower total cost with respect to the IG case. However, being less efficient than the counterfactual, the methanol production is 5% lower and the LCOF results to be slightly higher. Overall, the differences in terms of levelized cost of fuel are relatively small among the assessed cases, ranging from 29.7 €/GJ of the DGns case to 31.7 €/GJ of the DG case.

Table ES 4 – Main result of the economic analysis and levelized cost of fuel for an electrolyser investment cost of 700 €/kW.

Economic results	**DG-based plant**	**DGns-based plant**	**IG-based plant**	**SEG-based plant**
Total FCI, M€	284.80	253.42	220.26	215.44
Total FCI, €/kW$_{LHV}$	2048	1823	2114	2177
TCI, M€/y	39.33	35.00	30.42	29.75
O&M, M€/y	30.65	28.60	23.16	22.68
Purchased electricity cost, M€/y	28.45	32.93	15.24	14.80
Biomass cost, M€/y	13.32	13.32	13.32	13.32
Total costs, M€/y	111.76	109.85	82.14	80.56
Methanol production, t/y	177,318	186,116	137,758	130,621
LCOF, €/GJ	31.67	29.66	29.96	30.99

Once the number of hours of operation in enhanced and baseline operating modes and the corresponding average electricity prices are identified for a certain methanol selling price with the WTP approach described above, the profitability of the PBtM plant investment can be evaluated by computing the IRR. The DGns case proves to be profitable at lower methanol selling prices compared to all the other plants for both the electricity curves. The modified curve gives an economic advantage to all the configurations, reducing the breakeven methanol selling prices (by 62-46 €/t). The plant investment is profitable (i.e. IRR higher or equal to 10%) at relatively high capacity factors of the electrolysis unit (80.7-85.1% with modified curve, 94.3%-97% with the 2019 curve).

The main conclusions of this analysis are the following:

i. different gasification technologies involve different strategies to control the syngas module to operate with and without hydrogen input;

ii. the DG-based plant can take advantage of higher carbon efficiency of the gasification process, leading to higher overall plant carbon efficiency (~90%) in enhanced operation;

iii. due to the high oxygen demand, the DG-based plant obtains a great advantage from avoiding the O_2 storage system and from operating the plant between a minimum load satisfying the O_2 demand of DG at high electricity prices and a

maximum load to maximize methanol production and carbon efficiency at low electricity prices;

iv. in all the cases, the investment in the flexible PBtM plants is profitable for relatively high capacity factors (higher than 80%), meaning that the operational flexibility should be exploited by avoiding the consumption of high-price electricity rather than in the use of the limited amounts of low-price "excess" electricity.

Biomass-to-methanol and hydrogen plants with CCS

The techno-economic analysis of flexible Biomass-to-X plants with CCS (Poluzzi et al., 2022c) considers the following pathways (see block diagrams from Figure ES 11 to Figure ES 14):

- Biomass-to-Methanol plant, based on O_2-blown fluidized bed direct gasification (BtM DG);
- Biomass-to-Methanol plant, based on dual fluidized bed indirect gasification (BtM IG);
- Biomass-to-Hydrogen plant, based on O_2-blown fluidized bed direct gasification (BtH_2 DG);
- Biomass-to-Hydrogen plant, based on dual fluidized bed indirect gasification (BtH_2 IG).

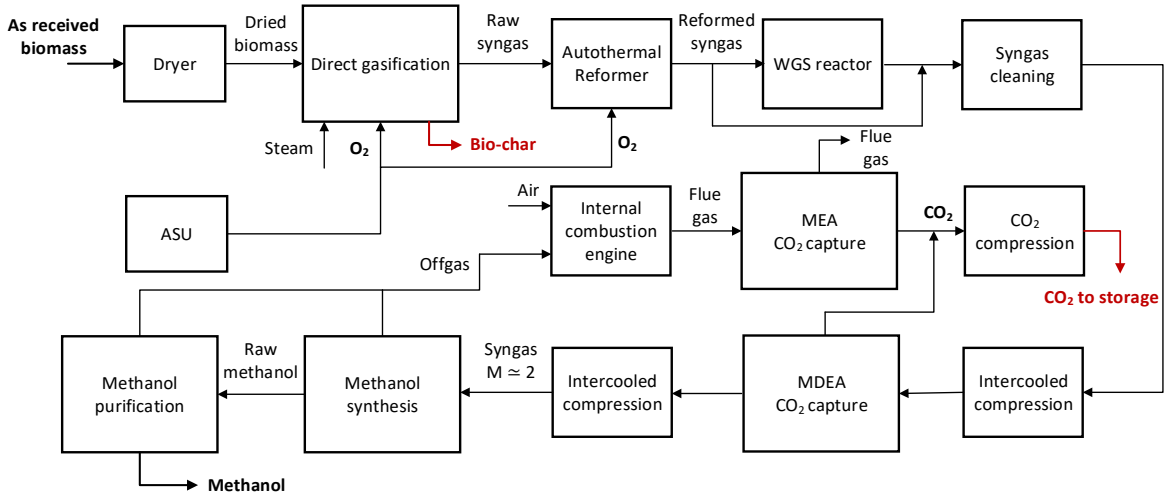

Figure ES 11 – Block diagram of the direct gasification-based Biomass-to-Methanol plant

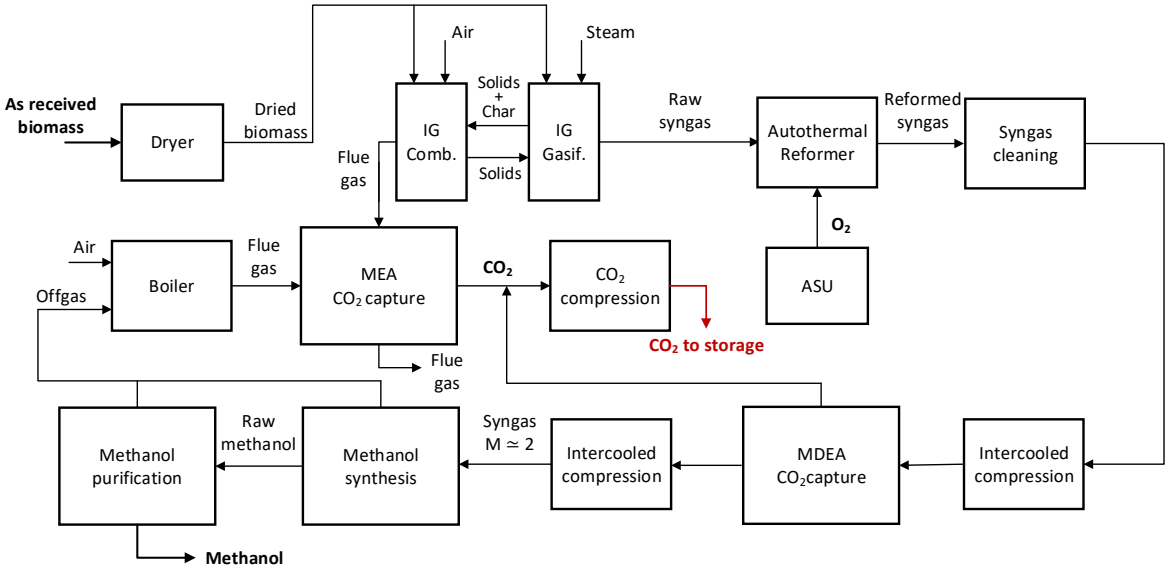

Figure ES 12 – Block diagram of the indirect gasification-based Biomass-to-Methanol plant

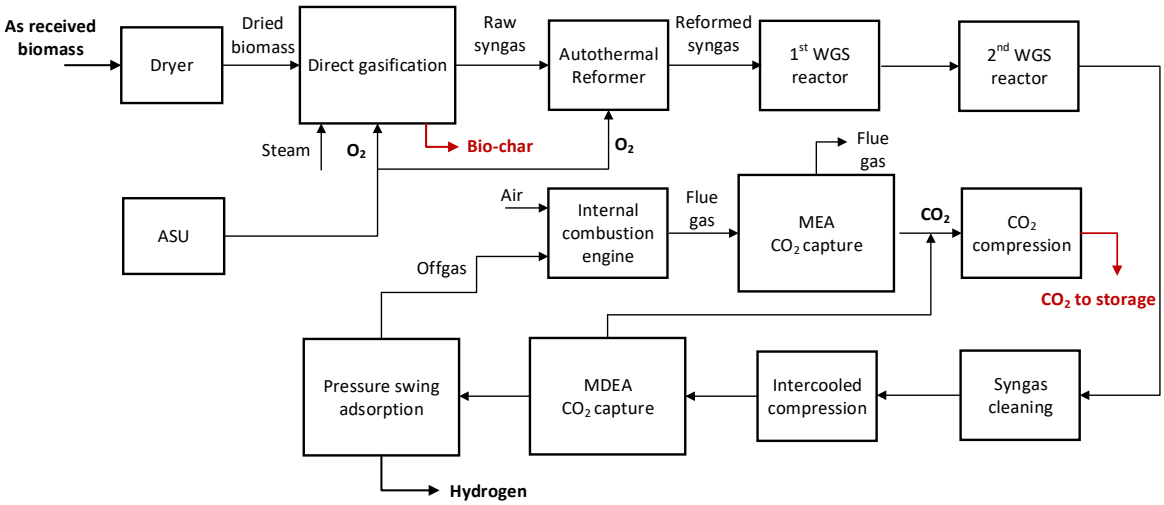

Figure ES 13 – Block diagram of the direct gasification-based Biomass-to-Hydrogen plant

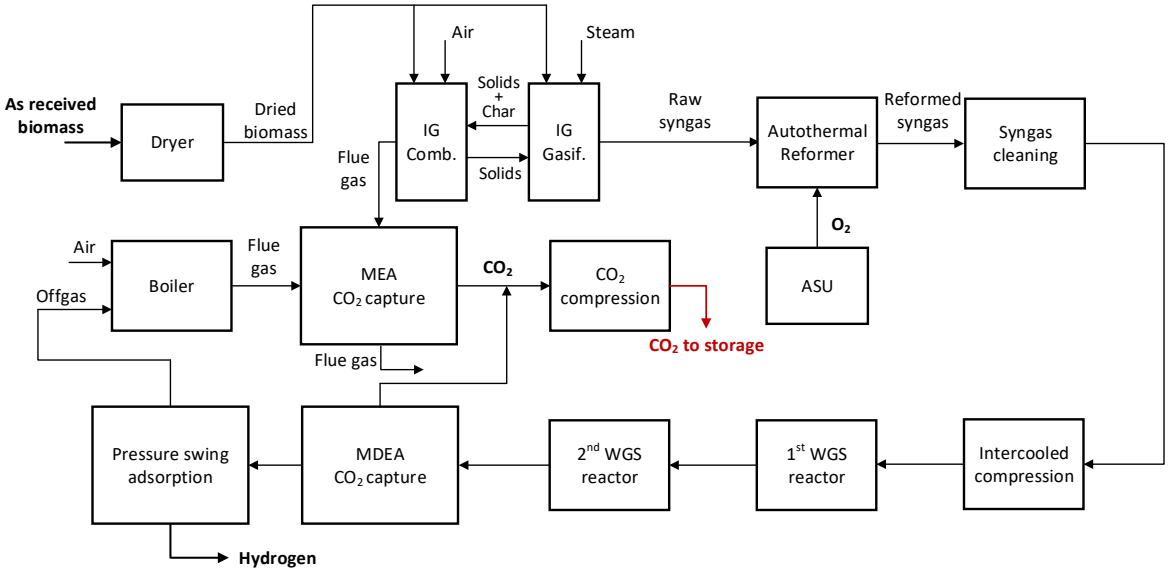

Figure ES 14 – Block diagram of the indirect gasification-based Biomass-to-Hydrogen plant

As stated in the introduction, multi-product plants operating flexibly to produce the good (methanol or hydrogen in this case) that generates the highest revenues may have an economic advantage. Therefore, also Biomass-to-Methanol and Hydrogen plants ($BtMH_2$ DG and $BtMH_2$ IG) are considered in the analysis. In such cases, all the components are designed to operate in both the operating conditions, i.e. methanol production mode and hydrogen production mode.

The technologies employed in the plants are modelled as described previously. The studied plants are designed to capture the CO_2 produced during the conversion of biomass into the final product. As a consequence, the carbon which is captured from the air during the biomass growth can be stored underground resulting in a negative emission process.

The technologies considered in this work for CO_2 separation are pre-combustion and post-combustion chemical absorption processes based on MDEA and MEA solvents respectively. In methanol production plants, CO_2 is removed by means of MDEA scrubbing in order to reach the target module necessary for the downstream synthesis. In hydrogen production plants, the CO_2 is removed from the syngas in order to obtain a high-purity CO_2 stream. The post-combustion technology may be employed in all the plant configurations in order to increase the overall CO_2 capture rate. The IG-based plants adopt the MEA scrubbing to separate the CO_2 from the flue gases coming both from the CFB combustor and from the PSA tail gas boiler. The DG-based plant uses the post-combustion technology to separate the CO_2 from the flue gas of the ICE which burns the off-gas of the methanol synthesis and purification. Being the selected amine scrubbing processes well-known commercial technologies, the CO_2 removal units are not modelled in detail, but the amount of CO_2 to be separated is either set (95% separation efficiency) or tailored to meet the syngas specifications (in case of CO_2 separation from syngas, in methanol production processes). The syngas conditioning design, which may include either one-stage or two stage WGS reactors combined with the MDEA scrubbing unit depends on the type of gasification technology and on the final product. Once separated in the respective amine scrubbing units, the high-purity CO_2 stream is compressed to 80 bar and then pumped up to 150 bar. In none of the biomass-to-X plants, heat is recovered with a steam cycle as the high heat demand for

CO_2 removal does not leave heat available for power generation or does not make it economically competitive to produce very small electric power output. Therefore, steam/water loops are adopted in all the configurations to transfer heat from waste heat sources to the heat users. A great amount of the recovered heat is used to satisfy the thermal duty for amine regeneration, for methanol purification, and to provide steam to the gasification unit. This can be partly supplied by the combustion of the tail gas from the methanol synthesis process and from the PSA for hydrogen purification. Off-gas from the methanol synthesis process and from the PSA for hydrogen purification are exploited either in a cogenerative ICE for electricity and steam production (in DG based plants), or in a boiler for steam production (in IG based plants). IG based plants face a higher heat demand compared to DG based plants due to an extensive use of the MEA-based CO_2 removal, which is more energy intensive.

The performance indexes are reported in the first part of Table ES 5. The biomass-to-X efficiencies are slightly higher in the hydrogen plants (67.6-68.5%) than in methanol plants (65.1-65.8%) mainly due to a less complex final product production from syngas. The carbon efficiencies show modest differences in methanol production plants, ranging from 42.3 to 42.8%.

In DG based plants, most of the CO_2 is captured with the pre-combustion MDEA process (50% and 86% in case of methanol and hydrogen production, respectively) and a much lower amount of CO_2 is captured post-combustion with MEA (2% and 9% for methanol and hydrogen production, respectively). On the contrary, in IG based plants, post-combustion capture is necessary to achieve high CO_2 capture efficiency, as 27% of the total inlet carbon is captured from the IG combustor (the remaining part from the tail gas boiler). The electric consumption of the investigated plants do not show substantial differences, as all plants need to import between 12.1 and 13.1 MW_e. In all plants, most of the electric consumption is associated to syngas compression, followed by CO_2 compression and O_2 production (in DG-based plants). The hydrogen production plants show higher CO_2 compression power, since higher portion of the inlet carbon is separated as CO_2. The DG-based plants feature higher ASU consumption due to higher oxygen demand. In the DG-based plants, the electric consumption is partly compensated by the electricity production of the ICE. This is not the case of the IG-based plants, where tail gas is burned in boilers rather than in the ICE, due to the higher heat demand for CO_2 separation.

The economic results are reported in the second part of Table ES 5. The multi-product plants are assumed to be operated for 50% of the time in methanol production mode and 50% of the time in hydrogen mode (see Table ES 1 for the other assumptions). The methanol production plants show the lowest yearly total costs, followed by the hydrogen production plants and the flexible multi-product plants. The hydrogen production plants show the highest CO_2 transport and storage cost because of the highest amount of CO_2 separated. The methanol production plants are characterized by lower LCOF, followed by the hydrogen production plants and the multi-product plants. By considering the same final product, the DG-based plants result in lower LCOF.

Table ES 5 – Techno-economic results of the Biomass-to-X plants with CCS.

Techno-economic results	**BtM DG**	**BtM IG**	**BtH_2 DG**	**BtH_2 IG**	**BtMH_2 DG**	**BtMH_2 IG**
Technical results						
Biomass-to-X efficiency (LHV basis),%	65.07	65.77	67.65	68.53	-	-
C in fuel, %	42.3	42.8	-	-	-	-

Techno-economic results	BtM DG	BtM IG	BtH_2 DG	BtH_2 IG	$BtMH_2$ DG	$BtMH_2$ IG
Captured CO_2 (MDEA unit), % of inlet carbon	50.3	26.3	85.8	64.0	-	-
Captured CO_2 (MEA unit), % of inlet carbon	1.9	29.0	8.7	34.1	-	-
Net electric output, MW	-9.93	-12.31	-7.55	-12.46	-	-
Economic results						
Total FCI, M€	174.60	186.09	210.56	218.77	229.77	237.59
TCI·CCF, M€/y	24.12	25.71	29.09	30.22	31.74	32.82
O&M, M€/y	17.71	18.82	20.82	21.76	22.51	23.36
Purchased electricity cost, M€/y	3.01	3.74	2.29	3.78	2.65	3.76
CO_2 transport and storage cost, M€/y	2.10	2.23	3.81	3.95	2.95	3.09
Biomass cost, M€/y	13.32	13.32	13.32	13.32	13.32	13.32
Total cost, M€/y	60.27	63.81	69.33	73.03	73.18	76.35
Methanol production, t/y	92,823	93,822	-	-	46,412	46,911
Hydrogen production, t/y	-	-	16,006	16,214	8,003	8,107
LCOF, €/GJ	32.63	34.18	36.07	37.51	38.83	40.03

Figure ES 15 shows the marginal CO_2 avoidance cost vs. the CO_2 capture ratio in the DG- and IG-based plants respectively. In the DG-based plants, about 5% of the CO_2 is avoided at zero marginal cost, stored in the unconverted biochar. The horizontal lines on the left hand side of the graph represent the marginal cost of adding CCS to a biomass-to-X plant (i.e. adding the CO_2 compression unit in the methanol production plant and adding MDEA scrubbing and CO_2 compression in the hydrogen production plant). On the right hand side, the step increase represents the marginal cost of adding the post-combustion MEA scrubbing unit and the corresponding CO_2 compression.

In the BtM DG plant, a CO_2 capture rate of 54.7% is reached at a cost of 40.8 €/t_{CO2} through compression (27.4 €/t_{CO2}) and transport and storage (13.4 €/t_{CO2}). By adding the MEA post-combustion capture unit and increasing the CO_2 compression capacity, the CO_2 capture rate is increased by 1.8% at a marginal cost of 204.9 €/t_{CO2}. In the BtH_2 DG plant, a CO_2 capture rate of 90.30% is reached at a cost of 52.2 €/t_{CO2} (38.8 €/t_{CO2} for capture + 13.4 €/t_{CO2} for transport and storage). The marginal cost of adding post-combustion CO_2 capture and increase capture rate up to 99% is 135.3 €/t_{CO2}.

In BtM IG plant, a CO_2 capture rate of 26.3% is reached at a cost of 45.8 €/t_{CO2} (32.4 €/t_{CO2} for capture + 13.4 €/t_{CO2} for transport and storage), through the addition of compressors for the CO_2 separated by the MDEA unit. By adding the MEA post-combustion capture unit and increasing the CO_2 compression capacity, the CO_2 capture rate is increased by 29% at a marginal cost of 105.1 €/t_{CO2}. In BtH_2 IG plant, a CO_2 capture rate of 64% is reached at 55.6 €/t_{CO2} by integrating the MDEA separation process and CO_2 compression (42.2 €/t_{CO2} for capture + 13.4 €/t_{CO2} for transport and storage). The addition of the MEA plant and the increase of the CO_2 compression unit allows increasing the capture rate up to 98.1%, at a marginal cost of 98.4 €/t_{CO2}. Post-combustion MEA scrubbing is needed in IG-based plants to reach high CO_2 capture rates.

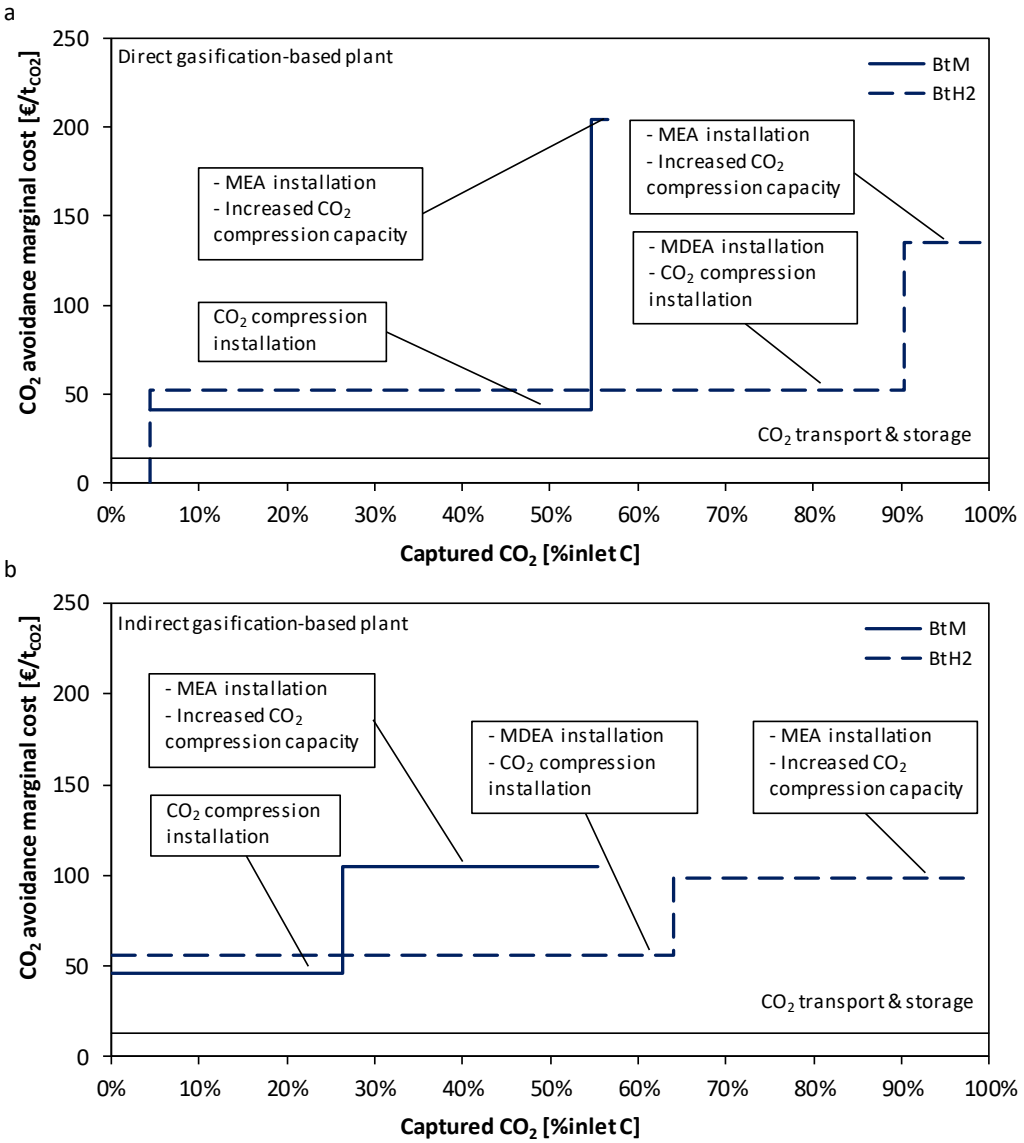

Figure ES 15 – CO_2 avoidance marginal cost vs. captured CO_2 (in DG-based plants, 4.5% of the inlet carbon is stored as biochar).

A simplified economic analysis involving flexible multi-product plant producing methanol and H_2 is conducted. Three different methanol selling prices (i.e. 450, 550, and 650 €/t) are selected, assumed to remain constant along the year. Two simple linear profiles are assumed for the cumulative hydrogen selling price (see Figure ES 16) which involve average yearly H_2 market prices of 4 and 2.5 €/kg respectively. CO_2 credits of 120 €/t_{CO2} are assumed for the stored CO_2.

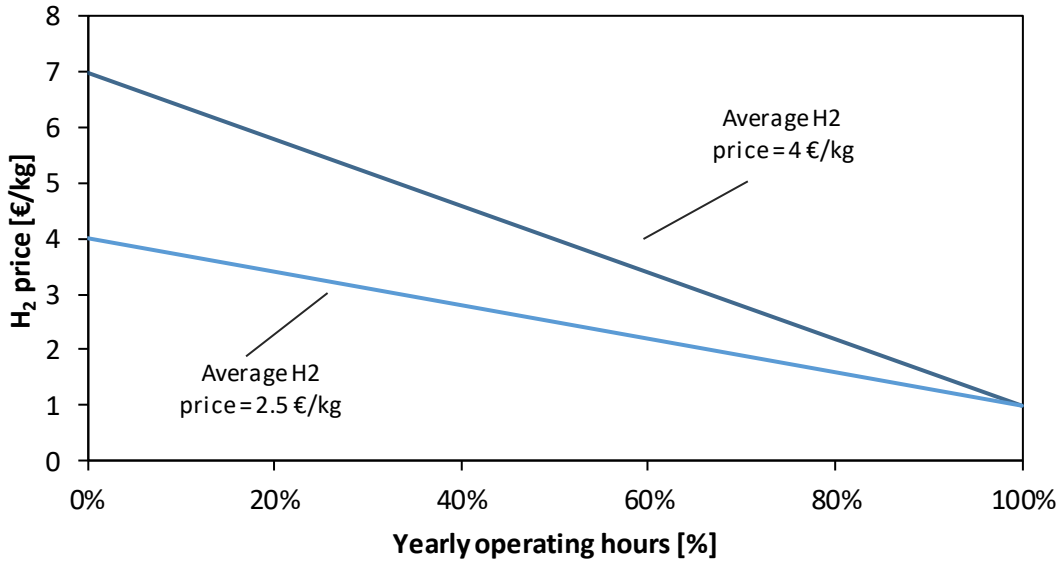

Figure ES 16 - Yearly hydrogen selling price profiles.

In Figure ES 17, the internal rate of return (IRR) of the flexible multi-product plants producing methanol and hydrogen is compared with the IRR of methanol and hydrogen plants delivering a single-product. On the x-axis, the fraction of hours in which the plants operate in hydrogen production mode is reported. Methanol plants are depicted as points on the left ordinate axis, since they never produce hydrogen. For a specified methanol price, the maximum IRR obtained by the multi-product plant must be compared with the highest IRR found on the hydrogen production plant curve and the value achieved by the methanol plant for that assumed price. In Figure ES 17a, considering the methanol selling prices (i.e. 650, 550 and 450 €/t), the multi-product plant should operate for about 70, 80 and 90% of the yearly operating hours in hydrogen mode and the remaining hours in methanol mode. IRRs of 22.1, 21.1 and 20.5% are higher than the optimal values generated by the single-product methanol plants (i.e. 20.4, 15.5 and 10.2%), but lower than the optimal value generate by the single-product hydrogen plant (i.e. 23%). Considering a lower hydrogen price (see Figure ES 17b), for the maximum methanol selling price curve (i.e. 650 €/t), the multi-product plant should operate for about 40% of the year in hydrogen mode and the remaining hours in methanol mode. In this case, the IRR of 14.3% is higher than the optimal value generated by the single-product hydrogen plant (i.e. 12.3%), but lower than the value generated by the single-product methanol plant (i.e. 20.4%). Considering lower methanol selling prices (i.e. 550 and 450 €/t), the multi-product plant should operate for 60% and 80% of the yearly operating hours in hydrogen mode. In this case, the IRRs of 12.2% and 10.8%, for the 550 and 450 €/t methanol prices respectively, are lower than the hydrogen single-product plant, but at least for the 450 €/t higher than the single-product methanol plant.

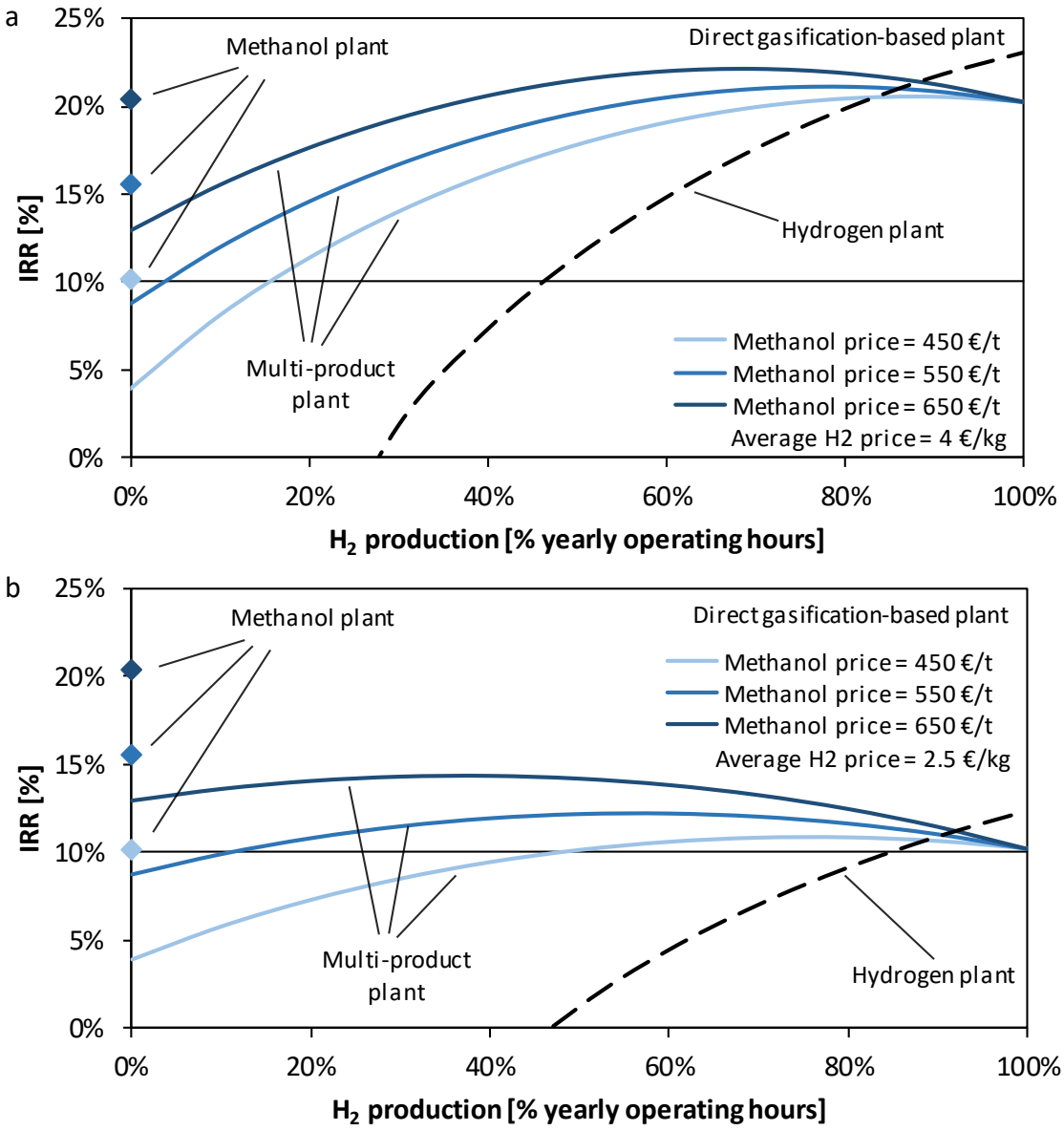

Figure ES 17 – IRR vs. yearly operating hours in hydrogen production mode: (a) yearly average H_2 price = 4 €/kg, (b) yearly average H_2 price = 2.5 €/kg.

The main conclusions of this techno-economic analysis are the following:

- in DG-based plants, most of the CO_2 is captured from syngas with MDEA solvent (i.e. 50-86%) and a much lower amount of CO_2 is captured from flue gas with MEA (i.e. 2- 9%). Conversely, in IG-based plants, MEA is necessary to achieve high CO_2 capture efficiency, as 27% of the total inlet carbon is captured from the IG combustor and 2-7% of the CO_2 is separated from the flue gas of the tail gas boiler.
- The maximum CO_2 capture rate achieved is 55-57% in methanol production plants and 98-99% in hydrogen production plants. In all the assessed cases, less than 2% of the inlet carbon is vented to the atmosphere as CO_2.

- Methanol production plants are characterized by lower LCOF (referred to the product LHV) than hydrogen plants: 32.6 - 34.2 €/GJ (or 649 - 680 €/t) vs. 36.1 - 37.5 €/GJ (or 4.3 - 4.5€/kg), if revenues from CO_2 storage are neglected. This is mainly due to the higher cost for CO_2 capture in hydrogen plants. By considering the same final product, the DG-based plants show slightly lower LCOF, mainly thanks to the lower CO_2 separation cost.
- When credits for CO_2 storage are included, breakeven price of 47-77 €/t_{CO2} make the plants with maximum CO_2 capture rate competitive with the corresponding plants without CCS. CO_2 credits of 148-158 €/t_{CO2} and of 131-138 €/t_{CO2} allow achieving current methanol and hydrogen production costs of around 400 €/t and 2 €/kg respectively.
- Multi-product flexible plants are never the worst case scenario despite the highest investment costs, thus offering a potential advantage from the financial risk perspective**.**

Table of Contents

Executive summary ..... **III**

Table of Contents ..... **XXXI**

List of Figures ..... **XXXIII**

List of Tables ..... **XXXV**

Chapter 1 Introduction **1**
1.1 Motivation of research 1
1.2 Biomass-to-X plants 2
1.3 Literature review 6
1.3.1 Power and biomass-to-X plants 6
1.3.2 Biomass-to-X plants with CCS 17
1.3.3 Economic competitivity of the Biomass-to-X processes 22
1.4 Scope of the research work and contribution to knowledge 26

Chapter 2 Methods **28**
2.1 Modelling and design 28
2.1.1 Biomass model and properties 28
2.1.2 Biomass pre-treatment 30
2.1.3 Gasification technologies 31
2.1.4 Sorption-enhanced gasification model 34
2.1.5 Syngas purification, conditioning and compression 37
2.1.6 Final product synthesis and purification 38
2.1.7 Heat recovery and thermal integration 42
2.2 Methods for techno-economic analysis 45
2.2.1 Key performance indicators 45
2.2.2 Potential carbon efficiency 47
2.2.3 Levelized cost approach 51
2.2.4 Willingness to pay approach 59

Chapter 3 Power and biomass-to-methanol plants **62**
3.1 Design optimization and economic viability of the electrolysis integration 62
3.1.1 Syngas production 67
3.1.2 Methanol production 70
3.1.3 Heat recovery and power generation 74
3.1.4 Process simulation results 76
3.1.5 Levelized cost of electro-fuel 80
3.1.6 Sensitivity analysis 82
3.1.7 Economic feasibility 84
3.1.8 Conclusions 85

3.2 Different gasification technologies comparison 87
3.2.1 Syngas production 88
3.2.2 Methanol production 91
3.2.3 Heat recovery and power generation 95
3.2.4 Process simulation results 97
3.2.5 Levelized cost of fuel 102
3.2.6 Economic feasibility 105
3.2.7 Environmental analysis 108
3.2.8 Conclusions 109

Chapter 4 Biomass-to-methanol and hydrogen plants with CCS 111
4.1 BECCS plants description 111
4.2 Syngas production 113
4.3 Biomass-to-methanol plants 115
4.4 Biomass-to-hydrogen plants 117
4.5 CO_2 capture 118
4.6 Thermal integration 118
4.7 Flexible methanol and hydrogen production 121
4.8 Process simulation results 121
4.9 Economic analysis 125
4.10 Conclusions 133

Chapter 5 Conclusions and outlook 136

Nomenclature 138

Bibliography 141

Appendix A 149
ERD and BRD configurations SEG-based power & biomass-to-methanol plants 152
Power & biomass-to-methanol plants different gasification technologies comparison. 167
Power & biomass-to-methanol plants capital costs 176

Appendix B 184
Biomass-to-methanol and hydrogen plants with CCS 191
Biomass-to-methanol and hydrogen plants with CCS capital costs 205

Acknowledgement 222

List of publications 223

List of Figures

Figure 1-1 – Biomass conversion pathways via gasification and corresponding qualitative destination of the carbon 5
Figure 1-2 – IRR (a, c, e) and operation revenue (b, d, f) maps for BtM, PBtM, BtP and BtH plants with and without CCS. Lines identify the boundary of the regions of the most profitable options for different values of electricity, CO_2, methanol, and hydrogen. 24
Figure 2-1 – Direct gasification process configuration. 31
Figure 2-2 – Indirect and sorption-enhanced gasification process configuration. In IG configuration, solids are represented by olivine; in SEG configuration solids are represented by limestone. 32
Figure 2-3 - Comparison of simulated syngas yield from SEG with literature (Fuchs et al., 2020) and USTUTT experimental data. 36
Figure 2-4 - Comparison of simulated compositions of syngas from SEG with literature (Fuchs et al., 2020) and FLEDGED experimental data from different campaigns. 37
Figure 2-5 – Aspen Plus vs. gPROMS composition profiles along methanol synthesis reactor axial coordinate (SEG EO ERD, see section 3.1 for more information). 40
Figure 2-6 - Scheme of the p-h superstructure representing the possible HRSC configurations. Colored boxes denote steam/water headers at fixed pressures and temperatures, which are connected by equipment units (pumps, economizers, evaporators, superheaters, valves), as described in Elsido et al. (2017). 43
Figure 2-7 - Sequence of process units that converts biomass into a final biogenic product. 47
Figure 2-8 – 'Carbon efficiency' and 'potential carbon efficiency' for methanol production (C:H:O=1:4:1), for two input material streams with carbon (left) and hydrogen (right) as limiting elements and addition of O_2 (b-B), H_2 (c-C), H_2O (d-D) and removal of CO_2 (e-E). 50
Figure 2-9 - Willingness to Pay approach with 2019 Denmark day-ahead market price curves. Breakeven points and resulting operating hours and electricity prices are shown for a methanol price of 450 €/t. 60
Figure 2-10 – Denmark cumulative electricity price and modified Denmark cumulative electricity price. 61
Figure 3-1 – Block diagram of the assessed power & biomass-to-methanol plant 64
Figure 3-2 - Syngas module as a function of the gasifier temperature from the 0D model of this work, compared with the data from literature (Pröll and Hofbauer, 2008a; Koppatz et al., 2009; Armbrust et al., 2014; Poboß, 2016; Alamia et al., 2017; Schmid et al., 2017; Fuchs et al., 2020) and with experimental campaigns conducted in the FLEDGED H2020 project framework at the University of Stuttgart (USTUTT) (Hafner et al., 2018, 2021; Hafner and Schmid, 2020). 68
Figure 3-3 - Energy balance of the SEG process. The inner circle refers to the input energy, the outer refers to the output energy. Left: baseline operation. Right: enhanced operation. 69
Figure 3-4 - Catalyst centerline temperature axial profiles. 73
Figure 3-5 – T-Q diagram of the ERD PBtM plant in enhanced operation. Heat exchangers sections codes are indicated in Table 3-9. 76
Figure 3-6 – Grand composite curve of the ERD PBtM plant in enhanced operation. 76

Figure 3-7 - Carbon efficiency, potential carbon efficiency and useful potential carbon efficiency of the process in baseline (top) and enhanced (bottom) operation for the ERD configuration. 79
Figure 3-8 - LCOe-F breakdown for the BRD and ERD cases. 82
Figure 3-9 - LCOe-F of the ERD PBtM plant as a function of the electrolyser capacity factor and of the average electricity price in enhanced operation, for an electrolyser cost of 700 €/kW. 83
Figure 3-10 - LCOe-F for the ERD PBtM plant as a function of the average electricity price in enhanced operation. The different cases refer to changes in the electrolysis capacity factor (80% and 20%) and in the electrolysis investment costs (700 €/kW and 400 €/kW). 84
Figure 3-11 –IRR as a function of the methanol selling price for an electrolyser investment cost of 400 €/kW. Curves are derived from the two electricity price curves shown in Figure 2-10. 85
Figure 3-12 - Block diagram of the DG-based power & biomass-to-methanol plant 87
Figure 3-13 - Block diagram of the IG-based power & biomass-to-methanol plant 88
Figure 3-14 - Block diagram of the SEG-based power & biomass-to-methanol plant 88
Figure 3-15 - Catalyst centerline temperature axial profiles. 93
Figure 3-16 - (A) Composite curve of IG-based plant baseline operation; (B) composite curve of DG-based plant baseline operation. 97
Figure 3-17 - Carbon efficiency, potential carbon efficiency and useful potential carbon efficiency of the process in baseline (a) and enhanced operation (b) for the direct, indirect and sorption-enhanced gasification-based plants. 101
Figure 3-18 – LCOF as a function of the average electricity price in enhanced operation for a) different electrolysis cost (i.e. 700 vs. 400 €/kW) and for b) different biomass cost (i.e. 46 €/t vs. 0 €/t). 105
Figure 3-19 – IRR of the DG-based plant as a function of the methanol selling price for an electrolyser investment cost of 400 €/kW. Curves are derived from the two electricity price curves shown in Figure 2-10. 106
Figure 3-20 – IRR of the DG- and DGns-based plants as a function of the methanol selling price for an electrolyser investment cost of 400 €/kW. Curves are derived from the two electricity price curves shown in Figure 2-10. 107
Figure 3-21 - IRR of the DGns-, IG- and SEG-based plants as a function of the methanol selling price for an electrolyser investment cost of 400 €/kW. Curves are derived from the two electricity price curves shown in Figure 2-10. 108
Figure 3-22 – CO_2 emissions of the PBtM plants vs. electricity grid emission factor. 109
Figure 4-1 – Block diagram of the direct gasification-based Biomass-to-Methanol plant 112
Figure 4-2 – Block diagram of the indirect gasification-based Biomass-to-Methanol plant 112
Figure 4-3 – Block diagram of the direct gasification-based Biomass-to-Hydrogen plant 113
Figure 4-4 – Block diagram of the indirect gasification-based Biomass-to-Hydrogen plant 113
Figure 4-5 – CO_2 avoidance marginal cost vs. captured CO_2 in DG-based plants (a) and in IG-based plants (b). In DG-based plants, 4.5% of the inlet carbon is stored as biochar. 128
Figure 4-6 – LCOF vs. CO_2 credits of BECCS plants: (a) BtM DG, (b) BtM IG, (c) BtH_2 DG, (d) BtH_2 IG. CCSp: installation of CO_2 compression. CCSm: installation of MEA and increase of CO_2 compression capacity. 130
Figure 4-7 – Yearly hydrogen selling price profiles. 131
Figure 4-8 – IRR vs. yearly operating hours in hydrogen production mode: (a) yearly average H_2 price = 4 €/kg, (b) yearly average H_2 price = 2.5 €/kg. 133

List of Tables

Table 1-1 - Summary of the selected recent literature on PBtX studies. Values in italics have been derived from the data in the papers. When not present in the reference, properties of fuel mixtures (e.g. LHV, density) are taken from JRC Technical Reports, 2014. When necessary, the 2019 conversion $/€ equal to 1.12 has been applied. 10
Table 1-2 – Summary of the selected recent literature on biomass-to-hydrogen plants. All the cost data are converted to 2019€. When not specified in the original paper, the currency year is assigned as: (year of publication – 1) 20
Table 1-3 - Assumptions for the economic analysis 25
Table 2-1 – Properties of as-received biomass 28
Table 2-2 - Non-conventional components sub-models 29
Table 2-3 - Coefficients for biomass specific heat 30
Table 2-4 - Comparison of simulated syngas composition with literature data for direct and indirect gasification. 33
Table 2-5 - Summary of parameters sources for the SEG model 36
Table 2-6 - Comparison of syngas compositions obtained by the 0D and 3D simulations by LUT. 37
Table 2-7 - Aspen Plus vs. gPROMS raw methanol composition. (see section 3.1 and 3.2 for more information) 41
Table 2-8 - Multiplying factors for estimating the total capital investment based on delivered-equipment cost. 54
Table 2-9 - Parameters and assumptions for the evaluation of the LCOF. 55
Table 2-10 – Capital costs detail 56
Table 2-11 – Global heat transfer coefficients dependent on working fluid thermodynamic conditions. 58
Table 3-1 - Plant stream properties ERD baseline operation 65
Table 3-2 - Plant stream properties ERD enhanced operation 66
Table 3-3 - SEG operating conditions and exit gas composition in baseline and enhanced operations. 68
Table 3-4 - Autothermal reformer operating conditions and exit gas composition in baseline and enhanced operations. 70
Table 3-5 - Syngas specifications upstream the methanol synthesis island in baseline and enhanced operating conditions. 71
Table 3-6 – Performance of methanol synthesis reactor for both ERD and BRD configurations ... 72
Table 3-7 - Characteristics of the raw methanol streams fed to the purification section for the assessed cases. 73
Table 3-8 - ICE and heat recovery steam cycle electric power outputs and net electric efficiencies. Steam flow rates at HP (120 bar), MP (32.2 bar) and LP (6.5 bar) turbine inlet are also reported. . 75
Table 3-9 – Heat sources and sinks of the ERD PBtM plant in enhanced operation 75
Table 3-10 - General performance of Power & Biomass-to-Methanol plant 77
Table 3-11 - Fixed capital investment costs of the units of the PBtM and the BtM plants used in the differential economic analysis. The units with the same investment cost in the different plants are not reported. 81
Table 3-12 – Main result of the economic analysis and levelized cost of e-fuel 82

Table 3-13 - Profitability of the plant investment for two different methanol selling prices and electrolyser investment costs. 84
Table 3-14 - Gasifiers operating conditions and exit gas composition. 89
Table 3-15 - Autothermal reformer operating conditions and exit gas composition. Syngas conditioning operating conditions. 91
Table 3-16 – Syngas specifications upstream the methanol synthesis island in baseline and enhanced operating conditions. 91
Table 3-17 - Performance of methanol synthesis. 93
Table 3-18 - Characteristics of the raw methanol streams fed to the purification section for the assessed cases. Methanol purification operating conditions. 94
Table 3-19 - ICE and heat recovery steam cycle electric power outputs and net electric efficiencies. Steam flow rates at HP (120 bar), MP (32.2 bar) and LP (6.5 bar) turbine inlet are also reported. . 95
Table 3-20 - General performance of the Power & Biomass-to-Methanol plants. 98
Table 3-21 – Fixed capital investment costs of the units of the PBtM plants. 103
Table 3-22 – Main result of the economic analysis and levelized cost of fuel for an electrolyser investment cost of 700 €/kW. 104
Table 4-1 – Gasifiers and autothermal reformer operating conditions and exit gas composition. . 114
Table 4-2 - Main features of the syngas conditioning island. 115
Table 4-3 - Main features of the methanol synthesis and purification processes. 116
Table 4-4 – Heat available and thermal loads of the assessed plants. 119
Table 4-5 - Overall performance of the assessed plants 123
Table 4-6 – Carbon balance of the BECCS plants. Percent values referred to the total inlet carbon. 124
Table 4-7 – Breakdown of the fixed capital investment costs of the biomass to methanol (BtM), biomass to hydrogen (BtH_2) and flexible biomass to methanol and hydrogen ($BtMH_2$) plants. 125
Table 4-8 - Main results of the economic analysis and levelized cost of fuel 127

Chapter 1
Introduction

1.1 Motivation of research

Biomass is a unique resource of renewable energy and renewable carbon. The amount of biomass for use in the energy, transport and chemical sectors is limited by the availability of land and by the competition with the food value chain. Therefore, it is of paramount importance to make the best use of the energy and the carbon in the biomass, according to the market and societal needs and to sustainability criteria (IEA, 2017; Camia et al., 2018).

In the past decades, the relatively low value of carbon compared to energy was such that biomass has been mostly used for heat and power generation through combustion, with unrestricted emission of CO_2. This is likely to change in the next decades if the commitment of governments and the regulations in limiting the CO_2 concentration in the atmosphere is confirmed, that will lead to an increase of the biogenic carbon value. Also, the rise of solar and wind power generation will likely cause a reduction of the average electricity prices and an increased value of the services to improve the resiliency of the electric energy system through energy storage and flexible power generation.

In this context, understanding the best use of biomass depending on the regional energy mix (Patrizio et al., 2021) and on the market and regulatory conditions is a strategic issue for industry and policymakers. The possible uses of biomass include:

i. combustion for power and heat generation, with or without CO_2 capture and storage;
ii. conversion into a carbon-based product (e.g. methane, methanol, Fischer-Tropsch, dimethyl ether) for the transport sector or the chemical industry, with or without capture and storage of the excess CO_2;
iii. conversion into a carbon-based product, with enhanced productivity through the conversion of the excess carbon with added green hydrogen in a power & biomass-to-X system;
iv. production of bio-hydrogen, with or without CO_2 capture and storage;
v. production of biochar and other products (e.g. power, liquids, hydrogen).

When final synthetic products are considered, biomass-to-X systems may produce either carbon- or hydrogen-based products which can be used in a wide range of sectors, from industry to transport. A large fraction of chemicals are carbon-based products, where

the carbon has a fossil origin. Bioenergy offers a solution to "defossilize" the chemical sector by substituting fossil carbon with biogenic carbon (Gabrielli et al., 2020). As regards the transport sector, liquid biofuels represent a valuable option for the decarbonization of heavy-duty road and off-road vehicles, shipping, and aviation due to the significant challenges in the electrification of these sectors. Biofuels are also suitable for reducing CO_2 emissions from light duty vehicles in the transition to electric and hydrogen-based mobility. In the coming decades, an increased share of advanced biofuels from low-risk ILUC (indirect land use change) feedstocks is expected and required by regulations (European Commission, 2021, 2022). Increasing the economic competitiveness of advanced biofuels is key for their wide deployment. The current estimated costs of advanced biofuels lie in the range of 17-44 €/GJ for biomass-based production and of 13-29 €/GJ for waste-based production, while the fossil fuel production cost varies between 8 and 14 €/GJ (Brown et al., 2020).

1.2 Biomass-to-X plants

This work focuses on plants for the conversion of second-generation biomass into liquid products and hydrogen via gasification-based pathways shown in Figure 1-1:

a. biomass-to-X, with emission of the excess CO_2 (BtX);
b. power & biomass-to-X, with reduced CO_2 emission and increased productivity thanks to green hydrogen addition by means of water electrolysis (PBtX);
c. biomass-to-X, with capture and storage of the excess CO_2 (BtX CCS).

The thesis investigates different types of gasification technologies, i.e. direct, indirect and sorption-enhanced gasification, and different final products, i.e. methanol and hydrogen. The considered gasification technologies are fluidised bed reactors which are suited to plants with dozens to hundreds MWs of biomass input. Entrained-flow gasification technologies are not addressed in this work since they are suited for larger plant sizes which cannot be logistically associated with biomass feedstock without being co-fed with coal.

All the investigated plants combine the same fundamental conversion steps, namely biomass drying, gasification, syngas purification, conditioning and compression, and final product synthesis and purification.

In the pre-treatment section, as-received woody biomass is fed to a belt dryer in order to reduce the moisture content from 45% to 15%. Biomass drying is necessary because all the water in the biomass would otherwise evaporate in the gasifier by using high quality heat coming from exothermic biomass oxidation. In the belt dryer, instead, water evaporation is induced by air which is heated through hot water.

Once pre-treated, the dried biomass is sent to the gasification island. Three different fluidized bed gasification technologies are investigated in this work.

In the direct gasification-based plant, the gasification process is thermally sustained through the partial oxidation of biomass by means of oxygen either from air separation unit (ASU) or as by-product from water electrolysis. Most of the inlet carbon remains in the nitrogen-free syngas as CO, CO_2 and CH_4, while a minor part is extracted from the fluidized bed as unconverted char. In the indirect gasification-based plants, a solid heat carrier material (i.e. olivine) circulates between a higher temperature combustor and a lower temperature gasifier to provide the heat required for biomass gasification. The heat is generated from the combustion with air of the unconverted char, that flows from the gasifier to the combustor,

and of additional biomass. In the sorption-enhanced gasification-based plants, CaO-rich solids are used as bed material and circulate between the gasifier and the combustor. In addition to behaving as a heat carrier as in the indirect gasification process, the circulating solids absorb CO_2 through the carbonation reaction ($CaO + CO_2 \leftrightarrow CaCO_3$). The produced $CaCO_3$ is calcined into CaO and CO_2 in the combustor by means of the combustion of the unconverted char flowing from the gasifier to the combustor and of additional biomass, if needed. Solids circulation is tuned to achieve a target CO_2 uptake, which is controlled by the equilibrium of the carbonation reaction. Therefore, by increasing the solids circulation rate, the gasifier temperature increases and the CO_2 separation reduces. In this way, it is possible to control the composition of the produced syngas. The main syngas chemical components should be in proper proportions to have a high conversion of the feed gas into the final product. This proportion is defined as the syngas module $M = (H_2 - CO_2)/(CO + CO_2)$, which has a specific value depending on the final product. In the sorption-enhanced gasifier, it is possible to obtain a tailored syngas with a target module, with no need of further syngas conditioning.

The aforementioned gasification processes produce a nitrogen-free syngas, which contains a significant amount of tar and methane. A catalytic auto-thermal reformer (ATR) unit is included downstream the gasifier and a high temperature filtration unit, to convert methane and tar into useful reactants for the synthesis (i.e. CO and H_2). Oxygen is fed either by means of ASU or as by-product of water electrolysis. In such a case, an oxygen storage system is foreseen in order to store the intermittent oxygen production from the electrolyser.

The reformed syngas must be further conditioned, purified and compressed to be fed to the downstream final product synthesis. In order to produce a tailored syngas for the downstream final product synthesis, the syngas conditioning section in direct and indirect gasification-based plants includes different processes such as water-gas shift (WGS), which allows to further shift the syngas composition towards hydrogen, and CO_2 capture, which allows to remove the excess carbon from the syngas. As already mentioned, the sorption-enhanced gasification-based plant does not need neither a WGS reactor nor a CO_2 capture unit, because the syngas composition may be tuned within the gasifier.

Syngas purification includes the removal of undesirable compounds, such as sulphur, chlorine and alkali, that would poison the downstream catalytic reactors. To this end a water scrubber, H_2S absorption by liquid Redox LO-CAT process (Echt et al., 2017) and adsorption with activated carbon are included in the plant.

The syngas needs to be compressed by means of one or more intercooled compressors, depending on the plant configuration, in order to reach the target pressure of the final product synthesis and purification (i.e. 90 bar for methanol production plants and 30 bar for hydrogen production plants).

Final product synthesis and purification allow to provide the product with the required purity specification. In methanol production plants, a conventional methanol synthesis technology is adopted, based on a boiling water reactor (BWR) where the syngas flows through tubes filled with catalyst and surrounded by boiling water at 238°C. Since the per-pass methanol yield is limited by thermodynamic equilibrium, most of the unconverted reactants are recycled back to the reactor. The crude methanol is cooled down to 40°C, separated from the light gases in a flash unit and then throttled to about 2 bar before purification. The purification section includes distillation columns aimed at stripping off the light gases from the crude methanol and at separating water from methanol, to reach the

target purity of 99.85%$_{wt}$. In hydrogen-production plants, hydrogen is produced in a pressure swing adsorption (PSA) system with a purity higher than 99.9%$_{vol}$.

Off-gas from methanol synthesis and purification, and PSA unit contains a significant amount of light gases, whose heating value is exploited for electricity and/or steam production, depending on the plant configuration. Steam cycle/loop is included in order to recover the heat from the different sections and to produce electricity and/or steam for internal consumption.

The presence and the location within the plant of the aforementioned process steps may change depending on the gasification technology and on the final product, therefore a case-specific description of the investigated plants is provided in the next sections.

Biomass gasification for advanced biofuel production is not commercially deployed at significant scale yet. However, the single process units (i.e. conventional gasifiers, ASU, cleaning technologies, WGS reactors, CO_2 removal, etc.) are commercially adopted in plants for the production of chemicals (hydrogen, methanol, ammonia, etc.) from fossil fuel gasification/reforming. Sorption-enhanced gasification is the less mature process, which was tested in the Guessing demo plant at TRL7 and has been object of demonstration for flexible operation at TRL5 in the H2020 FLEDGED project.

Biomass composition is characterized by different carbon-to-hydrogen ratio than the final biogenic product. Therefore, in "conventional" BtX systems, the excess carbon is removed as CO_2 to be subsequently vented to the atmosphere. PBtX and BtX CCS plants allow to valorise the excess biogenic carbon by using it for different purposes. In the PBtX pathway, the plant is integrated with a water electrolysis unit which generates hydrogen to be combined with the carbon-rich syngas from biomass gasification. The potential benefit of such a concept is to increase the utilization of the biogenic carbon in the biomass, enhancing the production of high value bio-product for a given size and cost of the biomass supply chain, pre-treatment and gasification equipment. Moreover, PBtX systems can potentially provide services to the electric grid through power-to-X energy storage. The BtX CCS pathway includes the capture of the CO_2 during the conversion of the biomass into the final product. As a consequence, the carbon which is captured from the air during the biomass growth can be stored underground resulting in a negative emission process. When hydrogen is the final product, all the biogenic carbon contained in the feedstock can be potentially captured. Given the current situation, the penetration in the market of these alternatives mainly depends on economic and environmental factors. The PBtX route is feasible only with a high penetration of non-programmable renewable energy sources (RES), while the BtX CCS pathway requires either a relatively high carbon tax or a reward for CO_2 removal from the atmosphere. If the product of BtX systems is hydrogen, a sufficiently developed hydrogen market is necessary.

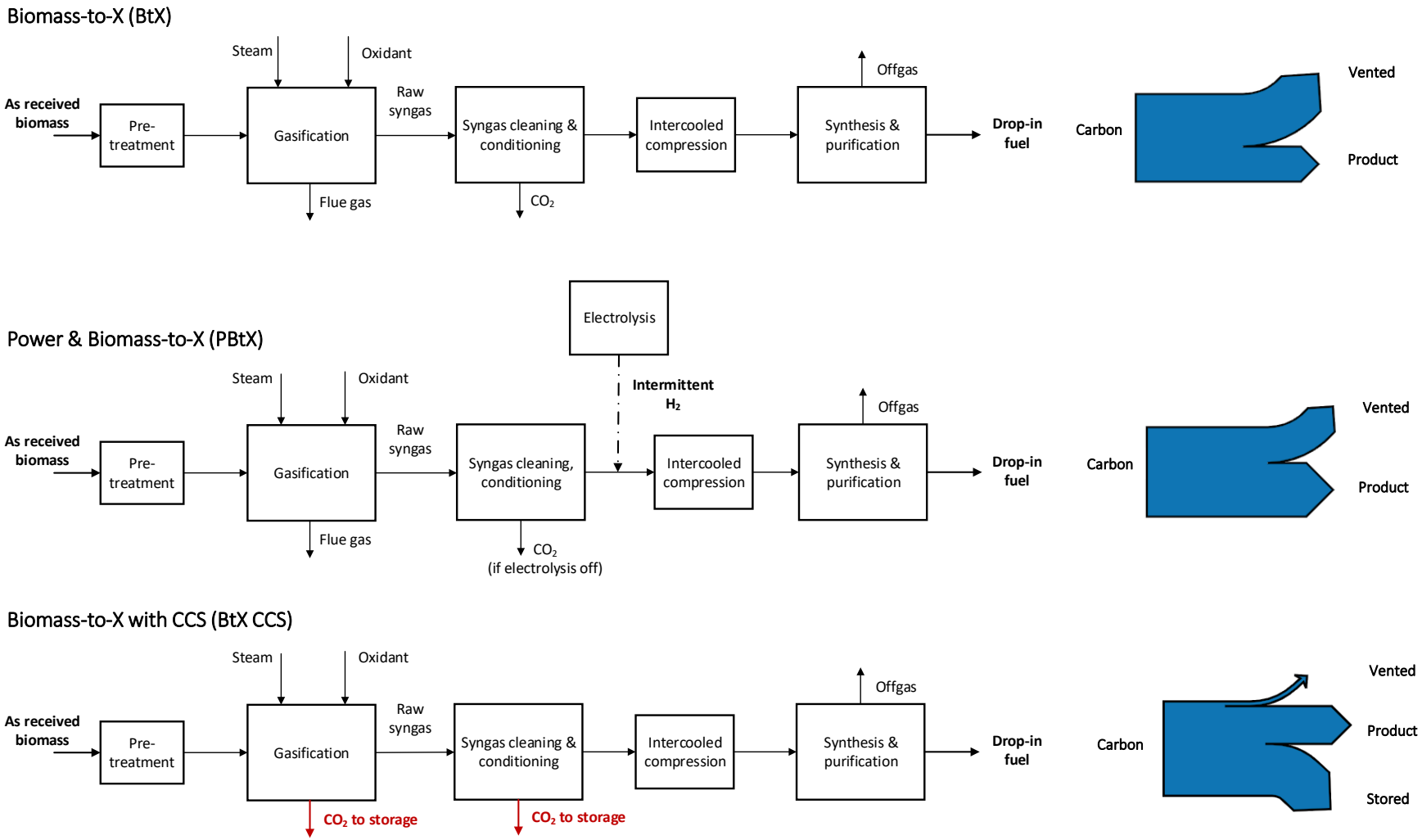

Figure 1-1 – Biomass conversion pathways via gasification and corresponding qualitative destination of the carbon

1.3 Literature review

A review of the recent literature on the relatively novel concepts of power and biomass-to-X plants and biomass-to-X plants with CCS is carried out in the next sub-sections. Section 1.3.1 and 1.3.3 are extensively developed in Poluzzi et al. (2021) and (Poluzzi et al., 2022c), respectively.

1.3.2 Power and biomass-to-X plants

In Table 1-1, a summary of selected scientific works on power & biomass-to-X (PBtX) plants is reported, considering synthetic natural gas (SNG), methanol (M), gasoline (G) via methanol-to-gasoline process, dimethyl ether (DME), Fischer-Tropsch liquids (FT) and jet fuel (JF) as final products. The main key performance indicators are reported, referring to the carbon utilization efficiency, the power-to-X (PtX) and hydrogen-to-X (HtX) energy efficiencies and to the cost of the product (in €/GJ_{LHV}). It has to be noted that PtX (eq. (1-1)) and HtX (eq. (1-2)) efficiencies refer to the marginal production efficiency of the product (*prod*) between the PBtX plant and the corresponding baseline BtX without hydrogen addition. Also, the cost of the e-product has been calculated (eq. (1-3)), as the marginal cost for the additional fuel produced in a PBtX plant, with respect to the corresponding BtX plant.

$$\eta_{PtX} = \frac{\left(\dot{m}_{prod} \cdot LHV_{prod}\right)_{PBtX} - \left(\dot{m}_{prod} \cdot LHV_{prod}\right)_{BtX}}{P_{el,electrolysis}} \tag{1-1}$$

$$\eta_{HtX} = \frac{\left(\dot{m}_{prod} \cdot LHV_{prod}\right)_{PBtX} - \left(\dot{m}_{prod} \cdot LHV_{prod}\right)_{BtX}}{\dot{m}_{H_2} \cdot LHV_{H_2}} \tag{1-2}$$

$$C_{e-prod} = \frac{\left(C_{prod} \cdot \dot{m}_{prod}\right)_{PBtX} - \left(C_{prod} \cdot \dot{m}_{prod}\right)_{BtX}}{\dot{m}_{prod,PBtX} - \dot{m}_{prod,BtX}} \tag{1-3}$$

In the literature, a number of plant configurations including different gasification technologies, conditioning units and biofuels have been assessed (see Table 1-1). Also, different types of electrolysis technologies can be integrated with BtX processes, implying different levels of flexibility of the overall plant.

Hannula (2015) examined the co-production of synthetic natural gas, methanol or gasoline (MTG) from biomass residues and electricity. The biomass feedstock is gasified with an oxygen-blown fluidized bed reactor. The BtX plants employ a WGS reactor for the control of the syngas composition. When hydrogen is added to the system, the WGS is bypassed. The acid gas removal (AGR) unit separates 98% of the CO_2 contained in the syngas independently on whether green hydrogen is added or not. The article compares PBtX, BtX and PtX plant configurations from a techno-economic point of view. The production cost for all the configurations are computed at fixed electricity price and annual operating hours. The economic competitiveness of operating the PBtX plant flexibly is

assessed with a simplified approach, by computing the breakeven electricity price at different annual operating hours that guarantees a profitable operation with respect to the reference BtX plant.

Hannula (2016) and Koponen and Hannula (2017) studied how to increase biofuels production from given amount of biomass by feeding external hydrogen from alkaline water electrolysis to a gasification-based biorefinery. Two gasification alternatives, i.e. oxygen blown and indirect gasification, and two different end-product alternatives, i.e. synthetic gasoline via methanol and synthetic natural gas, are assessed. In the PBtX plants, the CO_2 contained in the syngas is not separated and it is used as feedstock for the synthesis. The operational flexibility is not considered, therefore the PBtX plants imply a continuous external hydrogen supply and neither the WGS reactor nor the AGR unit for CO_2 separation are necessary. The study compares PBtX and BtX plant configurations from the techno-economic perspectives. The production costs are calculated at given electricity price and annual operating hours. The breakeven hydrogen price is calculated so as to obtain the same fuel production cost in BtX and PBtX configurations.

Albrecht et al. (2017) proposed the co-production of F-T fuels from biomass gasification and hydrogen addition from PEM electrolysis, which offers the potential to connect the device directly to fluctuating power sources thanks to its superior dynamic operation behavior. By choosing this type of electrolysis technology, the plant can operate more flexibly, although the flexibility is not explored within the article. The raw syngas from entrained flow biomass gasification is enriched with hydrogen upstream the RWGS reactor. The PBtX plant is compared with the conventional BtX process which includes both the WGS reactor and the AGR unit for CO_2 removal and with a PtX process. The fuel production cost is computed at fixed electricity price and annual operating hours.

Hillestad et al. (2018) presented a PBtX process for the production of Fischer-Tropsch (F-T) liquid fuels where external hydrogen is produced through high temperature steam electrolysis in a solid oxide electrolysis cell (SOEC). The extra hydrogen is mixed with the syngas both at high temperature to convert CO_2 into CO in a reverse water gas shift (RWGS) reactor and at low temperature in order to increase the H_2/CO ratio. SOEC requires less electrical power than alkaline water electrolysis, leading to high PtX efficiency, as shown in Table 1-1. However, the flexibility of the plant is limited because of the high operating temperature which is not compatible with intermittent operations. The PBtX plant is compared with a conventional BtX process which includes a WGS reactor and an AGR unit for CO_2 removal. The fuel production cost shown in Table 1-1 is calculated by fixing the electricity price, the annual operating hours and an optimistic investment cost for the SOEC.

Zhang et al. (2020) assessed two PBtX concepts with SOEC steam electrolysis and co-electrolysis, respectively. The first concept operates the SOEC with steam electrolysis which produces hydrogen and allows to avoid the WGS reactor and the AGR, aiming at very high carbon utilization. The second concept operates the SOEC with co-electrolysis by converting the CO_2 separated from the syngas. It aims at overcoming the flexibility limitations imposed by the SOEC through a configuration where the electrolyser does not affect the syngas conditioning process. When renewable electricity is not available, the CO_2 is captured from the syngas and stored, to be converted when renewable electricity becomes available. In the first operating mode, syngas is conditioned through the WGS reactor and CO_2 separation, while in the latter both the units are bypassed. The production cost of the PBtX plants is highly dependent on the price and the availability of renewable electricity. The concept with co-electrolysis allows for additional operational flexibility without renewable electricity,

resulting in higher annual production than the steam electrolysis concept, which interrupts the plant operation when renewable electricity is not available. The advantage of the steam electrolysis concept (see Table 1-1) is overcome by the co-electrolysis configuration in case of limited availability of renewable electricity along the year.

It is noteworthy, that the integration of an electrolysis system offers the opportunity of exploiting the coproduction of oxygen, to be used in the gasification process. On this respect, different criteria may be adopted to size the electrolysis unit, as assessed by Koytsoumpa et al. (2020), either to completely satisfy the plant oxygen demand or to retain the maximum amount of carbon in the final product.

The analysed literature assumes different plant sizes, different gasification and syngas conditioning processes, different electrolysis technologies and economic assumptions that do not allow a direct comparison of the quantitative results. Nevertheless, the existing literature allows to make the following main observations.

- The first main benefit of PBtX plants is the much higher carbon efficiency, i.e. the better utilization of the biogenic carbon. With PBtX configurations it is possible to achieve carbon efficiencies higher than 90%, vs. 25-40% of baseline BtX plants. The relatively low carbon efficiency of the PBtX systems in (Hannula, 2015). (42-49%) is due to the selected process configuration where only the CO in the syngas is converted and CO_2 is separated and vented.
- The HtX efficiency varies in a relatively narrow range in the reported studies (82-85% (Hannula, 2015, 2016; Albrecht et al., 2017; Hillestad et al., 2018)), independently from the final product. The only exception is gasoline production (Hannula, 2015, 2016), that is based on a methanol-to-gasoline (MTG) process downstream methanol synthesis, that introduces energy losses. Therefore, the PtX efficiency mainly depends on the efficiency of the electrolysis system. With an efficient thermal integration with the process, high temperature solid oxide electrolysers allow achieving a PtX efficiency approaching 80% (Hillestad et al., 2018; Zhang et al., 2020), to be compared with 50-58% of systems based on low temperature electrolysis (Hannula, 2015, 2016; Albrecht et al., 2017).
- In PBtX plants, the increased plant productivity favorably affects the two main cost items of a bioproduct, namely: (i) the biomass cost and (ii) the capital cost of the equipment for biomass gasification and syngas cleaning and conditioning. Both these items, that are directly linked to the input of biomass feedstock in the plant, are distributed over a higher amount of final product. Such economic benefit has to be compared to the additional cost for the production of the input hydrogen.
- The cost of green hydrogen is closely linked to: (i) the capital cost of the electrolysis system, (ii) the capacity factor of the electrolyser and (iii) the average price of electricity used for hydrogen production. As clearly shown by Hannula (2015), high capacity factors of the electrolysis system are needed to have competitive hydrogen production cost in a PBtX plant, unless (unrealistic) long periods of negative electricity price are assumed. This is the same conclusion obtained by Zhang et al. (2020), who showed the significant rise in the cost of the product, when the electrolysis capacity factor reduces. So, PBtX plants cannot be economically competitive if relying only on “excess

electricity" from renewable energy sources. This is the reason why all the reported economic analysis are carried out assuming high capacity factors, ranging from 82% to 94%, and the same capacity factor for the electrolysis system and the biomass gasification and biofuel synthesis processes.

- In the reported studies, different results have been obtained for the cost of the e-product. Hannula (2015) computed a higher cost of the products produced in PBtX plants than in the corresponding BtX plant. The resulting cost of the e-product is nearly twice as high as the cost of the corresponding bio-product. Higher differences (about four times higher e-product costs) have been obtained by Zhang et al. (2020) with a very different process, based on high temperature electrolysis and H_2O/CO_2 co-electrolysis. Albrecht et al. (2017) computed comparable costs for FT fuel via PBtX and BtX plants, resulting in a cost of the e-FT slightly higher or slightly lower than the bio-FT, depending on the revenues from the exported heat. From the data reported by Hillestad et al. (2018), a cost of the e-FT fuel 26% lower than the bio-FT has been computed, thanks to the optimistic investment cost of the SOEC unit and its high efficiency. From such contrasting results, it can be concluded that the economic competitiveness of a PBtX system is closely linked with the assumed cost of electrolysis and electricity (i.e. ultimately on the cost hydrogen), that will substantially depend on the evolution of the electrolysis technology and of the electricity market.
- It is interesting to compare the cost of the e-product of a PBtX plant with the cost of a PtX plant using CO_2 as carbon source. Hannula (2015) and Albrecht et al. (2017) performed a comparison with consistent assumptions, obtaining a lower cost of the e-product in the PBtX plant compared to the PtX plant. This can be attributed not only to higher PtX efficiency (Albrecht et al., 2017), but also to the lower marginal specific capital cost per unit of product of the PBtX plant compared to the capital cost of the PtX plant. For example, from the data in Albrecht et al. (2017), it is possible to compute a marginal specific capital cost for the production of the e-FT in the PBtX plant of 3580 €/kW_{prod}, as the ratio between the marginal cost of the PBtX system compared to the BtX one (355.8 M€) and the increased product output (99.4 MW_{LHV}) for the same biomass input. This cost is about 30% lower than the estimated specific capital cost for the production of e-FT in the PtX plants.

Table 1-1 - Summary of the selected recent literature on PBtX studies. Values in italics have been derived from the data in the papers. When not present in the reference, properties of fuel mixtures (e.g. LHV, density) are taken from JRC Technical Reports, 2014. When necessary, the 2019 conversion $/€ equal to 1.12 has been applied.

Reference	**Biomass input, gasification and syngas cleaning and conditioning technology**	**Electrolyser technology and power to LHV efficiency**	**Biofuel produced**	**Carbon efficiency**	**PtX efficiency**	**HtX efficiency**	**Main data for economic analysis**	**Cost of product**
(Hannula, 2015)	Biomass input: 100 MW, 50%wt moisture. O_2-blown fluidized bed gasification, syngas reforming, WGS reactor (bypassed in PBtX operation), CO_2 separation.	Alkaline η = 62%	M, SNG, G	BtX: *37.5%* (M) *32.2%* (G) *33.1%* (SNG) PBtX: *48.9%* (M) *42.1%* (G) *49.8%* (SNG)	*51.7%* (M) *44.6%* (G) *51.1%* (SNG)	*84.7%* (M) *73.1%* (G) *82.3%* (SNG)	Electrolysis cost: 589 €/kW (M) 571 €/kW (G) 565 €/kW (SNG) Electricity price: 50.4 €/MWh Capacity factor: 91% (8000 h/y) Biomass cost: 5 €/GJ TCI PBtX (per kW_{prod})[1]: 2320 €/kW (M) 3050 €/kW (G) 1925 €/kW (SNG) TCI BtX (per kW_{prod})[1]: 2335 €/kW (M) 3055 €/kW (G) 2000 €/kW (SNG)	PBtX: 24.4 €/GJ (M) 27.6 €/GJ (G) 22.7 €/GJ (SNG) BtX: 20.6 €/GJ (M) 22.6 €/GJ (G) 17.7 €/GJ (SNG) e-product: *36.9 €/GJ* (M) *44.0 €/GJ* (G) *32.6 €/GJ* (SNG)
(Hannula, 2015)	CO_2 as carbon source, direct CO_2 hydrogenation.	Alkaline η = 62%	M, SNG, G	PtX: *95.0%* (M) *81.7%* (G) *~100%* (SNG)	*51.5%* (M) *44.6%* (G) *51.1%* (SNG)	*84.4%* (M) *73.1%* (G) *82.3%* (SNG)	Electrolysis cost: 525 €/kW (M) 520 €/kW (G) 524 €/kW (SNG)	PtX: 40.0 €/GJ (M) 48.0 €/GJ (G) 36.8 €/GJ (SNG)

Reference	Biomass input, gasification and syngas cleaning and conditioning technology	Electrolyser technology and power to LHV efficiency	Biofuel produced	Carbon efficiency	PtX efficiency	HtX efficiency	Main data for economic analysis	Cost of product
							Electricity price: 50.4 €/MWh Capacity factor: 91% (8000 h/y) CO_2 cost: 40 €/t TCI (per kW_{prod})[1]: 1885 €/kW (M) 2615 €/kW (G) 1815 €/kW (SNG)	
(Hannula, 2016)	Biomass input: 100 MW, 50%wt moisture. O_2-blown fluidized bed gasification, syngas reforming. WGS reactor and CO_2 separation only in BtX configuration.	Alkaline, η = 67%	G, SNG	BtX: 30.5% (G) 32.5% (SNG) PBtX: 79.4% (G) 98.0% (SNG)	*48.4%* (G) *55.1%* (SNG)	*72.2%* (G) *82.3%* (SNG)	Electrolysis cost: 1000 €/kW Breakeven electricity price[2]: 35.4 €/MWh (G) 27.7 €/MWh (SNG) Capacity factor: 91% (8000 h/y) Biomass cost: 5 €/GJ TCI (per kW_{prod}): 2030 €/kW (G) 925 €/kW (SNG)	PBtX: 31.3 €/GJ (G) 21.4 €/GJ (SNG) BtX: 31.3 €/GJ (G) 21.4 €/GJ (SNG)
(Hannula, 2016)	Biomass input: 100 MW, 50%wt moisture.	Alkaline, η = 67%	G, SNG	BtX: 28.8% (G) 31.4% (SNG)	*49.7%* (G) *55.0%* (SNG)	*74.2%* (G) *82.1%* (SNG)	Electrolysis cost: 1000 €/kW	PBtX: 30.4 €/GJ (G) 20.4 €/GJ (SNG)

Reference	Biomass input, gasification and syngas cleaning and conditioning technology	Electrolyser technology and power to LHV efficiency	Biofuel produced	Carbon efficiency	PtX efficiency	HtX efficiency	Main data for economic analysis	Cost of product
	Indirect dual fluidized bed steam gasification, syngas reforming. WGS reactor and CO_2 separation only in BtX configuration.			PBtX: 58.4% (G) 67.0% (SNG)			Breakeven electricity price[2]: 33.9 €/MWh (G) 25.1 €/MWh (SNG) Capacity factor: 91% (8000 h/y) Biomass cost: 5 €/GJ TCI (per kW_{prod}): 2551 €/kW (G) 1287 €/kW (SNG)	BtX: 30.4 €/GJ (G) 20.4 €/GJ (SNG)
(Albrecht et al., 2017)	Biomass input: 98.3 MW, 10%wt moisture. Pyrolysis + entrained flow O_2-blown gasification, WGS and CO_2 separation (BtX) or rWGS (PBtX).	PEM η = 69.2%	FT	BtX: 24.9% PBtX: 97.7%	*58.2%*	*83.1%*	Electrolysis cost: 942 €/kW Electricity price: 105 €/MWh Capacity factor: 94% (8260 h/y) Biomass cost: 5.4 €/GJ TCI (per kW_{prod}): 5559 €/kW (PBtX) 11071 €/kW (BtX)	PBtX: 67.2 €/GJ[3] 70.0 €/GJ BtX: 64.1 €/GJ[3] 73.1 €/GJ e-product: *68.3 €/GJ*[3] *68.9 €/GJ*
(Albrecht et al., 2017)	CO_2 as carbon source. rWGS.	PEM η = 69.2%	FT	PtX: 98%	*50.6%*	*73.1%*	Electrolysis cost: 942 €/kW Electricity price: 105 €/MWh	PtX (small): 85.9 €/GJ[3] 89.1 €/GJ PtX (large):

Reference	Biomass input, gasification and syngas cleaning and conditioning technology	Electrolyser technology and power to LHV efficiency	Biofuel produced	Carbon efficiency	PtX efficiency	HtX efficiency	Main data for economic analysis	Cost of product
							Capacity factor: 94% (8260 h/y) CO_2 cost: 37.75 €/t TCI (per kW_{prod})[4]: 5364 €/kW (small) 4963 €/kW (large)	82.5 €/GJ[3] 85.6 €/GJ
(Hillestad et al., 2018)	Biomass input: 435 MW, 40%wt moisture. Torrefaction+ entrained flow O_2-blown gasification, rWGS, CO_2 separation.	SOEC η = 95.3%	FT	BtX: 37.8% PBtX: 91.3%	*78.6%*	*82.4%*	Electrolysis cost: 892.9 €/kW Electricity price: 44.6 €/MWh Electrolysis CF: 89% (7800 h/y) Biomass cost: 3.6 €/GJ TCI (per kW_{prod}): *4212 €/kW* (PBtX) *6430 €/kW* (BtX)	PBtX: *45 €/GJ* BtX: *61.7 €/GJ* e-product: *33.2 €/GJ*
(Zhang et al., 2020)	Biomass input: 60 MW, 4.8%wt moisture. Entrained flow O_2-blown gasification.	SOEC η = N/A	SNG, M, DME, JF	BtX: *27.7%* (SNG) *35.6%* (M) *36.1%* (DME) PBtX: *85.4%* (SNG) *85.9%* (M)	*75.3%* (SNG) *79.8%* (M) *81.8%* (DME) *68.3%* (JF)	N/A	Electrolysis cost: N/A Electricity price: 61.9 €/MWh Capacity factor: 82% (7200 h/y) Biomass cost: 5.1 €/GJ	PBtX: 20.3 €/GJ (SNG) 22.0 €/GJ (M) 23.7 €/GJ (DME) 33.1 €/GJ (JF) BtX: 8.5 €/GJ (SNG)

Reference	Biomass input, gasification and syngas cleaning and conditioning technology	Electrolyser technology and power to LHV efficiency	Biofuel produced	Carbon efficiency	PtX efficiency	HtX efficiency	Main data for economic analysis	Cost of product
				86.3% (DME)			TCI PBtX (per kW_{prod}): 1871 €/kW (SNG) 1747 €/kW (M) 1962 €/kW (DME) 3288 €/kW (JF)	11.0 €/GJ (M) 13.6 €/GJ (DME) 11.0 €/GJ (JF) e-product: *39.9 €/GJ* (SNG) *44.6 €/GJ* (M) *44.1 €/GJ* (DME)
(Zhang et al., 2020)	Biomass input: 60 MW, 4.8%wt moisture. Entrained flow O_2-blown gasification, WGS, CO_2 separation and conversion in SOEC.	SOEC with H_2O/CO_2 co-electrolysis. η = -	SNG, M, DME, JF	BtX: *27.7%* (SNG) *35.6%* (M) *36.1%* (DME) PBtX: *86.7%* (SNG) *85.0%* (M) *66.6%* (DME)	75.3% (SNG) 76.6% (M) 48.5% (DME)[5] 63.4% (JF)	N/A	Electrolysis cost: N/A Electricity price: 61.9 €/MWh Capacity factor: 82% (7200 h/y) Biomass cost: 5.1 €/GJ TCI (per kW_{prod}): N/A	PBtX: 22.0 €/GJ (SNG) 23.7 €/GJ (M) 31.4 €/GJ (DME) 38.1 €/GJ (JF) BtX: 8.5 €/GJ (SNG) 11.0 €/GJ (M) 13.6 €/GJ (DME) 11.0 €/GJ (JF) e-product: *45.4 €/GJ* (SNG) *53.1 €/GJ* (M) *140.7 €/GJ* (DME)

[1] Economic analysis performed on plants with the same product output of 200 MW_{LHV}.
[2] Breakeven electricity price to obtain the same cost of product of the baseline BtX plant.

[3] Revenues from heat export are taken into account.
[4] Two PtX systems are assessed with fuel output comparable to the corresponding BtX (small) and PBtX (large) plants.
[5] Low efficiency, due to additional heat demand.

Recent papers investigated new strategies to improve the techno-economic performance of PBtX plants.

Nielsen et al. (2022) studied the possibility to enhance the efficiency of FT liquid production plants integrated with SOEC. In the analysis, the authors examined the efficiency gains of the PBtX process as a result of redirecting the tail gas of the FT reactor to the anode of a SOEC as fuel input. The novel plant configuration is compared with the PBtX process where the tail gas is fed back to the gasifier. By means of supplying fuel to the SOEC, the electrical work input for the steam electrolysis can be lowered and fuel efficiencies between 74-90% can be reached with a remarkable improve from 66% of the benchmark PBtX process.

Putta et al. (2022) explored the optimal electrical energy input distribution between the gasifier and the electrolyser in PBtX processes producing FT liquids. The paper is based on the assumption that the addition of energy to a BtX process either in form of hydrogen by means of electrolysis or directly to the gasifier through electric heaters allows to improve the carbon efficiency. The authors proved that it is always beneficial to add part of the total energy added to the process to the gasifier with an optimal energy addition to the gasifier of 38.4% of the energy in the biomass feed.

Butera et al. (2020) and Butera et al. (2021) offered a potential solution to maximise the capacity factor of PBtX processes. The analysed plant integrates methanol production from biomass gasification with solid oxide cells which are operated in different modes, thus adapting the operation to fluctuating electricity prices. The plant operation can shift from methanol production at low electricity prices, by employing the solid oxide cells in electrolysis mode, to methanol and electricity co-production, and to electricity production at high prices, in fuel cell mode. The heat of the endothermic gasification reactions is provided by means of electric heating or partial oxidation in the gasifier. The novel flexible methanol production plant is then compared with two non-flexible single-mode PBtX plants from a techno-economic perspective. The flexible PBtX process shows to be the least cost-competitive case due to the highest investment cost. The flexible unit becomes the most competitive solution when imposing constraints on the use of electricity produced from fossil fuels to produce methanol, since it ensures higher capacity factors and methanol yields.

Predicting the potential deployment of power-to-X pathways requires to understand the features of future energy markets, hence the evolution of electricity prices, which will be highly influenced by the penetration of intermittent renewables and on the geographic location (Seel et al., 2018). The spread of technologies for the electrification of new sectors such as the transport sector and the production of heat for civil and industrial uses will impact on the demand side, affecting the electricity price distribution. In this respect, the techno-economic assessment of PtX and PBtX routes needs to jointly account for both these aspects.

McDonagh et al. (McDonagh et al., 2019) analysed the costs of SNG from a power-to-SNG system integrated in simulated Irish electricity markets with increased penetration of renewable energy sources. Their model investigated the interplay between the simulated electricity market price and the bid price on the run hours and the average electricity price, that are the most influencing factors of the produced e-SNG. Sorknæs et al. (Sorknæs et al., 2020) addressed the problem of re-designing the Danish electricity market under the assumption of a 100% renewable energy system, considering the mutual influence of renewable-based heating, gas, liquid fuels and electricity markets as an interdependent energy system. The study highlighted the significant influence that the demand side could have on the electricity price duration curve. A similar conclusion was obtained by Ruhnau

(Ruhnau, 2020), who assessed the effect of flexible electrolysis systems on stabilizing the value of solar and wind power generation.

Similarly, the economic performance of PBtX and e-fuel production plants is highly dependent on energy market conditions. Notwithstanding the inherent complexity that would be introduced by the uncertainty in electricity penetration and prices of future electrified markets (e.g., scale of electric mobility, diffusion of electrolysers, heat electrification for domestic and industrial use), the comprehensive system modelling of electricity supply and demand at electrofuels production plants is key to estimate their role and needs to be addressed further in future research.

1.3.3 Biomass-to-X plants with CCS

As previously detailed, BtX plants coupled with CCS are recently receiving attention due to the possibility of providing negative emissions by capturing and storing the CO_2 which is produced within the conversion process (i.e. bioenergy with carbon capture and storage -BECCS-). Moreover, when the final product is hydrogen the negative emission potential can be maximised while producing a high added value product which offers opportunities for the decarbonisation of a wide range of sectors (e.g. long-haul transport, chemicals, iron, and steel). For this reason, biomass-to-hydrogen (BtH_2) plants with carbon capture and storage are included in broader spectrum and scenarios analyses as a key option to meet CO_2 emissions reduction objectives.

Baker et al. (2020) investigated several BECCS pathways which may allow California to reach the target of carbon neutrality by 2045. The BtH_2 pathway via biomass gasification shows the lowest CO_2 removal cost (25-57 €/t_{CO2}) among all the analysed technologies (e.g. direct air capture, biogas-to-electricity, fast pyrolysis, etc.). The cost significantly depends on the type and on the origin of the inlet biomass. BtH_2 plants guarantee high capture rate, as up to 95% of the carbon contained in the feedstock can be captured.

Bui et al. (2020) analysed the potential to meet negative emissions targets of a series of BECCS plants, among which there are more mature technologies such as biomass-fired power plants and biomass-fuelled combined heat and power plants, and less mature ones as BtH_2 plants. The report showed that BtH_2 can play a major role in meeting CO_2 removal targets and that it is more cost-effective to deploy BtH_2 plants alongside more mature BECCS technologies (e.g. biomass-fuelled combined heat and power plants).

Hannula and Reiner (2019) examined the potential of carbon-neutral synthetic fuels (i.e. biofuel via gasification, and electrofuels from CO_2 and water using electricity) in decarbonizing the road transport. Synthetic fuel plants are expected to have advantages in long-haul light duty and/or heavy duty options where battery charging electric vehicles are less competitive. According to the International Energy Agency (IEA), 26 EJ/year of biofuels would be consumed globally in the transportation sector in 2050 (International Energy Agency, 2017). BECCS plants may cover that consumption in the most effective way, ensuring higher emission savings than biofuel plants without CCS and electrofuels. BECCS plants not only can produce negative emissions, but are also less sensitive to power sector emissions and they are not dependent on the scarce low-carbon electricity which may limit the deployment of several technologies in future.

The most significant techno-economic analyses in the scientific literature about BtH_2 plants are summarised in Table 1-2. The reported studies are mainly focused on large plants

(i.e. 100-1700 MW of biomass input) where, in some cases, biomass is co-fed with coal, and consider different gasification technologies, such as oxygen-blown fluidized bed, indirect dual fluidized bed, and entrained flow oxygen-blown gasification.

Larson et al. (2009) investigated large-scale gasification-based systems for producing different biofuels, namely Fischer-Tropsch (F-T) fuels, dimethyl ether (DME) and hydrogen. In the hydrogen production plant, biomass is gasified in an oxygen-blown fluidized bed reactor for producing syngas. Two sour shift reactors and CO_2 separation with Rectisol allow to maximise the production of hydrogen in the downstream pressure swing adsorption (PSA) system. The biomass-to-hydrogen process proves to be the most fuel efficient among all the analysed cases (about 59%). From an economic perspective, the costs of production are relatively low, favoured by the large size of the plants (i.e. 13.6 €/GJ for 893 MW of biomass input). The cost of producing hydrogen is the lowest (per GJ) among all the fuels examined in the article. The possibility of adding CCS to the plant is not investigated.

Salkuyeh et al. (2018) performed a techno-economic analysis of BtH_2 plants with and without CCS employing two different gasification technologies, namely dual fluidized bed indirect steam gasification and oxygen-blown entrained flow gasification. The entrained flow reactor allows to avoid the downstream syngas reforming and tar removal, but it increases the plant complexity and capital cost. The syngas conditioning section is composed by high-temperature and low-temperature water-gas shift (WGS) reactors in series, placed downstream sulphur cleaning, and by MDEA-based scrubbing as CO_2 removal unit. Hydrogen is produced through PSA. When CCS is included, the oxy-combustion of PSA tail gas is carried out. When CCS is included, steam and electricity produced by exploiting PSA tail gas are not sufficient to satisfy the internal demand, therefore additional natural gas is burned (3-8% of biomass input power) in order to increase steam and electricity production. The entrained flow gasification-based plant with CCS can capture almost all the CO_2 produced during the process. Conversely, the dual fluidized bed option captures only 60% of the produced CO_2 since only the CO_2 contained in the syngas is captured and the CO_2 from the combustor is emitted. The entrained flow gasification-based plant allows to achieve a higher fuel efficiency compared to the fluidised bed option (47.5% vs. 37.6%). It is important to highlight that the obtained fuel efficiencies are significantly lower than reported in other articles for similar gasification technologies. The reason of such low efficiencies cannot be derived from the information in the article. Although the two plant configurations with CCS share the same hydrogen production cost, the integration of CCS is less costly in the case of entrained flow gasification-based plant (6.6 €/t_{CO2} vs. 9.1 €/t_{CO2}).

Antonini et al. (2021) conducted a techno-environmental analysis of BtH_2 plants based on three different gasification technologies, namely indirect dual fluidized bed steam gasification (heat pipe reformer), sorption-enhanced oxygen-blown gasification and oxygen-blown entrained flow gasification. The heat pipe reforming and sorption-enhanced gasification-based plants share similar units downstream the gasification section, that include steam methane reforming, externally heated by combustion of PSA tail gas, and high-temperature WGS reactor. The entrained-flow gasification-based plant, instead, does not need syngas reforming, but it includes a low-temperature WGS reactor, downstream the high-temperature one, in order to convert the high amount of CO contained in the syngas. In all the configurations, CO_2 is removed through MDEA scrubbing and hydrogen is produced in a PSA unit. The biofuel plants are studied with and without CCS. When CCS is not included, the MDEA scrubbing unit is not present. Oxy-combustion within the combustor of the dual fluidized bed sorption-enhanced gasification-based plant guarantees additional

CO_2 capture. Sorption-enhanced and heat pipe reformer gasification-based plants are more fuel efficient than the entrained flow option, which requires more biomass per unit of hydrogen produced due to biomass energy loss in the pre-treatment process and less efficient gasification process. On the contrary, the entrained-flow gasification-based plant can achieve the highest CO_2 capture rate (i.e. 98%), since steam methane reforming is not needed and related emissions from tail gas combustion are avoided. The sorption-enhanced configuration can reach up to 92% of CO_2 captured by combining MDEA scrubbing with the oxy-combustion within the gasification section. The heat pipe reforming gasification option only achieves 60% of CO_2 capture rate, since a post-combustion CO_2 removal technology is not employed for the flue gas exiting the gasification section.

Arnaiz del Pozo et al. (2021) investigated the techno-economic potential of hydrogen production from large-scale coal/biomass (biomass 30%$_{wt}$) co-gasification plants with CO_2 capture. A benchmark plant is compared with other three plant configurations. The benchmark plant includes oxygen-blown entrained flow gasification, two sour-shift reactors, CO_2 removal with Selexol, PSA for hydrogen purification and a steam cycle. All the other plant configurations include entrained flow oxygen-blown gasification, high-temperature WGS reactor and membrane-assisted WGS, which replaces the Selexol absorption and the PSA unit. The first configuration produces power through oxy-combustion of the membrane-assisted WGS retentate to generate additional steam for the steam turbine. The second plant configuration introduces a more efficient entrained-flow gasification with slurry vaporization and power generation with a gas turbine fuelled by the purge stream of the CO_2 cryogenic purification unit. The third configuration removes the power cycle, allowing for electricity imports, and performing oxy-combustion of the retentate in order to increase steam production and therefore hydrogen production. All the proposed configurations are proven to be more fuel efficient than the benchmark (62.9-73% vs. 59.3%) and with a higher or very close CO_2 capture rate (91.7-100% vs. 93.8%). The relatively low hydrogen production cost achieved in all the plants of the study arises from the low cost of coal feedstock and the benefits of the economies of scale given by large hydrogen production capacities (13.3-15.7 €/GJ).

Hannula and Melin (2021) provided a techno-economic assessment of several biomass-to-X pathways, among which BtH_2 plant without and with CCS is studied. The plant without CCS includes oxygen-blown fluidized bed gasification, syngas reforming, two sour shift reactors, Rectisol-based CO_2 separation, PSA and a steam cycle. Compression of CO_2 is included when CCS is added, as separation of CO_2 is already present in the base case. A plant configuration where the CO_2 capture rate is maximised (CCS_{max}) is included in the analysis and it consists in capturing with MEA scrubbing the CO_2 contained in the flue gas produced by the combustion of the PSA tail gas and char in an auxiliary boiler. The plant with CCS reaches a CO_2 capture rate of about 90%. By adding MEA scrubbing, the capture rate is maximised up to 96.5%. The economic analysis is based on a First-of-a-kind (FOAK) plant assumption. The total capital investment of the biofuel demonstration plant GoBiGas is scaled up from 30 MW_{LHV} to 103 MW_{LHV} of biomass input. CCS components (i.e. CO_2 compression and post-combustion CO_2 capture) are added on top of the total capital investment. This analysis leads to a higher cost compared to other studies in the scientific literature. The integration of CCS starting from the base case costs about 20 €/t_{CO2}. A cost of 92 €/ t_{CO2} is required in order to maximise the CO_2 capture rate through the addition of MEA scrubbing.

Table 1-2 – Summary of the selected recent literature on biomass-to-hydrogen plants. All the cost data are converted to 2019€. When not specified in the original paper, the currency year is assigned as: (year of publication – 1).

Reference	**Biomass input, Gasification and syngas cleaning and conditioning technology**	**CO_2 capture efficiency**	**PSA H_2 recovery**	**Fuel efficiency**	**CO_2 capture rate**	**Main data for economic analysis**	**Cost of product**
(Larson et al., 2009)	Biomass input: 893 MW, 20%wt moisture. O_2-blown fluidized bed gasification, thermal/catalytic cracking, two sour shift reactors, Rectisol, PSA, steam cycle.	~100%	95%	58.9%	-	Biomass cost: 4.0 €/GJ TCI no CCS (per kW_{prod})[1]: 1018 €/kW TCI CCS (per kW_{prod})[1]: -	<u>No CCS:</u> 13.6 €/GJ <u>CCS:</u> -
(Salkuyeh et al., 2018)	Biomass input: 1677 MW, 5.8%wt moisture. Indirect dual fluidized bed steam gasification, syngas reforming, high-T and low-T WGS reactors, MDEA, PSA, steam cycle (boiler fed with oxygen and additional natural gas -CCS- or with air -no CCS-).	N/A	N/A	37.6%	60%	Biomass cost: 4.6 €/GJ TCI no CCS (per kW_{prod}): 982 €/kW TCI CCS (per kW_{prod}): 1293 €/kW	<u>No CCS:</u> 24.7 €/GJ <u>CCS:</u> 27.9 €/GJ CO_2 avoidance marginal cost: 9.1 €/t_{CO2}
(Salkuyeh et al., 2018)	Biomass input: 1327 MW, 5.8%wt moisture. Entrained flow O_2-blown gasification, high-T and low-T WGS reactors, MDEA, PSA, steam cycle (boiler fed with oxygen and additional natural gas -CCS- or with air -no CCS-).	N/A	N/A	47.5%	~100%	Biomass cost: 4.6 €/GJ TCI no CCS (per kW_{prod}): 1845 €/kW TCI CCS (per kW_{prod}): 2033 €/kW	<u>No CCS:</u> 27.1 €/GJ <u>CCS:</u> 27.9 €/GJ CO_2 avoidance marginal cost: 6.6 €/t_{CO2}
(Antonini et al., 2021)	Indirect dual fluidized bed steam gasification (heat pipe reformer), syngas reforming, high-T WGS reactor, MDEA (if CCS), PSA, steam cycle.	98%	90%	58-65%	60%	N/A	N/A
(Antonini et al., 2021)	Sorption-enhanced O_2-blown gasification, syngas reforming, high-T WGS reactor, MDEA (if CCS), PSA, steam cycle.	98%	90%	60-82%	60% (oxy-comb) 92% (oxy-comb + MDEA)	N/A	N/A
(Antonini et al., 2021)	Entrained flow O_2-blown gasification, high-T and low-T WGS reactors, MDEA (if CCS), PSA, steam cycle.	98%	90%	~55%	98%	N/A	N/A

Reference	Biomass input, Gasification and syngas cleaning and conditioning technology	CO_2 capture efficiency	PSA H_2 recovery	Fuel efficiency	CO_2 capture rate	Main data for economic analysis	Cost of product
(Arnaiz del Pozo et al., 2021)	Coal & Biomass input: 1255 MW, 30%wt biomass. Entrained flow O_2-blown gasification, two sour shift reactors, Selexol, PSA, steam cycle.	95%	90.5%	59.3%	93.8%	Biomass cost: 6.5 €/GJ Coal cost: 2.7 €/GJ TCI no CCS (per kWprod): - TCI CCS (per kWprod): ~1530 €/kW	No CCS: - CCS[2]: 15.7 €/GJ
(Arnaiz del Pozo et al., 2021)	Coal & Biomass input: 1255 MW, 30%wt biomass. Entrained flow O_2-blown gasification, high-T WGS reactor, membrane-assisted WGS. 1. Steam cycle. 2. More efficient gasification + gas turbine. 3. No power cycle (electricity import) + more steam to increase H_2 production.	-	-	1. 62.9% 2. 67.5% 3. 73.0%	1. ~100% 2. 91.7% 3. ~100%	Biomass cost: 6.5 €/GJ Coal cost: 2.7 €/GJ TCI no CCS (per kW_{prod}): - TCI CCS (per kW_{prod}): 1. ~1370 €/kW 2. ~1250 €/kW 3. ~1140 €/kW	No CCS: - CCS[2]: 1. 14.3 €/GJ 2. 13.8 €/GJ 3. 13.3 €/GJ
(Hannula and Melin, 2021)	Biomass input: 103 MW, 15%wt moisture. O_2-blown fluidized bed gasification, syngas reforming, two sour shift reactors, Rectisol, PSA, steam cycle, MEA (if CCS_{max}).	97% (Rectisol) 90% (MEA)	86%	56.9%	89.9% (Rectisol) 96.5% (Rectisol+MEA)	Biomass cost: 2.8 €/GJ TCI no CCS (per kW_{prod}): 6633 €/kW TCI CCS (per kW_{prod}): 6679 €/kW TCI CCS_{max} (per kW_{prod}): 6847 €/kW	No CCS: 38.0 €/GJ CCS: 41.2 €/GJ CO_2 avoidance marginal cost: 20.3 €/t_{CO2} CCS_{max}: 42.2 €/GJ CO_2 avoidance marginal cost: 92.2 €/t_{CO2}

[1] The overnight capital cost is reported.

[2] CO_2 credit of 50 €/t is included.

1.3.4 Economic competitivity of the Biomass-to-X processes

When integrated into the broader energy system, BtX plants need to deal with the variable price of electricity, that varies on hourly time-scales due to the intermittent solar and wind power generation, and of CO_2, hydrogen and carbon-based products, that may vary on weekly-monthly time scales depending on the respective markets. Therefore, the expected time-dependent relative value of power, carbon-based products, hydrogen and sequestered CO_2 may lead to the development of multi-product plants, to be operated flexibly in order to produce the good(s) with the highest added value.

The scope of this section is to provide insights on how the market price of the different goods (electricity, hydrogen and carbon-based products) and of carbon removal credits may affect the best use of biomass and on the positioning of PBtX and BtX CCS plants among the different competing uses of biomass. To this aim, a simple economic model has been defined, computing the Internal Rate of Return (IRR) and the operating revenue of (i) biomass-to-power (BtP), (ii) biomass-to-methanol (BtM), (iii) power & biomass-to-methanol (PBtM) and (iv) biomass-to-hydrogen (BtH) plants. For each of the four plant archetypes, configurations without and with CO_2 capture and storage have been considered. The economic indicators have been computed for different values of electricity, methanol and hydrogen selling price and of the captured CO_2. It has to be noted, that methanol has been selected as representative of a carbon-based product. The general qualitative conclusions obtained for methanol can be easily extended to other products.

The levelized annual cash flow CF_y (eq. (1-4)) is computed as the sum of the discounted annual investment, the operating costs (biomass feedstock, electricity and O&M) and revenues (selling of methanol, hydrogen, electricity, CO_2 emission allowance). The first term is calculated from the total $CAPEX$ by means of a Capital Recovery Factor (CRF) defined in eq. (1-5), that includes a constant discount rate (Weighted Annual Capital Cost, $WACC$) during the lifetime of the plant (LT). Revenues are proportional to the plant biomass input (B_{in}), the equivalent operating hours (h_{eq}), the specific yields of product ξ_i and its unitary price p_i. Under these assumptions, the IRR is computed as the breakeven $WACC$ value that gives a null net cash flow.

$$CF_y = B_{in} \cdot h_{eq} \cdot \sum \xi_i \cdot p_i - CAPEX \cdot CRF - OPEX \tag{1-4}$$

$$CRF = \sum_1^{LT} \frac{1}{(1+WACC)^i} = \frac{WACC \cdot (1+WACC)^{LT}}{(1+WACC)^{LT} - 1} \tag{1-5}$$

The lifetime of all the plants is assumed equal to 20 years and the capacity factor equal to 90% (i.e. about 8000 equivalent operating hours). All the costs are scaled to a reference biomass input of 300 MW_{LHV} (LHV 15.4 MJ/kg, carbon content 38%$_{wt}$, reference cost 18 €/MWh).

More specifically, the following technologies have been considered, with the assumptions summarized in Table 1-3:

i. Methanol synthesis via BtM plant based on oxygen-blown gasification and via PBtM plant involving additional hydrogen from low temperature electrolysis. Costs and efficiencies are taken from Hannula, (2015).

ii. Power production from biomass with and without CCS, considering a supercritical boiler and amine-based CO_2 capture. Costs and efficiencies are taken from Fajardy et al., (2021).

iii. Hydrogen production via oxygen-blown gasification and PSA separation. Costs and yields are taken from Bui et al., (2020) and Antonini et al., (2021).

iv. BtM and BtH plants with CCS considering a CO_2 compression station added to the existing CO_2 separation unit. Electricity consumption and additional costs for CO_2 compression are taken from IEAGHG, (2017). A cost of 10 €/t_{CO2} has also been assumed for CO_2 transport and storage, which is in the lower range of the expected costs for onshore geologic CO_2 storage (IEA, 2020).

It is important to highlight that values used in this analysis have been taken from different sources and a reliable quantitative comparison would require a careful data harmonization, especially in the method for determining the $CAPEX$, that has intrinsically high uncertainty and high impact on the cost of the products. Also, other features that may affect significantly the economics of a plant are not taken into account in this analysis, such as the revenues from operations in the secondary electricity market, that would increase the region of competitivity of BtP and PBtX plants, or the additional revenues from CHP configurations, that would favour BtP processes. Therefore, although based on quantitative values, this simplified analysis is intended to provide qualitative conclusions.

Figure 1-2 shows a map of the areas of the best plant from the point of view of IRR (left) and operating revenues (i.e. revenues minus $OPEX$, on the right) as function of the electricity price and of the value of the stored CO_2, for different methanol (MeOH) and hydrogen (H_2) prices.

Looking at the IRR maps, with methanol and hydrogen prices similar to the current ones (a), with intermediate electricity prices and low CO_2 value, the BtM system results the most competitive option, although with modest economic competitiveness, as the IRR is relatively low. Power production is favored at high electricity prices. BtM with CCS is the most profitable option if the CO_2 value rises above 20 €/t_{CO2}. PBtM system is the most competitive process for low electricity prices (below 25 €/MWh), unless the value of CO_2 rises above 30-50 €/t_{CO2}, making CO_2 sequestration more profitable than CO_2 conversion into e-methanol.

Increasing the value of methanol to 600 €/t (c), leads to improved economics for all the methanol production plants. The competitiveness of PBtM process expands towards the BtM region. BtP process remains competitive only for very high electricity prices (>150 €/MWh). BtH processes becomes competitive with high hydrogen price (e) and is favoured by high value of CO_2 when CCS is included.

Looking at the operating revenues maps (Figure 1-2, on the right), some differences emerge in the areas of convenience compared to the IRR maps. The area of convenience of the PBtM plant expands in the first two scenarios (b-d) compared to the IRR indicator (a-c). This means that it is economically competitive to run a PBtM plant for higher electricity prices (e.g. approaching 50 €/MWh when MeOH price is 600 €/t), but lower average electricity prices are needed to make PBtM the most profitable option from the IRR perspective and generate sufficient revenues to pay back the higher capital investment compared to the BtM cases. In the third scenario (f), the BtH area enlarges significantly when looking at the operating revenues. Similarly to the previous comment, this reflects the

behaviour of a case with higher operating revenues but higher capital costs than the other technologies at the boundaries.

The operating revenues charts also show that flexible plants may take advantage from the variable market prices over time. For example, depending on the electricity price (that varies on daily and seasonal time scales), on the hydrogen price (that in the future may fluctuate on a seasonal basis, depending on the availability of green hydrogen), on the CO_2 value (with expected variations on multi-year time scales) and the methanol price variability (dependent on the evolution of the demand), a flexible plant could switch its operating mode from BtM (without or with CCS), PBtM and BtH.

Figure 1-2 – IRR (a, c, e) and operation revenue (b, d, f) maps for BtM, PBtM, BtP and BtH plants with and without CCS. Lines identify the boundary of the regions of the most profitable options for different values of electricity, CO_2, methanol, and hydrogen.

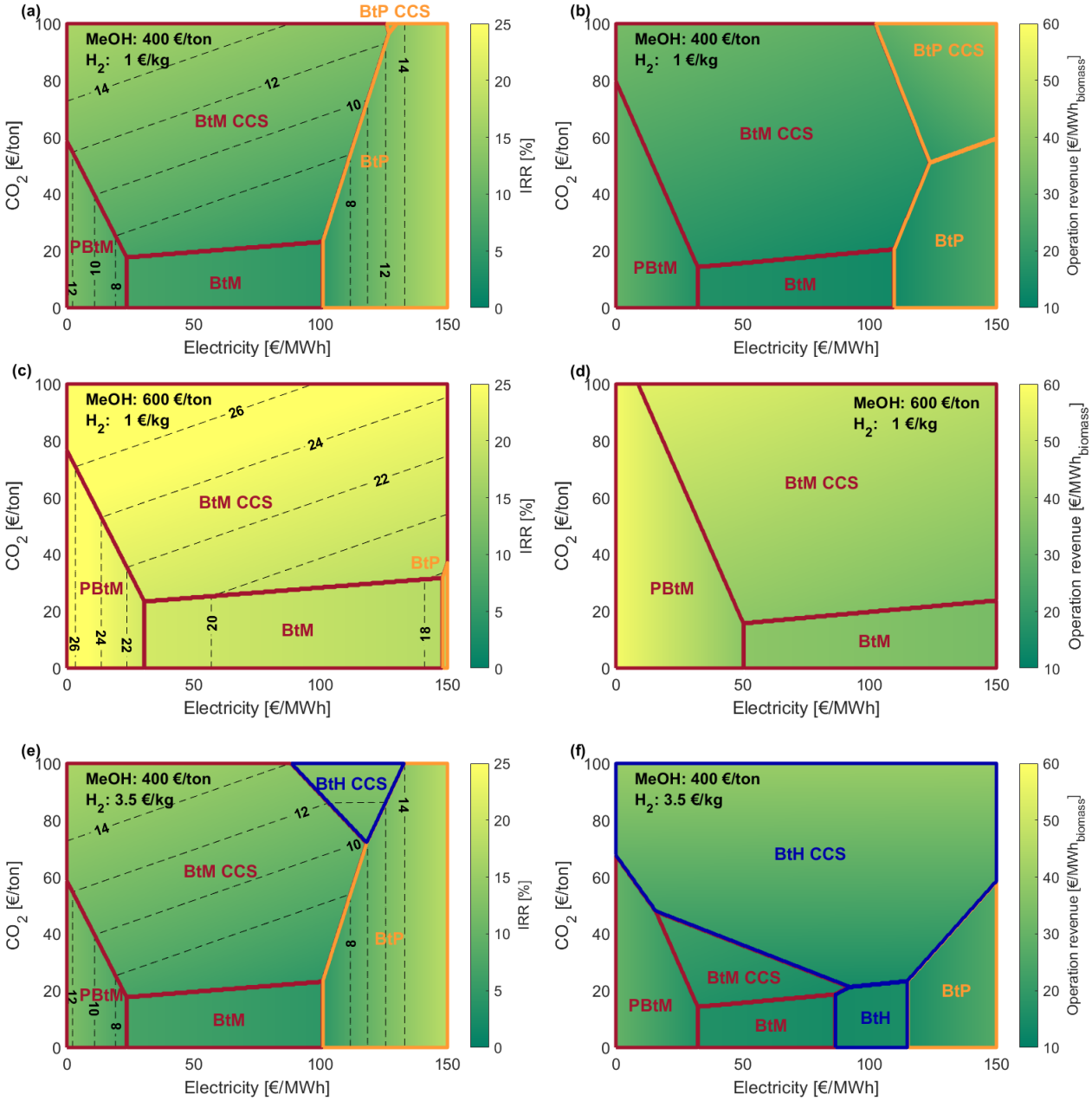

Table 1-3 - Assumptions for the economic analysis

	Yields				CAPEX	OPEX*	Carbon in products	Carbon stored	Carbon vent
	Electricity	**Methanol**	**Stored CO_2**	**Hydrogen**	**CAPEX**	**OPEX***	**Carbon in products**	**Carbon stored**	**Carbon vent**
	kWh_e/MWh_b	***kg/MWh_b***	***kg/MWh_b***	***kg/MWh_b***	***€$_{2017}$/kW_b***	***€/kW_b/y***	***$\%_w$ inlet C***	***$\%_w$ inlet C***	***$\%_w$ inlet C***
BtM	-40	108	-	-	1452	58.1	45.2	-	54.8
PBtM	-407	141	-	-	1725	69.0	59.0	-	41.0
BtM CCS	-54	108	174	-	1512	60.5	45.2	52.8	2.0
BtP	321	-	-	-	1118	29.1	-	-	100.0
BtP CCS	225	-	297	-	1891	31.6	-	90.0	10.0
BtH	27	-	-	14	2011	139.6	-	-	100.0
BtH CCS	2	-	323	14	2124	147.4	-	98.0	2.0

* In addition to reported plant OPEX, 10 €/t_{CO2} are included for CO_2 transport and storage costs in CCS cases.

1.4 Scope of the research work and contribution to knowledge

The evolution of the power, CO_2, H_2 and carbon-based product markets will increase the competition between different uses of biomass. In a carbon constrained world with high penetration of intermittent renewables, key drivers for the optimal exploitation of biomass will be the achievement of high efficiency in biogenic carbon utilization, either as a high-value product or as sequestered CO_2, and the efficient utilization of its dispatchable renewable energy content.

Recent literature on PBtX processes have assessed the techno-economic performance of such systems, highlighting the importance of low-cost hydrogen supply and the economic competitivity with respect to power-to-X systems based on the conversion of CO_2 from other sources. Recent works on BtX with CCS have highlighted the opportunity to provide a high added value final product and to produce negative emission at the same time. From a simplified economic analysis, section 1.3.4 showed that additional value may be obtained from operating biomass-to-X plants flexibly, e.g. modifying the electric power consumption, the destination of the biogenic carbon or the type of bio-product over time, following the market and regulatory conditions.

On this regard, the following main research gaps may be highlighted:

- none of the assessed recent as on PBtX systems investigates the design of the process units of plants conceived to operate flexibly. The economic performance of the plants are computed by fixing the electricity price and assuming that the electrolysis system operates continuously, at the same capacity factor of the biomass conversion process. The effect on the capital and operating costs of plants conceived to operate flexibly is currently unexplored in the open literature.
- The expected capacity factor of the electrolysis system of a PBtX plant is closely linked with the expected electricity price curve, which will depend on factors such as the geographic location, the type of renewable energy sources, their penetration in the regional grid and the willingness to pay of other potential users of electricity connected to the grid. Therefore, to understand the potential of PBtX plants and the value of their flexibility for the energy system, the integrated modelling of plants connected to electric grids of the future should be pursued.
- In future carbon-constrained world, the best bioenergy conversion pathway (e.g. electricity, H_2, methanol, etc.) will depend on the relative value/price of the products and of CO_2, that vary over time with different time scales. Multi-product plants able to operate flexibly to produce the good with the highest added value are not investigated in the scientific literature and are worth exploring from a techno-economic perspective.

In light of this, the present research work aims at assessing the energy, environmental and economic performance of flexible PBtX plants and of BtX plants with CCS. The thesis investigates different types of gasification technologies, i.e. direct, indirect and sorption-enhanced gasification, and different final products, i.e. methanol and hydrogen. The main objectives of the work are:

- selection of the most appropriate gasification and fuel synthesis technology for the integration with water electrolysis and CCS;
- identification of flexibility requirements both for the gasification and the final product synthesis;
- setting the design criteria of the main components on the basis of the flexibility requirements;
- evaluate the economic viability of the processes under different market conditions (e.g. electricity price, final product market value, CO_2 reward).

The research work is based on modelling and on the development of techno-economic analysis of different plant configurations. The technical part which includes heat and mass balances is performed with the process simulator Aspen Plus®.

The thesis is structured as follows:

- Chapter 2: a description of the main plant units together with details on modelling, validation and design is provided;
- Chapter 3: the techno-economic analysis of flexible power and biomass-to-methanol plants is discussed. A first analysis explores the optimal equipment design and plant operating criteria, while a second analysis compares plants based on different gasification technologies.
- Chapter 4: the techno-economic analysis of biomass-to-methanol and biomass-to-hydrogen plants with CCS is described. Furthermore, multi-product plants operating flexibly to produce the good (methanol or hydrogen) that generates the highest revenues are investigated.
- Chapter 5: conclusions and possible developments of the work are proposed.

Chapter 2
Methods

In this chapter, a description of simulation process model and design of the main units of Biomass-to-X plants is provided. Moreover, the methodology and the assumptions for the economic analysis are reported. Assumptions and calculation methods are consistent with our previous works on biomass-to-X plants (Poluzzi et al., 2022a, 2022b, 2022c).

2.1 Modelling and design

The process model is developed in Aspen Plus®, which allows to compute the mass and energy balances of the integrated plant. The computations are conducted for a biomass input of 100 MW_{LHV}.

For the thermodynamic properties, different models are considered for the different plant sections to improve the accuracy of calculations for the different processes. The general model is the RKS-BM that is complemented with the SRK model in the methanol synthesis section, the NRTL model in the methanol purification section, the ELECNRTL model in the water scrubber and the IAPWS-95 model in the steam and hot water loops.

A description of the plant units and of the methods for the simulation is given in the next sections. Extensive tables with the main calculation assumptions are reported in Appendix A and Appendix B.

2.1.1 Biomass model and properties

The proximate and the ultimate analysis of the as-received biomass are assumed from literature (Pröll and Hofbauer, 2008b) and are reported in Table 2-1.

Table 2-1 – Properties of as-received biomass

Parameter	Value
LHV, MJ/kg_{AR}	9.74
Moisture, $\%_{wt}$	45
Proximate analysis, $\%_{wt,dry}$	
Fixed Carbon	18.84
Volatile matter	80.0
Ash	1.16
Ultimate analysis, $\%_{wt,dry}$	
Carbon	51.19
Hydrogen	6.08
Nitrogen	0.2

Parameter	Value
Chlorine	0.05
Sulfur	0.02
Oxygen	41.3
Ash	1.16

Biomass is included in Aspen simulation as a non-conventional component, which allows defining its properties (specific heat, density, heat of combustion) without the knowledge of the detailed chemical structure of the substance. The same approach is also used to define the ash properties.

In Aspen Plus® a model is available for coal and it is used also for biomass and ashes with parameters changed accordingly to the specific application. Aspen Plus® HCOALGEN model has been used, that requires the definition of the ultimate and proximate analysis. Several sub-models and correlations are available for coal properties calculation. The general ones are selected and summarized in Table 2-2.

For biomass, the heat of combustion is given, considering the relations between LHV and HHV at different humidity, as shown in eq. (2-1), (2-2) and (2-3), where y_d are weight fraction on dry basis, Δh_{eva} is equal to 2.442 MJ/kg of water and LHV and HHV are expressed on dry basis.

$$LHV_d = LHV_{AR} \cdot (1 + y_{d,m}) \tag{2-1}$$

$$LHV_d = HHV_d - \left(y_{d,m} + y_{d,H} \cdot \frac{M_{w,water}}{M_{w,H_2}}\right) \cdot \Delta h_{eva} \tag{2-2}$$

$$LHV_{d,y'_{d,m}} = LHV_{d,y_{d,m}} + \left(y_{d,m} - y'_{d,m}\right) \cdot \Delta h_{eva} \tag{2-3}$$

The specific heat capacity is expressed with a polynomial formulation as shown in eq. (2-4), where $c_{p,d}$ is given on dry basis, j is each component of ultimate analysis and y_j are weight fraction on dry basis.

$$c_{p,d} = \sum_j \left(a_{1,j} + a_{2,j}T + a_{3,j}T^2 + a_{4,j}T^3\right) \cdot y_j \tag{2-4}$$

The specific heat capacity of dry wood can be estimated through the correlation of eq. (2-5).

$$c^0_{p,d} = 0.003867 \cdot T + 0.1031 \tag{2-5}$$

Table 2-2 - Non-conventional components sub-models

	BIOMASS		ASH	
Property	**Aspen Option**	**Value**	**Aspen Option**	**Value**
Heat of combustion	6 (HCOMB)	HHV dry basis	1 (BOIEC)	Standard correlation
Standard heat of formation	1	From heat of combustion	1	From heat of combustion

	BIOMASS		ASH	
Heat capacity	1 (CP1C)	Fitted on correlation for biomass (TenWolde et al., 1998)	1 (CP1C)	Standard correlation
Enthalpy basis	1	Standard state at 298.15 K and 1 bar	1	Standard state at 298.15 K and 1 bar

The heat capacity model from (TenWolde et al., 1998) also takes into account the additional contribution of energy absorbed by the wood-water bonds, according to eq. (2-6), where $c_{p,d}^0$ is the specific heat of dry wood, $c_{p,water}$ is the specific heat of water (about 4.186 kJ/kg K) and A is a correction term (eq. (2-7)) with T in K.

$$c_{p,d} = \frac{c_{p,d}^0 + y_{hum} \cdot c_{p,water}}{1 + y_{hum}} + A \tag{2-6}$$

$$A = (0.02355 \cdot T - 1.326 \cdot y_{hum} - 6.191) \cdot y_{hum} \tag{2-7}$$

This correction is valid between 280 and 420 K; above this temperature (fibre saturation temperature), the simple law of mixture is valid (A = 0). Parameters $a_{i,j}$ are regressed on this correlation, obtaining the coefficients in Table 2-3. Error between simplified polynomial approach in eq. (2-4), required by Aspen implementation and the more accurate model given in eq. (2-6) is about 2% between 10% and 50% water content.

Table 2-3 - Coefficients for biomass specific heat

	$a_{1,j}$	$a_{2,j}$	$a_{3,j}$	$a_{4,j}$
Biomass	0.5712	0.00257	-	-
Moisture	-6.9561	0.03768	-	-

For the specific heat capacity of ashes, the standard Aspen ashes are assumed.

2.1.2 Biomass pre-treatment

The biomass pre-treatment is the same for all the plant configurations. Biomass pretreatment includes a belt drier (Amos, 1998; Fagernäs et al., 2010). Heated air flows through the biomass bed, providing the heat for water evaporation. Hot water is used to heat the drying air by means of a heat exchanger. Air is blown through a thin static layer of material on a horizontally moving permeable belt.

The dryer is designed to provide a biomass with a moisture content of 15%$_{wt}$. The low-temperature belt dryer described by STELA (2019) is adopted in the process model. A hot water loop with temperatures ranging between 90 and 30°C provides the necessary thermal power for the dryer, which has a specific heat demand of 1 MWh/t$_{H2O}$ evaporated, resulting in a duty of about 13 MW$_{th}$. The power consumption is set to 32 kWh/t of dry feedstock (Hannula, 2016).

2.1.3 Gasification technologies

The thesis investigates different types of gasification technologies, i.e. direct (DG), indirect (IG) and sorption-enhanced gasification (SEG).

The direct gasifier is a pressurized circulating fluidized bed (CFB) which is fed with a mixture of steam and oxygen (see Figure 2-1). The amount of steam which is fed to the CFB as gasifying agent is determined to achieve the target steam-to-carbon (S/C) ratio of 1 at the reformer inlet. The oxygen input is provided either from ASU or as a by-product from water electrolysis. The gasifier heat and mass balances are calculated with a lumped parameter model. Gasification process parameters and assumptions needed to define the syngas composition at the gasifier outlet (i.e. the advancement of the WGS reaction in the gasifier, the content of CH_4 and higher hydrocarbons, and the char conversion) are calibrated to reproduce the syngas composition from the Varkaus plant (Palonen, 2012) (see Table 2-4). The gasifier operates at 870°C and 4 bar. The higher operating temperature with respect to IG and SEG guarantees a higher carbon conversion and a lower amount of methane in the outlet syngas compared to IG and SEG solutions.

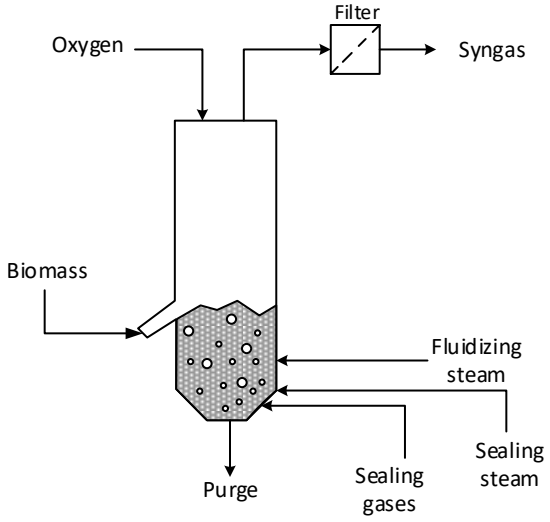

Figure 2-1 – Direct gasification process configuration.

The indirect gasifier is a dual fluidized bed, constituted by a bubbling fluidized bed (BFB) gasifier and a circulating fluidized bed (CFB) combustor (see Figure 2-2). Steam addition to the BFB as gasifying agent is determined to achieve the target S/C ratio of 1 at the reformer inlet. Steam is fed to the gasifier at 400°C. Similarly to the DG, the IG is calculated with a lumped parameter approach and the gasification process parameters needed to define the syngas composition at the gasifier outlet are calibrated to reproduce the syngas composition from the GoBiGas plant (Thunman et al., 2018) (see Table 2-4). The gasifier operates at 815°C and 1.4 bar.

Similar to the IG, the sorption-enhanced gasifier is a dual fluidized bed, constituted by a BFB gasifier/carbonator and a CFB combustor/calciner (see Figure 2-2). Low pressure steam is fed to the BFB reactor as gasifying agent to reach the target S/C of 1.5. The gasifier is modelled with a 0D model. Following the method proposed in Martínez et al. (2012), the

parameter $p_{\delta_{WGS}}$ is used to determine the approach to equilibrium of the water gas shift (WGS) reaction through eq. (2-8), where p_i is the partial pressure of the *i-th* species in the syngas and $K_p(T)$ is the WGS equilibrium constant from Fuchs et al. (2020).

$$p_{\delta_{WGS}} = log_{10}\left[\frac{\Pi_i p_i^{\nu_i}}{K_p(T)}\right] \tag{2-8}$$

The methane content in the syngas is given as a methane production per unit of dried biomass fed to the gasifier. The content of higher hydrocarbons, lumped with the molecule C_2H_4, is given as molar production per unit of produced methane.

Char conversion in the gasifier depends on the gasification temperature, through the expression derived from the data in Fuchs et al. (2020).

The uptake of carbon dioxide by CaO may be limited either by the chemical equilibrium or by the maximum conversion of CaO into $CaCO_3$. An approach to the equilibrium composition is considered, as indicated in Fuchs et al. (2020). The maximum conversion of CaO into $CaCO_3$ within the gasifier is calculated as function of the number of carbonation-calcination cycles, according to Grasa and Abanades (2006). In order to take account of kinetics limitation, the residence time and the distribution of the particles in the gasifier, a ratio between actual and maximum conversion of 0.75 is assumed for the sorbent. However, for all the investigated cases, CO_2 uptake resulted to be controlled by the thermodynamic limitation (i.e. by the CO_2 partial pressure) and to be never limited by the availability of active CaO in the circulating sorbent.

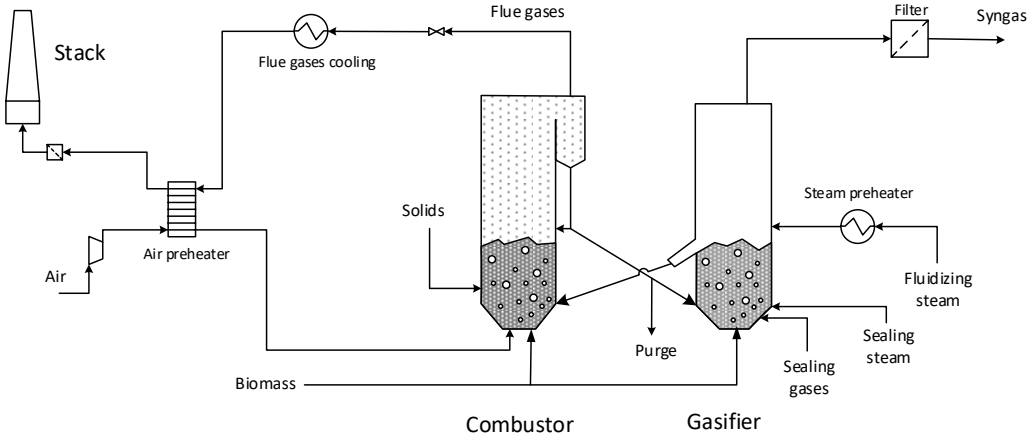

Figure 2-2 – Indirect and sorption-enhanced gasification process configuration. In IG configuration, solids are represented by olivine; in SEG configuration solids are represented by limestone.

The model is validated with data from literature (Pröll and Hofbauer, 2008a; Koppatz et al., 2009; Armbrust et al., 2014; Poboß, 2016; Alamia et al., 2017; Schmid et al., 2017; Fuchs et al., 2020) and with experimental campaigns conducted in the FLEDGED H2020 project framework at the University of Stuttgart (USTUTT) (Hafner et al., 2018, 2021; Hafner and Schmid, 2020) (see Figure 2-3, Figure 2-4 and Figure 3-2). The next section (2.1.4) contains further details on the SEG modelling.

Most assumptions hold both for the IG and the SEG options, since they are both dual fluidized bed systems. The gasifier model considers an almost complete separation of solids from gas. The solids entrained by gases out of the cyclones are assumed to be 0.01% of the circulating solids. The recirculated solids are fed to the combustor which performs the complete combustion of the unconverted char and of the additional biomass needed to achieve the target combustor temperature of 910°C. In the SEG combustor, complete calcination of $CaCO_3$ is achieved. In the combustor, the solids are assumed to be entrained by the gas with a certain solid mass flow per cross-section unit (G_S) at raiser outlet, by following the approach of Löffler et al. (2003). The outlet section of the combustor is designed to have a gas velocity of 5 m/s. The relation between entrained solids flow rate $\dot{m}_{es}$, G_S and gas velocity is given by eq. (2-9), where $\dot{m}_{gas}$ is gas mass flow rate, ρ_{gas} is gas density and v_{gas} the assumed gas velocity.

$$\dot{m}_{es} = G_S \cdot \frac{\dot{m}_{gas}}{\rho_{gas} \cdot v_{gas}} \tag{2-9}$$

The solids are separated by the outlet cyclone with a given efficiency which is specified to be 99.9% for calcium/olivine and 99% for ashes in order to take account of the different particle size distribution. The separated solids are partly sent to the gasifier and partly recirculated to the CFB combustor riser. A minimum solid purge from the bottom bed is required to avoid alkali and ashes collection in the reactor, therefore a mass flow rate equal to 1% of the inlet biomass is removed from the combustor. A makeup of limestone/olivine is added to the combustor to compensate the solids lost in the purge and from the cyclones. Combustion air is preheated by flue gases up to 270°C in design operation. The air flow rate is adjusted to obtain 3%$_{mol}$ of oxygen concentration in the flue gases. The connection between dual-fluidized bed system requires equal pressures in the two beds. Since the gasifier is operated above the atmospheric pressure to keep the whole syngas cooling and cleaning line at positive pressure, the combustor is also kept at pressure (~1.4 bar) through a backpressure valve before the stack.

In all the configurations, additional steam and air are also consumed with sealing purposes in biomass feeder, solid purge and filter cleaning. The content of other species in the syngas is estimated by assuming that all the sulphur in biomass is converted to H_2S, all chlorine to HCl and 10% of the nitrogen to NH_3.

The operating conditions are displayed in Table 3-3 (section 3.1.1) and in Table 3-14 (section 3.2.1).

Table 2-4 - Comparison of simulated syngas composition with literature data for direct and indirect gasification.

Syngas composition, %$_{mol}$ dry, N_2, Ar free	**Direct gasifier**		**Indirect gasifier**	
	This work	**Reference** (Palonen, 2012)	**This work**	**Reference** (Thunman et al., 2018)
CH_4	7.6	7.5	9.7	9.1
C_xH_y	3.4	3.0	2.6	2.4
CO	25.0	25.4	23.1	25.3
CO_2	29.6/29.8 [1]	32.8	19.9	21.0
H_2	34.1/34.3 [1]	31.3	44.7	42.2

[1] Outlet composition differences are related with the purity of the oxygen input stream. Oxygen stream purity is 100%$_{mol}$ from electrolysis and 95%$_{mol}$ from ASU.

2.1.4 Sorption-enhanced gasification model

As mentioned in the previous section, the SEG gasifier/carbonator is described by a 0D model implemented in Aspen Plus®, which performs mass balances and calculates the equilibrium of the chemical reactions (i.e. WGS and carbonation) at a given temperature. The resulting yield for each species is provided as input to a reactor model that calculates the energy balance. The calculator requires as input:

- composition and mass flow rate of the biomass;
- composition and mass flow rate of the recirculated solids from combustor/calciner;
- mass flow rate of other inlet flows (i.e. steam, additional oxygen, inerts);
- gasifier operating temperature;
- flow rate of fresh limestone fed to the system (F_0) in the combustor/calciner;
- steam-to-carbon molar ratio at gasifier inlet.

The model follows the following laws to compute the heat and mass balances of the gasifier/carbonator fed with woody biomass.

- Water Gas Shift reaction (WGS)

$$CO + H_2O \rightarrow CO_2 + H_2 \tag{2-10}$$

According to experimental evidence, this reaction it is not at equilibrium and the parameter $p_{\delta_{WGS}}$ is defined to indicate the approach to the equilibrium composition, following the approach proposed in Martínez et al. (2012), according to eq. (2-11).

$$p_{\delta_{WGS}} = log_{10}[\frac{\Pi_i p_i^{\nu_i}}{K_p(T)}] \tag{2-11}$$

$$K_p(T) = -2.4198 + 0.0003855\,T + \frac{2180.6}{T} \tag{2-12}$$

The numerator of equation (2-11) is related with partial pressure of species in the syngas, while the denominator is the equilibrium constant as function of temperature. The dependence on temperature of $p_{\delta_{WGS}}$ has been fitted on experimental data (Fuchs et al., 2020). The correlation in eq. (2-13) is used.

$$p_{\delta_{WGS}} = \begin{cases} 0.0092\,T - 6.5776, & T < 697°C \\ 1.661 \cdot 10^{-7}\,T^3 - 3.831029 \cdot 10^{-4} T^2 + 0.29533T - 76.1542, & T \geq 697°C \end{cases} \tag{2-13}$$

The solution of these equations gives a relation between CO, CO_2, H_2 and H_2O in the syngas.

- Methane content in the syngas is given as a methane production per unit of dry biomass fed to the gasifier (0.07 $kg_{CH4}/kg_{biom,dry}$). C_xH_y content is proportional to the methane content and is equal to 0.25 $kmol_{CxHy}/kmol_{CH4}$. These quantities are also fitted on experimental data from FLEDGED experimental campaigns. C_xH_y are simulated as equivalent to C_2H_4.
- The ratio between the unconverted char flowing from the gasifier to the combustor and the total biomass carbon content is expressed with the relation in eq.(2-14). Coefficients are fitted on data from literature (Fuchs et al., 2020).

$$X_{char} = 3.8124 \cdot 10^{-6} \cdot T^2 - 6.48735 \cdot 10^{-3} \cdot T + 3.0078924 \quad (2\text{-}14)$$

Char is assumed to be pure carbon and its amount is capped to the amount of fixed carbon in the biomass.

- CO_2 uptake by CaO may be limited either by the chemical equilibrium or by the maximum conversion of CaO into $CaCO_3$ in the gasifier. The equilibrium CO_2 concentration is calculated according to eq. (2-15).

$$\log_{10} x_{CO_2,eq} = 7.079 - \frac{8308}{T} \quad (2\text{-}15)$$

The maximum conversion of CaO into $CaCO_3$ in the gasifier is calculated as function of the number of carbonation-calcination cycles N, according to the model presented in Grasa and Abanades (2006) and summarized by eq. (2-16), (2-17) and (2-18).

$$X_{ave} = \sum_{N=1}^{\infty} X_N \cdot r_N \quad (2\text{-}16)$$

$$X_N = \frac{1}{\frac{1}{1 - X_r} + N \cdot k} + X_r \quad (2\text{-}17)$$

$$r_N = \frac{F_0 \cdot F_{Ca}^{N-1}}{(F_0 + F_{Ca})^N} \quad (2\text{-}18)$$

To consider kinetics limitation and the residence time distribution of the particles in the gasifier, a limitation in carbonation reaction yield is applied, according to the empirical relation reported in equation (2-19). The estimated value is then limited to avoid a volumetric fraction of CO_2 below the equilibrium of carbonation reaction, as in equation (2-20).

$$\chi = \begin{cases} 10^{-5.3070527 \cdot 10^{-3}\, T + 3.807265}, & T < 645°C \\ 10^{-1.30604 \cdot 10^{-5}\, T^2 + 0.0151752\, T - 3.987893}, & T \geq 645°C \end{cases} \quad (2\text{-}19)$$

$$x_{CO_2} / x_{CO_2,eq} = \max\{\chi; 1\} \quad (2\text{-}20)$$

In the model, CO_2 uptake computed according to equation (2-20), is then compared against the maximum conversion X_{ave} estimated with equation (2-16).

- The content of other species in the syngas are estimated assuming that all the sulfur in biomass is converted to H_2S, all chlorine to HCl and 0.1% of the nitrogen to NH_3.

In Table 2-5, the sources of parameters used in the SEG model are summarized.

Table 2-5 - Summary of parameters sources for the SEG model

Assumption	**Source**
Residual char in gasifier	Fuchs et al. 2020
Approach to equilibrium composition of WGS	Fuchs et al. 2020
Produced CH_4 : 0.07 $kg_{CH4}/kg_{bio,dry}$	FLEDGED (Hafner et al., 2017)
Produced C_xH_y : 0.250 $kmol_{C2H4}/kmol_{CH4}$	FLEDGED (Hafner et al., 2017)
Inert addition to gasifier	FLEDGED
S/C=1.5	FLEDGED

The obtained results of the SEG 0D model are compared with data from scientific literature (Pröll and Hofbauer, 2008a; Koppatz et al., 2009; Armbrust et al., 2014; Poboß, 2016; Alamia et al., 2017; Schmid et al., 2017; Fuchs et al., 2020) and with experimental data collected at University of Stuttgart (USTUTT) in the framework of the FLEDGED project (Hafner et al., 2018, 2021; Hafner and Schmid, 2020). Figure 2-3 and Figure 2-4 show the gas yield and the composition curves.

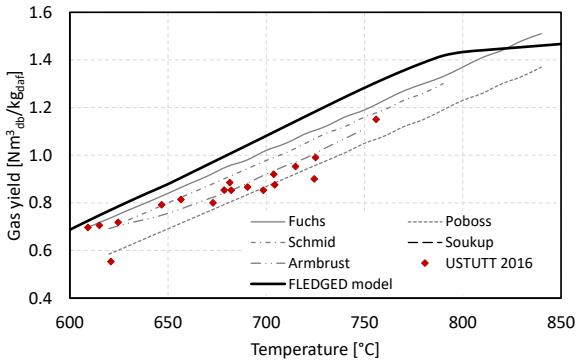

Figure 2-3 - Comparison of simulated syngas yield from SEG with literature (Fuchs et al., 2020) *and USTUTT experimental data.*

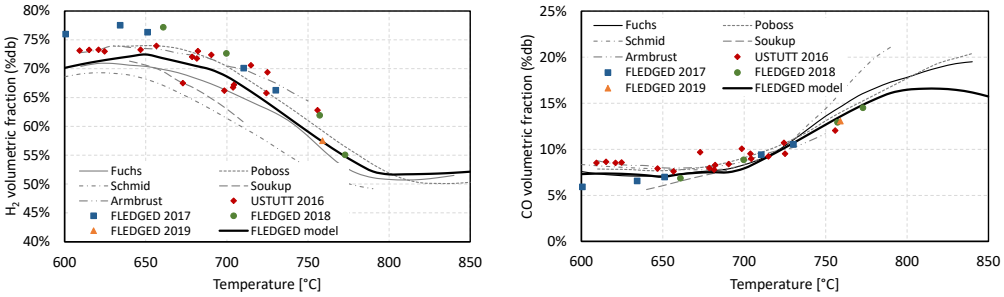

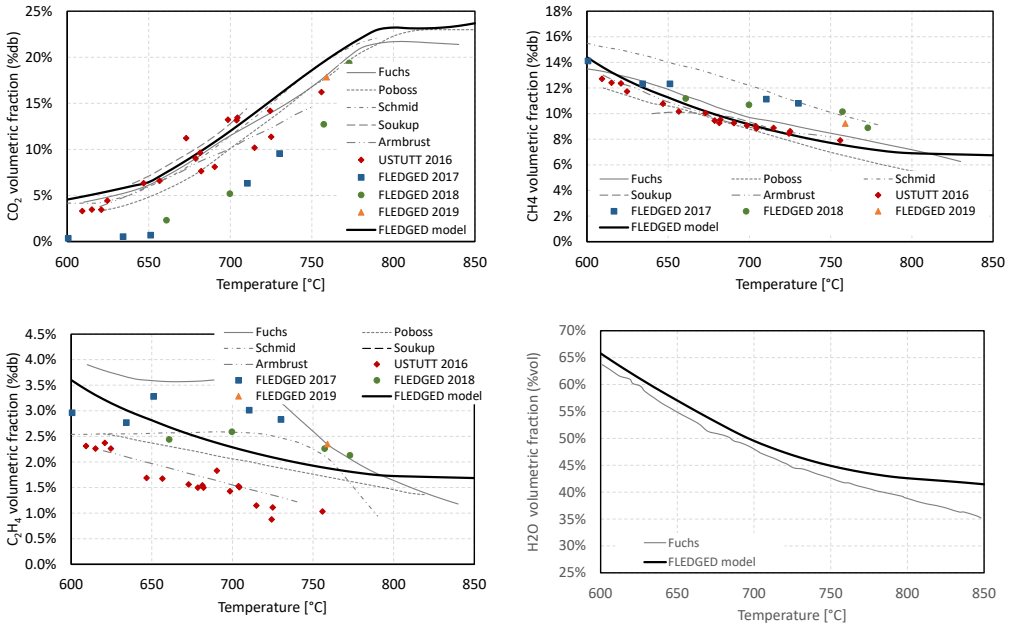

Figure 2-4 - Comparison of simulated compositions of syngas from SEG with literature (Fuchs et al., 2020) *and FLEDGED experimental data from different campaigns.*

The figures above show that the model satisfactorily reproduces experimental results and is fairly well aligned with the other models in the literature.

The results of the 0D model have also been compared with the 3D simulations performed by Lappeenranta University of Technology (LUT) in the framework of the FLEDGED project, as reported in Table 2-6.

Table 2-6 - Comparison of syngas compositions obtained by the 0D and 3D simulations by LUT.

Parameter	**Case F1**[1]		**Case F3**[1]	
Molar fraction	**Lumped**	**3D model**	**Lumped**	**3D model**
H_2O, %mol	48.9	53.0	44.4	50.1
H_2, $\%_{mol}$ dry, N_2, Ar free	65.6	60.6	52.0	50.5
CO_2, $\%_{mol}$ dry, N_2, Ar free	14.7	12.9	24.1	22.1
CO, $\%_{mol}$ dry, N_2, Ar free	9.0	11.0	15.1	13.9
CH_4, $\%_{mol}$ dry, N_2, Ar free	8.6	12.5	7.0	10.9
C_xH_y, $\%_{mol}$ dry, N_2, Ar free	2.1	3.0	1.7	2.6

[1] SEG operating points in FLEDGED project. The gasification temperature is 716°C and 772°C in F1 and F3 respectively.

2.1.5 Syngas purification, conditioning and compression

Downstream the gasification unit, the raw syngas undergoes a high temperature filtration before the raw gas reformer. The reforming unit is an ATR fed with oxygen produced by ASU or as a by-product by water electrolysis, using catalysts designed to operate on raw syngas (Kurkela et al., 2021). A restricted equilibrium calculation approach has been adopted for the ATR, assuming 90% methane conversion and complete conversion of higher hydrocarbons. The assumed methane conversion is slightly higher than the

conversion achieved in VTT lab-scale pilot plant (Kurkela et al., 2016). When, water electrolysis is integrated with the plant, an oxygen storage is associated with the reforming unit in order to store the intermittent oxygen production from the electrolysis and to provide a stable flow to the ATR. Information about the operating conditions of the ATR for all the configurations are reported in Table 3-4 (section 3.1.1) and in Table 3-15 (section 3.2.1). The higher oxygen demand to heat up the raw syngas to the reforming temperature is mainly related with the gasifier exit temperature and the reforming temperature.

As mentioned in section 1.2, syngas purification, conditioning and cleaning are necessary steps in order to produce a cleaned, tailored and compressed syngas for the downstream final product synthesis. The design of such plant sections depend on the gasification technology, on the final product, and on the plant configuration (i.e. presence of electrolyser or CCS equipment). Therefore, a detailed description is provided in Chapter 3 and Chapter 4.

2.1.6 Final product synthesis and purification

The methanol production plants must be fed with syngas with module $M = (H_2 - CO_2)/(CO + CO_2)$ of around 2, which is achieved within the syngas conditioning section by means of WGS reactor and/or CO_2 separation. The fresh syngas is first mixed with the unconverted recycled gas and then preheated in a feed/effluent heat exchanger, upstream the methanol synthesis reactor. The temperature of the inlet syngas to the methanol synthesis reactor is set according to the heat exchanger specifications. The outlet crude methanol is cooled down until the dew point temperature of the mixture is reached. The crude methanol is further cooled down to 40°C and separated in a flash unit from the light gases which are recycled back to the reactor.

The methanol synthesis process is performed in a multi-tubular fixed bed reactor filled with commercial $Cu/ZnO/Al_2O_3$ catalyst (CZA) pellets and externally cooled by boiling water (i.e. boiling water reactor, BWR). The methanol synthesis is modelled in Aspen Plus® by adopting the rigorous model for plug flow reactors. As mentioned above, the SRK equation of state is chosen to compute the thermodynamic properties since it is suited for the high temperature and pressure conditions within the reactor. The kinetic model proposed by Bussche and Froment (1996) is used in the analysis. Detailed information regarding the thermodynamics and the kinetics of the methanol reactor model can be found in Aspentech (2018). The methanol synthesis reactor presents fixed design criteria which are among others the tube length and diameter (i.e. 6 m and 0.04 m, respectively), the reactor pressure (i.e. 90 bar), the temperature of the boiling water (i.e. 238°C) and the catalyst-related specifications (see Table A 1 in Appendix A and Table B 1 in Appendix B). Moreover, the number of the tubes inside the reactor depends on the selected gas hourly space velocity (GHSV), referred to the volume of the reactor tubes. In this work, the plants are designed with a GHSV of 5000 h^{-1} and a recycle ratio (RR, defined as the molar flow rate of the recycle stream divided by the molar flow rate of the fresh syngas) of 5. The control criteria which are applied in off-design conditions depend on the composition and especially on the CO/CO_2 ratio of the fresh syngas (see Chapter 3).

The reactor model in Aspen Plus® is validated in collaboration with the Laboratory of Catalysis and Catalytic Processes (LCCP) research group at Politecnico di Milano. The reactor is analysed by using a 2D heterogeneous single tube model coupled with a 1D

description of the catalyst pellet, implemented in gPROMS® 5.0.2 software for the numerical solution. The model consists of:

- 2D gas phase i-species mass balances accounting for axial and radial concentration and temperature gradients;
- 2D gas and solid phase energy balances;
- 1D momentum balance in order to evaluate the pressure drops along the reactor tubes;
- 1D i-species mass balances of isothermal CZA cylindrical pellets accounting for the intraparticle diffusion phenomena that lowers the catalyst effectiveness factor.

The kinetic model proposed by Vanden Bussche and Froment (1996) is used in the analysis. The diffusivity and transport correlations are taken from literature while the gas mixture physical properties are calculated using the gPROMS® utility Multiflash. The model, validated against industrial data, is described extensively by Montebelli et al. (2013). The discretization methods used for the numerical solution of the model equations are the first-order backward finite-difference method (BFDM) for the reactor tube axial coordinate and the third-order orthogonal collocation on finite elements method (OCFEM) for the tube radial and the pellet coordinates. In the simulations is adopted a non-uniform grid of 60 axial points, obtained by a logarithm transformation implemented in gPROMS® with a transformation parameter $\alpha = 15$, while 3 and 4 collocation elements are used respectively for the radial coordinate and the catalyst pellet coordinate.

The model in gPROMS® is used to validate the output composition of the raw methanol in Aspen Plus. Figure 2-5 shows the composition profiles along the methanol synthesis reactor axial coordinate. The profiles differ along the axial coordinate, being the gPROMS model more accurate than the Aspen one. However, the composition of the raw methanol is relatively similar at the reactor outlet. Table 2-7 summarises the output composition of the raw methanol in all the cases discussed in Chapter 3. The more accurate gPROMS model is used to analyse the catalyst temperature which must be controlled in order to prevent excessive temperature hot-spot that may lead to catalyst deactivation.

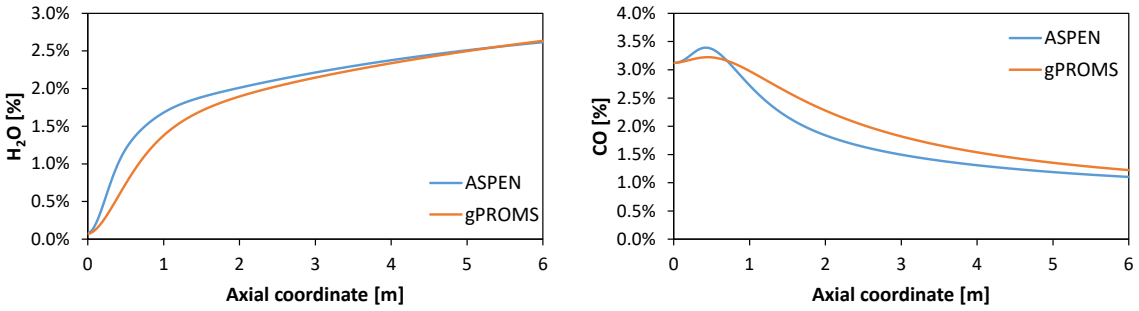

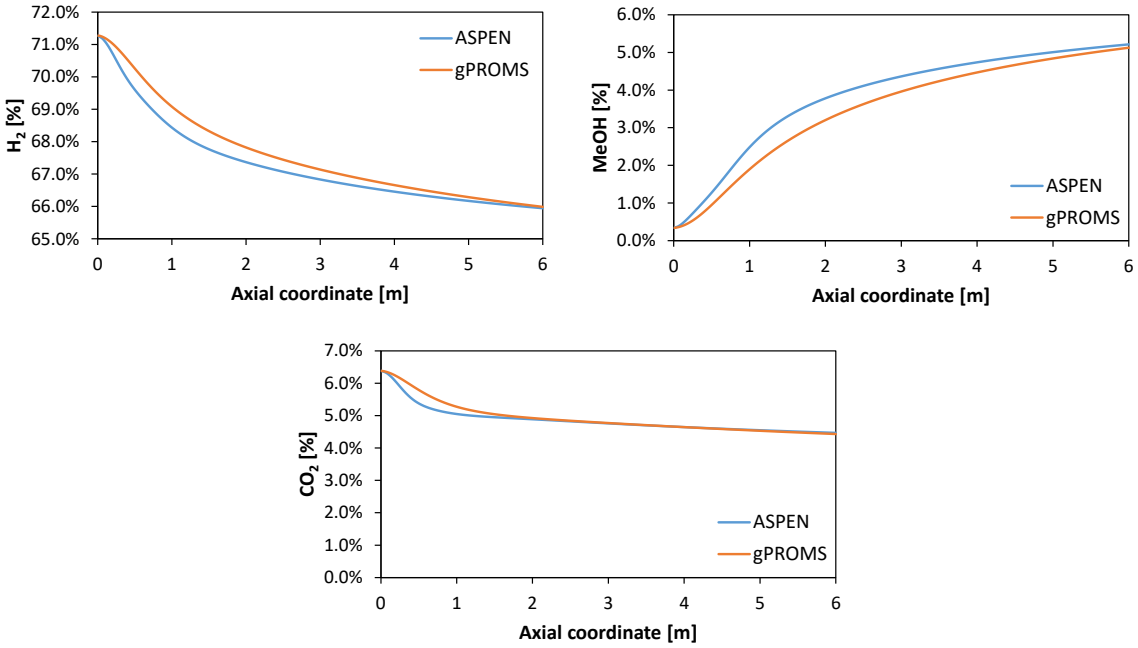

Figure 2-5 – Aspen Plus vs. gPROMS composition profiles along methanol synthesis reactor axial coordinate (SEG EO ERD, see section 3.1 for more information).

Table 2-7 - Aspen Plus vs. gPROMS raw methanol composition. (see section 3.1 and 3.2 for more information).

Parameters	DG BO		DG EO		IG BO		IG EO		SEG BO (ERD)		SEG EO (ERD)		SEG BO (BRD)		SEG EO (BRD)	
	Aspen	gPROMS	Aspen	gPROMS	Aspen	gPROMS	Aspen	gPROMS	Aspen	gPROMS	Aspen	gPROMS	Aspen	gPROMS	Aspen	gPROMS
H_2O, $\%_{mol}$	0.48	0.54	2.30	2.31	0.35	0.40	2.14	2.16	1.72	1.77	2.62	2.63	2.51	2.55	3.43	3.45
H_2, $\%_{mol}$	45.56	45.33	68.08	68.13	46.94	46.68	64.34	64.39	51.85	51.78	65.95	65.99	58.79	58.81	68.62	68.72
CO_2, $\%_{mol}$	1.00	0.94	3.29	3.27	0.95	0.90	3.23	3.20	2.57	2.51	4.47	4.43	5.10	5.05	9.57	9.49
CO, $\%_{mol}$	0.89	0.81	0.95	1.07	1.21	1.09	0.95	1.05	0.74	0.79	1.10	1.22	1.16	1.28	1.89	2.14
MeOH,	4.06	4.22	5.42	5.32	5.86	6.08	5.48	5.39	3.56	3.58	5.22	5.12	5.15	5.08	7.15	6.90
CH_4, $\%_{mol}$	12.16	12.20	5.24	5.23	13.61	13.66	7.64	7.63	10.41	10.41	5.46	5.44	7.34	7.33	2.58	2.57
N_2, $\%_{mol}$	35.85	35.96	14.70	14.67	31.08	31.19	16.22	16.18	29.15	29.16	15.19	15.16	19.94	19.91	6.76	6.73

The purification section is performed with a rate-based approach, to take into account the mass transfer occurring on each tray. The employed thermodynamic method is based on the Non-Random-Two-Liquid (NRTL) model (Renon and Prausnitz, 1968).

The raw product, rich in methanol and water and with the presence of other species (i.e. low boiling components and ethanol), enters the purification section at 2 bar and about 40°C. The methanol purification unit includes two distillation trayed columns in series, the stabilizing column which aims at removing most of the incondensable gases and concentration column which allows to concentrate the methanol up to the desired purity (i.e. 99.85%$_{wt}$) for the product, with at least 99% of recovery.

The design of the purification section and the control criteria for flexible operation are case-specific. Detailed descriptions are provided in Chapter 3 and Chapter 4.

In hydrogen production plants, the hydrogen fraction in the syngas is increased in the conditioning section by means of WGS reactors. The syngas is fed to a PSA system which provides hydrogen with a purity higher than 99.9%$_{vol}$ at 30 bar and a tail gas stream at atmospheric pressure. The hydrogen separation efficiency of the PSA is assumed to be 90% (Stöcker et al., 1998). The PSA unit is modelled as a black-box.

2.1.7 Heat recovery and thermal integration

Biomass-to-X plants make available significant amounts of heat to be recovered from many sources (e.g. hot syngas, flue gas, methanol synthesis, etc.). However, a significant amount of heat and steam is required by plant units, mainly amine regeneration, methanol purification and gasification unit. Therefore, the heat recovery and thermal integration design of the investigated plants is case-specific.

In power and biomass-to-methanol plants, the excess heat available is efficiently converted into electrical power by means of a heat recovery steam cycle (HRSC). On the other hand, the heat-related data depend on the operating mode calling for a flexible design of the heat exchanger network (HEN) and HRSC. For this reason, multiperiod methodologies must be used to find the optimal arrangement of the HEN and HRSC.

The design of the HRSC and HEN is performed using the multiperiod synthesis methodology proposed by Elsido et al. (2020, 2021) and developed within the Group of Energy Conversion systems at Politecnico di Milano. Given the list of hot and cold streams (i.e. syngas coolers, intercoolers, methanol reactor and the flue gases of the internal combustion engine) and the list of steam users (i.e. gasifier and MDEA regeneration) of each operating mode, the methodology finds the optimal HRSC and HEN design taking into account all the key technical design constraints, economics and the different operating modes.).

The objective function is the total annual cost of the heat recovery system (HEN and HRSC) of the plant, consisting in the sum of the annualized investment cost and the operating costs. The main technical constraints are set by the metal dusting metallurgical issue which may occur on the tubes of the syngas coolers for a temperature higher than 340°C (Grabke, 1995). To avoid such damaging phenomena, a “forbidden match” constraint is included in the optimization problem to forbid matching syngas coolers and steam superheaters in the metal dusting temperature range.

The superstructure combines the SYNHEAT superstructure (Yee and Grossmann, 1990) for the HEN with the *p-h* steam cycle superstructure (Martelli et al., 2017) shown in Figure 2-6. It includes up to three pressure levels for both evaporation (120 bar, 32 bar, 6.5 bar) and condensation (6.5 bar, 2 bar, 0.05 bar) and the extraction of superheated steam at different pressures. It is worth noting that the configuration shown is the most general one, and the optimization procedure might lead to the selection of only a portion of it. The pressure levels are set on the basis of process requirements (e.g. methanol reactor operating temperature) and superheating limitations of medium-grade steel tubes (525°C). The reheating temperature is set to 480°C to allow the extraction of steam at the required 182°C at 2 bar. Since the gasifier requires for the IG- and SEG-based plants superheated steam at low pressure and high temperature (400°C), a very low pressure reheater is included in the superstructure. In the DG configuration, steam extraction is required at 6.5 bar and 172°C, therefore an alternative de-superheater (DE-SH LP1 in Figure 2-6) is also included in the superstructure.

The Rankine cycle and HEN design problem is formulated as a challenging non-convex MINLP problem, which requires the ad hoc solution procedure proposed recently by Elsido et al. (2020, 2021) and approximately 13 hours of computational time.

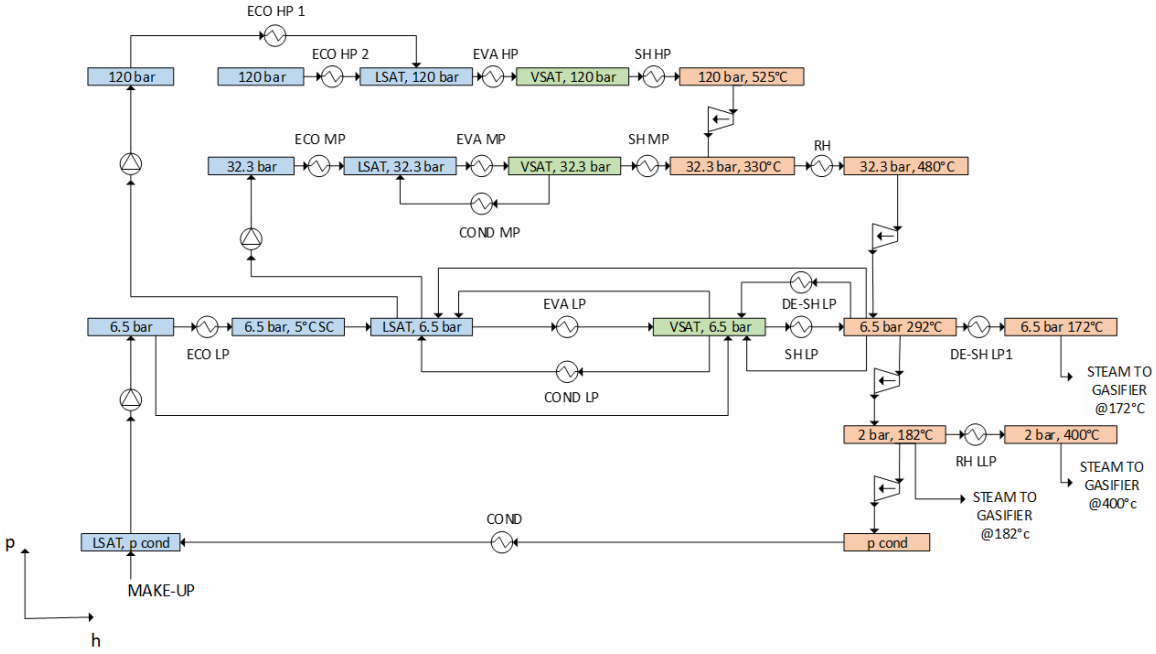

Figure 2-6 - Scheme of the p-h superstructure representing the possible HRSC configurations. Colored boxes denote steam/water headers at fixed pressures and temperatures, which are connected by equipment units (pumps, economizers, evaporators, superheaters, valves), as described in Elsido et al. (2017).

When CCS equipment (i.e. MDEA and mainly MEA scrubbing unit) is integrated with BtX plants, the high heat demand for CO_2 capture does not leave heat available for power generation or does not make it economically competitive to produce very small electric power output. Therefore, the investigated BtX CCS plants only adopt steam/water loops to transfer heat from waste heat sources to the heat users (see Chapter 4).

Additional waste heat is generated by the internal combustion engine (ICE) which uses the off-gas of the methanol synthesis and purification process, and of the PSA for hydrogen purification for electricity, steam, and hot water production. The performance map of the ICE as a function of its size *S* and load *L* are assessed using the linearized equation derived in Zatti et al. (2018) and reported below:

$$P_{el} = k_{1,el}L + k_{2,el}S + k_{3,el} \tag{2-21}$$

$$P_{th} = k_{1,th}L + k_{2,th}S + k_{3,th} \tag{2-22}$$

Where P_{el} and P_{th} are the electrical and thermal power output respectively, L is the load as thermal input power, S is the ICE size and k_1, k_2 and k_3 parameters obtained in Zatti et al. (2018) by best-fitting the part-load maps of commercially available gas-fired ICEs with power output larger than 4 MW. Variations of the exhaust temperature with loads have been neglected. The flue gases exit the ICE at 400°C and they are cooled down to 100°C. The rest of the heat is transferred to the cooling circuit of the ICE and can be recovered at low temperature, if required.

The high heat demand which is required in some configurations requires the installation of a boiler for steam production instead of the aforementioned ICE. In that case, the high temperature flue gases from the boiler are first cooled down to 160°C by steam generation and then to 80°C for combustion air pre-heating.

2.2 Methods for techno-economic analysis

2.2.1 Key performance indicators

To evaluate the performance of the assessed BtX plants, the following key performance indicators (KPIs) have been used.

The *fuel efficiency* ($\eta_{F,i}$) is the ratio between the chemical energy of the product stream and the chemical energy input to the process (both based on LHV). The fuel efficiency can be evaluated for the whole plant or for any plant process unit (i). In the enhanced operation mode of PBtX plants, the energy input includes also the contribution of the inlet hydrogen.

$$\eta_{F,i} = \frac{\dot{m}_{out,i} \cdot LHV_{out,i}}{\dot{m}_{in,i} \cdot LHV_{in,i}} \tag{2-23}$$

The *useful fuel efficiency* ($\eta_{F,i}^{u}$) accounts for the useful reactants (j) and the useful products (k) of the single plant unit (e.g. biomass as reactant and H_2 and CO as products for the gasification section, H_2 and CO as reactants and methanol as product for the methanol synthesis section).

$$\eta_{F,i}^{u} = \frac{\sum_{j=1}^{N} \dot{m}_{out,i,j} \cdot LHV_{out,i,j}}{\sum_{k=1}^{M} \dot{m}_{in,i,k} \cdot LHV_{in,i,k}} \tag{2-24}$$

The *carbon efficiency* (CE_i) can be defined as the ratio between the carbon molar flow rate in the stream $F_{C,i}$ at the exit of each process unit i and the carbon molar flow rate in the inlet biomass stream $F_{C,biom}$.

$$CE_i = \frac{F_{C,i}}{F_{C,biom}} \tag{2-25}$$

The achievable CE of a biofuel production plant is usually limited by the lack of hydrogen and the excess of oxygen in the feedstock, compared to the C:H:O ratio of the final product. The *potential carbon efficiency (PCE_i)* proposed by Poluzzi et al. (2020) is also used, to track the effect on the achievable CE of processes that entail not only carbon separation, but also involve oxygen, water or hydrogen addition. For the production of a generic fuel $C_{\chi_C} H_{\chi_H} O_{\chi_O}$, the *PCE* is defined as the ratio between the maximum carbon flow rate in the final fuel obtainable from stream i and the total carbon flow rate in the inlet biomass (eq. (2-26)). The maximum fuel production $F_{fuel,max,i}$ is defined to take into account the potential loss of carbon and hydrogen associated to the removal of the excess oxygen.

$$PCE_i = \frac{F_{fuel,max,i} \cdot \chi_C}{F_{C,biom}} \tag{2-26}$$

A *useful potential carbon efficiency (PCE_i^u)* can also be defined, considering only the useful molecules for the synthesis of the specific fuel. In this case, inert compounds in the fuel synthesis process (e.g. methane in the syngas for the synthesis of methanol) do not contribute in the calculation of the efficiency.

The *electric efficiency* (EE) indicates the conversion of the biomass chemical energy into electricity. The net electric output (P_{el}) accounts for the electricity produced by the steam turbines and by the internal combustion engine and for the electric consumption of the auxiliaries.

$$EE = \frac{P_{el}}{\dot{m}_{biom} \cdot LHV_{biom}} \tag{2-27}$$

The *equivalent fuel efficiency* ($\eta_{F,eq}$) accounts for the biomass saving associated with the electricity production of the plant. A steam cycle with 35% of electric efficiency ($\eta_{el,ref}$) is assumed as a reference, considering a biomass-fed subcritical steam power plant.

$$\eta_{F,eq} = \frac{\dot{m}_M \cdot LHV_M}{\dot{m}_{biom} \cdot LHV_{biom} - \frac{P_{el}}{\eta_{el,ref}}} \tag{2-28}$$

To account for the e-fuel production efficiency, the *power-to-fuel efficiency* (η_{PtF}) of eq. (2-29) is used, where the numerator is the additional fuel production in enhanced operation (EO) with respect to the baseline operation (BO) and P_{el} represents the net electric power output of the plant in enhanced operation and in baseline operation. Therefore, P_{el} includes the electricity production by the HRSC and the ICE, and the electricity consumption by the auxiliaries. In enhanced operation, P_{el} also includes the electricity consumption by the electrolyser, for which an electricity to hydrogen LHV efficiency of 69% is assumed (Bertuccioli et al., 2014; Schmidt et al., 2017).

$$\eta_{PtF} = \frac{(\dot{m}_M \cdot LHV_M)_{EO} - (\dot{m}_M \cdot LHV_M)_{BO}}{P_{el,EO} - P_{el,BO}} \tag{2-29}$$

In order to avoid the dependency on the efficiency of the electrolysis system, a *hydrogen-to-fuel efficiency* (η_{HtF}) is also used by considering the marginal contribution of hydrogen injection in fuel production (eq. ((*2-30*)).

$$\eta_{HtF} = \frac{(\dot{m}_M \cdot LHV_M)_{EO} - (\dot{m}_M \cdot LHV_M)_{BO}}{\dot{m}_{H_2} \cdot LHV_{H_2}} \tag{2-30}$$

The *carbon capture rate* (CCR) is the percentage of stored carbon with respect to the carbon contained in the feedstock.

$$CCR = \frac{F_{C,stored}}{F_{C,biom}} \tag{2-31}$$

2.2.2 Potential carbon efficiency

Biomass composition is characterized by different C:H:O ratios than the final biogenic product. Therefore, in biomass-to-X conversion plants, excess carbon and excess oxygen are typically removed in the form of CO_2, to be subsequently vented to the atmosphere. For example, plants based on biomass gasification involve a sequence of syngas conditioning steps including steam addition, water gas shift and CO_2 removal aimed at achieving the target C:H:O proportions at the inlet of the final product synthesis section. As previously mentioned, a new method based on a novel "*potential carbon efficiency*" (PCE) performance indicator is proposed to track the process performance along its process units (Poluzzi et al., 2020). The proposed method is applied to the plants investigated in this work. It must be highlighted that the PCE is not expected to give a different output than the carbon efficiency (CE) on the overall plant performance. On the other hand, the PCE provides a new insight into the effect that every single process unit has on the final CE. The PCE allows quantifying the potential variation of the achievable carbon efficiency in process units where no carbon separation occurs. Therefore, the PCE may be affected by the addition of a limiting element, such as hydrogen, through steam addition in a gasifier, or by the increase in oxygen content by means of oxygen injection in an autothermal reformer.

Considering a sequence of processes that convert biomass into a synthetic product (Figure 2-7), the carbon flow rate may change in each process unit due to carbon separation (e.g. CO_2 separation, unconverted char loss, unconverted tail gas to a combustor).

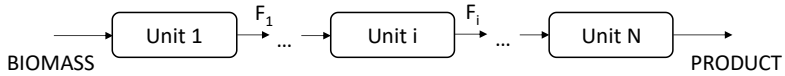

Figure 2-7 - Sequence of process units that converts biomass into a final biogenic product.

A *'carbon efficiency'* (CE) can be defined as the ratio between the carbon molar flow rate in the stream $F_{C,i}$ at the exit of each process unit i and the carbon molar flow rate in the inlet biomass stream $F_{C,biom}$ (eq.(2-25)).

This carbon efficiency index is a good overall performance indicator for a complete plant, but it is less significant as performance indicator for a single process unit, since it ignores the presence of hydrogen and oxygen that may limit the actual CE which can be ultimately achieved.

Considering a process for the production of a generic fuel $C_{\chi_C}H_{\chi_H}O_{\chi_O}$ and a generic material stream i exiting the process unit i with $F_{C,i}$,$F_{H,i}$ and $F_{O,i}$ molar flow rate of carbon, hydrogen and oxygen atoms respectively, the theoretical amount of fuel $F_{fuel,th,i}$ that can be produced from such stream may be calculated as the flow rate of the limiting element divided by its stoichiometric coefficient in the final fuel molecule (eq. (2-32)). The excess molar flow rate of carbon atoms $F_{exc,C,i}$ can then be calculated with eq. (2-33), which represents the amount of carbon in the stream i that needs to be removed in any of the downstream process units (e.g. as CO_2) or that can be converted into the final fuel only if additional atoms of the limiting element are added to the process.

$$F_{fuel,th,i} = \min\left(\frac{F_{C,i}}{\chi_C}; \frac{F_{H,i}}{\chi_H}; \frac{F_{O,i}}{\chi_O}\right) \quad (2\text{-}32)$$

$$F_{exc,C,i} = F_{C,i} - F_{fuel,th,i} \cdot \chi_C \quad (2\text{-}33)$$

Eq. (2-33) can be also referred to oxygen and hydrogen to calculate the excess flow rates $F_{exc,O,i}$ and $F_{exc,H,i}$. If excess oxygen is present in the stream (i.e. $F_{exc,O,i} > 0$), it will be removed in some stage of the process as CO_2 and/or H_2O. Therefore, the presence of excess oxygen involves that part of the hydrogen and carbon atoms will also be separated and will not be available for the synthesis of the final product. Therefore, a maximum fuel production $F_{fuel,max,i}$, lower than or equal to the theoretical fuel amount $F_{fuel,th,i}$, may be defined to take into account the potential loss of carbon and hydrogen associated to the removal of the excess oxygen (eq. (2-34)). The excess oxygen $F_{exc,O,i}$ is assumed to be first removed by the non-limiting element (i.e. the excess carbon $F_{exc,C,i}$ or the excess hydrogen $F_{exc,H,i}$, if any), that can remove a maximum amount of oxygen atoms equal to $2 \cdot F_{exc,C,i} + \frac{1}{2}F_{exc,H,i}$. If the residual oxygen is more than the amount removable with the excess carbon and hydrogen, (i.e. if $F_{exc,O,i} - 2 \cdot F_{exc,C,i} - \frac{1}{2}F_{exc,H,i} > 0$)), the maximum amount of fuel producible from the i^{th} stream is less than the theoretical one and can be expressed as in eq. (2-34).

$$F_{fuel,max,i} = F_{fuel,th,i} - \frac{\max\left(F_{exc,O,i} - 2 \cdot F_{exc,C,i} - \frac{1}{2}F_{exc,H,i}; 0\right)}{2\chi_C + \frac{1}{2}\chi_H - \chi_O} \quad (2\text{-}34)$$

Based on the definition of $F_{fuel,max,i}$, a *'potential carbon efficiency'* PCE_i is defined as the ratio between the maximum carbon flow rate in the final fuel obtainable from stream i and the total carbon flow rate in the inlet biomass (eq. (2-26)).

It must be specified that any other atom, which is present in the inlet biomass but not in the final product (e.g. nitrogen), does not influence the value of the indicator.

A useful potential carbon efficiency PCE_i^u can also be defined, considering only the useful molecules for the synthesis of the specific fuel. In this case, inert compounds in the fuel synthesis process (e.g. methane and higher hydrocarbons in the syngas in bio-methanol production plants) do not contribute in the calculation of the efficiency.

To better understand the effects of typical alterations of gas composition on the defined efficiencies, some examples are shown in Figure 2-8, considering a process designed to produce methanol (C:H:O = 1:4:1).

Two initial syngas compositions are considered, featuring carbon (column on the left) and hydrogen (column on the right) as limiting elements. The total amount of each atom is represented by the complete bar enclosed in the red contour. The yellow part of the bars represents the maximum amount of each atom that can end up in the final product. Therefore, they are in the same proportion as the corresponding atoms in the final product. The blue part of the bars shows the potential loss of carbon and hydrogen to separate the excess

oxygen as H_2O or CO_2. Oxygen excess is distributed to carbon and hydrogen in order to maximize the yield of final product. The red part of the bar (when present) represents the excess of hydrogen or carbon after the removal of the excess oxygen.

In the baseline case with carbon as limiting element (Figure 2-8a), all the excess oxygen can be removed as water, but the amount of hydrogen in that stream is such that excess hydrogen remains, to be removed in a downstream process. Since carbon does not need to be removed to achieve the correct stoichiometry for the production of methanol, the PCE of this stream is 100%. If a process is introduced requiring oxygen addition with an assumed O_2/C molar ratio of 0.4 (Figure 2-8b), the excess hydrogen is completely consumed and part of the oxygen needs to be removed also as CO_2. Therefore, although the CE remains 100% (no carbon is removed), the PCE reduces to 92%. If hydrogen or water are added to the baseline case (Figure 2-8c-d), the PCE does not change, as hydrogen was not the limiting element. Finally, if oxygen in the baseline stream is removed as CO_2 (Figure 2-8e), both theoretical and potential carbon efficiencies reduce and the excess hydrogen increases further.

In the baseline case with hydrogen as limiting element (Figure 2-8A), all the excess oxygen is potentially removed as CO_2, involving a reduction of the PCE to 63%. If more O_2 is added (Figure 2-8B), oxygen excess increases and is potentially removed as both H_2O and CO_2, causing a further reduction of the PCE to 42%. If H_2 is added in a sufficient amount (e.g. with H_2/C ratio of 0.4, as in Figure 2-8C), part of the excess oxygen can be removed as H_2O rather than as CO_2, causing an increase of the PCE (82%), compared to the baseline value. If more H_2 is added to the baseline stream, in a sufficient amount to bond with the excess oxygen, PCE would increase to 100%. If hydrogen is added in the form of H_2O (Figure 2-8D), the PCE also increases, as the amount of limiting element is increased. However, as the addition of water also involves an increase of the oxygen content, a maximum PCE (68% in this specific case) is achieved when the condition where no limiting element exists anymore is reached. Finally, if CO_2 is removed from the system (Figure 2-8E), the CE reduces, while the PCE remains equal to the baseline value of 63%.

	Limiting element: C Baseline composition: C:H:O = 1:5.5:1.2	Limiting element: H Baseline composition: C:H:O = 1:2.5:1.2
	Element in the final product; Element lost for removing excess oxygen; Excess element after oxygen removal; Available atoms	
Baseline	(a) 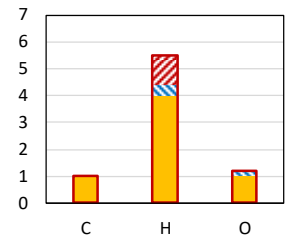 $CE = 100\%$ $PCE = 100\%$ $F_{fuel,th} = 1$ $F_{exc,C} = 0$ $F_{exc,H} = 1.5$ $F_{exc,O} = 0.2$ $F_{fuel,max} = 1$	(A) 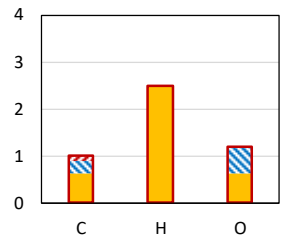 $CE = 100\%$ $PCE = 63\%$ $F_{fuel,th} = 0.63$ $F_{exc,C} = 0.375$ $F_{exc,H} = 0$ $F_{exc,O} = 0.575$ $F_{fuel,max} = 0.63$

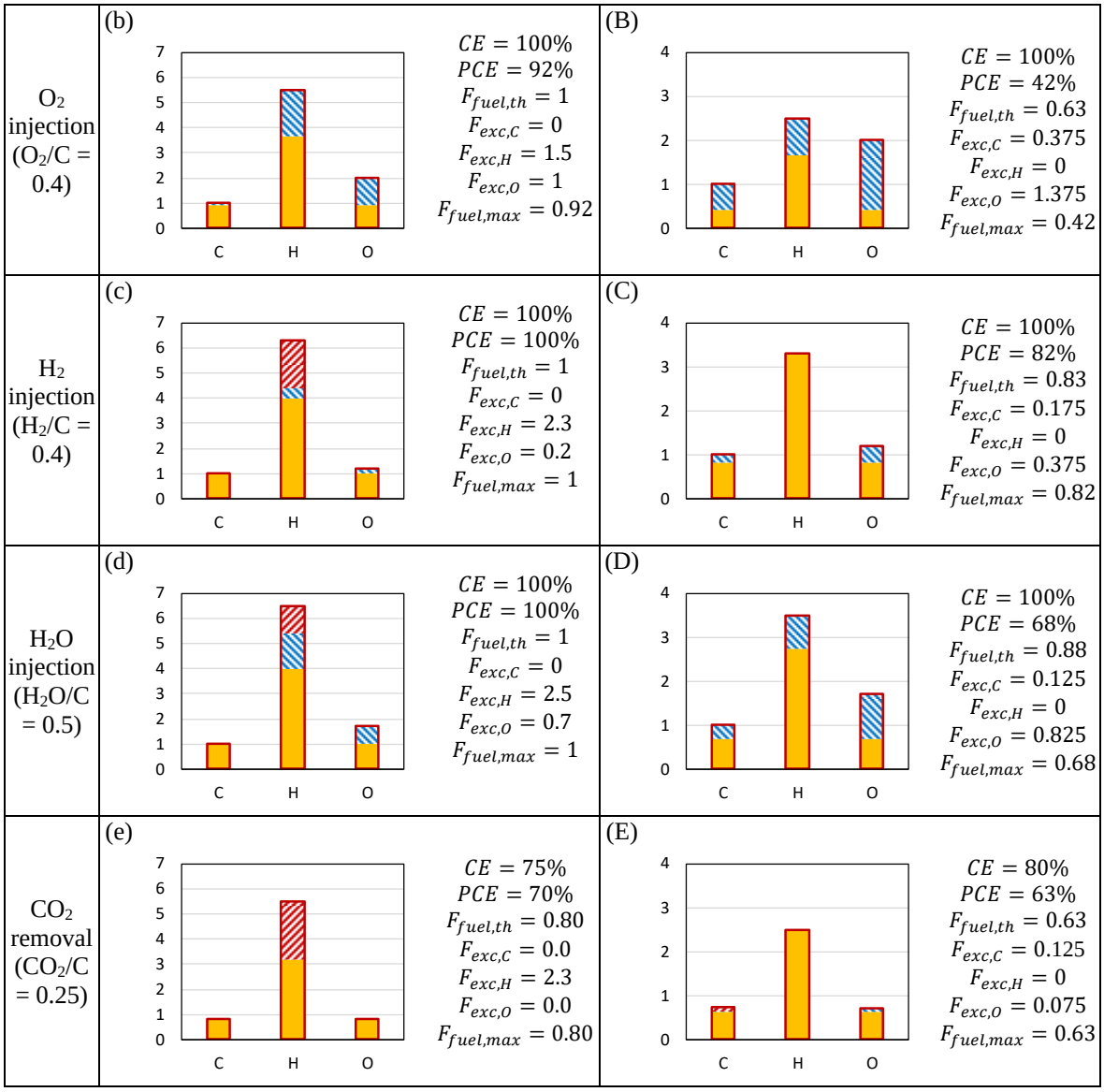

Figure 2-8 – 'Carbon efficiency' and 'potential carbon efficiency' for methanol production (C:H:O=1:4:1), for two input material streams with carbon (left) and hydrogen (right) as limiting elements and addition of O_2 (b-B), H_2 (c-C), H_2O (d-D) and removal of CO_2 (e-E).

From these generic examples, it is possible to observe the following behaviour of the two carbon efficiency indexes.

- The CE reduces only if carbon is removed from the system, either in the form of CO_2 (Figure 2-8e–E) or in the form of unconverted solid carbon. On the contrary, the PCE may also decrease if oxygen is added (Figure 2-8b–B) by an amount that is not compensated by a sufficient excess of hydrogen.
- The CE can only increase in the unusual case of the addition of carbon-containing molecules into the process. On the contrary, PCE increases when hydrogen is added either as H_2 to remove the excess oxygen (Figure 2-8C), or as H_2O when hydrogen is the limiting element (Figure 2-8D). Hydrogen

addition does not have any impact on the PCE, when hydrogen is not the limiting element (Figure 2-8c-d).

Therefore, the PCE is a useful index to evaluate a-priori the impact of sub-processes on the maximum fuel yield. In the following sections, the proposed approach is applied to different gasification technologies for the conversion of biomass into methanol. The same approach may be easily extended to other processes and other synthetic fuels.

2.2.3 Levelized cost approach

The economic analysis is performed by adopting the *Levelized Cost* approach. The levelized cost of the fuel is defined as the breakeven selling price that repays the total cost (C_{tot}) by producing a certain amount of fuel (M_{tot}) at the end of the plant lifetime (LT). It considers the total capital investment costs (TCI), utilities costs (C_{ut}), cost of feedstock ($C_{feedstock}$) and the fixed O&M costs ($C_{fixed\ O\&M}$), as shown in eq. (2-35), where $\dot{m}_{fuel}$ is the nominal fuel production rate and h_{eq} are the equivalent yearly operating hours, defined as the ratio between the actual amount of fuel produced in a certain period and the nominal flow rate.

$$LCOF = \frac{C_{tot}}{M_{tot}} = \frac{TCI \cdot CCF + C_{fixed\ O\&M} + C_{feedstock} + C_{ut}}{\dot{m}_{fuel} \cdot h_{eq}} \tag{2-35}$$

The flexible PBtM plants, which are analysed in this work, operate in the two different modes: baseline operation (without hydrogen injection) and enhanced operation (with hydrogen injection). The two modes differ in both productivity and operational cost, therefore they have to be weighted in order to calculate how they contribute to the total cost. In the assessment, the final LCOF is calculated by weighting the production and the operational costs on the hours for the two operation modes, according to eq. (2-36), where χ_{BO} and χ_{EO} are the fraction of total operating hours in baseline and enhanced mode, respectively and h is the annual plant availability.

$$LCOF = \frac{C_{tot}}{M_{tot}} = \frac{TCI \cdot CCF + C_{fixed\ O\&M} + C_{feedstock} + (C_{ut,BO} \cdot \chi_{BO} + C_{ut,EO} \cdot \chi_{EO})}{(\dot{m}_{fuel,BO} \cdot \chi_{BO} + \dot{m}_{fuel,EO} \cdot \chi_{EO}) \cdot h} \tag{2-36}$$

The Capex estimation approach is based on the *Percentage of Delivered-Equipment Cost Method*, which requires the determination of the delivered-equipment cost for estimating the fixed-capital investment (FCI), the working capital (WC) and the total capital investment (TCI). The other items included in the TCI computation are then estimated as percentage of the delivered-equipment cost. This is summarized in the following cost equations:

$$FCI_i = E_i \cdot (1 + \sum_{j}^{M} f_j) \tag{2-37}$$

$$WC_i = f_{WC} \cdot E_i \tag{2-38}$$

$$TCI = \sum_{i}^{N} (FCI_i + WC_i) \tag{2-39}$$

The FCI of the *i*-th plant component is estimated with the equation (2-37) where E_i is the delivered-equipment cost of the *i*-th component and f_j are the *M* multiplying factors reported in Table 2-8. The working capital is computed with the equation (2-38), where f_{WC} is one of the multiplying factors of the delivered-equipment cost reported in Table 2-8. Finally, the TCI is computed as the summation over the total number of components *N* of the FCI_i and WC_i. All the costs reported in this work refer to the year 2019.

To account for the investment depreciation and for the change in the value of money, a Capital Charge Factor can be introduced, representing the fraction of TCI assigned to each year of operation during its lifetime LT.

$$CCF = \frac{1}{\sum_{LT} \frac{1}{(1+\alpha)^n}} = \frac{\alpha(1+\alpha)^{LT}}{(1+\alpha)^{LT} - 1} \tag{2-40}$$

The discount rate α is a lumped parameter considering depreciation rate, inflation, expected return on investment (equity) and interests on capital of debt. The last contributions are sometimes labeled as WACC (Weighted Average Capital Cost).

In order to compute the Opex, the following costs are determined: utilities, maintenance and repairs, operating supplies, operating labor, laboratory costs, local taxes, insurance, and catalyst.

The main costs of the utilities are for the feedstock and for the electricity. A ligneous biomass price of 45.7 €/t (4.7 €/GJ) is taken from Hannula and Kurkela (2013). As regards the cost of electricity, the 2019 electricity prices of the day-ahead market of West Denmark (DK1) are considered in the calculations (ENTSO-E Transparency Platform, 2020). Denmark has been selected as it is the European country with the highest share of intermittent renewable energy sources and therefore may be representative of the energy mix of other European countries in the coming decade. The average electricity price can be derived as a function of the operating hours from the cumulative electricity price duration curve. In the BtX plants which include water electrolysis, once the electrolyser capacity factor is fixed (80% in this analysis, as reference value), an average electricity price of 34.3 €/MWh in enhanced operation and 55.3 €/MWh in baseline operation can be computed. As regards the catalyst cost, according to Tan et al. (2016) a typical price for the commercial CZA methanol catalyst is 18.12 €/kg with a catalyst lifetime of 4 years. In the BtX plants featuring CCS, the CO_2 transport and injection/storage costs are considered to be equal to 13.4 €/t, as reported in Hannula and Melin (2021). The cost corresponds to a 100 km pipeline transport from the conversion facility to the storage site and 2 km underground storage in deep saline formations.

The maintenance and repairs include the cost of maintenance labour and materials, including equipment spares, needed for the maintenance of the plant. The annual maintenance cost is taken as 5% of the fixed capital cost. The cost can be considered to be divided evenly between labour and materials. The operating supplies refer to all the miscellaneous materials required to operate the plant, which are not included neither in the raw materials nor in the maintenance materials, and they have been assumed equal to 10% of the total maintenance cost. The operating labour is the manpower needed to operate the

plant and it is directly involved with running the process. The costs should be calculated from an estimate of the number of shift and day personnel needed. Assuming highly automated plants, the operating labour has been assumed 10% of the total operating costs. As regards the laboratory costs, a value of 25% of the operating labour cost is assumed. For the local taxes and insurance, 1% of the fixed capital is considered for each.

A summary of the aforementioned key parameters which are used in the analysis is reported in Table 2-9.

Table 2-8 - Multiplying factors for estimating the total capital investment based on delivered-equipment cost.

	Percent of delivered-equipment cost for		
	Solid processing plant	***Solid-fluid processing plant***	***Fluid processing plant***
Direct costs			
Purchased equipment delivered	100	100	100
Purchased equipment installation	45	39	47
Instrumentation and controls (installed)	18	26	36
Piping (installed)	16	31	68
Electrical systems (installed)	10	10	11
Buildings (including services)	25	29	18
Yard improvements	15	12	10
Service facilities (installed)	40	55	70
Total direct plant cost	269	302	360
Indirect costs			
Engineering and supervision	33	32	33
Construction expenses	39	34	41
Legal expenses	4	4	4
Contractors fee	17	19	22
Contingency	35	37	44
Total indirect plant cost	128	126	144
Fixed-capital investment	397	428	504
Working capital	70	75	89
Total capital investment	467	503	593

Table 2-9 - Parameters and assumptions for the evaluation of the LCOF.

Economic parameters	**Value**
Discount rate, %	10
Lifetime, y	20
Capital Charge Factor, %	11.75
Availability, h/year	7884
Electrolyser capacity factor, %	80
Variable Opex	
Biomass feedstock cost, €/t	45.72
Denmark average electricity price, €/MWh	38.49
Denmark average electricity price, €/MWh (enhanced operation) [1]	34.30
Denmark average electricity price, €/MWh (baseline operation) [1]	55.26
CO_2 transport and injection/storage costs [2], €/t	13.39
Fixed Opex	
Maintenance and repairs, % FCI	5
Operating supplies, % FCI	0.5
Operating labor, % Opex	10
Laboratory costs, % Opex	2.5
Local taxes, % FCI	1
Insurances, % FCI	1
Catalyst cost, €/kg	18.12
Catalyst lifetime, y	4

[1] If the electrolyser is included in the analysis.

[2] If CCS is included in the analysis.

Part of the equipment cost estimate derives from in-house estimation in the framework of the FLEDGED project (Poluzzi et al., 2022a, 2022b). The purchase equipment delivered is increased to the fixed capital investment by using the Lang factors computed from Table 2-8. The remaining capital cost estimates are selected from scientific literature. The total direct cost of the equipment is obtained from the references, later the fixed capital investment is computed by means Lang factors derived from Table 2-8. The heat exchanger cost of the steam/water loops is computed by using the area as scaling parameter. The values of the global heat transfer coefficient (U) depending on the thermodynamic characteristics of the working fluids are reported in Table 2-11. The product of the area and the overall heat transfer coefficient (UA) is divided by U to compute the heat transfer area which is used in the economic evaluation.

Table 2-10 – Capital costs detail

Capital costs	Cost scaling parameter	Reference capacity	Scaling exponent	Reference purchase equipment delivered, M€	Lang factor	Reference
Biomass-to-syngas island						
Feedstock handling [1]	Feed, MWth	157	0.31	*6.94*	1.48	(Hannula, 2016) (2010 €)
Belt dryer [1]	Water evap., kg/s	0.34	0.28	*2.49*	1.48	(Hannula, 2016) (2010€)
ASU (O_2 at 1.05 bar) (air compr. included) [1]	Pure oxygen, t/d	1839	0.5	*47.96*	1.40	(Kreutz et al., 2005) (2002 $)
Oxygen compressor (from 1.05 bar)	Compressor work, MWel	0.41	0.67	0.44	5.04	In-house estimate (Poluzzi et al., 2022a, 2022b) (2019 €)
Oxygen storage	Storage volume, m^3	1.00	1.00	0.006	5.04	In-house estimate (Poluzzi et al., 2022a, 2022b) (2019 €)
Pressurized O_2 CFB gasifier [1]	Dry biom., kg/s	17.80	0.75	*49.38*	1.42	(Hannula, 2016) (2010€)
Atm steam CFB gasifier [1]	Dry biom., kg/s	17.80	0.75	*24.75*	1.42	(Hannula, 2016) (2010 €)
Combustor with fluegas treatment [1]	Fuel input, MWth	5.90	0.65	*7.73*	1.42	(Hannula, 2016) (2010 €)
Ceramic hot-gas filter [1]	Syngas, kmol/s	1.47	0.67	*8.91*	1.48	(Hannula, 2016) (2010 €)
Catalytic reformer [1]	Syngas, kmol/s	2.04	0.67	*28.55*	1.42	(Hannula, 2016) (2010 €)
Cleaning and conditioning island						
Scrubber	Syngas at cleaning inlet, kmol/s	0.64	0.67	0.27	5.04	In-house estimate (Poluzzi et al., 2022a, 2022b) (2019 €)
Liquid redox	Syngas at cleaning inlet, kmol/s	0.64	0.67	0.57	5.04	In-house estimate (Poluzzi et al., 2022a, 2022b) (2019 €)
Syngas compressor	Compressor work, MWel	7.01	0.67	7.50	5.04	In-house estimate (Poluzzi et al., 2022a, 2022b) (2019 €)
Activated carbon	Syngas at cleaning inlet, kmol/s	0.64	0.67	0.09	3.97	In-house estimate (Poluzzi et al., 2022a, 2022b) (2019 €)
Waste water treatment	Waste water, m^3/h	22.56	0.67	0.45	5.04	In-house estimate (Poluzzi et al., 2022a, 2022b) (2019 €)
WGS reactor (single-stage)	Syngas , kmol/s	0.26	0.67	1.60	4.28	In-house estimate (Poluzzi et al., 2022a, 2022b) (2019 €)
WGS reactor (two-stage) [2]	Syngas , kmol/s	0.26	0.67	4.00	4.28	In-house estimate (Poluzzi et al., 2022a, 2022b) (2019 €)

Capital costs	Cost scaling parameter	Reference capacity	Scaling exponent	Reference purchase equipment delivered, M€	Lang factor	Reference
CO_2 removal pre-combustion (MDEA) [1,3]	CO_2 captured, kg/h	46600	0.67	*16.69*	1.40	(IEAGHG, 2017b) (2015 €)
CO_2 removal post-combustion (MEA) [1]	CO_2 captured, kg/h	80048	0.67	*72.17*	1.40	(IEAGHG, 2017b) (2015 €)
Syngas-to-X island						
Methanol synthesis BWR [3]	Syngas molar flow, kmol/s	2.20	0.67	1.72	4.28	In-house estimate (Poluzzi et al., 2022a, 2022b) (2019 €)
Recycle compressor [3]	Compressor work, MWel	0.41	0.67	0.44	5.04	In-house estimate (Poluzzi et al., 2022a, 2022b) (2019 €)
Stabilizing column [3]	Raw methanol, kmol/s	0.15	0.67	0.10	5.04	In-house estimate (Poluzzi et al., 2022a, 2022b) (2019 €)
Concentration column [3]	Raw methanol, kmol/s	0.14	0.67	0.36	5.04	In-house estimate (Poluzzi et al., 2022a, 2022b) (2019 €)
PSA [1]	Syngas, m^3/s	4.63	1.00	*39.49*	1.42	(Riva et al., 2018) (2017€)
Heat recovery island						
CHP internal combustion engine [1]	Fuel input, kWth	13783	0.95	*2.48*	1.40	(Zatti et al., 2018) (2017 €)
Boiler [1]	Fuel input, kWth	10000	0.92	*0.60*	1.40	(Zatti et al., 2018) (2017 €)
ECO [3]	Area, m^2	10000	0.68	0.96	5.04	(Elsido et al., 2021) (2019 €)
EVA [3]	Area, m^2	5000	0.79	1.16	5.04	(Elsido et al., 2021) (2019 €)
SH [3]	Area, m^2	505	0.74	0.13	5.04	(Elsido et al., 2021) (2019 €)
Electricity-to-hydrogen island						
Electrolyser	Electrolyser size, MWel	1.00	1.00	0.70	1.00	In-house estimate (Poluzzi et al., 2022a, 2022b) (2019 €)
H_2 compressor	Compressor work, MWel	0.64	0.67	0.75	5.04	In-house estimate (Poluzzi et al., 2022a, 2022b) (2019 €)
CO_2 compression island						
CO_2 compression and dehydration unit [1]	Compressor work, MWel	3.01	0.67	*12.97*	1.40	(IEAGHG, 2017b) (2015 €)

[1] The cost reported in the column “reference equipment delivered" is a direct cost which includes installation and BOP. The corresponding Lang factors have been modified accordingly.

[2] The cost of the reference purchase equipment delivered has been modified in such a way that the cost for single-stage system is 40% of the cost of the two-stage system as indicated in Larson et al. (2009).
[3] In Chapter 3, case-specific in-house estimates are adopted (see from Table A 22 to Table A 25 in Appendix A).

Table 2-11 – Global heat transfer coefficients dependent on working fluid thermodynamic conditions.

U [W/m^2 K]	**Fluids**
60	Low pressure gas vs. water/steam
30	Low pressure gas vs. low pressure gas
400	High pressure gas vs. high pressure gas
500	High pressure gas vs. water/steam

2.2.4 Willingness to pay approach

With the aim of assessing the economic competitivity and the profitability of the flexible PBtM plants, it is necessary to identify the number of hours of operation in baseline and enhanced operating modes and the corresponding electricity prices. The fraction of the total operating hours in baseline and enhanced operation may be estimated with the 'Willingness to Pay' (WTP) methodology proposed by van Leeuwen and Mulder (2018).

The 'short-term WTP' expresses the breakeven electricity price that makes economically profitable to activate the electrolyser and operate in enhanced mode. Under such conditions, the revenues from the additional methanol production compensate the additional operational costs (electricity and water). The short-term WTP (WTP_{ST}) can be calculated from eq. (2-41), where $\dot{m}_{fuel}$ is the fuel production in enhanced operation (EO) and baseline operation (BO), p_{fuel} is the fuel selling price (€/kg), P_{el} is the net electrical power purchased in EO and in BO and c_{water} is the cost of water (quantitatively negligible compared to the cost of electricity).

$$\left(\dot{m}_{fuel,EO} - \dot{m}_{fuel,BO}\right) \cdot p_{fuel} = WTP_{ST} \cdot \left(P_{el,EO} - P_{el,BO}\right) + c_{water} \qquad (2\text{-}41)$$

Since all the contributions are proportional to the operational time, the result is independent of the capacity factor of the electrolysis unit. Taxes or grid fees are not accounted in this calculation. Moreover, the cost of water proves to be negligible compared to the cost of electricity.

The procedure is graphically illustrated in Figure 2-9. The cumulative price duration curve (green) is generated by ranking all the hourly prices of the 2019 day-ahead market of West Denmark (DK1) in ascending order. A certain point of the curve indicates how long during the year the price has been equal or lower than a certain value. The ascending (red) and descending (blue) average price curves are obtained by averaging the values of the cumulative curve starting from the lowest price and from the highest price, respectively. Therefore, the yearly average electricity price can be read on the right end of the red curve and on the left end of the blue curve. For example, if a methanol selling price of 450 €/t is assumed, a short term WTP of 46.5 €/MWh can be calculated from eq. (2-41). By comparing this value with the cumulative electricity price curve, the number of operating hours in enhanced operation can be estimated to be the 76.3%. For that electrolyser capacity factor, the value on the ascending average electricity price curve identifies the average electricity price in enhanced operating mode (33.7 €/MWh in this example) and the value on the descending average electricity price curve identifies the average electricity price in baseline operating mode (53.9 €/MWh).

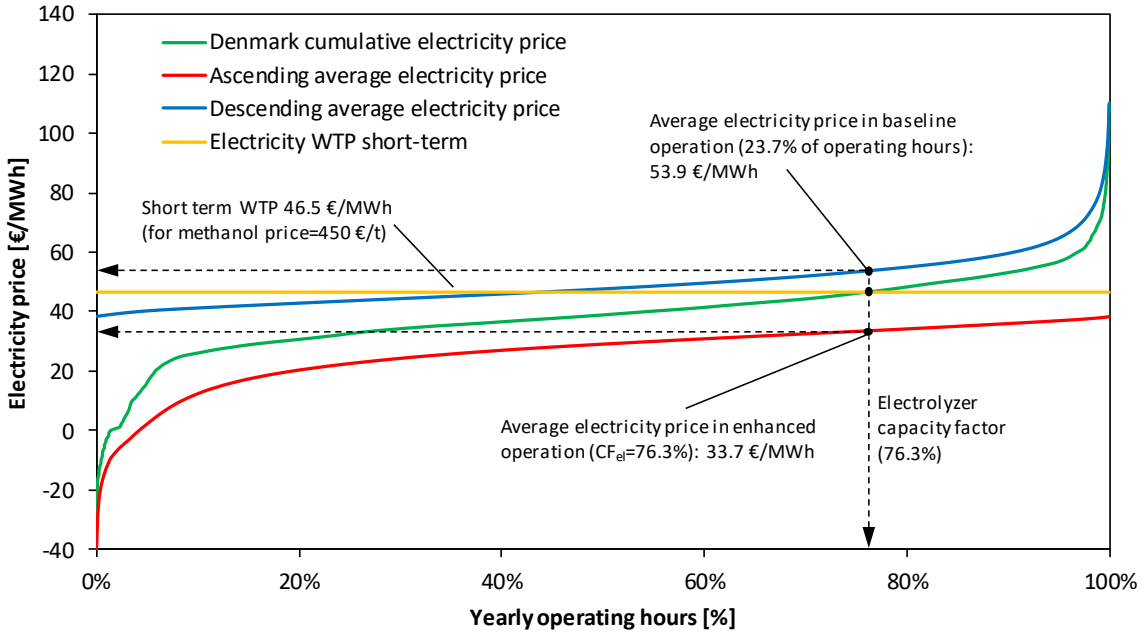

Figure 2-9 - Willingness to Pay approach with 2019 Denmark day-ahead market price curves. Breakeven points and resulting operating hours and electricity prices are shown for a methanol price of 450 €/t.

The electrolyser capacity factor is deeply influenced by the shape of the cumulative electricity price duration curve which depends on different factors such as the location, the penetration of renewable energy sources (RES), the type of RES technology, the price of the fuel and the technology of fossil fuel power plants and the type of final user (Afman et al., 2017; Seel et al., 2018; Ruhnau, 2020; Sorknæs et al., 2020). The general expected tendency is that by increasing the penetration of intermittent RES, the average electricity prices tend to reduce but the peak prices and the cost of grid balancing tend to increase. For the aforementioned reasons, a modified cumulative electricity price curve is added to the discussion, as shown in Figure 2-10. It must be stressed that this hypothetical curve has no ambition of representing any specific future price curve. The aim here is to show the sensitivity of the results on a different curve shape featuring lower average electricity prices and amplified peak prices that may be reasonably expected in future electric systems.

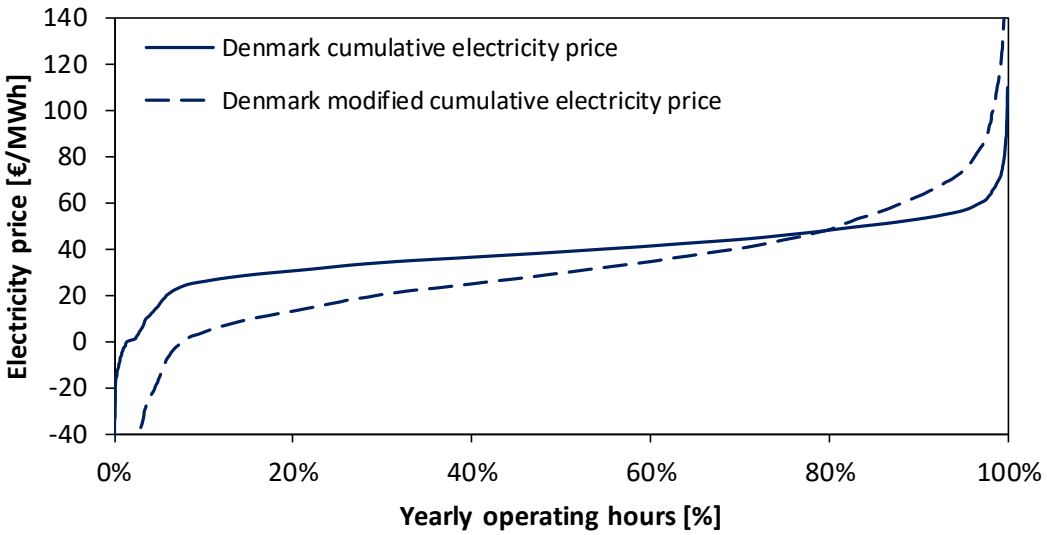

Figure 2-10 – Denmark cumulative electricity price and modified Denmark cumulative electricity price.

Chapter 3
Power and biomass-to-methanol plants

Power and biomass-to-X (PBtX) plants consist in integrating the bio-product production with water electrolysis. A PBtX plant is a producer of bio-/e-products, where the addition of green hydrogen increases the carbon utilization, avoids the release of CO_2 to the atmosphere and leads to higher output for a given feedstock.

In this chapter, techno-economic analyses on Power and biomass-to-methanol plants (PBtM) are reported. Section 3.1 and 3.2 are extensively developed in Poluzzi et al. (2022a) and Poluzzi et al. (2022b), respectively.

PBtX plants may benefit from being operated in a flexible way by modifying the electric power consumption and therefore the amount of hydrogen which is injected in the system. In this way, the system can be operated in the most profitable way by injecting hydrogen in periods of relatively low electricity prices and by cutting the hydrogen production and injection when it is uneconomical. However, none of the scientific works on PBtX systems discussed in in section 1.3 and 1.4 investigate the design of the process units and components conceived to operate flexibly. Moreover, the economic performance of this kind of systems is assessed by fixing the electricity price and by assuming a continuous operation of the electrolysis unit. The influence of a variable electricity price on the system operation is not satisfactorily analysed in the scientific literature.

This chapter provides techno-economic analyses of Power and biomass-to-methanol (PBtM) plants to be operated flexibly depending on the electricity price. The chapter is divided as follows:

- in section 3.1 the optimal equipment design and plant operating criteria following the water electrolysis integration are assessed;
- in section 3.2 plants based on different gasification technologies are compared.

3.1 Design optimization and economic viability of the electrolysis integration

In this section, the flexible PBtM plant shown in Figure 3-1 is assessed, using a low temperature electrolysis technology. The plant is based on the sorption-enhanced gasification (SEG) process, an indirect gasification system with in-situ CO_2 separation by CaO-based sorbent (see section 2.1.3). Following the idea presented in Martínez and Romano (2016), the SEG unit is operated flexibly by controlling the solids circulation rate in order to adjust CO_2 separation in the gasifier and produce a syngas with tailored composition for the downstream synthesis process (Pfeifer et al., 2009; Hawthorne et al.,

2012; Pitkäoja et al., 2020). The proposed system simplifies the syngas conditioning section through process intensification, by avoiding the water gas shift reactor and the CO_2 separation unit. Moreover, the gasification process can be operated flexibly by adapting the sorbent CO_2 uptake on the availability of intermittent hydrogen to be added upstream the methanol synthesis unit.

In addition to the originality of the proposed plant configuration, this section introduces the following main novelties compared to the existing literature in the calculation approach of PBtX plants:

- the economic optimal design of the plant components depends on the number of hours that the plant is expected to operate without hydrogen addition (baseline operation) and with hydrogen addition (enhanced operation), that are closely related to the variability of the electricity price. In this study, the optimal design criteria of all the plant components are provided on the basis of the two operating points. Furthermore, two design criteria are compared for the methanol synthesis section, which is sized on the flow rates of either the baseline operation mode or of the enhanced operation mode;
- the plants designed with the two above-mentioned criteria are calculated considering the off-design operation of the main process units, especially of the gasification island, of the heat recovery steam cycle and of the methanol synthesis and purification units;
- an economic analysis is carried out to compare the two design criteria. In this analysis, the link between the methanol selling price, the electricity price and the number of operating hours in enhanced operation is computed through the willingness to pay approach (van Leeuwen and Mulder, 2018), that takes into account the shape of the cumulative electricity price curve.

In the next sections, first, a technical analysis is conducted by discussing the aforementioned ideas. Then, a differential economic analysis is performed in order to evaluate the feasibility and the economic viability of the electrolyser installation. The economic competitiveness of the PBtM plant is computed with respect to a Biomass-to-Methanol (BtM) plant. The analysis is conducted by computing the e-Methanol production cost and the plant profitability when coupled with the electricity market.

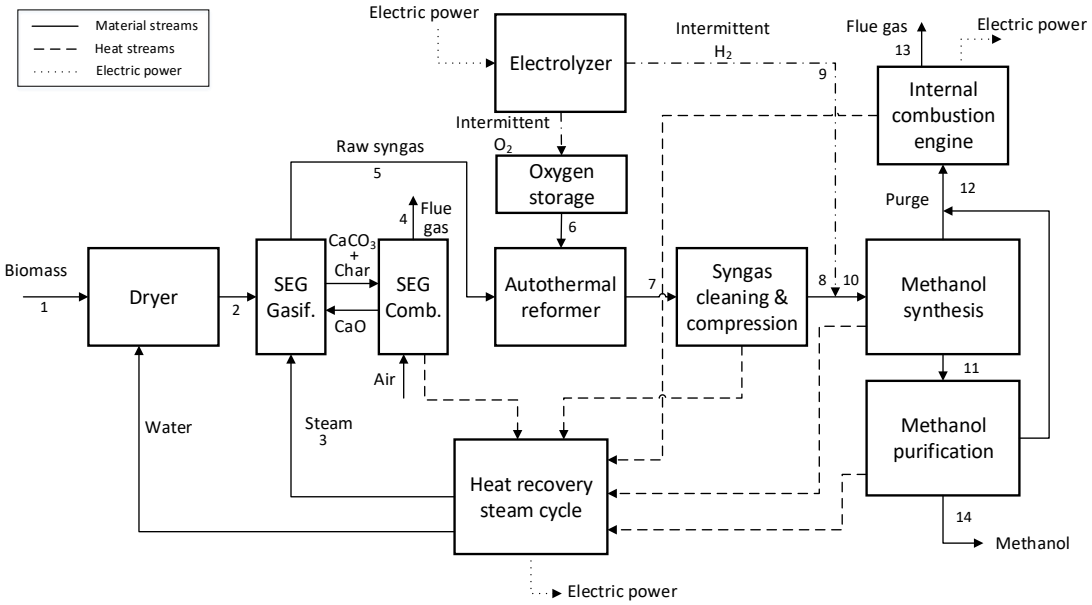

Figure 3-1 – Block diagram of the assessed power & biomass-to-methanol plant

The block diagram of the plant is shown in Figure 3-1 and the stream properties are displayed in Table 3-1 and Table 3-2 for baseline and enhanced operation, respectively. More detailed plant flowsheet and stream properties are included in Appendix A.

The plant unit operations must be designed to manage the intermittent addition of hydrogen, since the electrolyser is turned on only when the electricity price allows an economically viable hydrogen production. Therefore, two main operating points are assessed, namely (i) baseline operation (i.e. without hydrogen addition) and (ii) enhanced operation (i.e. with hydrogen addition).

The process model is developed in Aspen Plus®, which allows to compute the mass and energy balances of the integrated plant. The computations are conducted for a biomass input of 100 MW_{LHV}. The proximate and the ultimate analysis of the as-received biomass are assumed from literature (Pröll and Hofbauer, 2008b) and are reported in Table 2-1.

A detailed description of the methods for the simulation is reported in Chapter 2. An extensive table with the main calculation assumptions is reported in Table A 1 in Appendix A. The next sections are focused on the plant units and operating conditions.

Table 3-1 - Plant stream properties ERD baseline operation

Stream #	**1**	**2**	**3**	**4**	**5**	**6**	**7**	**8=10[1]**	**11**	**12**	**13**	**14**
Stream description	As-received biomass	Dried biomass	Fluidizing steam	Flue gas from combustor	Raw syngas	Oxygen to reformer	Reformed syngas	Syngas to synthesis	Methanol to purification	Purge to ICE	Flue gas from ICE	Methanol
Temperature, °C	25.00	80.00	182.00	156.12	714.07	25.00	800.00	122.68	41.65	35.94	360.00	64.12
Pressure, bar	1.01	1.01	2.00	1.05	1.23	30.00	1.10	92.00	2.00	1.36	1.01	1.01
Mass flow rate, kg/s	10.27	6.64	4.70	16.97	8.68	0.54	9.22	4.37	4.12	0.33	2.71	3.12
Mole flow rate, kmol/h	-	-	939.75	1843.68	2059.43	61.26	2285.44	1318.11	543.22	78.25	356.34	350.31
Composition, $\%_{mol}$	-	-	-	-	-	-	-	-	-	-	-	-
H_2O	-	-	100	0.91	49.11	-	42.25	-	33.76	0.29	17.75	0.19
H_2	-	-	-	-	32.91	-	40.58	70.36	0.16	49.22	-	-
CO_2	-	-	-	27.89	7.12	-	8.35	14.39	0.82	8.05	4.98	-
CO	-	-	-	-	4.39	-	7.45	12.92	-	0.71	-	-
Methanol	-	-	-	-	-	-	-	-	64.88	2.46	-	99.78
CH_4	-	-	-	-	4.30	-	0.39	0.67	0.23	11.26	-	-
C_xH_y	-	-	-	-	1.08	-	-	-	-	-	-	-
O_2	-	-	-	2.99	-	100	-	-	-	-	5.98	-
Ar	-	-	-	0.85	-	-	-	-	-	-	0.81	-
N_2	-	-	-	67.36	1.07	-	0.96	1.67	0.13	27.97	70.49	-
Ethanol	-	-	-	-	-	-	-	-	0.02	-	-	0.03
DME	-	-	-	-	-	-	-	-	-	0.03	-	-
LHV, MJ/kg	9.74	16.37	-	-	9.28	-	8.42	17.76	15.25	14.94	-	19.90
Power, MW_{LHV}	100.0	108.76	-	-	80.56	-	77.68	77.65	62.86	4.94	-	62.00

[1] In baseline operation, stream 8 coincides with stream 10 and hydrogen addition (i.e. stream 9) is not present.

Table 3-2 - Plant stream properties ERD enhanced operation

Stream #	**1**	**2**	**3**	**4**	**5**	**6**	**7**	**8**	**9**	**10**	**11**	**12**	**13**	**14**
Stream description	As-received biomass	Dried biomass	Fluidizing steam	Flue gas from combustor	Raw syngas	Oxygen to reformer	Reformed syngas	Syngas before enriching	Hydrogen	Syngas to synthesis	Methanol to purification	Purge to ICE	Flue gas from ICE	Methanol
Temperature, °C	25.00	80.00	182.00	143.95	771.80	25.00	800.00	120.52	25.00	118.51	40.90	32.52	360.00	64.11
Pressure, bar	1.01	1.01	2.00	1.05	1.23	30.00	1.10	92.00	30.00	92.00	2.00	1.36	1.01	1.01
Mass flow rate, kg/s	10.27	6.64	4.44	14.01	10.86	0.44	11.30	6.63	0.37	6.99	6.67	0.53	4.57	4.97
Mole flow rate, kmol/h	-	-	887.47	1615.16	2190.61	50.05	2404.05	1472.78	654.12	2126.90	875.27	143.62	603.44	559.06
Composition, $\%_{mol}$	-	-	-	-	-	-	-	-	-	-	-	-	-	-
H_2O	-	-	100	3.81	44.41	-	38.64	-	-	-	33.69	0.41	19.80	0.15
H_2	-	-	-	-	28.41	-	35.72	58.31	100	71.13	0.21	62.45	-	-
CO_2	-	-	-	17.76	13.19	-	13.13	21.31	-	14.75	1.52	13.28	5.44	-
CO	-	-	-	-	8.25	-	11.28	18.41	-	12.75	0.01	1.06	-	-
Methanol	-	-	-	-	-	-	-	-	-	-	64.35	2.57	-	99.81
CH_4	-	-	-	-	3.82	-	0.35	0.57	-	0.39	0.13	5.81	-	-
C_xH_y	-	-	-	-	0.96	-	-	-	-	-	-	-	-	-
O_2	-	-	-	3.00	-	100.00%	-	-	-	-	-	-	6.02	-
Ar	-	-	-	0.93	-	-	-	-	-	-	-	-	0.81	-
N_2	-	-	-	74.50	0.95	-	0.86	1.41	-	0.98	0.07	14.39	67.93	-
Ethanol	-	-	-	-	-	-	-	-	-	-	0.03	-	-	0.05
DME	-	-	-	-	-	-	-	-	-	-	-	0.02	-	-
LHV, MJ/kg	9.74	16.37	-	-	7.59	-	7.16	12.20	119.96	17.85	15.05	16.38	0.00	19.91
Power, MW_{LHV}	100.0	108.76	-	-	82.39	-	80.89	80.86	43.94	124.80	100.32	8.67	0.00	99.01

3.1.1 Syngas production

As-received woody biomass (stream 1) is fed to a belt dryer to reduce the moisture content from 45% to 15%. The dried biomass (stream 2) is sent to the fluidized bed sorption-enhanced gasifier, in which the gasification reaction takes place together with the removal of carbon dioxide through carbonation reaction ($CaO + CO_2 \leftrightarrow CaCO_3$). The produced $CaCO_3$ and the residual char are then transferred from the gasifier to the combustor fluidized bed. Here, the combustion of the char and of additional biomass provides the energy required for heating the solids and decomposing calcium carbonate back into calcium oxide. The circulation of hot solids from the combustor to the gasifier allows to thermally sustain the gasification process, through both the sensible heat of the circulating solids and the heat of the carbonation reaction. Solids circulation is tuned to achieve a target CO_2 uptake, which is controlled by the equilibrium of the carbonation reaction. Therefore, by increasing the solids circulation rate, the gasifier temperature increases and the CO_2 separation reduces. In this way, it is possible to obtain a tailored syngas with a target module $M = (H_2 - CO_2)/(CO + CO_2)$, with no need of downstream WGS and CO_2 capture sections.

The flexible operation of the sorption-enhanced gasification unit involves the production of syngas with a module close to 2 in baseline operation and lower than 1 in enhanced operation. The module is controlled by increasing the sorbent circulation rate which causes an increase of the gasification temperature from 714°C in baseline operation to 772°C in enhanced operation. The latter condition leads to zero CO_2 absorption in the gasifier due to thermodynamic limitation. In this way, the syngas retains the maximum amount of carbon (i.e. all the carbon except the unconverted char in the gasifier), which determines the maximum amount of hydrogen addition. Therefore, in enhanced operation the circulating CaO has the only function of heat carrier in the indirect gasification loop. Figure 3-2 compares the dependency of the syngas module on the gasifier temperature obtained with the 0D model in this work against experimental and modelling data in the literature.

Table 3-3 provides the details of the SEG reactor in the baseline and enhanced operating conditions. The char conversion is higher in enhanced operation, due to higher temperature gasification. This requires part of the input biomass to be fed to the combustor in order to achieve the target temperature. As a result of the mass and energy balances, the carbon efficiency of the SEG unit (i.e. the ratio between the carbon in the syngas stream and the inlet biogenic carbon) increases from 42.7 to 68.7% from baseline to enhanced operation. On the other hand, the increase of fuel efficiency (referred to the dried biomass) is minor, from 74.08 to 75.76%.

The combustor is designed in baseline operation, due to the higher flue gases flow rate resulting from the higher combustion power needed for sorbent calcination and from the released CO_2. In enhanced operation, the solid flux at the combustor riser outlet G_s decreases from 30 to 25.4 kg/m^2 s due to the lower mass flow rate and the lower gas density. At the same time, the solids circulation rate between the combustor and the gasifier increases from about 39 kg/s to 137 kg/s, as heat is transferred to the gasifier under a lower temperature variation of the circulating solids. This increased solids circulation corresponds to a minimum flux in the riser of 19.5 kg/m^2 s, which is lower than the actual solids flux, demonstrating that solids circulation can be sustained by the fluid-dynamics of the CFB combustor.

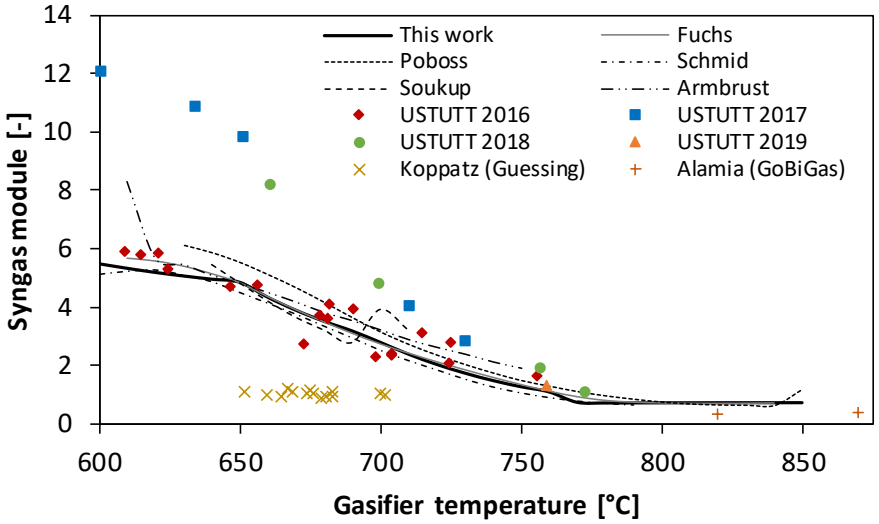

Figure 3-2 - Syngas module as a function of the gasifier temperature from the 0D model of this work, compared with the data from literature (Pröll and Hofbauer, 2008a; Koppatz et al., 2009; Armbrust et al., 2014; Poboß, 2016; Alamia et al., 2017; Schmid et al., 2017; Fuchs et al., 2020) *and with experimental campaigns conducted in the FLEDGED H2020 project framework at the University of Stuttgart (USTUTT)* (Hafner et al., 2018, 2021; Hafner and Schmid, 2020).

Table 3-3 - SEG operating conditions and exit gas composition in baseline and enhanced operations.

Parameter	Baseline operation	Enhanced operation
Gasifier exit temperature, °C	714.1[1]	771.8[2]
H_2, $\%_{mol}$ dry, N_2, Ar free	66.08	52.01
CO, $\%_{mol}$ dry, N_2, Ar free	8.82	15.11
CO_2, $\%_{mol}$ dry, N_2, Ar free	14.30	24.14
CH_4, $\%_{mol}$ dry, N_2, Ar free	8.64	6.99
C_xH_y, $\%_{mol}$ dry, N_2, Ar free	2.16	1.75
H_2O, $\%_{mol}$	49.12	44.42
Syngas module at gasifier outlet	2.24	0.71
Syngas flow rate, kmol/h	2059	2191
Char conversion in the gasifier, % of inlet C	68.06	72.81
Absorbed CO_2, % of inlet C	25.31	0.00
Biomass to gasifier, % of inlet biomass	100.0	94.34
Carbon efficiency, % of inlet C	42.71	68.69
Fuel efficiency, $\%_{LHV}$ of dried biomass	74.08	75.76
Flow rate of solids from combustor to gasifier, kg/s	39.29	137.16
CaO conversion in the gasifier, %	8.95	0.00
Gas superficial velocity at combustor outlet, m/s	5.00	4.38
Solid flux at combustor riser outlet (G_s), kg/m^2 s	30.01	25.44
Minimum solids flux to ensure the solids circulation, kg/m^2 s	5.58	19.48

[1] Gasification temperature is tuned to have a module equal to 2.05 upstream the methanol synthesis.
[2] Gasification temperature is tuned to have no absorbed CO_2 in the gasifier.

Figure 3-3 shows the energy balance of the SEG section in baseline and in enhanced operation, respectively on the left and on the right. The inner circle refers to the input energy to the SEG, the outer refers to the output energy.

The largest part of the input energy is associated to the chemical energy of biomass. Minor contributions derive from the sensible heat of the other streams fed to the SEG unit. In the enhanced operation, the sensible heat contribution associated with the input steam to the gasifier is twice as high the one in baseline operation. This is due to the fact that in enhanced operation the steam is fed to the gasifier at a higher temperature (400°C) than in baseline operation (182°C), which allows to decrease the additional biomass input required by the combustor. However, in baseline operation there is no need of additional biomass to the combustor and a higher steam input temperature would require combustor cooling or higher flue gas temperature.

In both the operating modes, about 72% of the energy output is represented by the chemical energy (LHV basis) of the raw syngas exiting the process. However, less than 49% is useful chemical energy associated to CO and H_2, which can be converted in the downstream synthesis process. More than 23% of the SEG output energy is associated to the heating value of methane and higher hydrocarbons which cannot be exploited for methanol production. This is the reason why a reforming unit downstream the gasification island is needed to achieve competitive performance of the overall plant. Significant contributions to the outlet energy flow are related to the sensible heat of the syngas exiting the gasifier and to the combustor flue gases. The higher contribution to the flue gas cooler for the baseline operation is due to the additional quantity of CO_2 released by sorbent calcination.

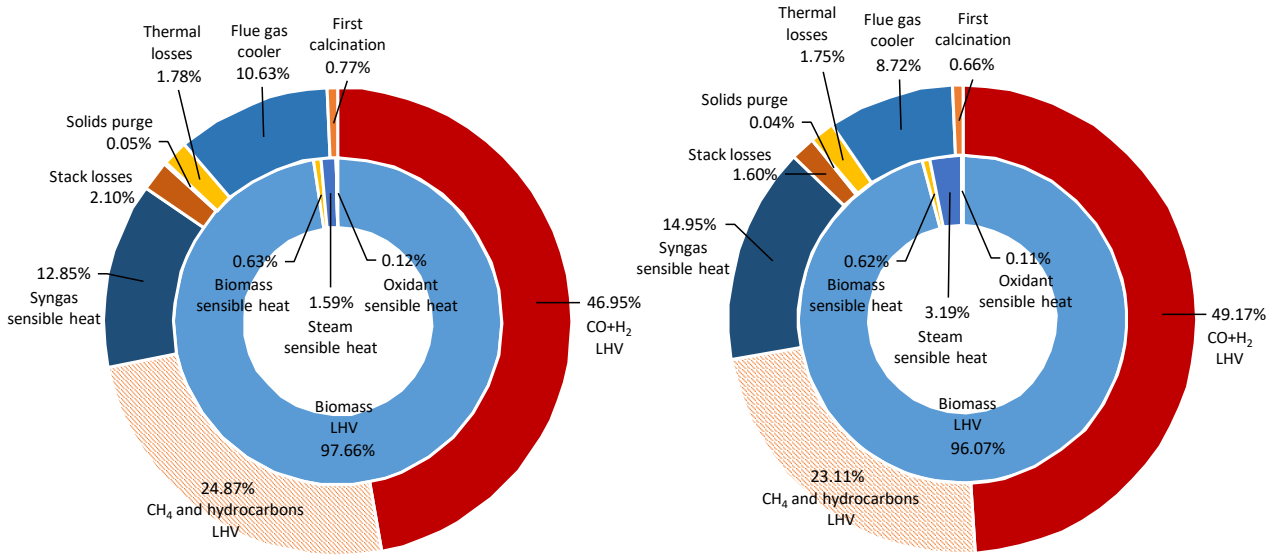

Figure 3-3 - Energy balance of the SEG process. The inner circle refers to the input energy, the outer refers to the output energy. Left: baseline operation. Right: enhanced operation.

Downstream the gasification unit, the raw syngas (stream 5) undergoes a high temperature filtration at the gasifier outlet temperature and is then fed to the raw gas reformer. Oxygen (stream 6) produced as a by-product from the water electrolysis is fed to the ATR to reach the exit temperature of 800°C. An oxygen storage is associated with the reforming unit in order to store the intermittent oxygen production from the electrolysis and to provide a stable flow to the ATR. The minimum capacity factor of the electrolyser which is required to produce the needed oxygen without external import or back-up ASU is 18.6%. By assuming 3 hours of back-up time, an oxygen storage size of about 149 m^3 is needed for storing gaseous oxygen at around 30 bar and ambient temperature. Information about the operating conditions of the ATR are reported in Table 3-4. The higher oxygen demand to heat up the raw syngas to the reforming temperature of the baseline operation is due to the lower gasifier exit temperature.

Table 3-4 - Autothermal reformer operating conditions and exit gas composition in baseline and enhanced operations.

Parameter	Baseline operation	Enhanced operation
Oxygen input, kmol/h	61.26	50.05
H_2, $\%_{mol}$ dry, N_2, Ar free	71.46	59.05
CO_2, $\%_{mol}$ dry, N_2, Ar free	14.71	21.71
CO, $\%_{mol}$ dry, N_2, Ar free	13.12	18.64
S/C at reformer inlet	2.73	1.63
Syngas module at reformer exit	2.04	0.93

Downstream the ATR, the reformed syngas (stream 7) is cooled down to 220°C and scrubbed with water. The scrubber inlet temperature is chosen to avoid the condensation of residual tars (Hannula and Kurkela, 2013). Ammonia and chlorine contained in the gas are removed in the scrubber.

Bulk sulphur removal is performed through a liquid Redox unit (LO-CAT process), where H_2S is converted into elemental sulphur and water by reaction with an iron oxygen carrier. The system is simulated as a black box, with data from (Kazemi et al., 2014).

After bulk cleaning, syngas is compressed in a 7-stage intercooled compressor, with an outlet pressure of about 90 bar and intercoolers outlet temperature of 40°C. Pressure ratio per stage β_{stage} is about 1.9, leading to gas temperature at the outlet of each compression stage 125°C. In enhanced operation, the volumetric flow rate at the syngas compressor inlet increases by 11.7% compared to the baseline operation. This variation can be managed and it is assumed not to affect the compression efficiency.

Activated carbon bed and sulphur scavenging units, used to remove trace contaminants that may poison the catalyst, are placed upstream the last compression stage at a pressure of about 48.6 bar.

The hydrogen enrichment step in the enhanced operation mode is realized just upstream the methanol synthesis section. The water electrolysis unit is designed to provide the maximum hydrogen enrichment in order to retain all the carbon in the syngas. This results in a 63.3 MW_{el} electrolyser which provides 0.37 kg/s of pure hydrogen (stream 9) at 30 bar, that is further compressed to about 90 bar by a 2-stage intercooled compressor without aftercooler before mixing with the syngas stream.

3.1.2 Methanol production

Once purified, conditioned and compressed, the fresh syngas (stream 10) is fed to the methanol synthesis island. The syngas specifications in both the operating modes are shown in Table 3-5. The composition of the fresh syngas shows limited variation in the baseline and in the enhanced operating modes. This also applies to the CO/CO_2 ratio and it largely results from the chemical equilibrium of the WGS reaction at the ATR outlet. The major difference between the baseline and enhanced operation cases lies in the flow rate, which is about 60% higher in the enhanced operation compared to the baseline.

The fresh syngas is first mixed with the unconverted recycled gas and then preheated in a feed/effluent heat exchanger, upstream the methanol synthesis reactor. The temperature of the inlet syngas to the methanol synthesis reactor is set according to the heat exchanger specifications. The outlet crude methanol is cooled down until the dew point temperature of the mixture is reached. The crude methanol is further cooled down to 40°C and separated in a flash unit from the light gases which are recycled back to the reactor.

Table 3-5 - Syngas specifications upstream the methanol synthesis island in baseline and enhanced operating conditions.

Parameter	Baseline operation	Enhanced operation
Temperature, °C	122.68	118.51
Pressure, bar	92.0	92.0
Mass flow rate, kg/s	4.37	6.99
Molar flow rate, kmol/h	1318.11	2126.90
H_2, $\%mol_{dry}$, N_2, Ar free	71.55	71.83
CO_2, $\%mol_{dry}$, N_2, Ar free	14.63	14.90
CO, $\%mol_{dry}$, N_2, Ar free	13.14	12.87
CH_4, $\%mol_{dry}$, N_2, Ar free	0.68	0.40
CO/CO_2	0.90	0.86

The methanol synthesis process and boiling water reactor design are based on the evaluation of the performance, reported in terms of carbon yield and methanol productivity, and on the analysis of the catalyst temperature which must be controlled in order to prevent excessive temperature hot-spot that may lead to catalyst deactivation by Cu cluster sintering (Twigg and Spencer, 2001).

The flexibility requirement also affects the methanol synthesis BWR, for which two different designs are proposed. The two alternatives entail different number of tubes and therefore different amounts of catalyst, selected either to keep high methanol yield in the enhanced operating mode (enhanced reactor design or ERD) or to limit the reactor investment costs (baseline reactor design or BRD). Both the ERD and BRD configurations have some fixed design criteria, among which are the tube length and diameter (i.e. 6 m and 0.04 m, respectively), the reactor pressure and the temperature of the boiling water (i.e. 90 bar and 238°C, respectively).

The number of tubes inside the reactor for each configuration depends on the selected gas hourly space velocity (GHSV), referred to the volume of the reactor tubes. The ERD configuration is designed with a GHSV of 5000 h^{-1} in enhanced operation with a recycle ratio (RR, defined as the molar flow rate of the recycle stream divided by the molar flow rate of the fresh syngas) of 5. In the baseline operation mode, the recycled molar flow rate is kept constant, fixed by the blower design, which involves an increase of RR. In this way, in the baseline operating mode the decrease of GHSV is limited and the overall methanol yield is maximized. The BRD configuration is designed with a GHSV of 5000 h^{-1} and with a RR of 5.0 in the baseline operating mode. When hydrogen is injected into the process, the recycled molar flow rate is kept constant, fixed by the blower design, and the RR reduces. In this way, a limited increase of the GHSV and a decrease of the overall methanol yield. Indeed, the yield performance is reversely correlated to the GHSV: high space velocity leads to lower methanol yield as consequence of the short gas/catalyst contact time (Table 3-6). Thus, the BRD solution is characterized by a lower methanol yield with respect to the ERD, but it guarantees savings on the reactor investment since less reactor tubes are employed. Furthermore, the BRD configuration shows an overall productivity which is higher with respect to the ERD. Differently to the yield, the productivity is indeed favoured by large GHSV.

The performance of the methanol synthesis reactor are reported in Table 3-6. The methanol yield is computed as follows, where F_i are the molar flow rates of the –i molecule.

$$Yield = \frac{F_{M,out} - F_{M,in}}{\left(F_{CO_2} + F_{CO}\right)_{in}} \tag{3-1}$$

Table 3-6 – Performance of methanol synthesis reactor for both ERD and BRD configurations

Parameters	ERD, baseline operation	ERD, enhanced operation	BRD, baseline operation	BRD, enhanced operation
Number of tubes	7580	7580	4704	4704
GHSV, h^{-1}	4684	5000	5000	5512
RR, molar basis	8.06	5.00	5.00	3.10
Recycle flow rate, kmol/h	10625	10625	6595	6595
Methanol yield per pass, %	48.61	46.50	43.07	37.23
Equilibrium yield per pass, %	62.14	64.31	57.92	55.82
Overall methanol yield, %	97.93	96.29	95.40	89.10
Syngas module at reactor inlet	8.60	6.84	5.71	3.98
Inert (CH_4, N_2) concentration at reactor inlet, $\%_{mol}$	37.25	18.71	25.00	8.20
Syngas temperature at reactor inlet, °C	183.3	172.3	175.1	167.8
Thermal power released by the reactor, MW	1.95	5.05	3.20	6.26
Methanol concentration at reactor outlet, $\%_{mol}$	3.56	5.22	5.15	7.14
Methanol concentration at flash unit outlet, $\%_{mol}$	64.88	64.35	64.75	64.30
Methanol productivity, $kg/day/kg_{cat}$	7.10	11.35	11.15	16.91

The inert concentration at the reactor inlet is directly related to the RR which is adopted in the specific operating mode. The thermal power released by the reactor is proportional to the inert amount.

The molar fraction of the reactants (H_2, CO_2 and CO) and products (H_2O and methanol) is higher in the enhanced operating modes. Conversely, the amount of inert gases (N_2 and CH_4) is far larger in the baseline operations (in particular in ERD where it approaches ∼40%), coherently with the higher inert concentration in the inlet streams. However, the methanol yield per passage is lower in the cases with H_2 addiction in absolute value and also if compared with the equilibrium one. This is due to the larger production of water that inhibits the reaction kinetics.

An important parameter to consider in the analysis is the maximum catalyst temperature. The hot-spot temperature should be limited, to avoid the CZA catalyst deactivation due to the Cu clusters sintering (Twigg and Spencer, 2001). The calculated catalyst centreline temperature axial profiles are reported in Figure 3-4. In all cases analysed, the temperature increases in the inlet zone of the reactor, driven by the heat provided by the boiling water (238°C). The heat released by the exothermic reactions makes the temperature increase to a hot-spot maximum (reached between 1-2 m for all the case analysed) and then the temperature flatters at the boiling water value due to the decrease of reaction rates related to the approach to the thermodynamic equilibrium. The parameter that mainly control the temperature in the four cases analysed is the amount of inert (N_2 + CH_4) at the reactor inlet. Indeed, the smoothest temperature profile with the lowest hot-spot (245°C) is obtained in the ERD baseline operating mode, due to dilution effect given by the largest amount of inert that is ∼37% in molar fraction. Instead, the highest hot-spot (252°C) is obtained in the BRD enhanced operating mode where the inert is only ∼8%. The other two cases, ERD enhanced operating mode and BRD baseline operating mode, have ∼19% and ∼25% of inert gas content respectively and show the same intermediate hot-spot temperature (248°C). The differences are however minimal due to the relatively low exothermicity of the methanol synthesis from CO_2 (ΔH_r= -49.4 kJ/mol_{CO2}) and since the effect of the lower inert concentration is partly compensated by the higher GHSV (i.e. higher flow velocity) and the larger thermal conductivity (related to the high conductivity of the molecular hydrogen) in

the enhanced operations. All in all, the maximum temperature are well below the critical temperature limit of 300 °C reported in literature for the catalyst CZA catalyst (Twigg and Spencer, 2001). Therefore, the reactor can manage efficiently the thermal duty in each of the cases analysed.

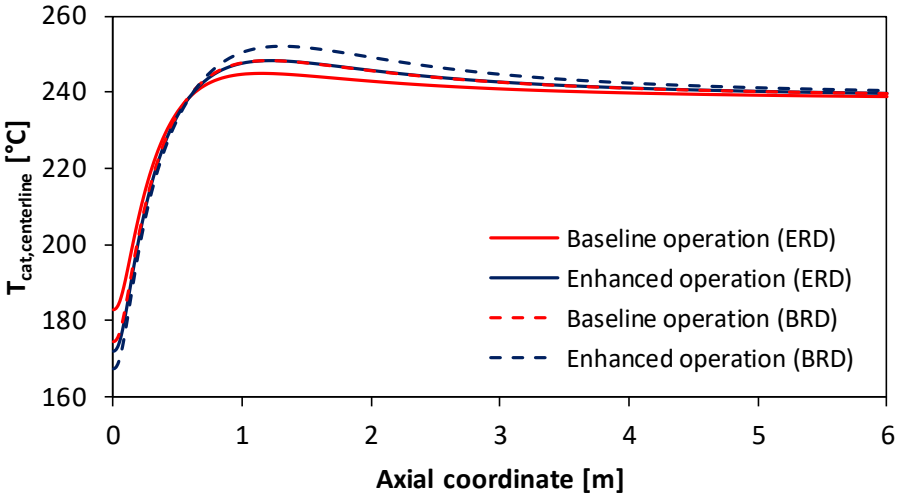

Figure 3-4 - Catalyst centerline temperature axial profiles.

Upstream the methanol purification island, the raw methanol is expanded to 2 bar by means of a valve and reaches a temperature of about 40 °C. The raw product is composed of methanol (~64%$_{mol}$), water (~33%$_{mol}$) and other components (mainly low boiling impurities and traces of ethanol), with a different composition for each considered case, as reported in Table 3-7. In the enhanced operation mode, the flowrate of methanol to be purified increases by 62% for the ERD case and by 55% for the BRD case with respect to baseline operation. Such flow rate variation must be managed by the purification unit.

The purification section is composed, for all the cases, of two distillation trayed columns in series. The first unit is a stabilizing column operating at 1.3 bar, aiming at removing the low boiling impurities. The heavier stabilized methanol-rich stream is fed to the second column, a concentration column run at atmospheric pressure, to obtain the methanol product stream with a purity of 99.85%$_{wt}$. The recovery in this stream of the methanol fed to the purification section is > 99%. The two columns are simulated with a rate-based approach, to take into account the mass transfer occurring on each tray.

The first column performs the separation with 23 valve trays, and the second one with 48 valve trays. The selected diameter allows to treat operate the columns in the two operating modes without significant issues of flooding or weeping, which would decrease the separation performance of the column. To this aim, for both the stabilizing unit and the concentration one, the dimensions are determined on the basis of the highest feed flowrate, resulting in diameters of 0.7 m for the stabilizing column and ~2 m for concentration column.

Table 3-7 - Characteristics of the raw methanol streams fed to the purification section for the assessed cases.

Parameter	ERD, baseline operation	ERD, enhanced operation	BRD, baseline operation	BRD, enhanced operation
Mass flow rate at purification inlet, kg/s	4.12	6.67	4.06	6.28
Molar flow rate at purification inlet, kmol/h	543.22	875.27	530.38	810.07

Parameter	ERD, baseline operation	ERD, enhanced operation	BRD, baseline operation	BRD, enhanced operation
Methanol concentration at purification inlet, $\%_{mol}$	64.88	64.35	64.75	64.30
H_2O concentration at purification inlet, $\%_{mol}$	33.76	33.69	33.03	31.78
Stabilizing column				
Condenser duty, MW	0.011	0.023	0.016	0.043
Reflux ratio	0.10	0.10	0.10	0.10
Reboiler duty, MW	0.66	1.08	0.66	1.04
Boilup ratio	0.13	0.13	0.13	0.14
Concentration column				
Condenser duty, MW	6.31	10.17	6.18	9.49
Reflux ratio	0.85	0.87	0.86	0.88
Reboiler duty, MW	6.24	10.06	6.11	9.39
Boilup ratio	3.01	3.01	3.09	3.23

In all the cases, the reflux ratio and the boilup ratio for the stabilizing column are low, in the range of 0.10-0.14, because of the low vapor being condensed at the top and because of the low amount of liquid being vaporized in the reboiler. As for the concentration column, which performs the separation between the two main components, higher amounts of circulating flowrates are needed, which involves high reflux and boilup ratios.

3.1.3 Heat recovery and power generation

The waste heat made available in the temperature range 1000 °C to 30 °C ranges from 79 MW for the enhanced operating mode to 66 MW for the baseline mode. A heat recovery steam cycle (HRSC) is used to recover such heat from the different plant sections and to convert it into electricity and steam for internal consumption. Moreover, the purge from the methanol synthesis and purification units (stream 12) contains a significant amount of light gases, whose heating value is exploited in a cogenerative internal combustion engine (ICE) for electricity and steam/hot water production.

The heat-related data depend on the operating mode calling for a flexible design of the heat exchanger network (HEN) and HRSC. For this reason, multiperiod methodologies are used to find the optimal arrangement of the HEN and HRSC (see section 2.1.7). The performance map of the ICE is evaluated in the same way as reported in section 2.1.7, by using linearized equations derived by Zatti et al. (2018).

In Table 3-8, the ICE and the heat recovery steam cycle electric power outputs and net electric efficiencies are shown for the different cases, with the reference BtM plant included. The highest electricity production from the ICE for the BRD enhanced operation is related to the lowest RR in the methanol synthesis unit and therefore to the highest purge flow rate. The same reasoning can be extended to the baseline ERD, which shows the lowest ICE electricity production due to the highest RR and the consequent lowest purge flow rate. As mentioned above, the net electric efficiency of the ICE decreases in baseline operation according with the decrease of the thermal power of the purge flow from the methanol synthesis and purification island. The ICE in the BtM plant displays higher electric power output and efficiency than ICE in the baseline operating modes because it operates in design condition.

As far as the HRSC design and performance are concerned, the optimal design substantially depends on the availability of high temperature heat and on the required steam exports of the different cases/operating modes. Due to the lower high temperature heat available in the ERD plant and the

higher methanol production, leading to higher heat demand for methanol purification, the optimal HRSC results to be without the HP evaporation level, differently from the BRD and the reference plants. As a result, also the efficiency and power output are significantly lower in the ERD plant.

Table 3-8 - ICE and heat recovery steam cycle electric power outputs and net electric efficiencies. Steam flow rates at HP (120 bar), MP (32.2 bar) and LP (6.5 bar) turbine inlet are also reported.

Parameter	ERD, baseline operation	ERD, enhanced operation	BRD, baseline operation	BRD, enhanced operation	Reference BtM plant
ICE					
Electric power, MW	2.15	4.00	2.73	7.91	3.17
Net electric efficiency, %	43.23%	46.40%	39.96%	46.40%	46.40%
HRSC					
HP/MP evaporation pressure levels, bar	32.2		120 / 32.2		120 / 32.2
Steam flow rate at HP turbine inlet, kg/s	-	-	8.1	7.5	8.5
Steam flow rate at MP turbine inlet, kg/s	7.4	4.5	9.6	10.3	9.5
Steam flow rate at LP turbine inlet, kg/s	7.2	6.1	9.3	9.9	9.2
Net electric power, MW	4.24	2.95	8.30	8.02	8.02
Net electric efficiency, %	20.52%	14.76%	29.31%	28.54%	30.38%

In Figure 3-5 and Figure 3-6, the complete temperature heat diagram and the grand composite curve of the PBtM plant with ERD design in enhanced operation mode are reported.

Table 3-9 – Heat sources and sinks of the ERD PBtM plant in enhanced operation

	Heat sources	Heat sinks
A	SEG combustor flue gas cooler	Superheater MP, Reheater MP, evaporator MP, economizer, superheater LP, concentration column reboiler
B	SEG combustor flue gas cooler	Air preheater
C	Syngas cooler	Economizer, evaporator MP, concentration column reboiler
D	Scrubber water cooler	Cooling water
E	Syngas compressor intercoolers	Belt dryer heat exchanger
F	Hydrogen compressor intercooler	Economizer, cooling water
G	Methanol synthesis reactor	Evaporator MP
H	Methanol cooler	Syngas feed preheater
I	Methanol condenser	Cooling water
J	HRSC condenser	Stabilizing column reboiler
K	Concentration column condenser	Belt dryer heat exchanger, economizer, cooling water
L	HRSC condenser	Concentration column reboiler
M	HRSC condenser	Belt dryer heat exchanger
N	ICE flue gas cooler and hot water production	Superheater LP, economizer, belt dryer heat exchanger

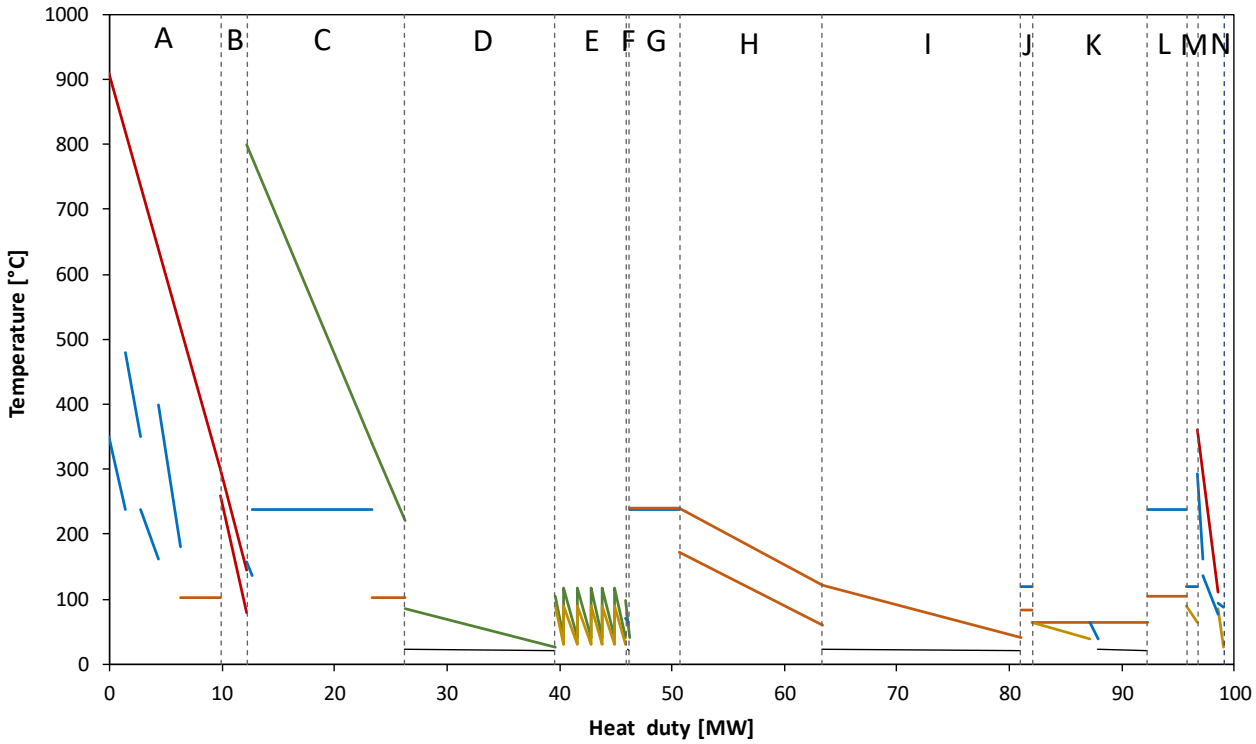

Figure 3-5 – T-Q diagram of the ERD PBtM plant in enhanced operation. Heat exchangers sections codes are indicated in Table 3-9.

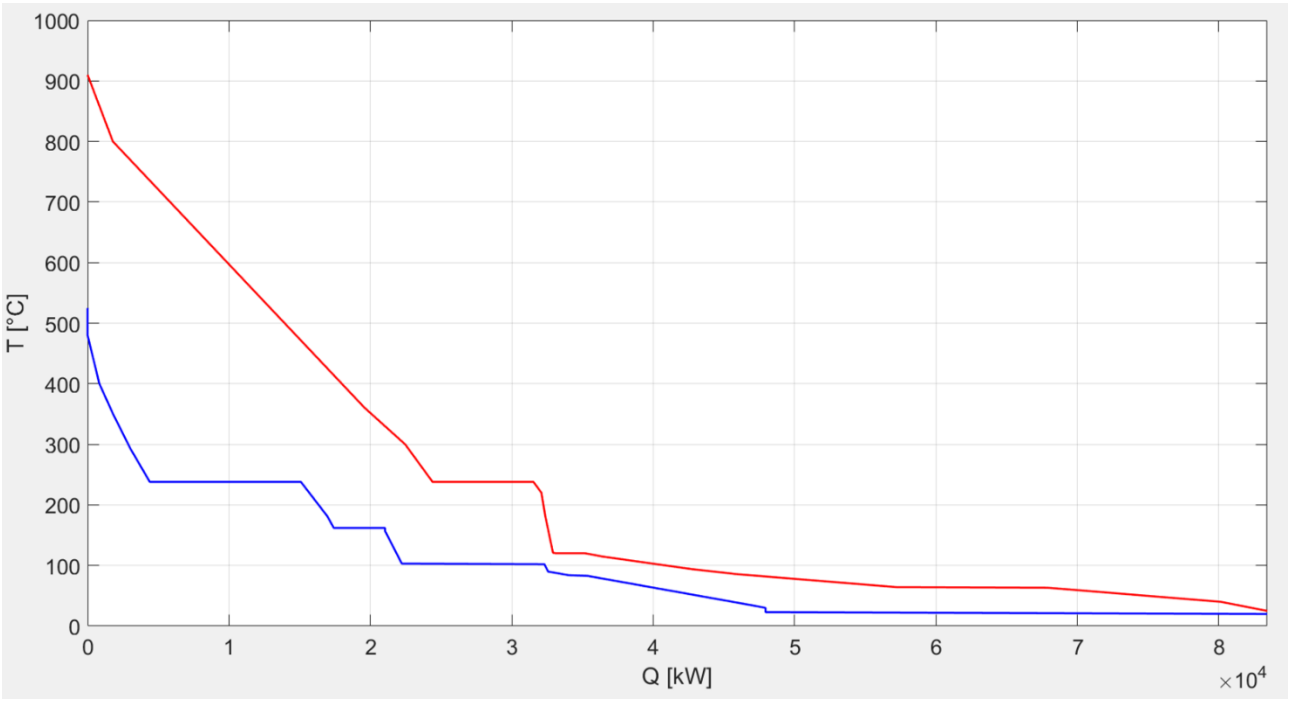

Figure 3-6 – Grand composite curve of the ERD PBtM plant in enhanced operation.

3.1.4 Process simulation results

The performance indexes of the assessed PBtM plants and of the reference BtM plant are reported in Table 3-10.

As mentioned above, the enhanced operation guarantees a higher utilization of the biogenic carbon contained in the feedstock compared to the baseline operation. The higher carbon utilization ensures a higher fuel efficiency and a higher useful fuel efficiency of the SEG unit.

The lower gasifier exit temperature and the higher methane content also cause a lower fuel efficiency of the reformer in baseline operation, due to the higher oxygen demand to heat up the raw syngas to the reforming temperature and to provide the heat for methane reforming. On the other hand, the gain in the useful fuel efficiency is higher in these cases, thanks to the higher amount of reformed CH_4.

As regards the methanol synthesis island, the higher yield of the baseline operation for both ERD and BRD configurations involves higher fuel efficiencies with respect to the enhanced operations. The difference of methanol yield and fuel efficiency between the baseline and the enhanced operations is relatively small for the ERD case, where methanol synthesis efficiency reduces by about 1 percentage point. On the other hand, in the BRD the fuel efficiency drops by about 5 points when operated in enhanced operation mode.

In the purification island, the BRD configuration in enhanced operation mode shows a slightly higher fuel efficiency and useful fuel efficiency due to the lowest content of water in the raw methanol feed.

The resulting fuel efficiency of the overall plant is higher in enhanced operation than in baseline operation for both ERD and BRD configurations. The ERD configuration is more fuel efficient than the BRD because of a more efficient methanol synthesis section. The fuel efficiency is 68.8% vs. 63.8% in enhanced operation for ERD and BRD cases respectively and 62.0% vs. 60.4% in baseline operation. The gap in global fuel efficiency between the two operating modes is lower in BRD configuration because the enhanced operation shows the lowest fuel efficiency of the methanol synthesis section (74.3%). The increase of carbon efficiency made possible by hydrogen addition is significant, especially with the ERD design, where it increases from 40.3% in baseline operation to 64.4% in enhanced operation mode.

The effect of hydrogen injection in boosting methanol production is higher in the ERD configuration than BRD and involves higher hydrogen-to-fuel (84.2% vs. 71.4%) and power-to-fuel efficiencies (57.5% vs. 52.3%).

The overall electric consumption in enhanced operation is dominated by the electrolysis consumption. The higher syngas mass flow rate and the inlet hydrogen also contribute in increasing the electric consumption for gas compression. The higher amount of waste water in the enhanced operating mode is due to the higher water flow rate produced as bottom product in the concentration column.

The technical performance of the reference BtM plant is identical to the BRD baseline operation as far as biomass conversion is concerned. However, since the oxygen is provided by a cryogenic ASU, there is an additional electric consumption, computed assuming a specific consumption of 0.272 kWh_{el}/kg_{O2} (Queneau and Marcuson, 1996).

Table 3-10 - General performance of Power & Biomass-to-Methanol plant

Performance indexes	ERD, baseline operation	ERD, enhanced operation	BRD, baseline operation	BRD, enhanced operation	Reference BtM plant
$\eta_{F,dry}$, %	108.75	108.75	108.75	108.75	108.75
$\eta_{F,SEG}$, %	74.08	75.76	74.08	75.76	74.08
$\eta^{u}_{F,SEG}$ (input: biomass; output: H_2, CO), %	48.40	51.51	48.40	51.51	48.40
$\eta_{F,ref}$, %	96.42	98.18	96.42	98.18	96.42
$\eta^{u}_{F,ref}$ (input and output: H_2, CO), %	143.78	141.03	143.78	141.03	143.78
$\eta_{F,pur}$, %	99.96	99.96	99.96	99.96	99.96
$\eta^{u}_{F,pur}$ (input and output: H_2, CO), %	100.00	99.99	100.00	99.99	100.00

Performance indexes	ERD, baseline operation	ERD, enhanced operation	BRD, baseline operation	BRD, enhanced operation	Reference BtM plant
$\eta_{F,MeOH\_syn}$, %	80.95	80.39	78.83	74.30	78.83
$\eta^{u}_{F,MeOH\_syn}$ (input: H_2, CO; output MeOH), %	82.56	81.22	80.44	75.12	80.44
$\eta_{F,MeOH\_pur}$, %	98.63	98.69	98.63	98.97	98.63
$\eta^{u}_{F,MeOH\_pur}$ (input and output: MeOH), %	99.24	99.16	99.17	99.37	99.17
$\eta_{F,global}$,%	62.00	68.78	60.37	63.75	60.37
$\eta_{F,eq}$, %	57.19	33.25	64.20	33.90	63.47
Carbon efficiency, %	40.34	64.40	39.27	59.67	39.27
Oxygen demand in the reformer, kg/s	0.54	0.44	0.54	0.44	0.54
Methanol production, kg/s	3.12	4.97	3.03	4.61	3.03
Methanol output, MW_{LHV}	62.00	99.01	60.37	91.76	60.37
Methanol yield, %	97.93	96.29	95.40	89.10	95.40
H_2 addition, kg/s	-	0.37	-	0.37	-
H_2 addition, MW_{LHV}		43.94		43.94	
Methanol production enhancement, %	-	59.63	-	51.93	-
η_{PtF}, $MW_{LHV,M}/MW_{el}$	-	57.48	-	52.27	-
η_{HtF}, $MW_{LHV,M}/MW_{H2}$	-	84.21	-	71.44	-
Net electric output, P_{el}, MW	-2.86	-67.24	2.03	-58.01	1.66
Electric generation, MW	6.38	6.95	11.02	15.92	11.19
Electric consumption, MW	9.24	74.19	8.99	73.93	9.53
Belt dryer	0.65	0.65	0.65	0.65	0.65
SEG air fan	0.75	0.73	0.75	0.73	0.75
Syngas compressor	7.15	7.95	7.15	7.95	7.15
Hydrogen compressor	-	0.88	-	0.88	-
Recycle compressor	0.67	0.67	0.41	0.41	0.41
Electrolyser	-	63.29	-	63.29	-
Other auxilieries[1]	0.03	0.03	0.03	0.03	0.03
ASU	-	-	-	-	0.53
Total waste water, kg/s	5.77	6.16	5.73	5.97	5.73

[1] Other auxiliaries include Liquid Redox and water scrubber pump.

In Figure 3-7, the trend of the carbon efficiency, potential carbon efficiency and useful potential carbon efficiency is reported for the baseline and for the enhanced operating mode of the ERD configuration. The trend of the carbon efficiency indexes is qualitatively the same in the BRD plants, which are not shown. The evolution of all these indicators is followed along intermediate streams within the plant by following the approach adopted in Poluzzi et al., (2020) (see section 2.2.2). In the bar chart, the total amount of each atom is represented by the complete bar enclosed in the red contour. The yellow part of the bars represents the maximum amount of each atom that can end up in the final product, therefore, they are in the same proportion as the corresponding atoms in the final product. The blue part of the bars shows the potential loss of carbon and hydrogen to separate the excess oxygen as H_2O or CO_2. Oxygen excess is distributed to carbon and hydrogen in order to maximize the yield of final product. The red part of the bar (when present) represents the excess of hydrogen or carbon after the removal of the excess oxygen.

As-received biomass features a carbon-to-hydrogen ratio much higher than that of methanol (0.70 vs. 0.25) and the oxygen excess causes the PCE to be equal to 70%. By means of the drying process, part of the water is removed from the biomass and this results in a PCE decrease to about 47%. In the dried biomass, hydrogen becomes the limiting element, therefore the oxygen excess can be removed as CO_2 without affecting the maximum fuel yield, as excess carbon remains available (red portion of the C bar).

As shown in Figure 3-7 (top) which describes the baseline operation, the PCE decreases to about 43% in the SEG unit. This is due to the loss of carbon from the gasifier to the combustor, where the char is burned and the absorbed CO_2 is vented. This represents the main loss of carbon, which is

intrinsic in indirect gasification processes and is responsible for the lower carbon efficiencies achievable compared to systems based on direct gasification processes, as discussed in (Poluzzi et al., 2020). As a result of the carbon loss in the gasifier, carbon becomes the limiting element in the raw gas, that features a hydrogen excess (red portion of the bar). CE also drops in the gasifier to the same value of the PCE, due to carbon separation through both the unconverted char and the absorbed CO_2. Simultaneously, the PCE_u reduces to about 27% because of the presence of CH_4 and C_xH_y, which are inert in the downstream methanol synthesis. No substantial variation of the PCE occurs across the reformer for the assumed conditions, as the added oxygen can bond with the excess hydrogen and be entirely removed as water. On the other hand, the PCE_u increases to about 42% due to the conversion of the hydrocarbons into useful reactants (H_2 and CO). As the extent of CO_2 separation in the SEG is tuned to achieve the target syngas module after the reformer, no change of PCE and CE is observed in the conditioning step, which consists in a simple water separation. The final overall carbon efficiency in baseline operation is about 40.3% for the ERD configuration and about 39.3% for the BRD configuration. The slight difference between the two is mainly due to the different performance of the methanol synthesis section.

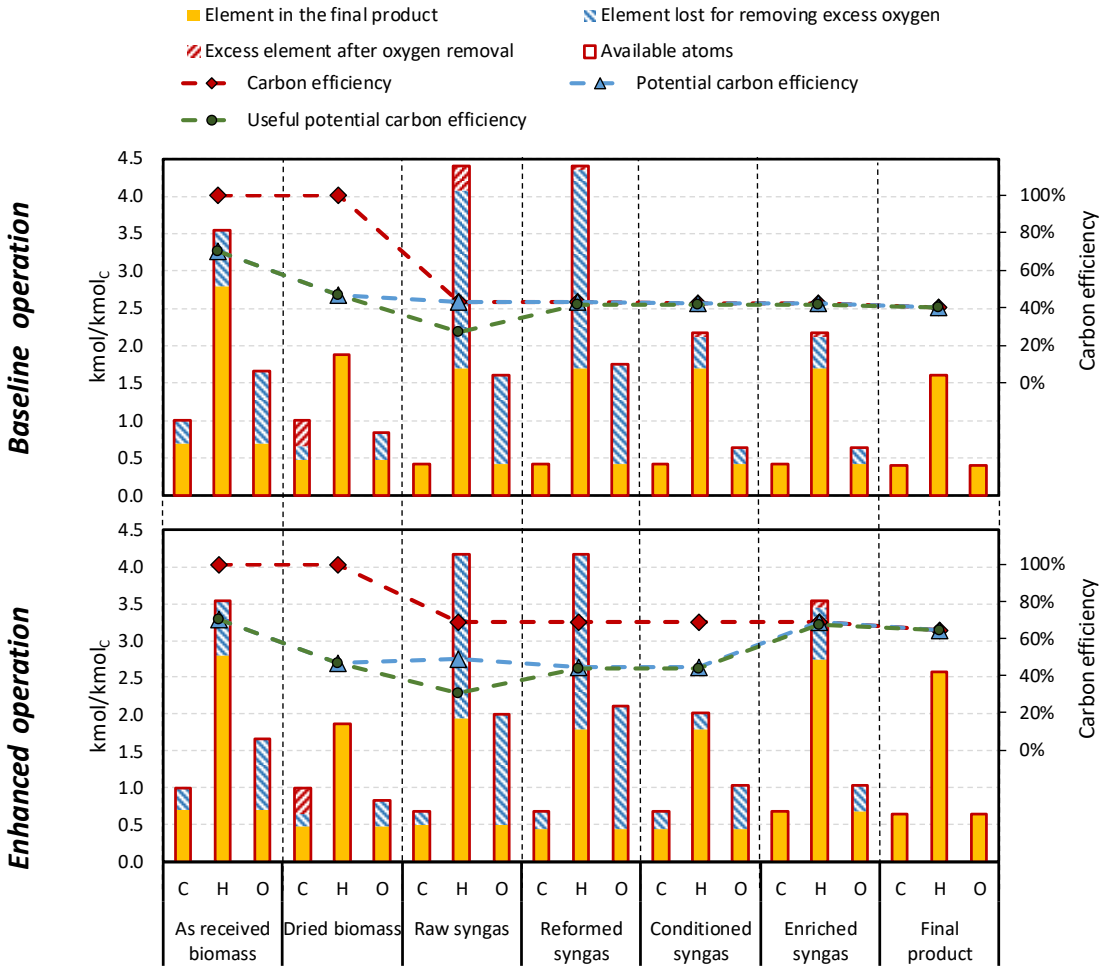

Figure 3-7 - Carbon efficiency, potential carbon efficiency and useful potential carbon efficiency of the process in baseline (top) and enhanced (bottom) operation for the ERD configuration.

In enhanced operation, carbon separation is controlled by increasing the solid circulation rate and therefore the gasifier temperature compared to the baseline operation. The raw syngas features a higher CE compared to the baseline operation (about 69%), since less carbon is separated in the gasifier. The PCE of the raw syngas in enhanced operation is about 6% higher than baseline operation

thanks to a higher content of carbon, which was the limiting element in the baseline operating mode. The PCE reduces within the reformer from about 49% to 45%. Then, CE and PCE do not change through the cleaning and conditioning step. The gap between the CE and the PCE represents the gain of carbon efficiency that may be achieved by hydrogen addition. This gap is filled in the enriching stage, where the PCE increases to the same value of the CE. As shown in the bar chart, the added hydrogen allows to recover the carbon which is potentially lost to remove the excess oxygen, behaving as an oxygen acceptor. The final overall carbon efficiency in enhanced operation is about 64.4% for the ERD configuration and about 59.7% for the BRD configuration. The difference between the two is mainly due to the different performance of the methanol synthesis section, which is amplified compared to the baseline operation cases.

3.1.5 Levelized cost of electro-fuel

The method applied for the economic analysis of the PBtM plants is the *Levelized Cost* approach (see section 2.2.3). In this part, a differential economic analysis approach is adopted with the aim of quantifying the economic impact of the electrolysis integration in the assessed biofuel production plants.

The costs of the PBtM plants are compared with the costs of a BtM plant, whose main differences are the absence of the electrolysis system and the presence of an ASU to produce oxygen for the reformer. The objective of the differential approach is to evaluate if flexible PBtM plants are economically competitive with the reference BtM plant. In this regard, the Levelized Cost of the e-Fuel (LCOe-F) can be defined as in eq.(3-2), where ΔC_{tot} is the difference in total costs between PBtM and BtM plants, which results from the sum of the differential TCI and the differential $C_{O\&M}$, and $\dot{m}_{e\text{-}fuel}$ is the additional e-Methanol (e-MeOH) produced thanks to the electrolysis integration.

$$LCOe\text{-}F = \frac{\Delta C_{tot}}{e\text{-}M_{tot}} = \frac{\Delta TCI \cdot CCF + \Delta C_{fixed\ O\&M} + \Delta C_{ut}}{\dot{m}_{e\text{-}fuel} \cdot h_{eq}} \tag{3-2}$$

A detailed description of the approach, the main assumptions and parameters for the economic analysis is present in section 2.2.3.

In Table 3-11, the fixed capital investment costs of the assessed plants are reported. Process units that do not differ in BtM and PBtM plants (e.g. biomass drying, gasifier and reformer) are not reported in the table as they do not affect the differential economic analysis. The PBtM plants benefit from the absence of the ASU, which is present in the BtM case. However, as already reported in section 3.1.1, an oxygen storage is needed for the ATR. In this case, a 30 bar gaseous oxygen storage sized to cover 3 hours of continuous operation is considered, whose costs was estimated to be about 45% the avoided ASU cost. The capital investment for the syngas compressor is slightly higher for PBtM plants, since they are designed for a higher flow rate. The ERD option shows higher costs for both the methanol synthesis reactor and the recycle compressor, i.e. 11.9 M€ and 3.2 M€ respectively, compared to 7.4 M€ and 2.2 M€ of the BtM and BRD cases. As regards the two distillation columns, the PBtM plants display slightly higher capital investment, as both are designed for the enhanced operation. The advantage in capital cost of the BRD flexible plant, that benefits from a smaller methanol synthesis unit, is compensated by the higher cost of the power island, needed to recover the energy from the purge gas from the MeOH synthesis unit. Finally, the PBtM configurations exhibit a major additional cost for hydrogen production in the electrolysis unit and compression, which count for about 75-95% of the total differential FCI. The assumed specific cost for the electrolysis system is 700 €/kW_e which is consistent with the current alkaline technology and with the future cost estimations of PEM technology (Bertuccioli et al., 2014; International Energy Agency, 2019).

Overall, the cost of the larger steam cycle of the BRD plant with respect to the ERD plant, overcompensates the lower cost of the methanol synthesis island, resulting in higher differential FCI.

Table 3-11 - Fixed capital investment costs of the units of the PBtM and the BtM plants used in the differential economic analysis. The units with the same investment cost in the different plants are not reported.

Fixed capital investment, M€	Reference BtM plant	BRD PBtM plant	ERD PBtM plant
Biomass-to-syngas island			
ASU (with O_2 compressor)	10.74	-	-
Oxygen storage	-	4.51	4.51
Cleaning and conditioning island			
Syngas compressor	19.88	21.35	21.35
Other units	6.72	6.94	6.98
Syngas-to-methanol island			
Methanol synthesis BWR	7.35	7.35	11.86
Recycle compressor	2.21	2.21	3.15
Stabilizing column	0.45	0.49	0.49
Concentration column	1.49	1.84	1.86
Power island			
CHP internal combustion engine	1.78	4.27	2.23
HRSC	33.43	40.45	26.13
Electricity-to-hydrogen island			
Electrolyser	-	44.31	44.31
H_2 compressor	-	4.66	4.66
Total differential FCI	-	63.87	51.11

A degree of freedom in the plant design is the size of the oxygen storage. The optimal size depends on the frequency of electrolyser switching. By assuming to store oxygen at the same production pressure of 30 bar and at 25°C, the resulting density is 39.4 kg/m^3. With a reformer oxygen consumption in baseline operation of 0.54 kg/s, the volume of buffer storage for 3-hour operation without electrolysis is 149 m^3. An insufficient size of the storage may lead to the need of importing oxygen from an external producer or switching the electrolyser on at low load to produce the exact amount of oxygen needed in the plant, when the electricity price is higher than the breakeven price.

When operated at full load, the oxygen produced by the electrolyser is 4.4 times higher than the flow rate of oxygen required in the reformer (10.53 t/h vs. 1.96 t/h). Therefore, the minimum capacity factor of the electrolyser to produce the oxygen required in the ATR without external import or back-up ASU is 18.6%. Possible revenues from the sale of the excess oxygen are not included in this analysis, although an economic income of about 2.9 M€ (about 20% of the annual electricity cost) may be obtained assuming an oxygen selling price of 54 €/t.

In Table 3-12, the main economic results of the levelized cost approach are shown. The ERD PBtM plant shows 1.5% higher differential total costs with respect to the BRD configuration, but ensures 24% higher e-Methanol production, leading to ~20% lower LCOe-F of the produced methanol. Although a consistent comparison with other studies is not possible, it is interesting to observe that the obtained LCOe-F costs lie in the upper range of the biomethanol costs obtained in the relevant literature reported in Table 1-1.

Table 3-12 – Main result of the economic analysis and levelized cost of e-fuel

Economic results	BRD PBtM plant	ERD PBtM plant
Differential TCI, M€/y	7.50	6.00
Differencial fixed O&M, M€/y	6.50	5.99
Differential purchased electricity cost, M€/y	12.88	15.30
Differential total costs, M€/y	26.88	27.29
e-Methanol production, t/y	35768	44530
LCOe-F, €/t	751.4	612.92
LCOe-F, €/GJ	37.76	30.80

In Figure 3-8, the LCOe-F breakdown is reported. The main contribution is associated to the purchase of electricity, whose share is about 48% and 56% in BRD and ERD plants, respectively. The share of the electrolyser capital cost is about 20% in both cases. The fixed Opex share is in the range 22-24%, with BRD as upper bound. Other costs, resulting from the net contribution of the avoided ASU and the other capital investments, contribute by about 9% in BRD and 3% in ERD plants.

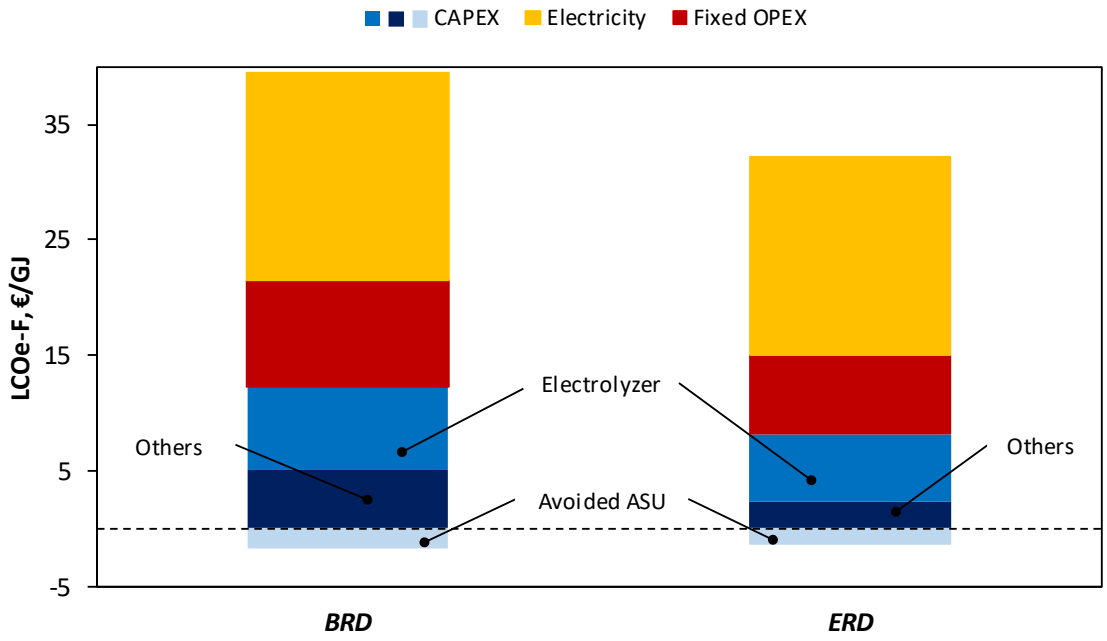

Figure 3-8 - LCOe-F breakdown for the BRD and ERD cases.

Overall, from this analysis, it can be concluded that designs aimed at high power-to-methanol conversion efficiencies (i.e. the ERD design in this case study) should be preferred due to the high cost of hydrogen production compared to the cost associated to oversizing the equipment for fuel synthesis.

3.1.6 Sensitivity analysis

The LCOe-F is deeply influenced by the operating hours in enhanced operation and by the average electricity price. In Figure 3-9, the dependency of the electrolyser capacity factor and the average electricity price on the LCOe-F is shown for the ERD case. Increasing CF_{el} from 20 to 80%, leads to a reduction of the LCOe-F by about 30 €/GJ, independently of the average electricity price in enhanced operation.

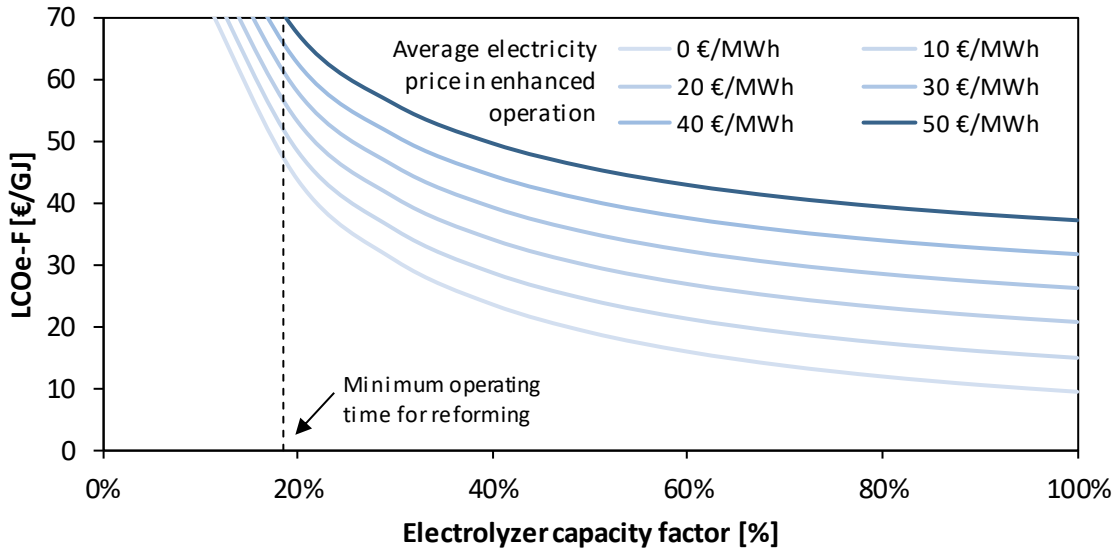

Figure 3-9 - LCOe-F of the ERD PBtM plant as a function of the electrolyser capacity factor and of the average electricity price in enhanced operation, for an electrolyser cost of 700 €/kW.

The electrolyser investment cost is also a key factor influencing the LCOe-F. Figure 3-10 shows the effect of a reduction of the electrolyser investment cost from 700 €/kW to 400 €/kW, considered as a potential cost in favorable long-term scenarios (Blanco et al., 2018). The benefit of a reduction of the cost of electrolysis is much higher for low capacity factors, where the costs of green hydrogen are dominated by the Capex. For CF_{el} of 20%, the LCOe-F cost reduces by 16.6 €/GJ with a low cost electrolyser. For capacity factor of 80%, the LCOe-F reduction is 4.8 €/GJ, i.e. -15.6% with the reference electricity price.

These results show that the impact of increasing the capacity factor from 20% to 80% on the cost of the e-fuel is significantly higher than the impact of a reduction of the electrolyser capital cost, once the pre-requisite of high electrolyser capacity factor is met.

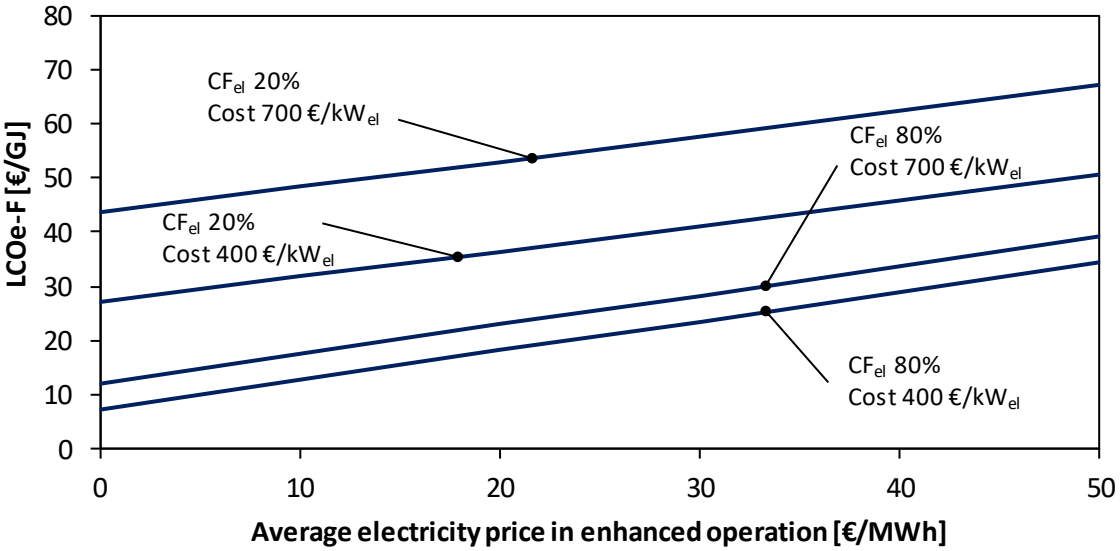

Figure 3-10 - LCOe-F for the ERD PBtM plant as a function of the average electricity price in enhanced operation. The different cases refer to changes in the electrolysis capacity factor (80% and 20%) and in the electrolysis investment costs (700 €/kW and 400 €/kW).

3.1.7 Economic feasibility

The 'Willingness to pay' (WTP) approach, presented in section 2.2.4, allows to identify the number of hours of operation in baseline and enhanced modes and the corresponding average electricity prices for a certain methanol selling price. From this data, the profitability of the PBtM plant investment compared to the reference BtM option can be evaluated by computing the Net Present Value (NPV) and the Internal Rate of Return (IRR).

In Table 3-13, NPV and IRR are reported for two methanol selling prices, that lead to two different capacity factor of the electrolysis unit through the WTP methodology. The calculation is performed with two different capital investment of the electrolysis unit. A methanol selling price of 450 €/t (i.e. same order the market price of fossil methanol) involves an electrolysis capacity factor of 76.3%. At this condition, the investment results unprofitable (negative NPV) compared to the reference BtM plant, independently of the electrolyser cost. If the methanol selling price increases to 600 €/t, the electrolyser capacity factor increases to 97.8% and the PBtM plant becomes competitive, especially with the low electrolyser cost.

Table 3-13 - Profitability of the plant investment for two different methanol selling prices and electrolyser investment costs.

Parameter	**Value**			
Methanol price, €/t	**450**		**600**	
CF_{el}	76.31%		97.75%	
Electricity price, €/MWh (enhanced operation)	33.73		37.73	
Electricity price, €/MWh (baseline operation)	53.86		71.85	
Electrolyser cost, €/kW	**700**	**400**	**700**	**400**
NPV	-60.79	-24.62	-3.68	32.49
IRR	-	-8.61%	8.93%	24.70%

The results discussed above show that a profitable investment requires high methanol selling price, that involves very high capacity factor. This means that the added value of a flexible PBtM

plant is limited compared to an inflexible PBtM plant that always keeps the electrolyser in operation. However, this result strongly depends on the shape of the cumulative electricity price curve.

In Figure 3-11, the IRR is reported as a function of the methanol selling price for an electroylser investment cost of 400 €/kW. The functions are derived from the 2019 Denmark electricity price curve and from the modified curve. The solid lines refer to the flexible PBtM plant, where the increase of the MeOH selling price involves an increase of the electrolyser capacity factor, with the method described previously. The dashed lines refer to inflexible plants, with 100% capacity factor of the electrolysis system, purchasing the electricity at the yearly average electricity price of the current price curve (38.5 €/MWh) and of the modified curve (30.4 €/MWh). The IRR value of 10% defines the region above which the PBtM plants are considered profitable with respect to the reference BtM plant.

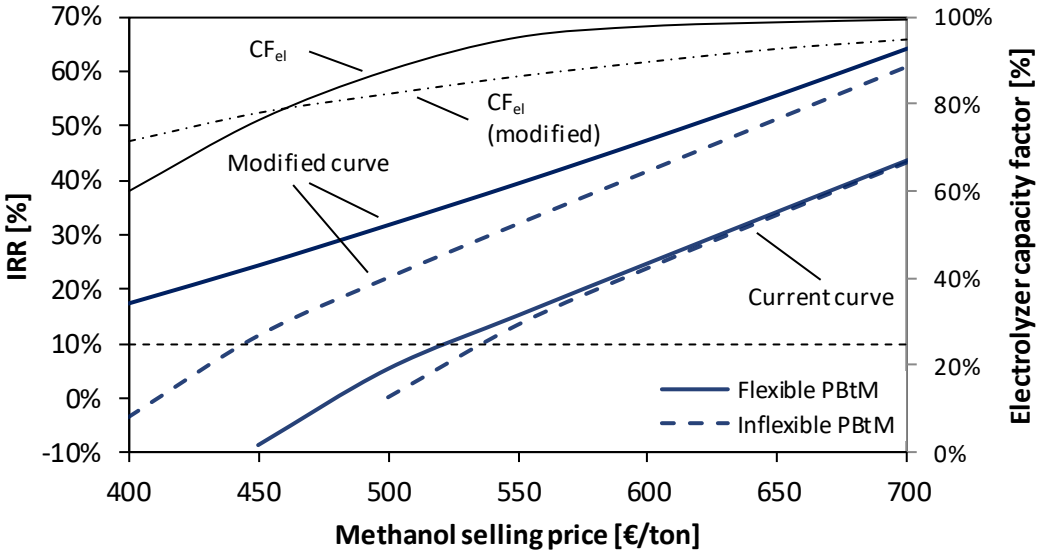

Figure 3-11 –IRR as a function of the methanol selling price for an electrolyser investment cost of 400 €/kW. Curves are derived from the two electricity price curves shown in Figure 2-10.

The curves which derive from the current Danish electricity prices ('current' curve) display profitable investment compared to the BtM route at methanol selling prices higher than about 525 €/t. The curves derived from the modified data show profitable investment compared with the reference option at significantly lower methanol selling prices. This is due to the lower average electricity price of the modified curve with respect to the Denmark one. For both the cases, it can be observed that the solid line is always above the dashed line, meaning that flexible operation of the electrolyser always leads to a more profitable investment than an inflexible plant. However, with the current electricity price curve, the solid and dashed lines are very close for a wide range of methanol prices, indicating a little advantage of flexible operation. On the contrary, with the modified electricity price curve, the flexible PBtM plant becomes significantly more profitable than the inflexible PBtM plant.

3.1.8 Conclusions

This section assessed, from techno-economic perspectives, different design and operational criteria of Power & Biomass-to-Methanol (PBtM) plants capable to operate flexibly without hydrogen addition (baseline mode) and with hydrogen addition (enhanced mode). Two designs are compared for the methanol synthesis reactor, with different number of tubes, selected either to keep high methanol yield in the enhanced operating mode (enhanced reactor design) or to limit the reactor investment cost (baseline reactor design).

The following main conclusions can be listed from this analysis:

- Due to the high cost of hydrogen from electrolysis in comparison with the cost of oversizing the methanol synthesis unit, enhanced reactor design is to be preferred over baseline reactor design. Oversizing of the reactor allows significantly higher carbon efficiency in enhanced operating mode (64.4% vs. 59.7%), higher power-to-MeOH efficiency (57.5% vs. 52.3%) and 20% lower cost of the e-MeOH (30.80 vs. 37.76 €/GJ_{LHV}) with the baseline assumptions of this analysis (i.e. 80% of electrolyser capacity factor and 2019 Denmark day-ahead market electricity price).
- Due to the high cost of the electrolysis system, competitive cost of the produced e-MeOH can only be achieved with high electrolyser capacity factors. The impact of increasing the capacity factor from 20% to 80% on the cost of the e-fuel is significantly higher than the impact of a reduction of the electrolyser capital cost, once the pre-requisite of high electrolyser capacity factor is met. A reduction of the cost of the electrolyser from 700 to 400 €/kW_{el} operating with a capacity factor of 80%, involves a reduction of the LCOe-F by 4.8 €/GJ. On the other hand, increasing the capacity factor from 20 to 80% with an electrolysis cost of 700 €/kW, leads to a reduction of the LCOe-F by about 30 €/GJ.
- The high electrolyser capacity factor, needed to make economically competitive a PBtM plant, may reduce the advantage of a plant designed for flexible operations. In fact, with the 2019 Denmark electricity price curve, a limited economic advantage has been calculated for a flexible plant compared to an inflexible plant always operating in enhanced operating mode regardless of the hourly electricity price. Nevertheless, the attractiveness of the flexible plant may increase significantly in future scenarios with very high penetration of intermittent renewables, leading to low average electricity prices, but also longer periods of high peak prices.
- A prerequisite to make PBtM plants economically competitive is that the bio-MeOH and e-MeOH selling price must be sufficiently high to determine high “willingness to pay” price for the electric energy and therefore high electrolyser capacity factors. With the 2019 Denmark electricity price curve, an e-MeOH selling higher than about 500 €/t are required.

3.2 Different gasification technologies comparison

This section provides a further analysis of PBtM plants to be operated flexibly depending on the electricity price. The main novelties compared to the scientific literature are the following:

- a comparative techno-economic analysis of PBtM plants based on three different gasification technologies (direct, indirect and sorption-enhanced gasification) is carried out;
- the design and operational criteria of the plants conceived to operate flexibly in baseline (i.e. without hydrogen addition) and enhanced operation (i.e. with hydrogen addition) are assessed, comparing the characteristics of the different gasification technologies;
- the economic competitivity of flexibly operated plants when integrated with the electricity market is discussed, compared to inflexible plants conceived to operate with constant hydrogen input.

In Figure 3-12, Figure 3-13 and Figure 3-14, the block diagrams of the assessed PBtM plants, based on oxygen-blown direct gasification (DG), indirect gasification (IG) and sorption-enhanced gasification (SEG) are shown. The properties of the main streams indicated in the figures are reported in Appendix A (from Table A 16 to Table A 21).

The plant unit operations are designed to manage the intermittent addition of hydrogen, since the electrolyser is turned on only when the electricity price allows an economically viable hydrogen production. Therefore, two main operating points are assessed, namely (i) baseline operation (i.e. without hydrogen addition) and (ii) enhanced operation (i.e. with hydrogen addition).

The process model is developed in Aspen Plus®, which allows to compute the mass and energy balances of the integrated plant. The computations are conducted for a biomass input of 100 MW_{LHV}. The proximate and the ultimate analysis of the as-received biomass are assumed from literature Pröll and Hofbauer, (2008b) and are reported in Table 2-1.

A detailed description of the methods for the simulation is reported in Chapter 2. An extensive table with the main calculation assumptions is reported in Table A 1 in Appendix A. The next sections are focused on the plant units and operating conditions.

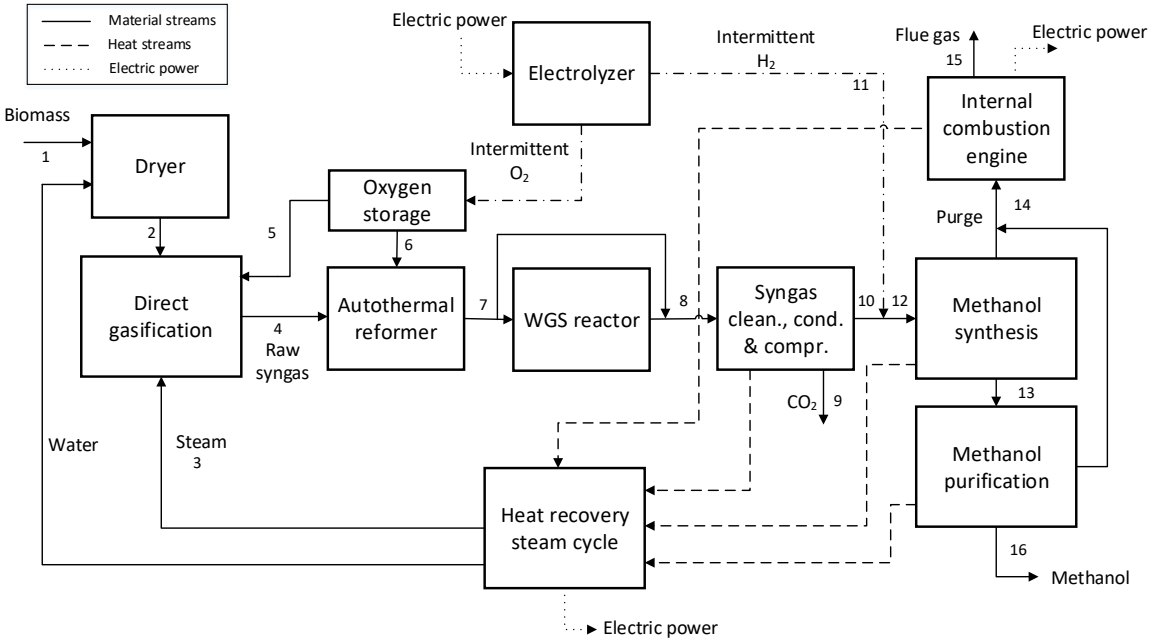

Figure 3-12 - Block diagram of the DG-based power & biomass-to-methanol plant

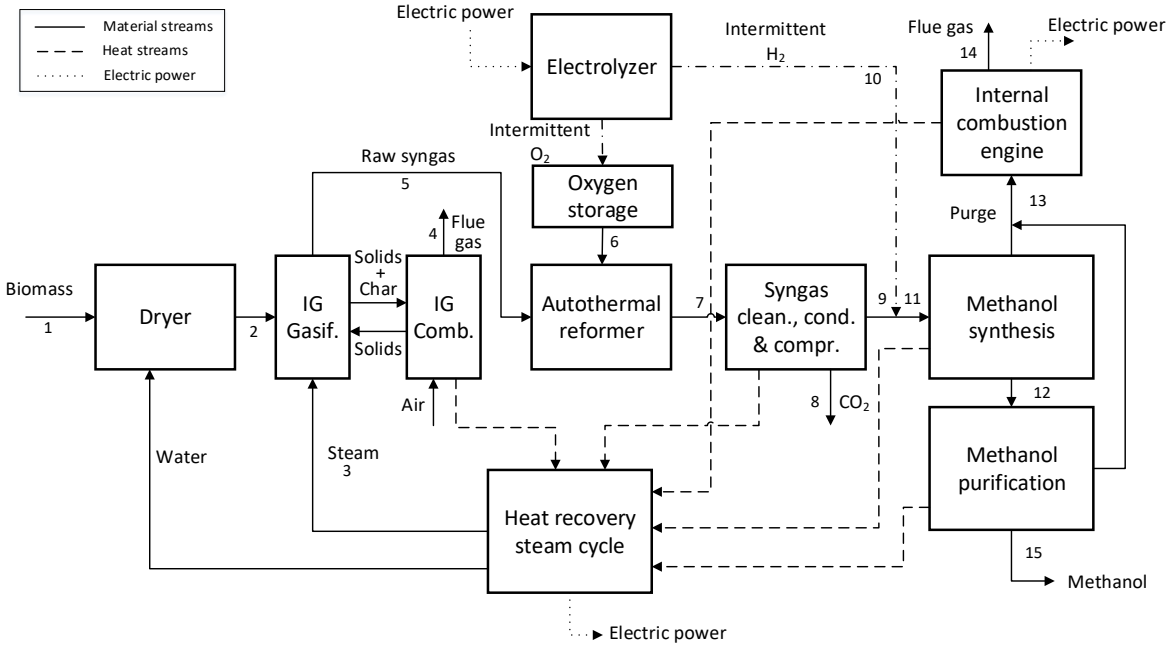

Figure 3-13 - Block diagram of the IG-based power & biomass-to-methanol plant

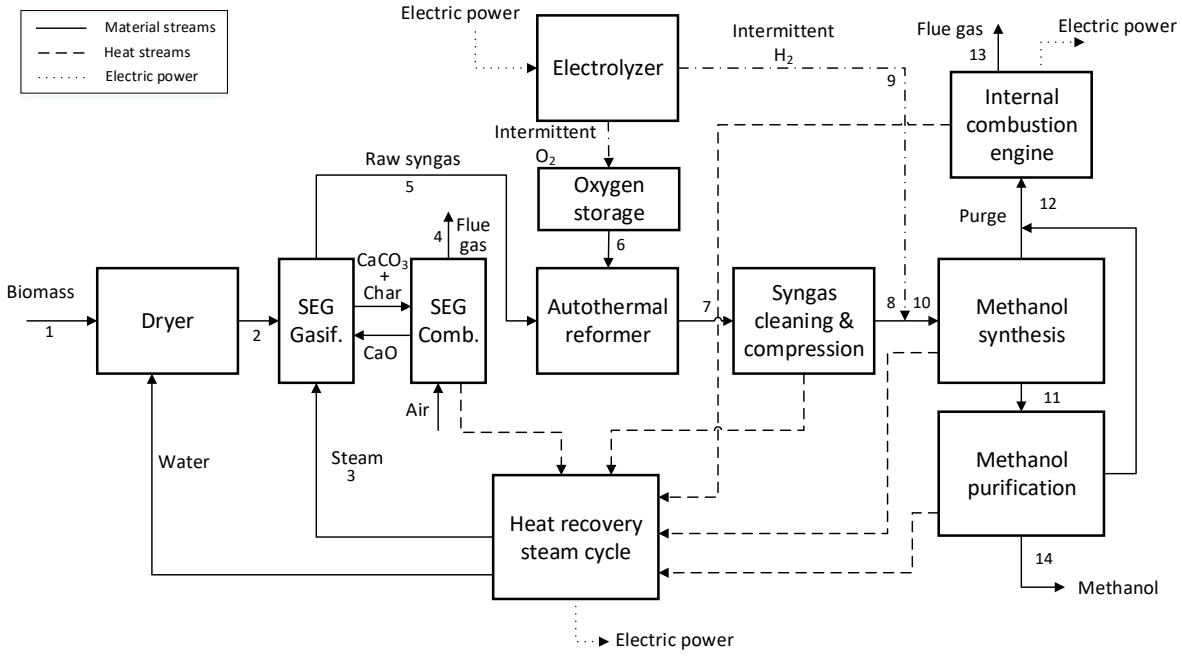

Figure 3-14 - Block diagram of the SEG-based power & biomass-to-methanol plant

3.2.1 Syngas production

As-received woody biomass (stream 1) is fed to a belt dryer to reduce the moisture content from 45% to 15% and the dried biomass (stream 2) is sent to the gasification island.

A detailed description of the gasification technologies and models has been carried out in section 2.1.3 and 2.1.4.

The operating conditions are displayed in Table 3-14 and the comparison of the simulated syngas composition with literature data for DG and IG is reported in Table 2-4.

The flexible operation of the sorption-enhanced gasification unit entails the production of syngas with a module close to 2 in baseline operation and lower than 1 in enhanced operation. Following the approach modelled and tested in the scientific literature (Pröll and Hofbauer, 2008a; Koppatz et al., 2009; Armbrust et al., 2014; Poboß, 2016; Schmid et al., 2017; Fuchs et al., 2020; Hafner and Schmid, 2020; Hafner et al., 2021; Pitkäoja et al., 2021), the module is controlled by increasing the sorbent circulation rate which causes an increase of the gasification temperature from 714°C in baseline operation to 772°C in enhanced operation. The latter condition leads to zero CO_2 absorption in the gasifier due to thermodynamic limitation. In this way, the syngas retains the maximum amount of carbon (i.e. all the carbon except the unconverted char in the gasifier), which determines the maximum amount of hydrogen addition. Therefore, in enhanced operation the circulating CaO has the only function of heat carrier in the indirect gasification loop.

The DG and the IG options produce a syngas with the same characteristics in both the operating conditions. The control criteria for the plant operation with intermittent hydrogen addition are applied in the conditioning section, as discussed afterwards.

Table 3-14 - Gasifiers operating conditions and exit gas composition.

Parameter	**DG**	**IG**	**SEG BO**	**SEG EO**
Gasifier outlet temperature, °C	870.0	815.0	714.1[1]	771.8[2]
Gasifier outlet pressure, bar	4.0	1.4	1.4	1.4
H_2, $\%_{mol}$ dry, N_2, Ar free	34.1	44.7	66.1	52.0
CO, $\%_{mol}$ dry, N_2, Ar free	25.0	23.1	8.8	15.1
CO_2, $\%_{mol}$ dry, N_2, Ar free	29.8	19.9	14.3	24.1
CH_4, $\%_{mol}$ dry, N_2, Ar free	7.6	9.7	8.6	7.0
C_xHy, $\%_{mol}$ dry, N_2, Ar free	3.4	2.6	2.2	1.8
H_2O, $\%_{mol}$	40.5	36.3	49.1	44.4
Syngas module at gasifier outlet	0.08	0.58	2.24	0.71
Syngas flow rate, kmol/h	2044	1710	2059	2191
Char conversion in the gasifier, % of inlet C	95.50	83.00	68.06	72.81
Biomass to gasifier, % of inlet biomass	100.0	86.20	100.0	94.34
Oxygen input, kg/s	1.84	-	-	-
Carbon efficiency, % of inlet C	95.50	71.55	42.71	68.69
Fuel efficiency, $\%_{LHV}$ of dried biomass	79.36	78.06	74.08	75.76
Flow rate of solids from combustor to gasifier, kg/s	-	168.69	39.29	137.16
Gas superficial velocity at combustor outlet, m/s	-	5.00	5.00	4.38
Solid flux at combustor riser outlet (G_s), kg/m^2 s	-	13.57	30.01	25.44

[1] Gasification temperature is tuned to have a module equal to 2.05 upstream the methanol synthesis.

[2] Gasification temperature is tuned to have no absorbed CO_2 in the gasifier.

Downstream the gasification unit, the raw syngas undergoes a high temperature filtration before the raw gas reformer. The ATR is fed with oxygen produced as a by-product from water electrolysis. An oxygen storage is associated with the reforming unit in order to store the intermittent oxygen production from the electrolysis and to provide a stable flow to the ATR. The minimum capacity factor of the electrolyser which is required to produce the needed oxygen without external import or back-up ASU is 15.1%, 18.6% and 41% for IG, SEG and DG-based plant, respectively. By assuming 3 hours of back-up time, an oxygen storage size of about 130, 149 and 670 m^3 is needed for storing gaseous oxygen at around 30 bar and ambient temperature in IG-, SEG- and DG-based plant, respectively. The higher minimum plant capacity factor and volume storage for the DG-based plant is related to the need of providing oxygen not only to the ATR but also to the gasifier unit. Due to the high volume of the storage which implies significant capital costs and safety-related aspects, a DG

configuration without the storage is added to the discussion in section 3.2.5. Information about the operating conditions of the ATR for all the configurations are reported in Table 3-15. The higher oxygen demand to heat up the raw syngas to the reforming temperature is mainly related with the gasifier exit temperature and the reforming temperature.

Downstream the ATR of the DG-based plant, the syngas is cooled to 300°C and fed to the sour WGS reactor which allows to adjust the syngas composition prior to the CO_2 removal step. In baseline operation, about 40.6% of the syngas is fed to the WGS reactor and the rest is bypassed. In enhanced operation, the WGS reactor is entirely bypassed and no shift occur. In IG- and SEG-based plants, this reactor is not present.

In all the configurations, the syngas is cooled down to 220°C and scrubbed with water. The scrubber inlet temperature is chosen to avoid the condensation of residual tars (Hannula and Kurkela, 2013). Ammonia and chlorine contained in the gas are removed in the scrubber.

Bulk sulfur removal is performed through a liquid Redox unit (LO-CAT process), where H_2S is converted into elemental sulfur and water by reaction with an iron oxygen carrier. The system is simulated as a black box, with data from Kazemi et al. (2014).

After bulk cleaning, in DG- and IG-based plants, the syngas undergoes a compression to 30 bar through a 4-stage and a 6–stage intercooled compressor, respectively. In the SEG-based plant, the syngas is compressed in a 7-stage intercooled compressor, with an outlet pressure of about 90 bar. In all the configurations, the intercoolers outlet temperature is 40°C and the pressure ratio per stage β_{stage} is about 1.8, leading to gas temperature at the outlet of each compression stage below 125°C. In SEG-based plants, the volumetric flow rate at the syngas compressor inlet increases by 11.7% in the enhanced operation compared to the baseline. This variation can be managed by the compressor control system and it is assumed not to affect the compression efficiency. In DG- and IG-based plants, a CO_2 removal unit based on MDEA allows to remove 90% of the CO_2 contained in the syngas in baseline operation. The unit is bypassed in enhanced operation in order to retain all the carbon in the syngas. The SEG configuration does not need such a unit, because the syngas composition is tuned within the gasifier.

In DG- and IG-based plants, a second intercooled compressor with 2 stages allows to increase the pressure to about 90 bar.

Activated carbon bed and sulfur scavenging units, which are used to remove trace contaminants that may poison the catalyst, are placed upstream the last compression stage at a pressure of about 50 bar.

The H_2 enrichment step in the enhanced operation mode is realized just upstream the second intercooled compressor for DG- and IG-based plant, being the hydrogen available at 30 bar. For SEG configuration, the H_2 addition is realized just upstream the methanol synthesis section, therefore the hydrogen stream at 30 bar is further compressed to about 90 bar by a 2-stage intercooled compressor without aftercooler before mixing with the syngas stream. The water electrolysis unit is designed to provide the maximum hydrogen enrichment in order to retain all the carbon in the syngas. This results in a 129, 67.5, 63.3 MW_{el} electrolyser for DG-, IG- and SEG-based plants, respectively.

As already mentioned, in the DG configuration, the syngas module is controlled by controlling amount of syngas which bypasses the WGS reactor in baseline operation and by bypassing the WGS reactor and the CO_2 removal unit in enhanced operation. In the IG-based plant, the CO_2 removal unit is bypassed in enhanced operation. In the SEG configuration, syngas module is tuned within the gasifier depending on the hydrogen availability, by modifying the solids circulation rate.

Table 3-15 - Autothermal reformer operating conditions and exit gas composition. Syngas conditioning operating conditions.

Parameter	DG	IG	SEG BO	SEG EO
Reformer outlet temperature, °C	915.0	800.0	800.0	800.0
Oxygen input, kmol/h	67.8	53.2	61.26	50.05
H_2, $\%_{mol}$ dry, N_2, Ar free	45.80	56.45	71.46	59.05
CO_2, $\%_{mol}$ dry, N_2, Ar free	24.40	17.89	14.71	21.71
CO, $\%_{mol}$ dry, N_2, Ar free	29.17	24.90	13.12	18.64
S/C at reformer inlet	1.0	1.0	2.73	1.63
Syngas module at reformer exit	0.40	0.90	2.04	0.93
Amount of syngas bypassed in WGS, %	59.42	-	-	-
CO_2 separation efficiency, % of inlet CO_2	90	90	-	-

3.2.2 Methanol production

Downstream the syngas purification, conditioning and compression steps, the fresh syngas is fed to the methanol synthesis island. The syngas specifications for the three plant configurations in both the operating modes are shown in Table 3-16. As regards the DG- and IG-based plants, the composition of the fresh syngas shows a major variation between baseline and enhanced operating mode. This is a consequence of the different conditioning units that the syngas has to undergo depending on the operating mode. The difference between baseline and enhanced operation is also reflected in the CO/CO_2 ratio, which shows a substantial reduction in enhanced operation. Unlike the aforementioned cases, the SEG-based plant features a fresh syngas composition with a limited variation between the baseline and the enhanced operating modes. This also applies to the CO/CO_2 ratio and it largely results from the chemical equilibrium of the WGS reaction at the ATR outlet. The largest difference between the baseline and enhanced operation cases lies in the flow rate, which is about 60% higher in the enhanced operation compared to the baseline. When it comes to the DG- and IG-based plants, the difference between the operation points is accompanied with a difference in the flow rate, which is about 135% higher in DG-EO (on molar basis) compared to DG-BO and about 75% higher in IG-EO compared to IG-BO.

The fresh syngas is first mixed with the unconverted recycled gas and then preheated in a feed/effluent heat exchanger, upstream the methanol synthesis reactor. The temperature of the inlet syngas to the methanol synthesis reactor is set according to the heat exchanger specifications. The outlet crude methanol is cooled down until the dew point temperature of the mixture is reached. The crude methanol is further cooled down to 40°C and separated in a flash unit from the light gases which are recycled back to the reactor.

Table 3-16 – Syngas specifications upstream the methanol synthesis island in baseline and enhanced operating conditions.

Parameter	DG BO	DG EO	IG BO	IG EO	SEG BO	SEG EO
Temperature, °C	114.5	112.3	115.0	112.5	122.7	118.5
Pressure, bar	92.0	92.0	92.0	92.0	92.0	92.0
Mass flow rate, kg/s	3.81	9.31	3.71	6.9	4.37	6.99
Molar flow rate, kmol/h	1225	2877	1213	2139	1318	2127
H_2, $\%_{mol}$ dry, N_2, Ar free	68.03	71.22	67.32	70.81	71.55	71.83
CO_2, $\%_{mol}$ dry, N_2, Ar free	4.03	12.86	2.11	11.97	14.63	14.90
CO, $\%_{mol}$ dry, N_2, Ar free	27.18	15.60	29.70	16.73	13.14	12.87
CH_4, $\%_{mol}$ dry, N_2, Ar free	0.76	0.32	0.87	0.49	0.68	0.40
CO/CO_2	6.74	1.21	14.04	1.40	0.90	0.86

The flexibility requirement also affects the methanol synthesis boiling water reactor, which is designed by taking into account the two different operating points. All the plant configurations have some fixed design criteria, among which are the tube length and diameter (i.e. 6 m and 0.04 m, respectively), the reactor pressure and the temperature of the boiling water (i.e. 90 bar and 238°C, respectively). The number of tubes inside the reactor for each configuration depends on the selected gas hourly space velocity (GHSV), referred to the volume of the reactor tubes.

All the plant options are designed with a GHSV of 5000 h^{-1} in enhanced operation with a recycle ratio (RR, defined as the molar flow rate of the recycle stream divided by the molar flow rate of the fresh syngas) of 5. As extensively discussed in section 3.1, it is economically preferable to size the methanol reactor on the enhanced operation condition, rather than on the baseline operation. The control criteria which are applied in the baseline operation mode depends on the composition and especially on the CO/CO_2 ratio of the fresh syngas. As regards the SEG-based plant, which has the lowest CO/CO_2 ratio and therefore potentially the poorest performance in terms of methanol yield, the recycled molar flow rate is kept constant, fixed by the blower design, which involves an increase of RR in baseline operation. In the DG- and the IG-based plants, the recycled molar flow rate is controlled in order to reach 99% of overall methanol yield. For both the configurations, the recycled molar flow rate which guarantees 99% yield is lower than the molar flow rate in the design EO condition.

The performance of the methanol synthesis unit is evaluated considering the methanol carbon yield defined in equation (3-1) and methanol productivity, in which the methanol species mass flow rate downstream the flash unit is considered. The temperature profiles are also analyzed in order to verify that the threshold limit of 300 °C is not exceeded, in order to prevent the catalyst deactivation by Cu cluster sintering (Twigg and Spencer, 2001).

The methanol synthesis performance of the SEG-based plant is extensively described in section 3.1, therefore the description below is mainly focused on the DG- and IG-based plants. The performance and operating conditions of the methanol synthesis are displayed in Table 3-17.

The equilibrium yield per pass is higher in both the DG and IG BO cases, due to the larger CO/CO_2 ratio at the reactor inlet that thermodynamically favors the carbon conversion. The higher molar fraction of CO_2 in the EO cases, results also in a larger water production that hinders the methanol synthesis kinetics (Vanden Bussche and Froment, 1996). Indeed, despite the equilibrium yield per pass is not reached for any condition analyzed, its approach is faster in the two BO cases. Moreover, the equilibrium approach in BO is pushed by the lower GHSV.

The methanol yield and equilibrium yield per pass of the two DG EO and IG EO cases are almost equal due to the similar operating conditions. Instead, the difference in methanol yield of DG BO and IG BO is more significant (65.6% vs. 71%), as consequence of the different GHSV (3274 h^{-1} vs. 3054 h^{-1}) and the different CO/CO_2 ratio that affects the thermodynamic equilibrium. The equilibrium yield in DG BO is indeed ~3% lower with respect to BO IG due to the larger content of CO_2 in the feed. The productivity is far larger in the EO as consequence of the larger feed streams used. The methanol productivity obtained with DG BO is the lowest, less than half of the EO cases. Worth of notice is also the large amount of inert recycled in the loop BO, that are more than 40%, as a consequence of the large recycle ratios. Compared to DG and IG cases, SEG shows lower methanol yield per pass as a consequence of the lower CO/CO_2 ratio (lower than 1 in the SEG case) while the productivity is still directly related to the flow rate streams.

The centreline catalyst temperature axial profiles are reported in Figure 3-15. In the inlet zone of the reactor, the temperature increases passing through a maximum, due to the heat released by the exothermic reaction involved in the methanol synthesis process. Then, the temperature decreases down to the coolant level (238 °C) due to the progressive approach to the equilibrium, which lowers the reaction rates. The SEG cases have both mild temperature profiles as a consequence of the large GHSV (4684 h^{-1} and 5000 h^{-1}) and low CO/CO_2 ratio. The SEG BO shows the lowest hot spot due to the high inert concentration (37.25%). The catalyst temperature profiles are almost overlapped in the

DG and IG EO cases, due to the similar operating condition, inlet composition and GHSV. The hot spot is also less pronounced with respect to the BO cases because of the larger GHSV (5000 h^{-1}) that improves the heat exchange by convection. The highest temperature hot spot is reached with the IG BO that is operated with the lowest GHSV (3054 h^{-1}) and highest CO/CO_2 ratio. Nevertheless, the maximum temperature are moderate and never exceeds 260 °C that is far less than the temperature limit of 300 °C (Twigg and Spencer, 2001), meaning that the reactor design is appropriate for the heat management for any analysed condition.

Table 3-17 - Performance of methanol synthesis.

Parameters	DG BO	DG EO	IG BO	IG EO	SEG BO	SEG EO
Number of tubes	10263	10263	7629	7629	7580	7580
GHSV, h^{-1}	3274	5000	3054	5000	4684	5000
RR, molar basis	8.23	5.0	5.5	5.0	8.06	5.00
Recycle flow rate, kmol/h	10080	14385	6625	10693	10625	10625
Methanol yield per pass, %	65.59	54.31	71.00	54.91	48.61	46.50
Equilibrium yield per pass, %	78.22	70.36	81.41	69.10	62.14	64.31
Overall methanol yield, %	99.00	97.37	99.00	97.38	97.93	96.29
Syngas module at reactor inlet	9.69	8.05	7.57	7.69	8.60	6.84
Inert (CH_4, N_2) concentration at reactor inlet, $\%_{mol}$	44.50	18.11	40.39	21.65	37.25	18.71
Syngas temperature at reactor inlet, °C	195.1	173.3	187.8	175.2	183.3	172.3
Thermal power released by the reactor, MW	5.52	8.40	6.70	6.71	1.95	5.05
Methanol concentration at reactor outlet, $\%_{mol}$	4.06	5.42	5.86	5.48	3.56	5.22
Methanol concentration at flash unit outlet, $\%_{mol}$	87.54	68.22	92.52	69.88	64.88	64.35
Methanol productivity, $kg/day/kg_{cat}$	5.53	11.78	7.53	11.86	7.10	11.35

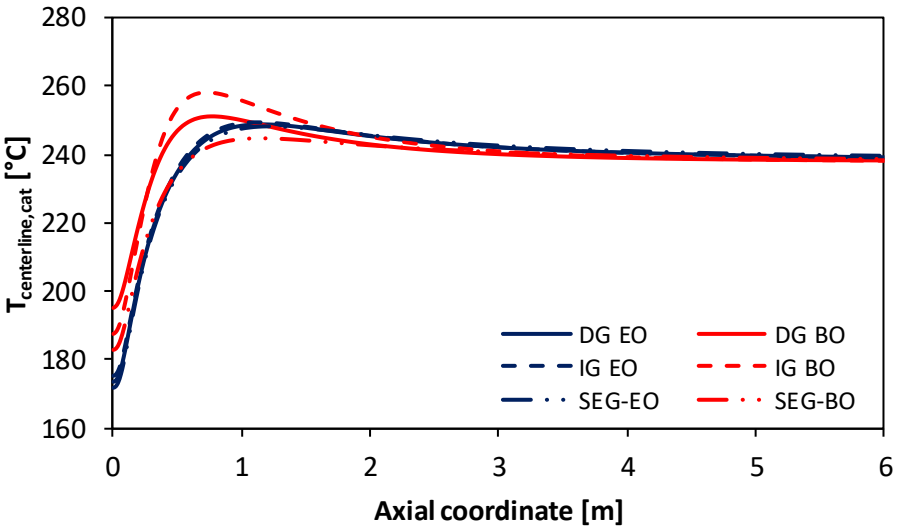

Figure 3-15 - Catalyst centerline temperature axial profiles.

The raw product, rich in methanol and water and with the presence of other species (low boiling components and ethanol), enters the purification section at 2 bar and 41-42°C (depending on the case).

As regards the SEG-based plant, the design and control criteria for the purification section have been extensively described in section 3.1. In this case, the flowrate of methanol to be purified increases by 62% in enhanced operation compared to baseline operation, while the composition remains fairly constant (see Table 3-18). On the contrary, both the flowrate and the composition of the remaining cases vary significantly between baseline and enhanced operation. In the DG case, a stream with a 2.7 times higher flow rate than the baseline case, and with much lower methanol content than the baseline case (68.2% vs. 87.5%) is produced. In the case of IG, the flowrate in enhanced operation doubles compared to the baseline operation and the methanol mole fraction reduces to 69.9% from 92.5% of the baseline operation.

The purification section has been designed considering that the units should be able to work in flexible mode. The plant is composed of two distillation column in series, the first one aiming at removing most of the incondensable gases and the second one aimed at concentrating the methanol up to the desired purity (99.85%$_{wt}$) for the product, with at least 99% of recovery.

Because of the characteristics of the streams to be treated, which all present a low and similar amount of low boiling impurities (the sum of mole fractions of methanol, ethanol and water is for all the cases about 0.98), for the first column (the stabilizing column), the separation can be accomplished with 23 trays. The optimal diameter is 0.9 m, 0.75 m and 0.66 m for the DG, IG and SEG cases, respectively.

The second column (the concentration column) performs most of the operation for achieving the desired purity of the methanol product and its performance is significantly influenced by the flowrate and the composition of the feed stream. In particular, for the stream produced in the DG configuration, the operation for separating methanol and water, with a mole fraction of about 70% and 30% for the enhanced operation, is more demanding than the one for separating the mixture composed of about 89% methanol and 11% water for the baseline operation, resulting in a higher reflux ratio. In addition, the much higher flowrate of the enhanced operation causes higher circulating flowrates inside the column, therefore requiring a too large column diameter for a well performing operation in the baseline case. Similar considerations can be done also for the purification of the stream produced in the IG-based plant.

On the basis of these considerations, and taking into account that a column able to treat both the streams in enhanced operation and in baseline one in flexible mode is needed, a recycle of the product streams rich in methanol and in water has been considered for the baseline operation. A stream fed to the concentration column with about 70% of the flowrate of the stream in the enhanced operation and a similar composition as for methanol and water is obtained. In this way, a column operating at atmospheric pressure at the top, with 48 trays and a diameter of 2.5 m in the DG-based plant and of 2.1 m in the IG case, can perform the separation for both the enhanced operation case and the baseline one. The operating costs for the operation in the baseline case are increased, because the concentration column needs to treat a higher flowrate and with a higher water content in the feed stream, however on the overall economic analysis this can be acceptable, also because the baseline operation is run for few time and discontinuously in a year. As already mentioned, in the SEG-based plant, the relatively small difference in flowrate and the constant composition of the feed in the two operating modes allows to manage the separation without recycle of the product streams. In this case, the diameter of the concentration column results to be equal to 2 m.

Table 3-18 - Characteristics of the raw methanol streams fed to the purification section for the assessed cases. Methanol purification operating conditions.

Parameter	DG BO	DG EO	IG BO	IG EO	SEG BO	SEG EO
Mass flow rate at purification inlet, kg/s	3.59	8.98	3.51	6.62	4.12	6.67
Molar flow rate at purification inlet, kmol/h	425	1160	406	848	543	875
Methanol concentration at purification inlet, %$_{mol}$	87.54	68.22	92.52	69.88	64.88	64.35

Parameter	DG BO	DG EO	IG BO	IG EO	SEG BO	SEG EO
H_2O concentration at purification inlet, $\%_{mol}$	10.87	30.08	5.65	28.33	33.76	33.69
Stabilizing column						
Condenser duty, MW	0.009	0.027	0.010	0.021	0.011	0.023
Reflux ratio	0.10	0.10	0.10	0.10	0.10	0.10
Reboiler duty, MW	0.44	1.37	0.47	1.03	0.66	1.08
Concentration column						
Condenser duty, MW	10.01	14.21	7.33	10.62	6.31	10.17
Reflux ratio	0.82	0.86	0.85	0.85	0.85	0.87
Reboiler duty, MW	9.94	14.07	7.19	10.49	6.24	10.06

3.2.3 Heat recovery and power generation

The waste heat available between the temperatures of 1000°C and 30°C is approximately 82 MW in the enhanced operating mode and 60 MW in the baseline mode. A heat recovery steam cycle (HRSC) is used to recover such heat and to convert it into steam for the process and electric power. Furthermore, an internal combustion engine (ICE) exploits the off-gas of the methanol synthesis and purification units for electricity and steam/hot water production.

The design of the HRSC and heat exchanger network (HEN) is performed using the multiperiod synthesis methodology reported in section 2.1.7. The performance map of the ICE is evaluated in the way described in section 2.1.7, by using linearized equations derived by Zatti et al. (2018).

The ICE and HRSC electric power outputs and net electric efficiencies are shown in Table 3-19 for the different cases. The DG EO case holds the highest electricity production because of the highest purge flow rate of the series, which is a consequent of the highest hydrogen addition in all the considered cases. The IG EO and SEG EO cases are characterized by similar conditions upstream the methanol synthesis which lead to a similar electricity production. In BO, all the cases are characterized by higher RRs in the methanol synthesis with respect to the corresponding EO. Consequently, lower purge flow rates are fed to the ICE leading to lower electricity production. Moreover, the net electric efficiency of the ICE decreases in baseline operation due to the lower thermal power of the purge flow from the methanol synthesis and purification island. Concerning the HRSC design and performance, the optimization depends on the availability of high temperature heat and on the steam exports required by the various operating modes. Due to the extraction of steam at a higher pressure (6.5 bar vs 2 bar) in the DG cases, the flow through the LP turbine is significantly reduced, thus reflecting in a lower electricity production and efficiency of the steam cycle. In addition, the stronger differences between baseline and enhanced operation of the DG case with respect to the IG case, reflect on a higher difference in terms of performance between BO and EO. The main reasons are two: (i) the high difference in steam required for the MDEA, (ii) the higher amount of available heat in the EO, in particular from the syngas cooler, methanol reactor and the condenser. These differences are lower in the IG case, thus yielding a small efficiency difference between BO and EO.

Table 3-19 - ICE and heat recovery steam cycle electric power outputs and net electric efficiencies. Steam flow rates at HP (120 bar), MP (32.2 bar) and LP (6.5 bar) turbine inlet are also reported.

Parameter	DG BO	DG EO	IG BO	IG EO	SEG BO	SEG EO
ICE						
Electric power, MW	1.78	4.44	2.02	3.75	2.15	4.00
Net electric efficiency, %	41.19	46.40	43.26	46.40	43.23	46.40
HRSC						

Parameter	DG BO	DG EO	IG BO	IG EO	SEG BO	SEG EO
HP/MP evaporation pressure levels, bar	32.2	32.2	32.2	32.2	32.2	
Steam flow rate at HP turbine inlet, kg/s	0.0	0.0	0.0	0.0	0.0	0.0
Steam flow rate at MP turbine inlet, kg/s	3.62	8.40	8.59	8.52	7.4	4.5
Steam flow rate at LP turbine inlet, kg/s	1.12	6.04	8.26	8.11	7.2	6.1
Net electric power, MW	1.87	4.34	4.94	4.88	4.24	2.95
Net electric efficiency, %	9.93	22.74	25.45	26.54	20.52	14.76

Figure 3-16, the composite curves of the baseline operation of the IG and DG cases are reported. It can be seen that no pinch-point is reached in both the cases: this is due to the forbidden match constraints between syngas coolers and steam superheaters set to avoid metal dusting of the tubes.

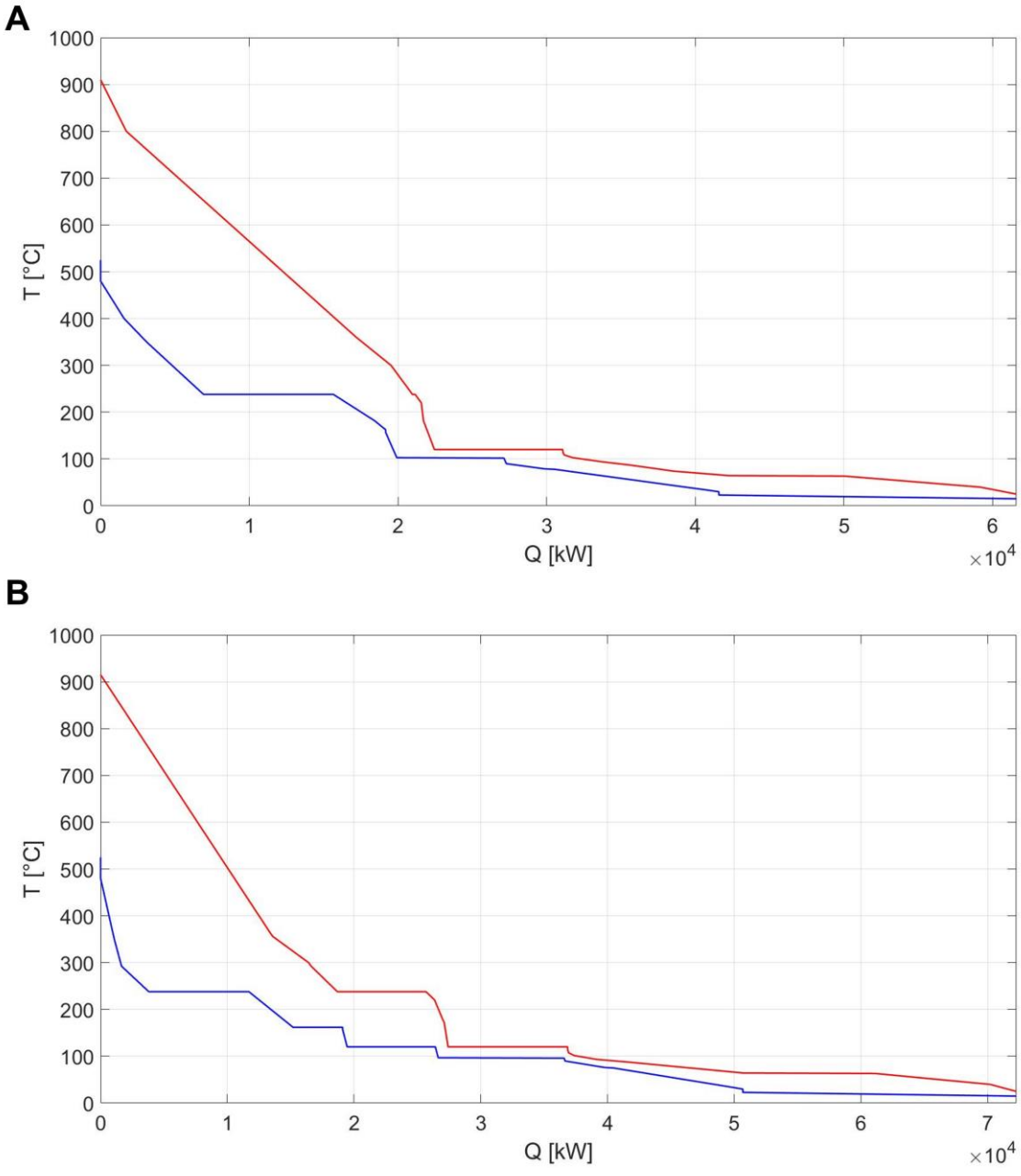

Figure 3-16 - (A) Composite curve of IG-based plant baseline operation; (B) composite curve of DG-based plant baseline operation.

3.2.4 Process simulation results

The performance indexes of the assessed PBtM plants are reported in Table 3-20.

In enhanced operation (the prevailing operating mode), the DG-based plant holds the highest overall fuel efficiency of the series (73.3%), followed by the IG case (71.0%) and the SEG-based plant (68.8%).

Looking at the fuel efficiencies of the individual process units, the main differences are associated to the gasification process and the reforming. The DG case shows the highest gasifier fuel efficiency mainly because of the use of oxygen as oxidant instead of air and of the higher carbon conversion. Although the carbon utilization of the indirect gasifier is lower than the aforementioned case, the fuel efficiencies are not very different in value. This is due to the fact that the indirect gasifier can benefit from the injection of superheated steam at 400°C, that can be safely produced from combustor off-gas cooling with no risk of metal dusting, in contrast to the DG-based plant. The higher the syngas flow rate and the difference between the gasifier and the reformer exit temperature, the lower the fuel efficiency of the reformer due to the higher oxygen demand to heat up the raw syngas to the reforming temperature. Consequently, the IG-based plant is characterized by the highest reformer fuel efficiency. For the same reason, the reformer fuel efficiency of the SEG case in baseline operation is lower with respect to the same value in enhanced operation. As regards the fuel efficiencies of the synthesis and of the purification sections, the differences among the cases are modest and mainly related with the differences of CO/CO_2 ratio of the syngas.

The resulting fuel efficiencies of the overall plant are higher in enhanced operation than in baseline operation for all the configurations. The carbon efficiencies of all the plants in the series show modest differences in baseline operation. The rise of carbon efficiency achievable by hydrogen enrichment is significant, especially with the DG-based plant which retains most of the carbon in the syngas, and where it increases from 42.6% in baseline operation to 90.5% in enhanced operation mode.

The higher margin in hydrogen addition for the DG-based plant allows the methanol production to increase by 112.3% in enhanced operation, while in the IG and SEG cases, hydrogen addition boosts the methanol output by 57.3% and 59.6% respectively.

As to the hydrogen-to-fuel efficiency, the SEG-based plant shows the highest value of 84.2%, followed by the DG case with 82.2% and by the IG one with 81.1%. The reason of this trend can be explained by looking at the molecules that contribute to the carbon flow rate increases in enhanced operation. In the IG-based plant, the enhancement of carbon flow rate occurs exclusively through an increase of the CO_2 flow rate. In the DG and SEG configurations, instead, the increase of carbon flow rate takes place through an increase of both the CO and CO_2 flow rates (74% of the increased carbon flow rate is associated to CO_2 and 26% to CO in the DG plant, while 55% and 45% of the carbon flow rate increase are associated to CO_2 and CO respectively in the SEG plant). This is due to the different syngas conditioning techniques in the selected configurations (i.e. presence of WGS reactor and/or CO_2 removal unit). The trend also reflects on the CO/CO_2 ratio variation: high variation for the IG case (i.e. 14 to 1.4), modest variation for the DG case (i.e. 6.7 to 1.2) and almost unchanged ratio for the SEG case. The higher the increased carbon flow rate is associated to CO_2, the higher the amount of hydrogen which is consumed by the reversed WGS reaction in the methanol synthesis unit and the lower the hydrogen-to-fuel efficiency.

The power-to-fuel efficiency does not follow the same trend of the HtF efficiency. This is because the PtF efficiency also depends on the effect of the modified operating conditions on the heat recovery steam cycle and on the consumption of auxiliaries, leading to variation of the steam

generated, the utility consumptions and ultimately to the electric balance, that are not only linked univocally to the consumption of the electrolysis system. The calculated PtF efficiency ranges from 56.5% of the IG case to 58.5% of the DG plant, confirming the values reported in the literature for PBtX plants based low temperature electrolysis systems (see the related discussion in the introduction).

Table 3-20 - General performance of the Power & Biomass-to-Methanol plants.

Performance indexes	DG BO	DG EO	IG BO	IG EO	SEG BO	SEG EO
$\eta_{F,dry}$, %	108.75	108.75	108.75	108.75	108.75	108.75
$\eta_{F,gasifier}$, %	79.36	79.36	78.06	78.06	74.08	75.76
$\eta^{u}_{F,gasifier}$(input: biomass; output: H_2, CO), %	46.76	46.76	47.47	47.47	48.40	51.51
$\eta_{F,ref}$, %	97.43	97.43	99.20	99.20	96.42	98.18
$\eta^{u}_{F,ref}$ (input and output: H_2, CO), %	161.32	161.32	158.60	158.60	143.78	141.03
$\eta_{F,pur}$, %	98.34	99.94	99.97	99.97	99.96	99.96
$\eta^{u}_{F,pur}$ (input and output: H_2, CO), %	98.34	99.98	99.99	99.99	100.00	99.99
η_{F,M_syn}, %	80.45	81.19	80.05	80.65	80.95	80.39
η^{u}_{F,M_syn} (input: H_2, CO; output M), %	81.71	81.75	81.39	81.61	82.56	81.22
η_{F,M_pur} , %	97.16	98.65	98.29	98.62	98.63	98.69
η^{u}_{F,M_pur} (input and output: M), %	98.07	99.13	99.39	99.21	99.24	99.16
$\eta_{F,global}$,%	65.48	73.35	66.24	70.97	62.00	68.78
$\eta_{F,eq}$, %	58.49	28.85	61.95	34.23	57.19	33.25
Carbon efficiency, %	42.63	90.46	43.13	67.79	40.34	64.40
Oxygen demand, kg/s	2.45	2.45	0.47	0.47	0.54	0.44
Methanol production, kg/s	3.29	6.99	3.33	5.23	3.12	4.97
Methanol output, MW_{LHV}	65.48	139.07	66.23	104.19	62.00	99.01
Methanol yield, %	99.00	97.37	99.00	97.38	97.93	96.29
H_2 addition, kg/s	-	0.75	-	0.39	-	0.37
H_2 addition, MW_{LHV}	-	89.58	-	46.83		43.94
Methanol production enhancement, %	-	112.30	-	57.29	-	59.63
η_{PtF}, $MW_{LHV,M}/MW_{el}$	-	58.48	-	56.54	-	57.48
η_{HtF}, $MW_{LHV,M}/MW_{H2}$	-	82.15	-	81.07	-	84.21
Net electric output, P_{el}, MW	-4.06	-129.89	-2.35	-69.49	-2.86	-67.24
Electric generation, MW	3.65	8.78	6.96	8.63	6.38	6.95
Electric consumption, MW	7.71	138.67	9.31	78.13	9.24	74.19
Belt dryer	0.65	0.65	0.65	0.65	0.65	0.65
Gasifier air fan	-	-	0.67	0.67	0.75	0.73
Syngas compressor 1	4.51	4.20	5.77	5.77	7.15	7.95
Hydrogen compressor		-	-		-	0.88
Syngas compressor 2	1.67	3.85	1.66	2.88	-	-
Recycle compressor	0.62	0.90	0.41	0.67	0.67	0.67
MDEA electric consumption	0.23	-	0.12	-	-	-
Electrolyser	-	129.04	-	67.46	-	63.29
Other auxilieries[1]	0.03	0.03	0.02	0.02	0.03	0.03
Total waste water, kg/s	3.63	5.76	2.81	3.91	5.77	6.16

[1] Other auxiliaries include Liquid Redox and water scrubber pump.

In Figure 3-17a, the trend of the carbon efficiency, potential carbon efficiency and useful potential carbon efficiency is reported for the baseline operating mode of all the selected configurations. The evolution of the aforementioned indicators is observed along intermediate

streams within the plant by following the approach proposed by Poluzzi et al. (2020) (see section 2.2.2). In the bar chart, the total amount of each atom is represented by the complete bar enclosed in the red contour. The yellow part of the bars embodies the maximum amount of each atom that can end up in the final product, therefore they are in the same proportion as the corresponding atoms in the final product. The blue part of the bars displays the potential loss of carbon and hydrogen to separate the excess oxygen as H_2O or CO_2. Oxygen excess is allocated to carbon and hydrogen in order to maximize the yield of final product. The red part of the bar (when present) represents the excess of hydrogen or carbon after the removal of the excess oxygen.

In all the selected configurations, as-received biomass presents a carbon-to-hydrogen ratio much higher than that of methanol (0.70 vs. 0.25) and the oxygen excess causes the PCE to be equal to 70%. By means of the drying process, part of the water is removed from the biomass and this results in a PCE reduction to about 47%. In the dried biomass, hydrogen becomes the limiting element, therefore the oxygen excess can be removed as CO_2 without affecting the maximum fuel yield, as excess carbon remains available (red portion of the C bar).

In the DG case, the PCE rises to 51% across the gasifier thanks to the addition of steam. This leads to a raw syngas composition where no limiting element is present anymore (the red portion of the bar disappears). Simultaneously, the PCE_u reduces to 27% because of the production of CH_4 and C_xH_y, which are inert for the methanol synthesis. In the reformer, the PCE reduces (from 51% to 45%) because of oxygen addition, that may need to be separated downstream by causing a reduction of the potential amount of carbon and hydrogen ending up in the final product. On the other hand, the PCE_u increases to 44% due to the conversion of the hydrocarbons into useful reactants (H_2 and CO). The syngas conditioning step slightly affects the PCE, as these steps ultimately allocate oxygen atoms between H_2O and CO_2, which are then separated. As regards the CE indicator, a slight reduction occurs upstream the conditioning step due to the loss of unconverted carbon in the gasifier. Most of the CE reduction occurs in the CO_2 removal unit, where carbon is separated from the syngas. After this step, the CE and the PCE achieve the same value. In the fuel synthesis section, CE and PCE reduce by the same amount due to the incomplete conversion of the feed into methanol, which affects the two indexes in the same way. The PCE_u reaches the same value of the aforementioned indicators (43%) after the purification step, where the CH_4 is separated from the raw methanol stream.

In the IG-based plant, across the gasifier, the CE reduces to 72% and the PCE increases to 50%. The decrease of CE and the slightly lower increase of PCE compared to the DG case is due to the loss of carbon from the gasifier to the combustor, where the char is burned together with part of the input biomass. Also, the PCE_u undergoes a great reduction (to 28%) because of the production of CH_4 and of C_xH_y. Across the reformer, the PCE reduces to 46% due to oxygen addition, while the CE remains constant and the PCE_u increases. Syngas cleaning and conditioning slightly affect the PCE, while the CE reduces due to CO_2 separation. After the synthesis and purification steps, all the indicators reach the same value and result in a final overall carbon efficiency of 43%.

In the SEG case, the lowest PCE is obtained at the gasifier outlet, equal to 43%. This is due to the higher heat input to the combustor, also needed for the calcination of the CaO-based CO_2 sorbent. As a result of the carbon loss, carbon becomes the limiting element in the raw gas, that presents a hydrogen excess (red portion of the bar). No substantial variation of the PCE occurs across the reformer for the assumed conditions, as the added oxygen can bond with the excess hydrogen and be entirely removed as water. CE also drops in the gasifier to the same value of the PCE, due to carbon separation through both the unconverted char and the absorbed CO_2. As the extent of CO_2 separation in the SEG is tuned to achieve the target syngas module downstream the reformer, no variation of PCE and CE is observed in the conditioning step. The final overall carbon efficiency of the SEG-based system is 40%, which is the lowest of the series.

All the plants, previously presented in baseline operation, are shown in enhanced operation in Figure 3-17b. As regards the DG- and the IG-based plants, the same carbon efficiency trends of baseline operation are observed up to the reformed syngas. No substantial variations compared to the

baseline case are observed for the PCE of the conditioned syngas in the IG case. In the DG-based plant, instead, the PCE of the conditioned syngas decreases by about 3% compared to the corresponding baseline case. This is due to the WGS unit bypass, that leads to a syngas with a higher water content compared to the baseline case, causing a loss of hydrogen with the condensed water higher than needed compared to the oxygen excess in the syngas. As a result, after condensed water is separated, hydrogen becomes the limiting element and excess carbon appears. In the SEG-based plants, the raw syngas features a higher CE compared to the baseline operation (about 69%), since less carbon is separated in the gasifier. The PCE of the raw syngas in enhanced operation is about 6% higher than baseline operation thanks to a higher content of carbon, which was the limiting element in the baseline operating mode. The PCE reduces within the reformer from about 49% to 45%. Then, CE and PCE do not change through the cleaning and conditioning step. In all the plants, the gap between the CE and the PCE represents the gain of carbon efficiency that may be achieved by hydrogen addition. This gap is filled in the enriching stage, where the PCE increases to the same value of the CE. As shown in the bar chart, the added hydrogen allows to recover the carbon which is potentially lost to remove the excess oxygen, behaving as an oxygen acceptor. The final overall carbon efficiencies are 90%, 68% and 64% for the DG, IG and SEG cases, respectively.

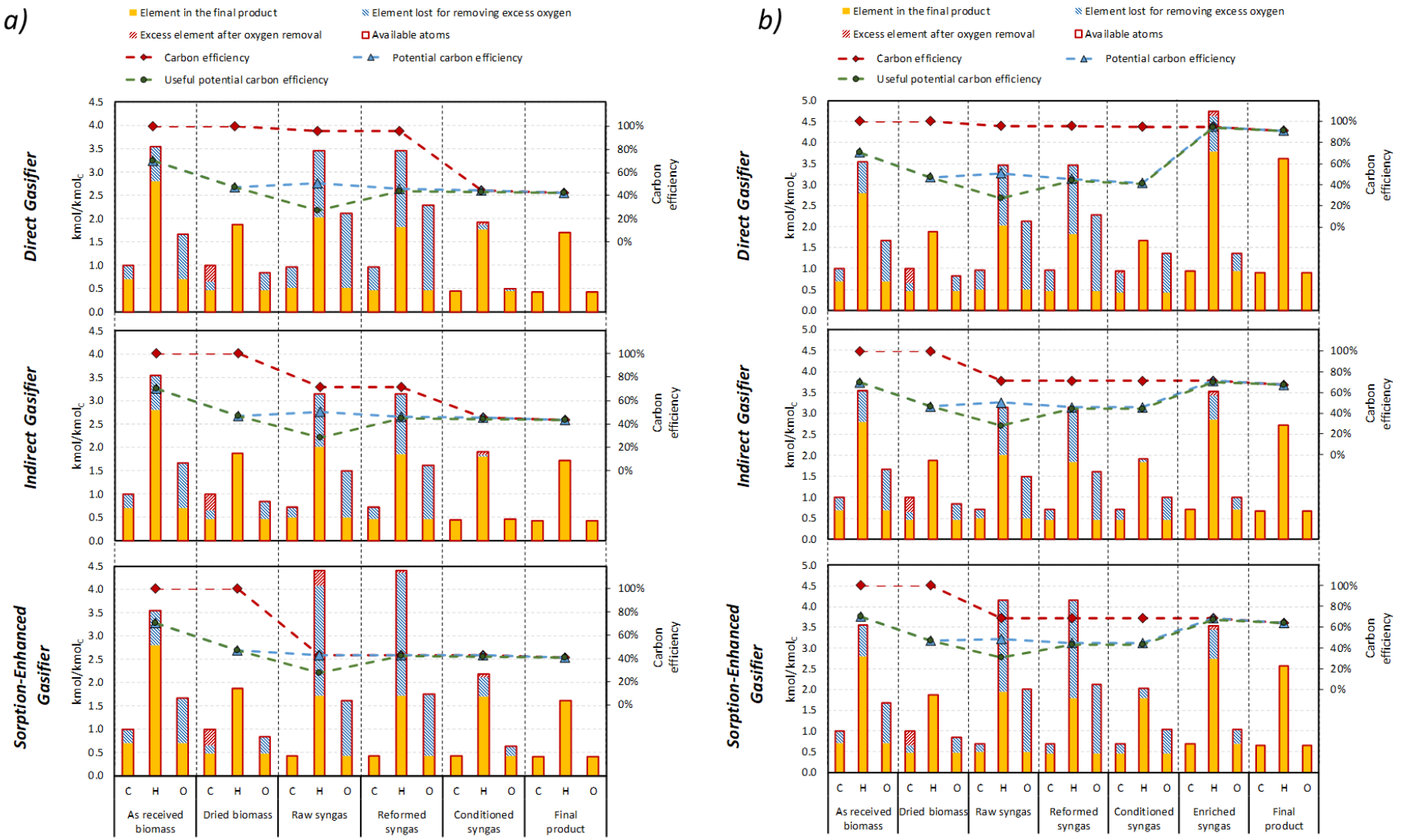

Figure 3-17 - Carbon efficiency, potential carbon efficiency and useful potential carbon efficiency of the process in baseline (a) and enhanced operation (b) for the direct, indirect and sorption-enhanced gasification-based plants.

3.2.5 Levelized cost of fuel

The economic analysis is performed by adopting the *Levelized Cost* approach for the three PBtM plants. A detailed description of the approach, the main assumptions and parameters for the economic analysis is present in section 2.2.3. The levelized cost of fuel (LCOF) is computed as shown in eq. (2-36).

In Table 3-21, the fixed capital investment costs of the assessed plants are reported. The PBtM plants benefit from the absence of high capital cost ASU. However, as already reported in section 3.2.1, an oxygen storage is needed for the ATR. In this case, a 30 bar gaseous oxygen storage sized to cover 3 hours of continuous operation is considered. The oxygen storage vessels represent about 2% of the total fixed cost both for the IG and for the SEG case and about 7% of the costs in the DG-based plant. Therefore, an additional DG-based plant is considered, named DGns (no storage) in Table 3-21, where the electrolyser operates between a minimum load (baseline operation) and the maximum load (enhanced operation). The minimum load corresponds to 41%, which is the minimum capacity factor for the electrolyser in order to guarantee the supply of the required amount of oxygen for the ATR. As can be observed in Table 3-21, the biomass-to-syngas island capital cost of the DGns case is the lowest of the series, because of the advantage of not installing the oxygen storage unit and because of the lower gasifier cost compared to the IG and SEG ones. IG- and SEG-based plants have similar capital cost for the biomass-to-syngas island because similar equipment is adopted in the two configurations (i.e. dual fluidized bed gasifier in both). As regards the cleaning and conditioning island, the differences between the cases are mainly due to the presence of the WGS reactor and of the CO_2 removal unit. The DG-based plant holds the highest cost cleaning and conditioning island because of the presence of both such units. However, in the DGns case, the WGS reactor is not installed because the target module for the methanol synthesis is reached through the addition of hydrogen in the minimum electrolyser load operation and CO_2 removal. Also the IG-based plants does not install the WGS, therefore the capital cost for the cleaning and conditioning section is similar to the DGns case. The SEG-based plant benefits from process intensification and does not need neither the WGS reactor nor the CO_2 removal unit. This results in the lowest cleaning and conditioning island capital cost, 47% lower than the DG case and about 33% lower than DGns and IG plants. As regards the syngas-to-methanol island, the DG- and DGns-based plants are characterized by about 31% higher capital cost, mainly because of the higher number of tubes in the methanol synthesis reactor. The power island capital costs are very similar for all the cases. The cost of the electrolysis system accounts for the 32% of the total FCI for the DG- and DGns-based plants, 18% for the IG case and 19% for the SEG plant, including H_2 compression. The assumed specific cost for the electrolysis system is 700 €/kW_e, which is consistent with the current alkaline technology and with the future cost estimations of PEM technology (Bertuccioli et al., 2014; International Energy Agency, 2019).

Overall, the DG-based plant is characterized by the highest total FCI of the series, because it has the largest electrolysis system and the largest oxygen storage. When the storage is not installed, the total FCI decreases by 11%, also because of the absence of the WGS reactor. The SEG-based plant exhibits the lowest total FCI of the series thanks to process intensification. When FCI is referred to the methanol production in EO (i.e. the prevalent operating mode), the DG-based plants show the lowest specific costs of the series, as the highest absolute FCI are compensated by the highest methanol productivity.

Table 3-21 – Fixed capital investment costs of the units of the PBtM plants.

Fixed capital investment	DG-based plant	DGns-based plant	IG-based plant	SEG-based plant
Biomass-to-syngas island, M€	**90.02**	**69.76**	**85.40**	**92.42**
Oxygen storage	20.26	-	3.92	4.51
Feedstock handling	8.91	8.91	8.91	8.91
Belt dryer	7.11	7.11	7.11	7.11
Pressurized O_2 CFB gasifier	29.58	29.58	-	-
Steam CFB gasifier	-	-	13.27	14.82
Combustor with fluegas treatment	-	-	30.76	31.76
Ceramic hot-gas filter	6.96	6.96	6.18	7.29
Catalytic reformer	17.19	17.19	15.26	18.01
Cleaning and conditioning island, M€	**53.47**	**42.35**	**41.35**	**28.34**
Scrubber	1.38	1.38	1.24	1.41
Liquid redox	2.88	2.88	2.58	2.94
Syngas compressor 1	14.60	13.92	17.23	21.35
Syngas compressor 2	13.14	13.14	10.81	-
Activated carbon	0.37	0.37	0.33	0.38
Waste water treatment	2.16	2.16	1.66	2.26
WGS reactor	6.85	-	-	-
CO_2 removal pre-combustion (MDEA)	12.10	8.51	7.50	-
Syngas-to-methanol island, M€	**22.99**	**22.99**	**17.59**	**17.36**
Methanol synthesis BWR	16.00	16.00	11.96	11.86
Recycle compressor	3.95	3.95	3.17	3.15
Stabilizing column	0.58	0.58	0.49	0.49
Concentration column	2.46	2.46	1.98	1.86
Power island, M€	**27.99**	**27.99**	**28.70**	**28.36**
CHP internal combustion engine	2.45	2.45	2.09	2.23
HRSC	25.54	25.54	26.61	26.13
Hydrogen production island, M€	**90.32**	**90.32**	**47.22**	**48.97**
Electrolyser	90.32	90.32	47.22	44.31
H_2 compressor	-	-	-	4.66
Total FCI, M€	**284.80**	**253.42**	**220.26**	**215.44**
Total FCI, €/kW$_{th}$	**2048**	**1823**	**2114**	**2177**

Table 3-22 displays the main economic results of the levelized cost approach, computed assuming that all the plants operate in enhanced mode for 80% of the time. The O&M costs follow the same trend as the TCI. Among the various cost items reported in the maintenance and the operating labor correspond to about the 45% and the 25% of the total O&M, respectively. The DG and DGns cases feature the highest purchased electricity cost, as they incorporate the largest electrolysis systems and the highest production of hydrogen. Among these two, the DGns plant shows the highest purchased electricity cost, since the electrolysis unit is turned on for all the operating hours of the plant. The DGns configuration shows the lowest LCOF of the series, thanks to the highest methanol production. The SEG-based plant is characterized by a slightly lower total cost with respect to the IG case. However, being less efficient than the counterfactual, the methanol production is 5% lower and the LCOF results to be slightly higher. Overall, the differences in terms of levelized cost of fuel are relatively small among the assessed cases, ranging from 29.7 €/GJ of the DGns case to 31.7 €/GJ of the DG case.

Table 3-22 – Main result of the economic analysis and levelized cost of fuel for an electrolyser investment cost of 700 €/kW.

Economic results	**DG-based plant**	**DGns-based plant**	**IG-based plant**	**SEG-based plant**
TCI, M€/y	39.33	35.00	30.42	29.75
O&M, M€/y	30.65	28.60	23.16	22.68
Purchased electricity cost, M€/y	28.45	32.93	15.24	14.80
Biomass cost, M€/y	13.32	13.32	13.32	13.32
Total costs, M€/y	111.76	109.85	82.14	80.56
Methanol production, t/y	177,318	186,116	137,758	130,621
LCOF, €/t	630.28	590.25	596.29	616.71
LCOF, €/GJ	31.67	29.66	29.96	30.99

In Figure 3-18a, the dependency of the LCOF on the average electricity price in EO and on the electrolysis capital cost is depicted. Both the DG-based plants show a clear advantage in decreasing the electrolyser cost, since it represents a major cost item. In Figure 3-18b, the LCOF is reported as a function of the average electricity price in EO and of the cost of the feedstock biomass which is kept at the reference value of 46 €/t in one case and at 0 €/t in the other case. The dual fluidized bed configurations (i.e. IG and SEG) exhibit better economic performance at high electricity prices, when free biomass is available. This is due to the fact that the feedstock cost has a higher share on the LCOF in IG and SEG cases compared to their DG counterfactuals.

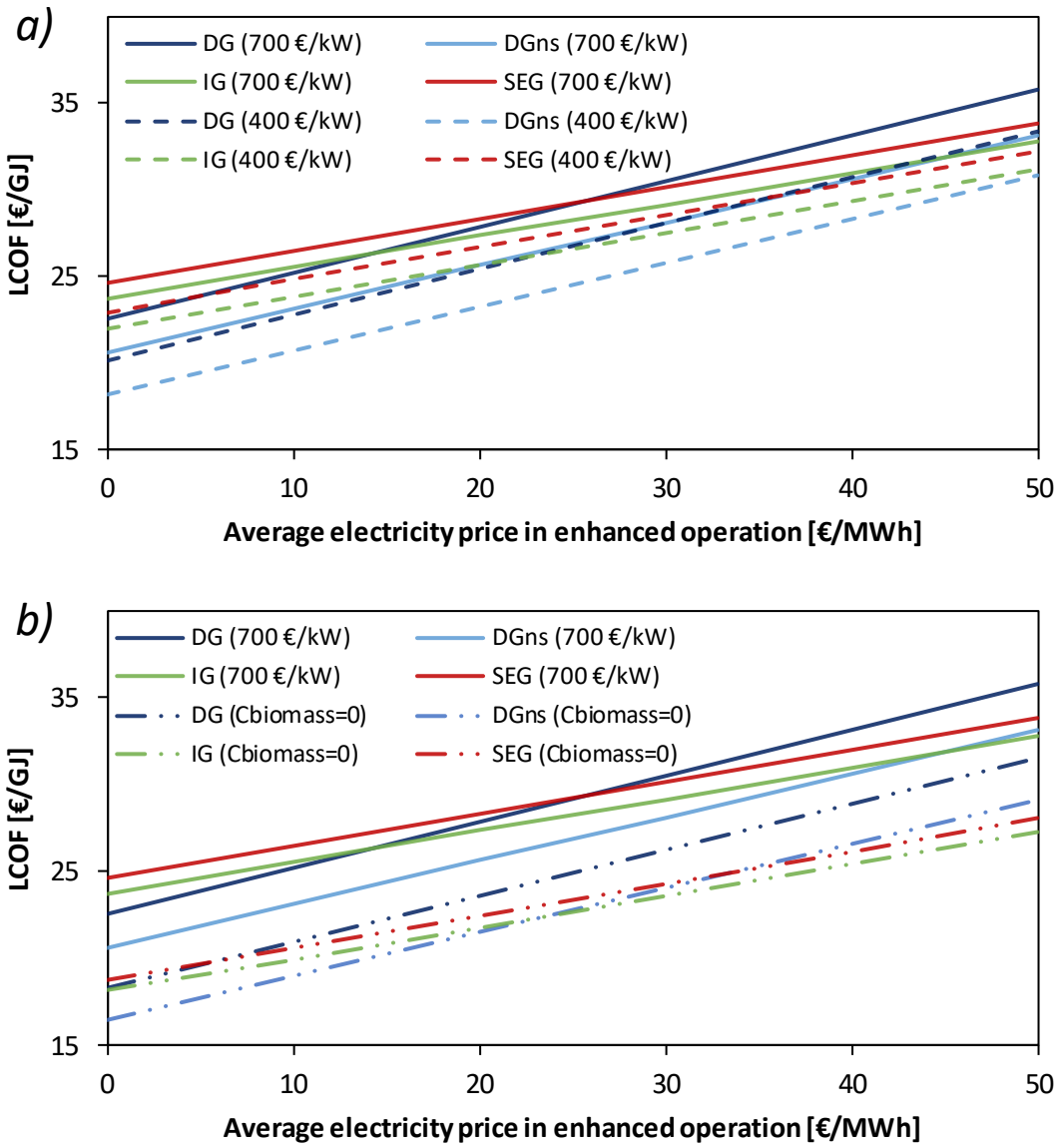

Figure 3-18 – LCOF as a function of the average electricity price in enhanced operation for a) different electrolysis cost (i.e. 700 vs. 400 €/kW) and for b) different biomass cost (i.e. 46 €/t vs. 0 €/t).

3.2.6 Economic feasibility

The 'Willingness to pay' (WTP) approach, presented in section 2.2.4, allows to identify the number of hours of operation in baseline and enhanced modes and the corresponding average electricity prices for a certain methanol selling price. From this data, the profitability of the PBtM plant investment can be evaluated by computing the Internal Rate of Return (IRR).

In Figure 3-19, the Internal Rate of Return (IRR) of the DG-based plant is reported as a function of the methanol selling price for an electrolyser investment cost of 400 €/kW. The functions are derived from the 2019 Denmark electricity price curve and from the modified curve. The solid lines refer to the flexible DG-based plant, where the increase of the methanol selling price involves an increase of the electrolyser capacity factor, with the method described previously. The dashed lines refer to the inflexible DG-based plant, with 100% capacity factor of the electrolysis system, purchasing electricity at the yearly average electricity price of the current price curve (38.5 €/MWh)

and of the modified curve (30.4 €/MWh). The IRR value of 10% defines the region above which the selected PBtM plants are considered profitable.

The curves which derive from the current Danish electricity prices ('current' curve) display profitable investment at methanol selling prices higher than about 575 €/t. In this case, a profitable investment requires a high methanol selling price, that involves a very high capacity factor of the electrolyser (CF_{el} approaches 100%). This means that the added value of a flexible PBtM plant is limited compared to an inflexible plant that always keeps the electrolyser in operation. On the contrary, the curves derived from the modified electricity price curve show profitable investment at lower methanol selling prices. This is due to the lower average electricity price of the modified curve with respect to the Denmark one. In this case, the advantage of flexible operation in terms of profitability is more marked, which is witnessed by the fact that the solid line is above the dashed one for a wide range of methanol prices. The breakeven methanol selling price results to be about 510 €/t for the flexible PBtM plant and 535 €/t for the inflexible plant.

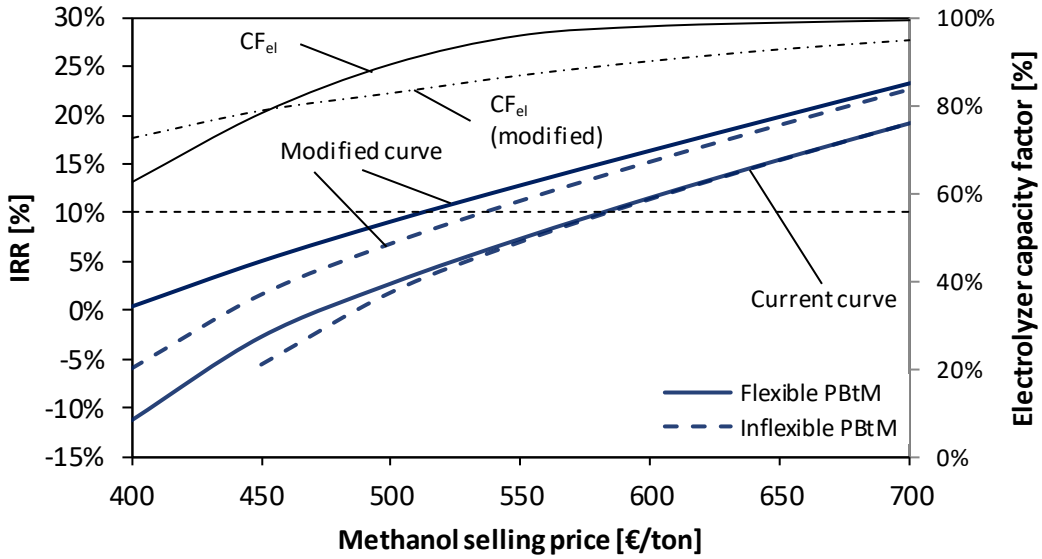

Figure 3-19 – IRR of the DG-based plant as a function of the methanol selling price for an electrolyser investment cost of 400 €/kW. Curves are derived from the two electricity price curves shown in Figure 2-10.

In Figure 3-20, the IRR of the flexible DG and DGns plants is shown as a function of the methanol selling price for the current and for the modified electricity curve. The DGns case is profitable at lower methanol selling prices compared to the DG case for both the electricity curves. The modified curve gives an economic advantage to both plants, reducing the breakeven methanol selling price by 62-70 €/t.

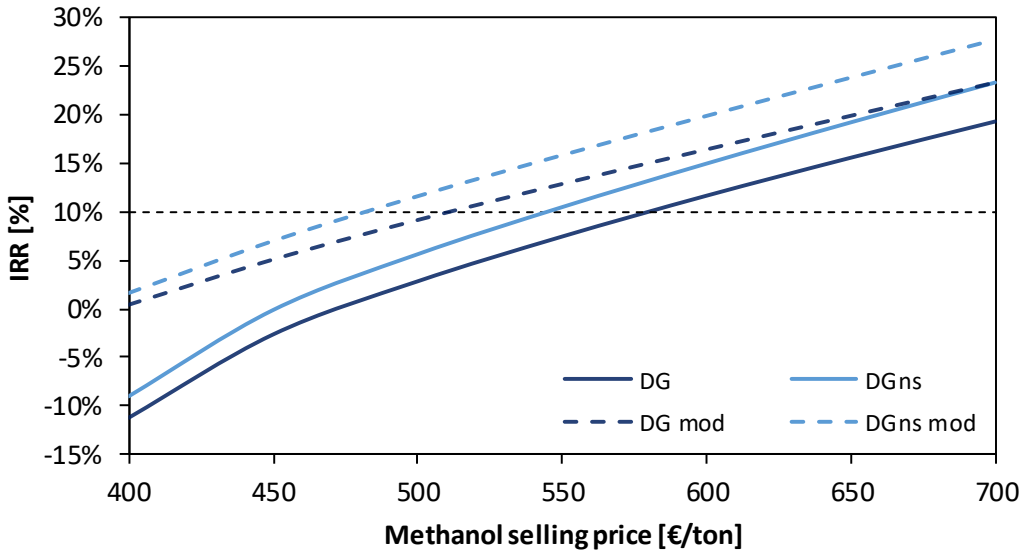

Figure 3-20 – IRR of the DG- and DGns-based plants as a function of the methanol selling price for an electrolyser investment cost of 400 €/kW. Curves are derived from the two electricity price curves shown in Figure 2-10.

In Figure 3-21, the IRR of the DGns-, IG- and SEG-based plants is compared as a function of the methanol selling price. The DGns case is profitable at lower methanol selling prices compared to the other cases for both the electricity curves. The modified curve gives an economic advantage to all the configurations, reducing the breakeven methanol selling price by 62, 50 and 46 €/t for DGns, IG and SEG respectively. The plant investment is profitable (i.e. IRR higher or equal to 10%) at relatively high capacity factors of the electrolysis unit. With the modified electricity price curve, the capacity factors which guarantee a profitable investment are higher than 80.7, 82.9 and 85.1% for DGns, IG and SEG respectively. With the 2019 electricity curve, the capacity factors are even higher and reach 94.3, 95.3 and 97.0% for DGns, IG and SEG respectively.

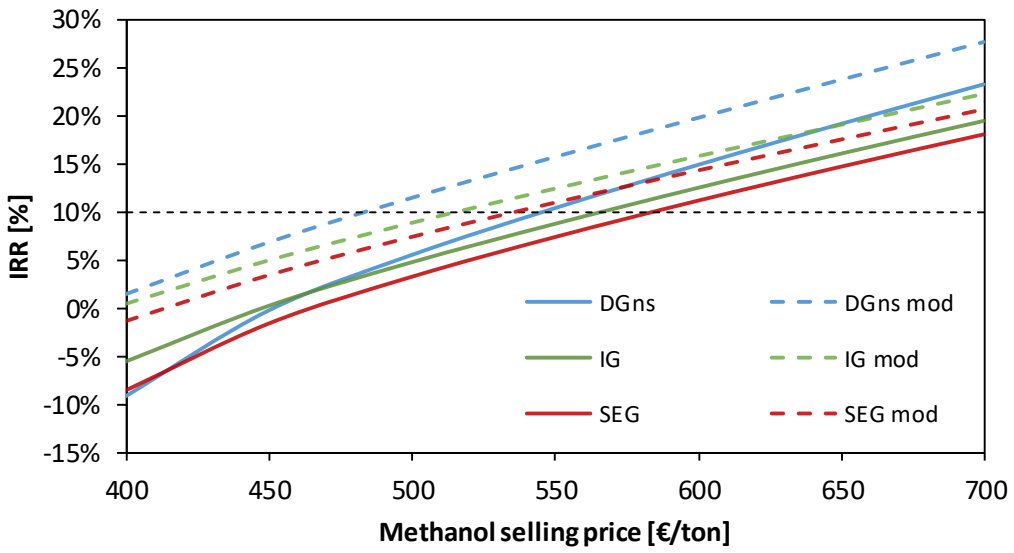

Figure 3-21 - IRR of the DGns-, IG- and SEG-based plants as a function of the methanol selling price for an electrolyser investment cost of 400 €/kW. Curves are derived from the two electricity price curves shown in Figure 2-10.

3.2.7 Environmental analysis

It has to be noted that the environmental and economic impacts of indirect CO_2 emissions associated to the electricity consumed by the electrolyser are not accounted in this study. In other words, it is assumed that zero-emissions electricity is consumed by the electrolyser (which is not the case of the average power generation plant in the current Denmark energy mix).

The reason behind the aforementioned assumption can be found in in Figure 3-22 in which the CO_2 emissions of the assessed PBtM plants are depicted as a function of the electricity grid emission factor. The vertical dashed lines at 3.6, 59, 112.3, and 236.7 g_{CO2}/MJ denote the carbon intensity of Sweden, Denmark, Italy and Poland electricity generation mix in 2018 according to the European Environmental Agency (EEA) database. The horizontal line represents the typical emission of a methanol production plant from natural gas which amounts to about 470 kg_{CO2}/t_M (Ingham, 2017). By considering an electrolyser capacity factor of 80%, the assessed PBtM plants requires an electricity grid emission factor of 26.8, 28, 40.7 and 39.8 g_{CO2}/MJ for DG-, DGns-, IG-, and SEG-based plants respectively, in order to produce the same amount of emissions of the conventional methanol production plant.

Therefore, the use of near zero-emission electricity is a pre-requisite in the production of hydrogen from electrolysis and of related e-products, to make them environmentally sustainable and with lower carbon footprint than conventional products (International Energy Agency, 2019).

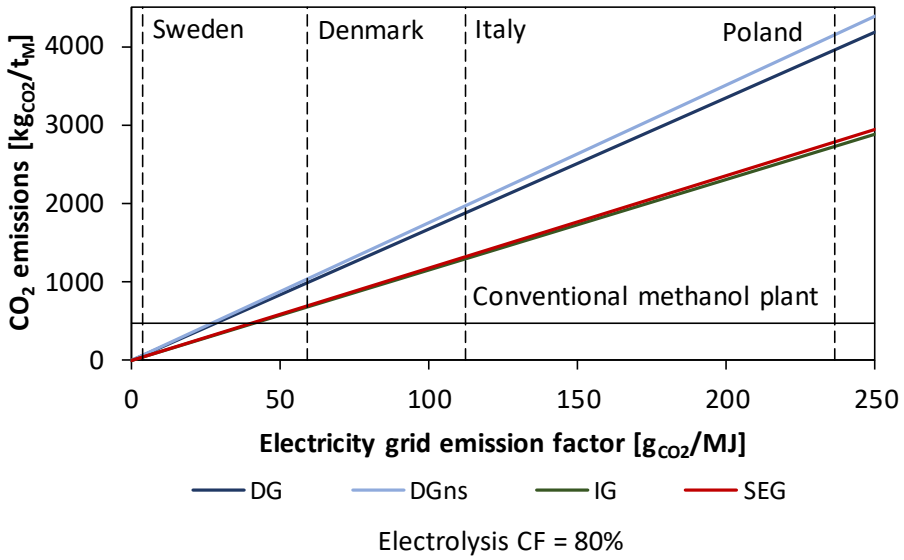

Figure 3-22 – CO_2 emissions of the PBtM plants vs. electricity grid emission factor.

3.2.8 Conclusions

This section evaluated from techno-economic perspectives the design and the operational criteria of a series of Power-to-Methanol (PBtM) plants employing different gasification technologies, namely direct gasification (DG), indirect gasification (IG) and sorption-enhanced gasification (SEG). This kind of plants are capable to operate flexibly without hydrogen addition (baseline operation) and with hydrogen addition (enhanced operation). The main technical conclusions can be summarized as follows:

- No technical criticality has been highlighted in the design and operation of flexible PBtX plants. However, different gasification technologies involve different strategies to control the syngas module to operate with and without hydrogen input (i.e. presence of WGS reactor and/or CO_2 removal unit). The different gasification technologies lead to different values of the CO/CO_2 ratio in the feed of the methanol synthesis unit. The operational criteria of the methanol synthesis section change accordingly. From a design perspective, no issues have been detected regarding the risk of hot spots in the methanol reactor in any operating conditions, provided that recycle rate is increased in baseline operation. On the other hand, the reduced flow rate of produced methanol in baseline operation may cause malfunctioning of the purification columns, therefore a recycle may be needed to keep the columns operating efficiently.
- The DG-based plant can take advantage of higher carbon efficiency (CE) of the gasification process, leading to higher overall plant carbon efficiency (~90%) in enhanced operation. The SEG and IG cases achieve similar maximum CE in enhanced operation (64.4% SEG and 67.8% IG), though significantly lower than DG due to CO_2 loss from the combustor. A higher CE would only be possible by recovering the CO_2 in the flue gas with a post combustion CO_2 capture or through oxyfuel combustion.
- Hydrogen-to-fuel (HtF) efficiency ranges between 81 and 84%, while Power-to-Fuel (PtF) efficiency between 56 and 58%, with low temperature electrolysis system.

The main results from the economic analysis can be summarized as follows:

- Due to the high oxygen demand in the gasifier, the DG-based plant obtains a great advantage from avoiding an inevitably large O_2 storage system. Therefore, it appears economically preferable to operate the plant between a minimum load satisfying the O_2

demand of DG at high electricity prices and a maximum load to maximize methanol production and carbon efficiency at low electricity prices. This allows avoiding a large O_2 storage with significant benefits for Capex and safety issues.

- In all cases, the flexible PBtX plants can take advantage of electricity price curves with low average electricity prices and high peak prices. Without sufficiently long and high peak electricity prices, an inflexible plant with the electrolysis always in operation would lead to limited economic penalty compared to a flexible plant.
- The specific fixed capital investment (FCI) ranges between 1823 and 2048 €/kW of methanol output in enhanced operation. The LCOFs range between 29.7 and 31.7 €/GJ_{LHV}. Economic advantages would derive from a decrease in the electrolysis capital investment, especially for the DG-based plants which employ the largest electrolysis system. In particular, a reduction of the capital cost of the electrolysis system from 700 €/kW to 400 €/kW involves a decrease of the specific FCI by 15.3%, 13.6%, 9.2%, 8.8% in DGns, DG, IG and SEG respectively. The LCOF decreases by 7.9%, 7.8%, 5.5% and 5.3% in DGns, DG, IG and SEG respectively.
- The methanol breakeven selling prices range between 545-582 €/t with the current reference Denmark electricity price curve (yearly average electricity price of 38.5 €/MWh, average electricity price in enhanced operation of 34.3 €/MWh) and between 484-535 €/t with the assumed modified electricity price curve of a future energy mix with increased penetration of intermittent renewables (yearly average electricity price of 30.4 €/MWh, average electricity price in enhanced operation of 20.6 €/MWh).
- In all the cases, the investment in the assessed flexible PBtM plants is profitable for relatively high capacity factors (higher than 80%), meaning that the operational flexibility should be exploited by avoiding the consumption of high-price electricity rather than in the use of the limited amounts of low-price “excess” electricity.

Chapter 4
Biomass-to-methanol and hydrogen plants with CCS

In this chapter, a techno-economic analysis of biomass-to-methanol and biomass-to-hydrogen plants with CCS is carried out, with the following main original outcomes:

i. the calculation of the cost of CO_2 avoided for different products (methanol and hydrogen), different gasification technologies (direct oxygen-blown and indirect gasification) and different CO_2 capture strategies (pre-combustion MDEA-based and post-combustion MEA-based CO_2 capture);

ii. the assessment of the economic impact of the design of plants with flexible production of methanol and hydrogen, when hydrogen is subject to time-dependent market price.

4.1 BECCS plants description

The following BECCS plants have been assessed in this analysis:

- Biomass-to-Methanol plant, based on O_2-blown fluidized bed direct gasification (BtM DG);
- Biomass-to-Methanol plant, based on dual fluidized bed indirect gasification (BtM IG);
- Biomass-to-Hydrogen plant, based on O_2-blown fluidized bed direct gasification (BtH_2 DG);
- Biomass-to-Hydrogen plant, based on dual fluidized bed indirect gasification (BtH_2 IG).

The block diagrams of the four assessed processes are shown in Figure 4-1Figure 4-4. All the plant configurations combine the same fundamental conversion steps, namely biomass drying, gasification, syngas purification, conditioning and compression, final product synthesis and purification, and CO_2 removal and compression. All the plants are self-sufficient in terms of heat and steam balance, while grid electricity can be imported.

A description of the calculation methods is given in Chapter 2. Extensive tables with the properties of the main streams and the main calculation assumptions are reported in Appendix B. Assumptions and calculation method are consistent with the work on power and biomass to methanol plants in Chapter 3. The next sections focus on plant units and operating conditions.

The process models are developed in Aspen Plus®, which is used to compute the mass and energy balances of the integrated plants. The computations are conducted for a biomass input of 100 MW_{LHV}. The proximate and the ultimate analysis of the as-received woody biomass are assumed from literature (Pröll and Hofbauer, 2008b) and are reported in Table 2-1.

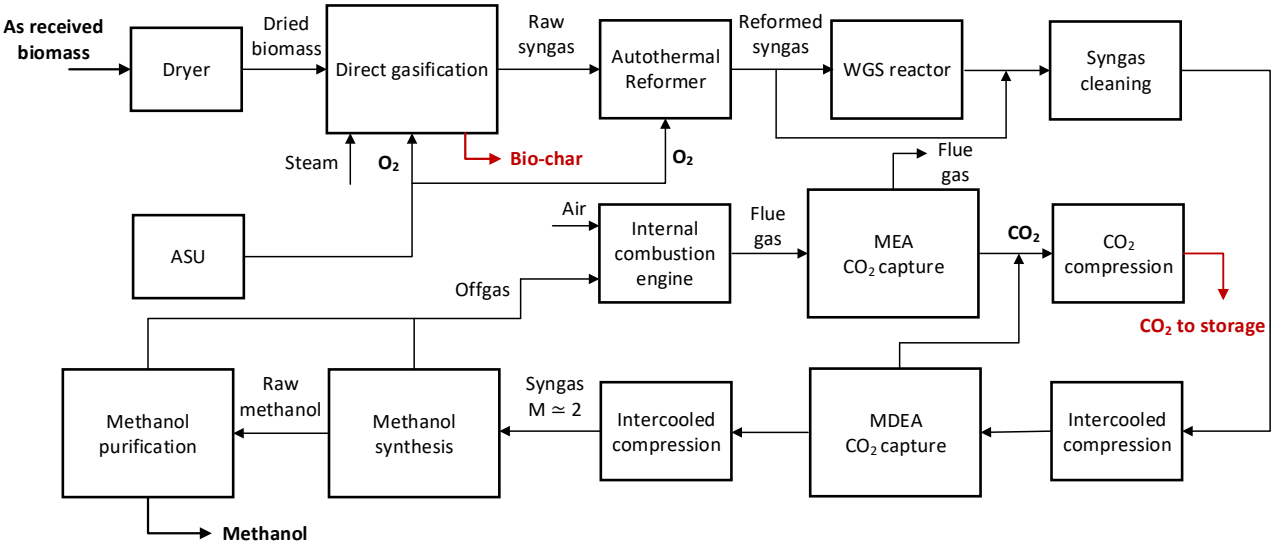

Figure 4-1 – Block diagram of the direct gasification-based Biomass-to-Methanol plant

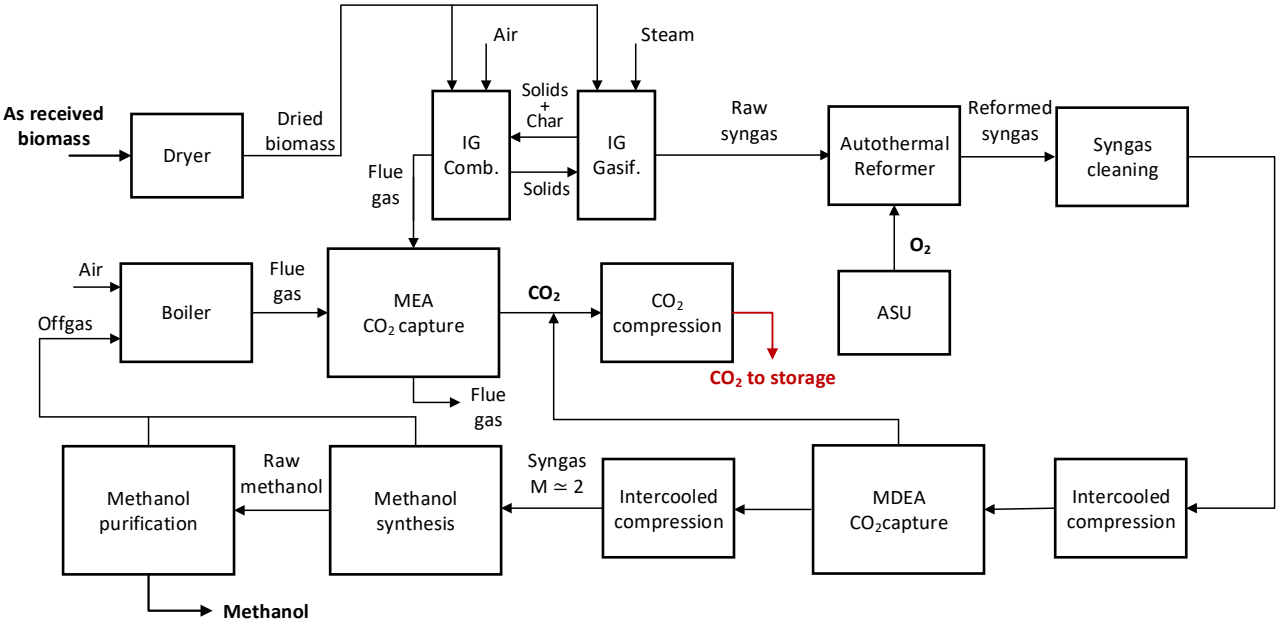

Figure 4-2 – Block diagram of the indirect gasification-based Biomass-to-Methanol plant

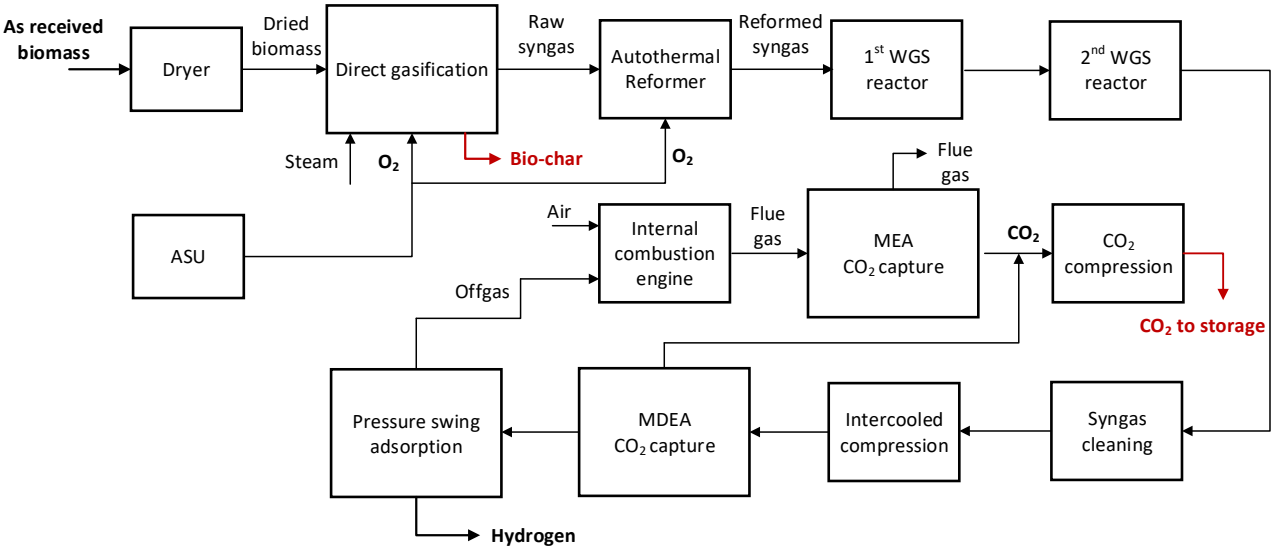

Figure 4-3 – Block diagram of the direct gasification-based Biomass-to-Hydrogen plant

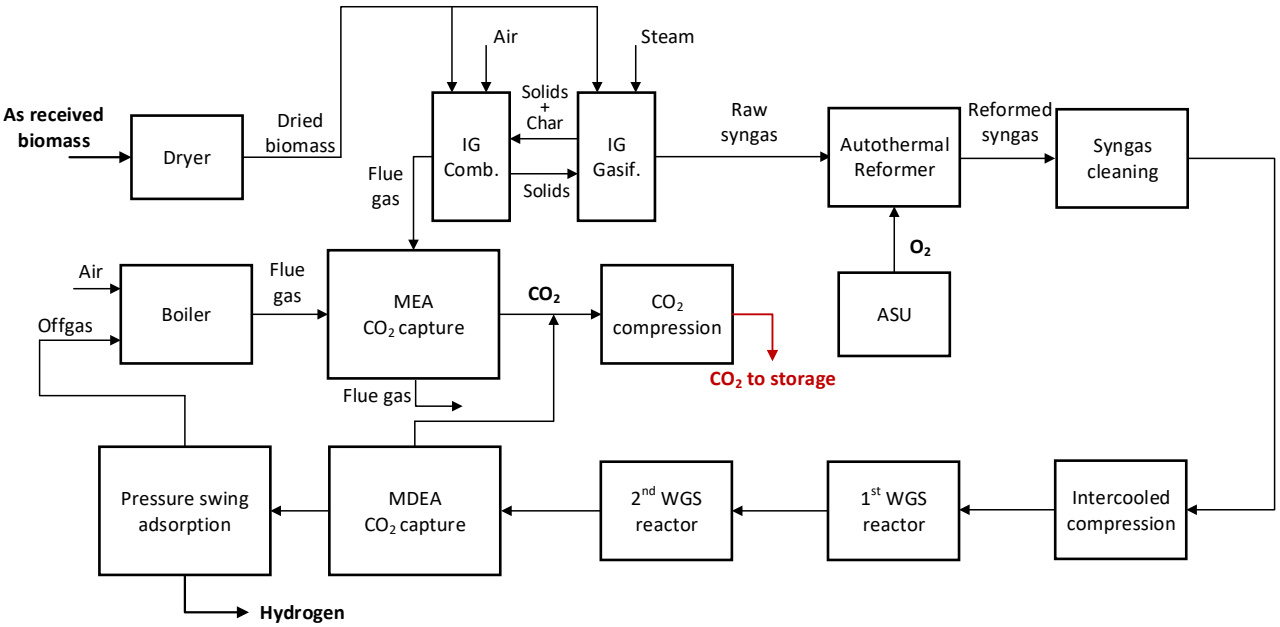

Figure 4-4 – Block diagram of the indirect gasification-based Biomass-to-Hydrogen plant

4.2 Syngas production

As-received woody biomass is fed to a belt dryer to reduce the moisture content from 45% to 15%, before feeding the gasification island. A detailed description of the belt drier and design specifications can be found in section 2.1.2.

In the direct gasification-based plants (Figure 4-1 and Figure 4-3), the gasifier is a pressurized circulating fluidized bed (CFB) which is fed with a mixture of steam and oxygen. Therefore, the gasification process is thermally sustained through the partial oxidation of biomass by means of oxygen from an air separation unit (ASU). Most of the inlet carbon remains in the nitrogen-free syngas as CO, CO_2 and CH_4, while a minor part is extracted from the fluidized bed as unconverted char.

In the indirect gasification-based plants (Figure 4-2 and Figure 4-4), the gasifier is a dual fluidized bed, constituted by a bubbling fluidized bed (BFB) gasifier and a circulating fluidized bed (CFB) combustor. A solid heat carrier material (e.g. olivine) circulates between the higher

temperature combustor and the lower temperature gasifier to provide the heat required for biomass gasification. The heat is generated from the combustion with air of the unconverted char, that flows from the gasifier to the combustor, and of additional biomass. A post-combustion CO_2 removal unit based on MEA scrubbing allows to capture CO_2 from the flue gas generated in the combustor.

A detailed description of the model and the design specifications of the gasification technologies, and the comparison of the simulated syngas composition with literature data both for DG and IG can be found in section 2.1.3. The operating conditions are displayed in Table 4-1.

The aforementioned gasification processes generate a nitrogen-free syngas, which contains a significant amount of tar and methane. A catalytic auto-thermal reformer (ATR) unit is included downstream the gasifier and a high temperature filtration unit, in order to convert methane and tar into CO and H_2. The ATR is fed with oxygen produced by an ASU with a purity of $95\%_{mol}$ (Giuffrida et al., 2010), using catalysts designed to operate on raw syngas (Kurkela et al., 2021). A restricted equilibrium calculation approach has been adopted for the ATR, assuming 90% methane conversion and complete conversion of higher hydrocarbons. Information about the operating conditions of the ATR for both the configurations are reported in Table 4-1.

The reformed syngas must be further conditioned, cleaned and compressed before the final product synthesis and purification. In all the configurations, a water scrubber allows to remove soluble contaminants contained in the syngas, such as ammonia and chlorine. Bulk sulfur removal is performed through a liquid Redox unit (LO-CAT process (Echt et al., 2017)), where H_2S is converted into elemental sulfur and water by reaction with an iron oxygen carrier. The system is simulated as a black box, with data from (Kazemi et al., 2014). Activated carbon bed and sulfur scavenging units, which are used to remove trace contaminants, are placed upstream the last compression stage at a pressure of about 50 bar in methanol production plants, and upstream the PSA at about 30 bar in hydrogen production plants.

Table 4-1 – Gasifiers and autothermal reformer operating conditions and exit gas composition.

Parameter	**DG**	**IG**
Gasification		
Gasifier outlet temperature, °C	870.0	815.0
Gasifier outlet pressure, bar	4.0	1.4
H_2, $\%_{mol}$ dry, N_2, Ar free	34.3	44.7
CO, $\%_{mol}$ dry, N_2, Ar free	25.0	23.1
CO_2, $\%_{mol}$ dry, N_2, Ar free	29.6	19.9
CH_4, $\%_{mol}$ dry, N_2, Ar free	7.6	9.7
C_xHy, $\%_{mol}$ dry, N_2, Ar free	3.4	2.6
H_2O, $\%_{mol}$	40.2	36.3
Syngas module at gasifier outlet	0.09	0.58
Syngas flow rate, kmol/h	2058	1707
Char conversion in the gasifier, % of inlet C	95.50	83.00
Biomass to gasifier, % of inlet biomass	100.0	86.0
Oxygen input, kg/s	1.93	-
Carbon efficiency, % of inlet C	95.50	71.39
Fuel efficiency, $\%_{LHV}$ of dried biomass	79.62	77.89
Flow rate of solids from combustor to gasifier, kg/s	-	169.32
Syngas reforming		
Reformer outlet temperature, °C	915.0	800.0
Oxygen input, kmol/h	71.2	55.5
H_2, $\%_{mol}$ dry, N_2, Ar free	45.93	56.46
CO_2, $\%_{mol}$ dry, N_2, Ar free	24.28	17.87
CO, $\%_{mol}$ dry, N_2, Ar free	29.17	24.91

Parameter	DG	IG
S/C at reformer inlet	1.0	1.0
Syngas module at reformer exit	0.41	0.90

4.3 Biomass-to-methanol plants

The methanol production plants must be fed with syngas with module $M = (H_2 - CO_2)/(CO + CO_2)$ of around 2, which is achieved through syngas conditioning by means of WGS reactor and/or CO_2 removal unit.

Downstream the ATR in the DG-based plant, the syngas is cooled down to 220°C and partly (about 27.4% of the total flow rate) fed to the adiabatic sour WGS reactor, which allows to adjust the syngas composition prior to the CO_2 removal step. The WGS inlet temperature is close to the lower end of the temperature range given by Ullmann's encyclopedia (2005) for raw gas shift (200-500°C). A lower inlet temperature may also cause the condensation of residual tars (Hannula and Kurkela, 2013). In the IG-based plant, the WGS reactor is not present since the syngas composition does not require adjustments prior to CO_2 removal.

After bulk cleaning, syngas undergoes a compression to 30 bar through a 4-stage and a 6–stage intercooled compressor in DG- and IG-based plants, respectively. In all the configurations, the intercoolers outlet temperature is 40°C and the pressure ratio per stage β_{stage} is about 1.8, leading to gas temperature at the outlet of each compression stage below 115°C.

A pre-combustion CO_2 removal unit based on MDEA scrubbing at 30 bar allows to remove the CO_2 contained in the syngas. In the DG-based plant, 95% of the CO_2 is separated from the syngas (Brandl et al., 2021), while in the IG-based plant, 90% of the CO_2 is removed to achieve the target module upstream the methanol synthesis.

In BtM plants, a 2 stage intercooled compressor allows to increase the pressure of the conditioned syngas to about 90 bar, which is the operating pressure of the methanol synthesis reactor. Downstream the syngas purification, conditioning and compression steps, the fresh syngas with a module of 2.05 is fed to the methanol synthesis island.

The main features of the syngas conditioning process and the delivered syngas properties are summarized in Table 4-2.

Table 4-2 - Main features of the syngas conditioning island.

Parameter	BtM DG	BtM IG	BtH_2 DG	BtH_2 IG
Syngas conditioning				
WGS bypass, %	72.56	-	-	-
WGS reactor(s) inlet temperature, °C	220	-	220/220	300/180
Steam addition to WGS reactor, kg/s	-	-	-	3.0
CO_2 separation efficiency, % of inlet CO_2	95	90	95	95
Conditioned syngas properties				
Temperature, °C	115.2	115.0	40.0	40.0
Pressure, bar	92.0	92.0	30.2	30.2
Mass flow rate, kg/s	3.83	3.73	1.70	1.39
Molar flow rate, kmol/h	1218	1214	1234	1218
H_2, $\%_{mol}$ dry, N_2, Ar free	67.33	67.32	93.41	94.77
CO_2, $\%_{mol}$ dry, N_2, Ar free	1.94	2.12	3.27	2.44
CO, $\%_{mol}$ dry, N_2, Ar free	29.96	29.69	2.56	1.93
CH_4, $\%_{mol}$ dry, N_2, Ar free	0.77	0.87	0.76	0.86
CO/CO_2	15.44	14.02		

The fresh syngas is first mixed with the unconverted recycled gas and then preheated in a feed/effluent heat exchanger, upstream the methanol synthesis reactor. The stream from the methanol reactor is cooled down to 40°C and separated in a flash unit from the light gases which are recycled back to the reactor.

Methanol synthesis is performed in a multi-tubular fixed bed reactor filled with commercial $Cu/ZnO/Al_2O_3$ catalyst (CZA) pellets and externally cooled by boiling water (i.e. boiling water reactor, BWR). The methanol synthesis is modeled in Aspen Plus as a plug flow reactor with the kinetic model proposed by Bussche and Froment (1996). Detailed information on the thermodynamics and the kinetics of the methanol reactor model can be found in 2.1.6.. The methanol synthesis reactor features tube length of 6 m and diameter of 40 mm, boiling water temperature of 238°C and catalyst specifications reported in Appendix B. Moreover, the number of tubes in the reactor depends on the selected gas hourly space velocity (GHSV), referred to the volume of the reactor tubes. In this work, the plants are designed with a GHSV of 5000 h^{-1} and a recycle ratio (RR, defined as the molar flow rate of the recycle stream divided by the molar flow rate of the fresh syngas) of 5.

The performance of the methanol synthesis unit is evaluated through the methanol carbon yield defined in eq. (4-1) and the methanol productivity (defined as the methanol produced per unit mass of catalyst), both referred to the methanol flow rate downstream the flash separator.

$$Yield = \frac{F_{M,out} - F_{M,in}}{\left(F_{CO_2} + F_{CO}\right)_{in}} \qquad (4\text{-}1)$$

The two methanol production plants have the same design specifications and very similar CO/CO_2 ratio of the inlet syngas. As a consequence, the size and performance of the two systems are comparable (Table 4-3).

Table 4-3 - Main features of the methanol synthesis and purification processes.

Parameters	**BtM DG**	**BtM IG**
Methanol synthesis		
Number of tubes	4345	4331
GHSV, h^{-1}	5000	5000
RR, molar basis	5.0	5.0
Recycle flow rate, kmol/h	6090	6071
Methanol yield per pass, %	63.74	69.33
Overall methanol yield, %	98.31	98.77
Syngas module at reactor inlet	5.66	6.81
Inert (CH_4, N_2,Ar) concentration at reactor inlet, $\%_{mol}$	44.90	40.15
Syngas temperature at reactor inlet, °C	187.4	186.35
Thermal power released by the reactor, MW	6.95	6.86
Methanol concentration at reactor outlet, $\%_{mol}$	6.22	6.29
Methanol concentration at flash unit outlet, $\%_{mol}$	93.07	92.54
Methanol productivity, $kg/day/kg_{cat}$	13.03	13.21
Methanol purification		
Inlet mass flow rate, kg/s	3.46	3.50
Inlet molar flow rate, kmol/h	398	405
Inlet methanol concentration, $\%_{mol}$	93.07	92.54
Inlet H_2O concentration, $\%_{mol}$	4.77	5.51
Stabilizing column		
Condenser duty, MW	0.013	0.012
Reflux ratio	0.11	0.11
Reboiler duty, MW	0.84	0.85

Concentration column		
Condenser duty, MW	5.84	5.97
Reflux ratio	0.63	0.64
Reboiler duty, MW	5.68	5.81

The raw product, rich in methanol and water and with other trace species (low boiling components and ethanol), enters the purification section at 2 bar and about 40°C, after throttling. Two distillation columns in series are employed, the first one removing most of the incondensable gases and the second one aimed at concentrating the methanol up to the desired purity of 99.85%$_{wt}$. Methanol recovery is at least 99.5%$_{mol}$ in both columns. The first column, i.e. the stabilizing column, accomplishes the separation with 20 trays, while the second one, i.e. the concentration column, performs the separation with 40 trays. The performance of the two plants is similar, as shown in Table 4-3.

The purge from the methanol synthesis and purification units contains significant amount of light gases, whose heating value is exploited either in a cogenerative internal combustion engine (ICE) for electricity and steam production in case of DG-based plants or in a boiler for steam production in case of IG-based plants.

4.4 Biomass-to-hydrogen plants

The hydrogen production plants are designed with two WGS reactors with intercooling in order to increase the hydrogen fraction in the syngas. In the DG-based plant, two adiabatic sour WGS reactors are placed upstream the compression step and operate at about 4 bar, similar to the gasifier. Both WGS reactors operate with an inlet temperature of 220°C. The overall CO conversion in the WGS section is 93.1%. The first and second WGS reactors convert 75.5% and 71.9% of the inlet CO, respectively. In the IG-based configuration, the WGS section is placed downstream syngas cleaning and compression and operates at about 30 bar. The first is a high-temperature WGS reactor with iron-based catalyst, fed with syngas at 300°C, complying with the temperature range indicated by Ullmann's encyclopedia (2005) (300-510°C). Upstream the reactor, the syngas is mixed with superheated steam at 250°C, with flow rate tuned to reach a reduction factor $R = (p_{CO} + p_{H_2})/(p_{CO_2} + p_{H_2O})$ equal to 1.3, where p_i is the partial pressure of the given species. Such a value is selected in order to avoid over-reduction of Fe_3O_4 in Fe-based high-temperature shift catalysts (Lee et al., 2013). Since the syngas contains a very low amount of water at this step, a relatively high quantity of superheated steam (3.0 kg/s) must be added in order to reach the target value of the reduction factor. The second reactor is a low-temperature shift with copper-based catalyst. Syngas is fed at 180°C, complying with the temperature range for low-temperature shift (180-270°C) (Ullmann's encyclopedia, 2005). The first and second WGS reactors convert 63.4% and 82.2% of the inlet CO, respectively, leading to an overall CO conversion of 93.5%.

Syngas compression to 30 bar is carried out through a 4-stage and a 6–stage intercooled compressor, respectively in DG- and IG-based plants. In all the configurations, the intercoolers outlet temperature is 40°C and the pressure ratio per stage β_{stage} is about 1.8, leading to gas temperature at the outlet of each compression stage below 115°C.

In both DG- and IG-based plants, a pre-combustion CO_2 removal unit based on MDEA scrubbing at 30 bar allows to remove 95% of the CO_2 contained in the syngas.

Downstream CO_2 removal, H_2-rich syngas at 30 bar is fed to the PSA unit without additional compression. The syngas specifications for the plant configurations are shown in Table 4-2. The products of the PSA system are hydrogen with a purity higher than 99.99%$_{vol}$ at 30 bar and a tail gas stream at atmospheric pressure. The hydrogen separation efficiency of the PSA is assumed to be 90% (Stöcker et al., 1998).

The heating value of the light gases in the PSA tail gas is exploited either in a cogenerative internal combustion engine (ICE) for electricity and steam production in the DG-based plant or in a boiler for steam production in the IG-based plant, as discussed in section 4.6.

4.5 CO_2 capture

The studied plants are designed to capture the CO_2 produced during the conversion of biomass into the final product. As a consequence, the carbon which is captured from the air during the biomass growth can be stored underground resulting in a negative emission process.

The technologies considered in this analysis for CO_2 separation are pre-combustion and post-combustion chemical absorption processes based on MDEA and MEA solvents respectively. In methanol production plants, CO_2 is removed by means of MDEA scrubbing in order to reach the target module necessary for the downstream synthesis. In hydrogen production plants, the CO_2 is removed from the syngas in order to obtain a high-purity CO_2 stream. The post-combustion technology may be employed in all the plant configurations in order to increase the overall CO_2 capture rate. The IG-based plants adopt the MEA scrubbing to separate the CO_2 from the flue gases coming both from the CFB combustor and from the PSA tail gas boiler. The DG-based plant uses the post-combustion technology in order to separate the CO_2 from the flue gas of the ICE which burns the off-gas of the methanol synthesis and purification. The amount of high-purity CO_2 coming from the amine scrubbing units changes significantly according to the gasification technology and the product. As shown in Appendix B, the mass flow rate of separated CO_2 with MDEA ranges between 2.79 kg/s of the BtM IG case, where most of the carbon is retained in the product and released as CO_2 from the combustor, and 9.09 kg/s of the BtH_2 DG case, where most of the carbon has to be separated as CO_2 from the syngas. The mass flow rate of separated CO_2 with MEA is 0.20 and 0.92 kg/s for BtM DG and BtH_2 DG respectively. For IG-based plants, 2.88 kg/s are separated from the flue gas of the CFB combustor and 0.19 and 0.73 kg/s from the flue gas of the boiler for BtM IG and BtH_2 IG respectively.

Being the selected amine scrubbing processes well-known commercial technologies, the CO_2 removal units are not modelled in detail, but the amount of CO_2 to be separated is either set to 90-95%, as mentioned in sections 4.3 and 4.4. The reboiler duty of the stripping column is set to 1 MJ/kg_{CO2} for MDEA (Meissner, III and Wagner, 1983; Moioli et al., 2016, 2017) and 3.7 MJ/kg_{CO2} for MEA scrubbing (Gale, 2017). The electric consumption of the two technologies, that has a little impact on the overall electricity balance, is derived from IEAGHG (2017b). CO_2 is assumed to be released from the stripping columns with 100% purity (dry basis) at nearly atmospheric pressure.

Once separated in the respective amine scrubbing units, the captured CO_2 stream is sent to the compression unit, composed by an intercooled compressor followed by a pump. The 5-stage intercooled compressor pressurizes the CO_2 up to 80 bar with a pressure ratio per stage of about 2.3 and intercoolers outlet temperature of 40°C. Downstream the last compressor, the supercritical CO_2 is pumped up to 150 bar. The overall electric consumption of the compression process is 0.11 kWh_{el}/kg_{CO2}, which is consistent with the literature (Hannula and Kurkela, 2013).

4.6 Thermal integration

Biomass-to-X plants make available significant amounts of heat to be recovered from many sources (e.g. hot syngas, flue gas, methanol synthesis, etc.). However, a great amount of the recovered heat is needed to provide heat for amine regeneration, for methanol purification, and to generate steam for the gasification unit. This can be partly supplied by the combustion of the tail gas from the methanol synthesis process and from the PSA for hydrogen purification. Such off-gas are exploited either in a cogenerative ICE for electricity and steam production (in DG-based plants), or in a boiler

for steam production (in IG-based plants). IG-based plants face a higher heat demand compared to DG-based plants due to the larger capacity of the post-combustion CO_2 separation process, which is more energy intensive. In the DG-based plants, the energy balance of the ICE is evaluated by using linearized equations derived from Zatti et al. (2018). Such equations allow to compute the electric power, the net electric efficiency, the thermal power and thermal efficiency of the ICE. The ICEs feature electric efficiency between 44.7 and 46.4% and thermal efficiency between 44.4 and 45.6%. The flue gases exit the ICE at 400°C and are cooled down to 100°C by recovering 18.6-19.8% of the fuel energy input. The rest of the heat is transferred to the cooling circuit of the ICE and can be recovered at low temperature, if required. In the IG-based plants, the high temperature flue gases from the boiler are first cooled down to 160°C by steam generation and then to 80°C for combustion air pre-heating.

In Table 4-4, the heat available and the thermal loads are shown for each plant configuration. The available high temperature heat is much higher in the IG-based plants compared to the DG cases. This is due to the high temperature flue gas from the CFB combustor and to the tail gas boiler. The methanol production plants require boiling water for the cooling of the reactor, which is not present in the hydrogen production plants. The availability of low temperature heat is similar among the BECCS plants. The methanol production plants can exploit a considerable amount of thermal power from the methanol cooler upstream the flash unit and the purification section. The hydrogen production plants have a higher heat recovery potential in the CO_2 compression section due to the higher CO_2 mass flow rate. The DG-based plants can exploit the heat recovery from the cooling circuit of the ICE.

As previously mentioned, the IG-based plants require larger amount of heat due to the higher amount of CO_2 separated with the post-combustion capture technology. The BtM DG-based plant has similar thermal consumption of the BtH_2 DG configuration because the heat required by the reboiler of the methanol concentration column balances the higher heat requirement of the CO_2 removal units which handle a higher mass flow rate to be separated. The same happens with the IG-based plants which share similar amount of high temperature heat consumption. The low temperature heat demand is the same for all the configurations and is related with the hot water requirement of the belt dryer. Steam generation is required for the gasification unit mainly for fluidizing the bed and for sealing and cleaning purposes. In BtH_2 IG, superheated steam is required for the high temperature WGS reactor in order to avoid catalyst over-reduction, as described in section 4.4.

Table 4-4 – Heat available and thermal loads of the assessed plants..

Thermal loads	**BtM DG**	**BtM IG**	**BtH_2 DG**	**BtH_2 IG**
High-medium temperature heat available (suitable for steam generation, amine regeneration, and methanol purification), MW_{th}	*24.24*	*32.46*	*21.20*	*35.95*
Flue gas cooler	-	9.64	-	9.64
Syngas cooler 1	16.80	11.27	16.79	11.27
Syngas cooler 2[1]	-	-	3.73	-
Clean syngas cooler 1	-	-	-	1.90
Clean syngas cooler 2[2]	-	-	-	1.67
Methanol synthesis	6.95	6.86	-	-
ICE flue gas	0.49	-	0.68	-
Tail gas boiler	-	4.69	-	11.47
Low temperature heat available (suitable for biomass drying), MW_{th}	*16.92*	*17.08*	*14.33*	*15.14*
Syngas compressor intercoolers 1	4.25	5.78	5.33	5.02
Syngas compressor intercoolers 2[3]	0.78	0.77	-	-
Clean syngas cooler 3	-	-	-	5.59
Methanol cooler	7.75	7.98	-	-
CO_2 compressor intercoolers	2.41	2.55	4.36	4.53
ICE low temperature water cooler	1.73	-	4.64	-
Medium temperature heat demand, MW_{th}	*12.58*	*20.83*	*12.49*	*20.14*

Thermal loads	**BtM DG**	**BtM IG**	**BtH$_2$ DG**	**BtH$_2$ IG**
Stabilizing column reboiler, MW_{th}	0.84	0.85	-	-
Concentration column reboiler, MW_{th}	5.68	5.81	-	-
Pre-combustion CO_2 capture (MDEA), MW_{th}	5.32	2.79	9.09	6.78
Post-combustion CO_2 capture (MEA) (comb. fraction), MW_{th}	-	10.66	-	10.67
Post-combustion CO_2 capture (MEA) (ICE/boiler fraction), MW_{th}	0.74	0.72	3.40	2.69
Low temperature heat demand (for biomass drying), MW_{th}	*13.04*	*13.04*	*13.04*	*13.04*
Steam generation, $\dot{m}$ [kg/s] / T [°C] / p [bar]	2.66/200/6[4] 0.80/200/6	2.62/400/4[4] 0.69/180/4	2.66/200/6[4] 0.80/200/6	2.62/400/4[4] 0.69/180/4 3.00/250/33

[1] Syngas cooler 2 is placed in between the sour WGS reactors. Syngas cooler 1 is the heat exchanger immediately downstream the gasification and reforming section.
[2] Clean syngas cooler 2 is placed downstream the low-temperature WGS reactor. Clean syngas cooler 1 is in between high-temperature and low temperature WGS reactors.
[3] Syngas compressor intercoolers 2 correspond to the compressor which performs the compression prior to the methanol synthesis (up to 90 bar).
[4] The first row corresponds to the gasifier fluidization steam. The second row includes steam for sealing and cleaning purposes in the gasification section. The third row is the steam addition to the high-temperature WGS in BtH$_2$ IG.

The thermal integration for all the configurations depends on the heat available and the thermal loads within the plant. In none of the biomass-to-X plants, heat is recovered with a steam cycle as the high heat demand for CO_2 removal does not leave heat available for power generation or does not make it economically competitive to produce very small electric power output. Furthermore, the technical constraint related with the metal dusting (Grabke, 1995), which forbids to superheat the steam with the syngas cooler, involves low superheating temperature and low steam cycle efficiency. Therefore, steam/water loops are adopted in all the configurations to transfer heat from waste heat sources to the heat users. The TQ diagrams of the four plants are reported from Figure B 1 to Figure B 4 (Appendix B).

In the BtM DG plant, as shown in the temperature heat diagram in Figure B 1, two water loops at different evaporation pressures are adopted. In the high pressure loop, the evaporation pressure (32.2 bar) is fixed by the methanol reactor. The saturated steam from the BWR is condensed back to provide heat to the distillation column reboilers. The evaporation pressure of the low pressure loop is 6 bar. In the syngas cooler upstream the WGS reactor, steam is evaporated. Part of it is slightly superheated to 200°C and fed to the gasifier and the remaining part is supplied to the MDEA and MEA reboilers.

Similarly to the previous configuration, the BtM IG plant (Figure B 2) adopts two water loops for heat recovery. As in the previous case, the high pressure loop at 32.2 bar is fixed by methanol reactor cooling. Saturated steam is sent to the distillation column reboilers. In the low pressure loop, the evaporation takes place at 4 bar with part of the cooling of the flue gas from the CFB combustor, the syngas cooling upstream the water scrubber and the flue gas cooler downstream the boiler. Part of the saturated steam is preheated to 400°C (fluidizing steam) and to 180°C (steam for cleaning and sealing purposes) through the heat provided by the flue gas from the CFB combustor. The remaining part of the produced steam supplies heat to the MDEA and MEA reboilers.

The BtH$_2$ DG plant (Figure B 3) has one low pressure water loop at 6 bar. The evaporation is carried out in the syngas cooling section and with part of the flue gas cooler downstream the ICE. The saturated steam is partly superheated to 200°C and sent to the gasifier. The remaining steam provides heat for the regeneration of MDEA and MEA.

The BtH$_2$ IG plant (Figure B 4) adopts two water evaporation levels. The high pressure level is needed to provide steam to the WGS reactors. Steam is evaporated at 33 bar and slightly superheated to 250 °C in the syngas cooler upstream the water scrubber. The low pressure loop operates at 4 bar. The heat sources exploited for steam evaporation are the hot syngas upstream the water scrubber, the

flue gas from the CFB combustor and from the tail gas boiler, and the hot syngas downstream the high-temperature and the low-temperature WGS. Part of the saturated steam is preheated to 400°C (fluidizing steam) and to 180°C (steam for cleaning and sealing) through the heat provided by the flue gas from the CFB combustor. The remaining part of the steam supplies heat to the MDEA and MEA reboilers. A make-up is provided to balance out the process steam consumed in the gasifier and the WGS unit.

In all the configurations, low temperature heat is used to provide the heat needed in the belt drier (Table 4-4). A water loop from 90 to 30°C supplies about 13 MW_{th} for the biomass drying.

4.7 Flexible methanol and hydrogen production

Methanol price varies over time, depending on the global market. Even though hydrogen is not currently traded as a commodity, this may change in the future, when increasingly amounts of green hydrogen may be produced from renewables and its availability and price may change on seasonal basis. In such context, multi-product plants may take economic advantage from operating flexibly to produce the good (methanol or hydrogen in this case) that generates the highest revenues. In order to design a plant which flexibly produces methanol and hydrogen, all the components must be designed to operate in both the operating conditions, i.e. methanol production mode and hydrogen production mode.

In both Biomass-to-Methanol & Hydrogen plants based on direct gasification ($BtMH_2$ DG) and on indirect gasification ($BtMH_2$ IG), the gasification island is designed and operated stably, since its operation is independent of the operating mode. On the other hand, the process units downstream the gasifier and the reformer can be designed for methanol or hydrogen operation mode and may be bypassed depending on the operating point.

In the DG-based plant, two WGS reactors are present for the production of hydrogen. In methanol production mode, WGS reactors should be partly or totally bypassed. Downstream the scrubber all the plant components are designed on the hydrogen production case due to the higher flow rate in this configuration (more syngas shift and therefore less water removed in the scrubber purge). The methanol synthesis and purification islands (including the 2nd syngas compressor) and the hydrogen production island are both installed to provide the different products according to the market needs. The CO_2 capture and compression units are designed on the hydrogen production case, since a higher CO_2 flow rate is separated in hydrogen production mode. The high pressure steam generation loop is dedicated to the methanol production (methanol synthesis reactor and distillation columns). The low pressure loop is present in both the configurations and it is designed on the hydrogen production mode.

In the IG-based plant, the methanol and hydrogen production plants are identical up to the syngas compressor (same flow rates, pressures and temperatures of the streams). Downstream the compression stage, the hydrogen production mode needs two WGS reactors in order to maximize the hydrogen production. In the methanol production mode, WGS reactors should be partly or totally bypassed. As in the previous case, methanol and hydrogen production islands are both installed and the units for CO_2 capture are designed on the hydrogen production mode. A high pressure steam generation loop is dedicated to methanol production (methanol synthesis reactor and distillation columns). Another high pressure level is necessary to provide the steam requirement for the WGS in the hydrogen case. In this case, the syngas cooler and the flue gas cooler provide heat both to the high pressure and the low pressure levels.

4.8 Process simulation results

The described performance indexes alongside with other significant quantities are reported in

Table 4-5.

The DG-based plants show the highest gasifier fuel efficiency ($\eta_{F,gas}$) which is mainly due to the use of oxygen as oxidant instead of air. The benefit of oxygen-blown gasification counterbalance the overall lower char conversion in the gasification system and the feed of steam at lower temperature. The lower fuel efficiency of the reformer ($\eta_{F,ref}$) in the DG configurations with respect to the IG cases is due to the higher syngas flow rate and to the higher difference between the gasifier and reformer exit temperatures, that cause a higher oxygen demand to heat up the raw syngas to the reforming temperature. The loss of fuel efficiency in the purification and conditioning step ($\eta_{F,pur\text{-}co}$) is due to the exothermicity of the WGS reaction. The higher efficiency loss of the hydrogen production plants is due to the higher advancement of the WGS reaction. As regards the fuel efficiencies of the synthesis ($\eta_{F,syn}$) and of the purification sections (η_{F,f_pur}) in the methanol production plants, the differences among the cases are modest and mainly related with the differences of CO/CO_2 ratio of the syngas. The loss of efficiency in the methanol synthesis is due both to the exothermicity of the reaction and to the tail gas extraction. In both plants, almost 80% of the fresh syngas thermal power ends up into crude methanol, about 5% is released with the tail gas and about 15% is lost with the exothermic reaction. The loss of efficiency in the last step of the hydrogen production plants is due to the loss of hydrogen and other fuel gases (e.g. CH_4, CO) as tail gas from the PSA unit. The resulting overall fuel efficiencies are slightly higher in the hydrogen plants (67.6-68.5%) than in the methanol plants (65.1-65.8%). The bio-hydrogen plant studied by Hannula et al. (Hannula and Melin, 2021), which shares similar plant configuration of the BtH_2 DG plant assessed in this analysis, features a global fuel efficiency of 56.9% referred to the biomass LHV downstream the dryer (vs. 62.2% of BtH_2 DG referred to dried biomass). The difference is mainly due to the higher hydrogen separation efficiency in the PSA of the BtH_2 DG plant assumed in this work (90% vs. 86%). Overall, the aforementioned fuel efficiencies obtained in this work are in the high range of the interval of values reported for similar plants in the literature (see section 1.3.3).

The carbon efficiencies show modest differences in methanol production plants, ranging from 42.3 to 42.8%.

The electric consumption of the investigated plants do not show substantial differences, as all plants need to import between 12.1 and 13.1 MW_e. In all plants, most of the electric consumption is associated to syngas compression, followed by CO_2 compression and O_2 production (in DG-based plants). The hydrogen production plants show higher CO_2 compression power, since higher portion of the inlet carbon is separated as CO_2. The DG-based plants feature higher ASU consumption due to higher oxygen demand. In the DG-based plants, the electric consumption is partly compensated by the electricity production of the ICE. This is not the case of the IG-based plants, where tail gas is burned in boilers rather than in the ICE, due to the higher heat demand for CO_2 separation.

The steam produced within the plants partly allows to satisfy the heat demand of the thermal loads and partly is consumed in the gasifier and in the high-temperature WGS reactor (only in BtH_2 IG). In DG-based plants, a higher amount of water is injected in the gasifier to reach the target steam-to-carbon ratio upstream the reformer, since a higher amount of carbon is retained in the syngas. As a consequence, considering only the contribution to the gasifier, a higher amount of water make-up is required in DG-based plants. However, in BtH_2 IG, superheated steam is added before the high-temperature shift reactor to avoid catalyst over-reduction.

The injected steam is partly converted into hydrogen through gasification, reforming and/or WGS and partly condensed back to liquid water. Most of the condensed water comes from the water scrubber purge. From 8 to 27% of the total waste water derives from flue gas cooling, before MEA-based CO_2 absorption. The waste water can be recovered and re-used within the plant after treatment. Methanol production plants do not require a net water addition, while hydrogen production plant need a net addition. This is related to the fact that in hydrogen production plants more syngas is shifted and therefore more water is converted into hydrogen.

Table 4-5 - Overall performance of the assessed plants

Performance indexes	**BtM DG**	**BtM IG**	**BtH_2 DG**	**BtH_2 IG**
$\eta_{F,dryer}$, %	108.75	108.75	108.75	108.75
$\eta_{F,gas}$, %	79.62	77.89	79.62	77.89
$\eta_{F,ref}$, %	97.47	99.26	97.47	99.26
$\eta_{F,pur\text{-}co,}$ %	98.70	99.97	94.33	95.46
$\eta_{F,syn}$, %	79.48	79.83	-	-
$\eta_{F,f\_pur,}$ %	98.27	98.03	84.97	85.38
$\eta_{F,global}$, %	**65.07**	**65.77**	**67.65**	**68.53**
$\eta_{F,eq}$, %	**50.35**	**48.29**	**55.36**	**50.15**
Carbon efficiency, %	**42.34**	**42.81**	-	-
Carbon capture rate, %	**56.60**	**55.34**	**98.98**	**98.14**
Oxygen demand, kg/s	2.57	0.50	2.57	0.50
Biofuel production, kg/s	3.27	3.31	0.56	0.57
Biofuel output, MW_{LHV}	65.07	65.77	67.65	68.53
Net electric output, P_{el}, MW	-9.93	-12.31	-7.55	-12.46
Electric generation, MW	2.17	-	5.55	-
Electric consumption, MW	12.10	12.31	13.10	12.46
Belt dryer electric consumption	0.65	0.65	0.65	0.65
Gasification combustor air fan	-	0.68	-	0.68
Gasification oxygen compressor	0.24	-	0.24	-
Syngas compressor 1	4.49	5.77	5.58	5.98
Syngas compressor 2	1.66	1.66	-	-
Methanol loop recycle compressor	0.38	0.38	-	-
MDEA electric consumption	0.23	0.12	0.40	0.30
MEA electric consumption	0.02	0.28	0.08	0.32
ASU[1]	2.27	0.49	2.27	0.49
CO_2 compression	2.13	2.25	3.85	4.00
Other auxilieries[2]	0.03	0.03	0.03	0.04
Total waste water, kg/s	3.84	3.71	2.52	5.35
Water make-up, kg/s	3.46	3.30	3.46	6.30
Net water consumption, kg/s	-0.38	-0.41	0.94	0.95

[1] Specific consumption depending on size from (Queneau and Marcuson, 1996).

[2] Other auxiliaries include Liquid Redox, water scrubber pump and water loop pumps.

Table 4-6 shows the fate of carbon in the assessed plants. The biogenic carbon which is contained in the biomass can be retained in the final product (in case of methanol production), captured and stored, and vented as CO_2. Most of the carbon is captured through pre- and post-combustion CO_2 technologies. In the direct gasifier, a small quantity of bio-char is also released with the fluidized bed solids purge. In all the plant configurations, less than 2% of the biogenic carbon is vented to the atmosphere as CO_2. In DG-based plants, most of the CO_2 is captured with the pre-combustion MDEA process (50% and 86% in case of methanol and hydrogen production, respectively) and a much lower amount of CO_2 is captured post-combustion with MEA (2% and 9% for methanol and hydrogen production, respectively). On the contrary, in IG-based plants, post-combustion capture is necessary to achieve high CO_2 capture efficiency, as 27% of the total inlet carbon is captured from the IG combustor. On the whole, CO_2 vented to the atmosphere is about 1% of the inlet carbon in the DG-based plants and 2% in the IG based-plants.

Table 4-6 – Carbon balance of the BECCS plants. Percent values referred to the total inlet carbon.

	C in fuel	**Captured CO_2 (MDEA)**	**Captured CO_2 (MEA, from gasification unit)**	**Captured CO_2 (MEA, from vented gas combustion in ICE/boiler)**	**Bio-char**	**Vented CO_2**
BtM DG	42.3 %	50.3 %	-	1.9 %	4.5 %	1.1 %
BtM IG	42.8 %	26.3 %	27.2 %	1.8 %	-	1.9 %
BtH_2 DG	-	85.8 %	-	8.7 %	4.5 %	1.0 %
BtH_2 IG	-	64.0 %	27.2 %	6.9 %	-	1.9 %

4.9 Economic analysis

The economic analysis is performed by using the *Levelized Cost* approach. A detailed description of the approach, the main assumptions and parameters for the economic analysis are present in section 2.2.3. The levelized cost of fuel (LCOF) is computed as shown in eq. (2-35).

The method for Capex and Opex estimation is extensively described in section 2.2.3. The main assumptions are summarized in Table 2-9. All the costs reported refer to the year 2019. The details of the capital costs of the plant equipment are reported in Appendix B. The CO_2 transport and injection/storage costs are considered to be equal to 13.4 €/t. The assumed cost corresponds to a 100 km pipeline transport from the conversion facility to the storage site and 2 km underground storage in deep saline formations (Hannula and Melin, 2021).

The detail of the fixed capital investment (FCI) costs of the BECCS plants is shown in Table 4-7. Alongside with the BtM and BtH_2 plants, the flexible plants (i.e. $BtMH_2$ DG and $BtMH_2$ IG) described in section 4.7, are included in the table. The biomass-to-syngas island cost differs depending on the gasification technology. However, the cost of the DG- and IG-based plants is similar, as the higher cost of the ASU in the DG-based plants is offset by the higher cost of the dual fluidized bed gasification. The methanol production plants hold the lowest syngas purification, conditioning and compression cost, since they do not have or have a smaller WGS section. The flexible methanol and hydrogen production plants have the highest syngas purification, conditioning and compression cost, since they require both the higher cost WGS section for hydrogen production, and the cost for CO_2 separation and additional compression sections for methanol production. The DG-based plants for methanol production show a higher syngas purification, conditioning and compression cost compared to the IG-based plants, because of the more complex syngas conditioning process and the higher flow rate of captured CO_2. The higher complexity of the methanol synthesis and purification island compared to the PSA unit leads to a higher cost of the methanol synthesis section compared to hydrogen purification. Again, the flexible $BtMH_2$ plants feature the highest capital investment cost, as they include the equipment for the delivery of both products. The heat recovery section is slightly more expensive in the DG-based plants due to the installation of the CHP internal combustion engine instead of the boiler.

The fixed capital investment (FCI) of plants without CCS can be approximately derived by summing up all the aforementioned cost items. The simplifying assumption is that without CO_2 scrubbing units, a different design of the heat recovery would likely be preferable and might include a steam cycle for power production. On the other hand, MDEA scrubbing cannot be avoided to reach the target module in the methanol production plants. The FCI of plants without CCS results to be lower in the methanol production plants and in the IG-based plants. When CCS is considered, MEA scrubbing, CO_2 capture and compression units in all the plants, and MDEA in BtH_2 plants must be added. In hydrogen production plants with CCS, MDEA technology is necessary to obtain high-purity CO_2 stream not diluted with other compounds in the PSA off-gas. The capital costs increases from a minimum of 12% in BtM DG-based plant (174.6 vs. 155.9 M€) up to a maximum of 43% in the BtH_2 IG plant (218.8 vs. 153.2 M€). Overall, the IG-based plants with CCS have the highest FCI due the larger size of the post-combustion CO_2 capture unit.

In the flexible $BtMH_2$ plants, the equipment for CCS represents about 16% and 24% of the FCI in the DG-based and IG-based plants respectively. The inclusion of the methanol synthesis process involves an increase of 9-14% of the FCI compared to the corresponding BtH_2 plants.

Table 4-7 – Breakdown of the fixed capital investment costs of the biomass to methanol (BtM), biomass to hydrogen (BtH_2) and flexible biomass to methanol and hydrogen ($BtMH_2$) plants.

Fixed capital investment	BtM DG	BtM IG	BtH_2 DG	BtH_2 IG	$BtMH_2$ DG	$BtMH_2$ IG
Biomass-to-syngas, M€	**95.54**	**92.22**	**95.54**	**92.22**	**95.54**	**92.22**

Fixed capital investment	**BtM DG**	**BtM IG**	**BtH_2 DG**	**BtH_2 IG**	**$BtMH_2$ DG**	**$BtMH_2$ IG**
Feedstock handling	8.91	8.91	8.91	8.91	8.91	8.91
Belt dryer	7.11	7.11	7.11	7.11	7.11	7.11
ASU	23.32	10.25	23.32	10.25	23.32	10.25
O_2 compressor	2.35	0.43	2.35	0.43	2.35	0.43
Pressurized O_2 CFB gasifier	29.58	-	29.58	-	29.58	-
Steam CFB gasifier	-	13.25	-	13.25	-	13.25
Combustor with fluegas treatment	-	30.87	-	30.87	-	30.87
Ceramic hot-gas filter	6.99	6.17	6.99	6.17	6.99	6.17
Catalytic reformer	17.27	15.24	17.27	15.24	17.27	15.24
Syngas purification, conditioning and compression, M€	**46.42**	**38.54**	**54.00**	**52.19**	**74.89**	**68.02**
Scrubber	1.38	1.23	1.38	1.23	1.38	1.23
Liquid redox	2.90	2.58	2.90	2.58	2.90	2.58
Syngas compressor 1	14.56	17.23	16.84	17.65	16.84	17.65
Syngas compressor 2	7.49	7.48	-	-	7.49	7.48
Activated carbon	0.37	0.33	0.37	0.33	0.37	0.33
Waste water treatment	1.53	1.34	1.02	1.70	1.53	1.70
WGS reactor	5.30	-	31.48	28.70	31.48	28.70
CO_2 removal pre-combustion (MDEA)	12.89	8.35	-	-	12.89	8.35
Methanol and hydrogen production, M€	**10.99**	**10.98**	**5.65**	**5.10**	**16.64**	**16.09**
Methanol synthesis BWR	6.97	6.95	-	-	6.97	6.95
Recycle compressor	2.10	2.09	-	-	2.10	2.09
Stabilizing column	0.41	0.41	-	-	0.41	0.41
Concentration column	1.52	1.53	-	-	1.52	1.53
PSA	-	-	5.65	5.10	5.65	5.10
Heat recovery, M€	**2.97**	**2.52**	**5.55**	**3.72**	**5.77**	**4.09**
CHP internal combustion engine	1.29	-	3.03	-	3.03	-
Boiler	-	0.43	-	0.97	-	0.97
Heat exchangers	1.68	2.09	2.52	2.76	2.73	3.12
Total FCI without CCS, M€	**155.91**	**144.26**	**160.74**	**153.25**	**192.83**	**180.42**
CO_2 separation and compression, M€	**18.69**	**41.83**	**49.83**	**65.52**	**36.94**	**57.17**
CO_2 removal pre-combustion (MDEA)	-	-	18.44	15.16	+5.56[2]	+6.81[2]
Decreased PSA cost[1]	-	-	-2.02	-1.52	-2.02	-1.52
CO_2 removal post-combustion (MEA)	4.29	26.85	11.96	29.89	11.96	29.89
CO_2 compression and dehydration unit	14.40	14.98	21.44	21.99	21.44	21.99
Total FCI, M€	**174.60**	**186.09**	**210.56**	**218.77**	**229.77**	**237.59**

[1] BtH_2 plants without CCS include higher size PSA unit because a higher amount of syngas needs to be treated when CO_2 is not separated by MDEA process. The decreased cost of PSA when MDEA is added to the plant is taken into account.

[2] In $BtMH_2$ plants, the MDEA unit is designed on methanol production without CCS and on hydrogen production with CCS. These values correspond to the incremental cost of the MDEA process when designed on hydrogen production rather than on methanol production.

Table 4-8 shows the main results of the economic analysis based on the levelized cost approach. The multi-product plants are assumed to be operated for 50% of the time in methanol production mode and 50% of the time in hydrogen mode. The methanol production plants show the lowest yearly total costs, followed by the hydrogen production plants and the flexible multi-product plants. The hydrogen production plants show the highest CO_2 transport and storage cost because of the highest amount of CO_2 separated. The methanol production plants are characterized by lower LCOF, followed by the hydrogen production plants and the multi-product plants. By considering the same final product, the DG-based plants result in lower LCOF. Compared to the bio-hydrogen plant assessed by Hannula and Melin (2021), who estimated a hydrogen cost of 42.2 €/GJ (section 1.3.3), 13% lower LCOF have been obtained in this work for the BtH_2 DG plant, mainly due to the fact that Hannula et al. referred to a First-of-a-kind (FOAK) plant, involving higher total capital investment than in this work, that refers to N^{th}-of-a-kind (NOAK) cost assumptions.

Table 4-8 - Main results of the economic analysis and levelized cost of fuel

Economic results	**BtM DG**	**BtM IG**	**BtH_2 DG**	**BtH_2 IG**	**$BtMH_2$ DG**	**$BtMH_2$ IG**
TCI·CCF, M€/y	24.12	25.71	29.09	30.22	31.74	32.82
O&M, M€/y	17.71	18.82	20.82	21.76	22.51	23.36
Purchased electricity cost, M€/y	3.01	3.74	2.29	3.78	2.65	3.76
CO_2 transport and storage cost, M€/y	2.10	2.23	3.81	3.95	2.95	3.09
Biomass cost, M€/y	13.32	13.32	13.32	13.32	13.32	13.32
Total cost, M€/y	60.27	63.81	69.33	73.03	73.18	76.35
Methanol production, t/y	92,823	93,822	-	-	46,412	46,911
Hydrogen production, t/y	-	-	16,006	16,214	8,003	8,107
LCOF, €/t	649	680	4,331	4,505	-	-
LCOF, €/GJ	32.63	34.18	36.07	37.51	38.83	40.03

Figure 4-5 shows the marginal CO_2 avoidance cost vs. the captured CO_2 in the DG- and IG-based plants respectively. In the DG-based plants, about 5% of the CO_2 is avoided at zero marginal cost, stored in the unconverted biochar. The horizontal lines on the left hand side of the graph represent the marginal cost of adding CCS to a biomass-to-X plant (i.e. adding the CO_2 compression unit in the methanol production plant and adding MDEA scrubbing and CO_2 compression in the hydrogen production plant). On the right hand side, the step increase represents the marginal cost of adding the post-combustion MEA scrubbing unit and the corresponding CO_2 compression.

In the plot, the following assumptions are adopted for the sake of simplicity: i) the scale effects on the capital cost of the equipment for CO_2 capture, transport and storage are not taken into account (if more CO_2 is captured, the CO_2 avoidance cost should decrease, generating declining lines instead of horizontal ones); ii) the absence of MDEA and MEA units would favor the heat integration of the plant with a steam cycle for power production, affecting the economics of the plants without CO_2 capture or with partial capture.

In the BtM DG plant, a CO_2 capture rate of 54.7% is reached at a cost of 40.8 €/t_{CO2} through compression (27.4 €/t_{CO2}) and transport and storage (13.4 €/t_{CO2}). By adding the MEA post-combustion capture unit and increasing the CO_2 compression capacity, the CO_2 capture rate is increased by 1.8% at a marginal cost of 204.9 €/t_{CO2}. In the BtH_2 DG plant, a CO_2 capture rate of 90.30% is reached at a cost of 52.2 €/t_{CO2} (38.8 €/t_{CO2} for capture + 13.4 €/t_{CO2} for transport and storage). The marginal cost of adding post-combustion CO_2 capture and increase capture rate up to 99% is 135.3 €/t_{CO2}.

In BtM IG plant, a CO_2 capture rate of 26.3% is reached at a cost of 45.8 €/t_{CO2} (32.4 €/t_{CO2} for capture + 13.4 €/t_{CO2} for transport and storage), through the addition of compressors for the CO_2 separated by the MDEA unit. By adding the MEA post-combustion capture unit and increasing the

CO_2 compression capacity, the CO_2 capture rate is increased by 29% at a marginal cost of 105.1 €/t_{CO2}. In BtH_2 IG plant, a CO_2 capture rate of 64% is reached at 55.6 €/t_{CO2} by integrating the MDEA separation process and CO_2 compression (42.2 €/t_{CO2} for capture + 13.4 €/t_{CO2} for transport and storage). The addition of the MEA plant and the increase of the CO_2 compression unit allows increasing the capture rate up to 98.1%, at a marginal cost of 98.4 €/t_{CO2}. Post-combustion MEA scrubbing is needed in IG-based plants to reach high CO_2 capture rates.

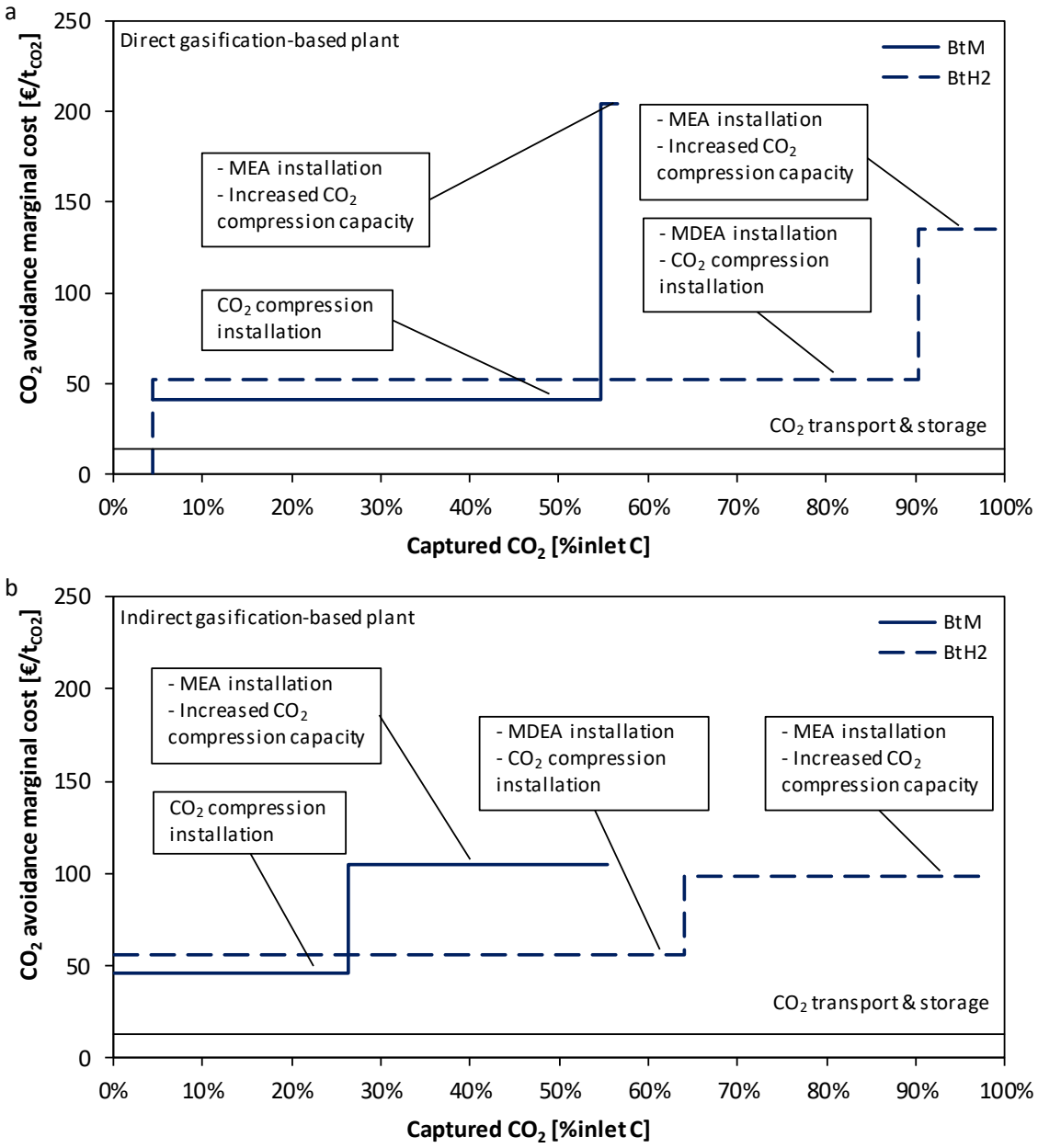

Figure 4-5 – CO_2 avoidance marginal cost vs. captured CO_2 in DG-based plants (a) and in IG-based plants (b). In DG-based plants, 4.5% of the inlet carbon is stored as biochar.

BECCS plants benefit from CO_2 credits that reward their capacity of removing CO_2 from the atmosphere. Figure 4-6 shows the LCOF as a function of the CO_2 credits for plants with no CCS, partial CCS (CCSp, achieved via CO_2 compression in BtM, and CO_2 separation and compression in BtH_2 plants) and maximum CCS (CCSm, achieved via MEA-based CO_2 separation and increased CO_2 compression capacity).

The BtM DG plant (Figure 4-6a) needs 40.84 €/t_{CO2} and 46.76 €/t_{CO2} in CCSp and CCSm cases respectively to reach the production cost of 28.66 €/GJ of the case without CCS. The two CCS configurations hold very similar trend of the LCOF in the selected CO_2 credits range since they capture a very similar amount of CO_2. BtM IG plant (Figure 4-6b) requires 45.76 and 76.87 €/t_{CO2} in CCSp and CCSm cases respectively to reach the production cost of 27.33 €/GJ of the case with no CCS. For CO_2 credits higher than 105.1 €/t_{CO2} (i.e. the marginal cost to achieve the highest capture rate), the CCSm configuration becomes economically more competitive than the CCSp case.

The BtH_2 DG plant (Figure 4-6c) must be rewarded with 52.23 and 59.85 €/t_{CO2} in CCSp and CCSm respectively to achieve 27.22 €/GJ of the case without CCS. CO_2 credits of 135.3 €/t_{CO2} makes the CCSm configuration more competitive than CCSp. BtH_2 IG plant (Figure 4-6d) needs 55.63 and 70.48 €/t_{CO2} in CCSp and CCSm respectively to reach the same LCOF of 26.83 €/GJ of the case with no CCS. CO_2 credits of 98.4 €/t_{CO2}, again equal to the marginal cost for maximum capture, are necessary to make CCSm the most competitive case.

It is also worth observing that hydrogen production plants show steeper lines compared to the methanol plants thanks to the higher amount of captured CO_2 per GJ of delivered product. Therefore, BtH_2 plants become economically favourable at higher CO_2 credits.

In CCSm cases, CO_2 credits of 148 €/t_{CO2} for DG-based and 158 €/t_{CO2} for IG-based allow achieving methanol production cost of around 400 €/t (i.e. 20.1 €/GJ) and credits of 131 €/t_{CO2} for DG-based and 138 €/t_{CO2} for IG-based allow achieving H_2 production costs of 2 €/kg (i.e. 16.7 €/GJ).

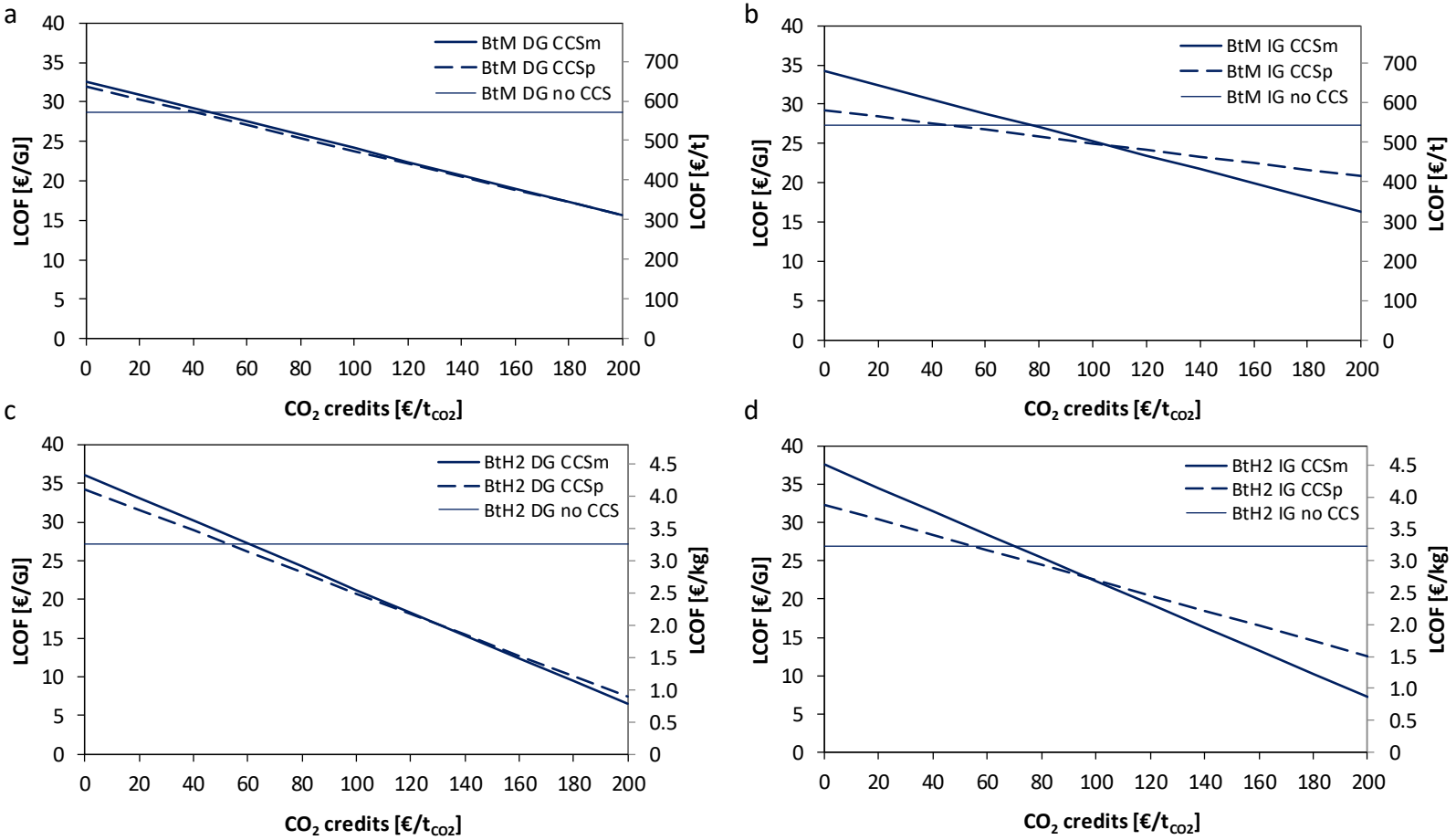

Figure 4-6 – LCOF vs. CO_2 credits of BECCS plants: (a) BtM DG, (b) BtM IG, (c) BtH_2 DG, (d) BtH_2 IG. CCSp: installation of CO_2 compression. CCSm: installation of MEA and increase of CO_2 compression capacity.

As previously mentioned, in a context where the expected time-dependent relative value of power, carbon-based products, hydrogen, and sequestered CO_2 determines a significant variation of the revenues of bioenergy plants, multi-product plants to be operated flexibly to produce the goods with the highest added value may gain an economic advantage. For a simplified economic analysis of a flexible methanol and H_2 plant, three different methanol selling prices (i.e. 450, 550, and 650 €/t) are selected, assumed to remain constant along the year. Two simple linear profiles are assumed for the cumulative hydrogen selling price (see Figure 4-7), ranging between a high price of 7 €/kg or 4 €/kg, representative of periods with low availability of renewable electricity and green H_2, and a low price of 1 €/kg, representative of periods with high availability of renewable electricity and green H_2. These two scenarios involve an average yearly H_2 market price of 4 and 2.5 €/kg. The rationale behind the assumption of hydrogen price profile is that water electrolysis is expected to become the leading technology for hydrogen production in the long-period. Therefore, the breakeven hydrogen selling price will be influenced by the electricity price, inheriting its volatility, possibly shrunk by some degree depending on the availability and cost of H_2 storage. CO_2 credits of 120 €/t_{CO2} are assumed for the stored CO_2 in these calculations.

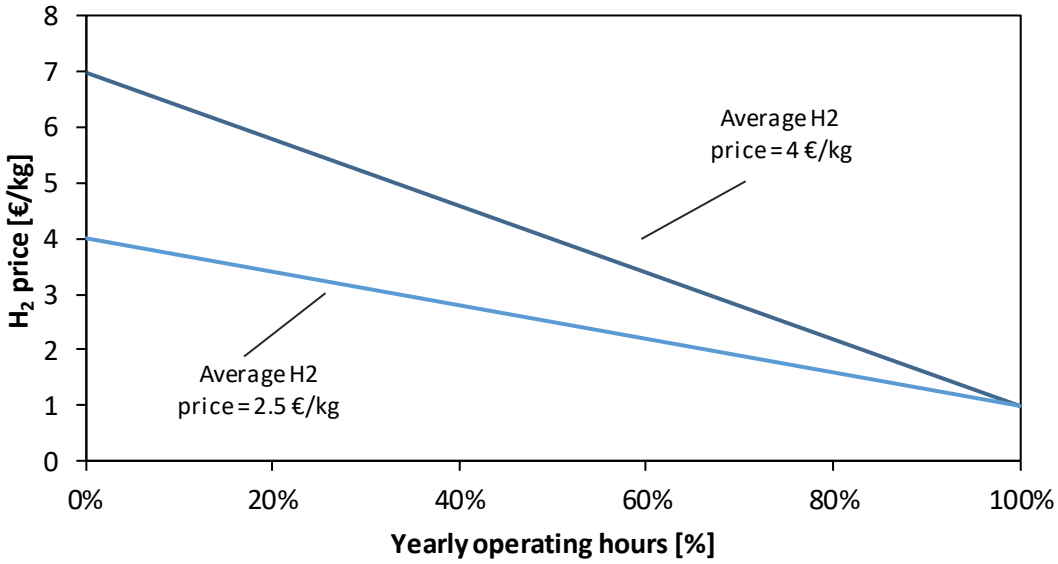

Figure 4-7 – Yearly hydrogen selling price profiles.

In Figure 4-8a-b, the internal rate of return (IRR) of the flexible multi-product plants producing methanol and hydrogen is compared with the IRR of methanol and hydrogen plants delivering a single-product. On the x-axis, the fraction of hours in which the plants operate producing hydrogen is reported. Methanol plants are depicted as points on the left ordinate axis, since they never produce hydrogen. The hydrogen plant curve shows an increasing trend with the yearly operating hours. Therefore, 100% of the yearly operating hours corresponds to the optimal condition. It has to be noted that the optimal number of operating hours could be lower than 100%, in case the operational costs (biomass and power purchase, variable O&M) overtake the hydrogen selling price, making the interruption of the plant operation economically convenient. For a specified methanol price, the maximum IRR obtained by the multi-product plant must be compared with the highest IRR found on the hydrogen production plant curve and the value achieved by the methanol plant for that assumed price. As shown in Figure 4-8a, for methanol selling prices of 650, 550 and 450 €/t,

the economically optimum of the multi-product plant is achieved when it operates for about 70, 80 and 90% of the in hydrogen mode and the remaining hours in methanol mode. IRRs of 22.1, 21.1 and 20.5% are higher than the optimal values generated by the single-product methanol plants (i.e. 20.4, 15.5 and 10.2%), but lower than the optimal value generate by the single-product hydrogen plant (i.e. 23%).

Considering the lower hydrogen price scenario (Figure 4-8b), for the maximum methanol selling price curve (i.e. 650 €/t), the multi-product plant should operate for about 40% of the time in hydrogen mode and the remaining hours in methanol mode. In this case, the IRR of 14.3% is higher than the optimal value generated by the single-product hydrogen plant (i.e. 12.3%), but lower than the value generated by the single-product methanol plant (i.e. 20.4%). Considering lower methanol selling prices (i.e. 550 and 450 €/t), the multi-product plant should operate for 60% and 80% of the yearly operating hours in hydrogen mode. In this case, the IRRs of 12.2% and 10.8%, for the 550 and 450 €/t methanol prices respectively, are lower than the hydrogen single-product plant, but at least for the 450 €/t higher than the single-product methanol plant.

Overall, with the assumptions of this study, multi-product plants result in slightly higher or slightly lower IRR of the single-product plant with the highest revenues. On the other hand, they are never the worst case scenario despite the highest investment costs, thus offering a potential advantage from the financial risk perspective thanks to lower exposure to market price volatility.

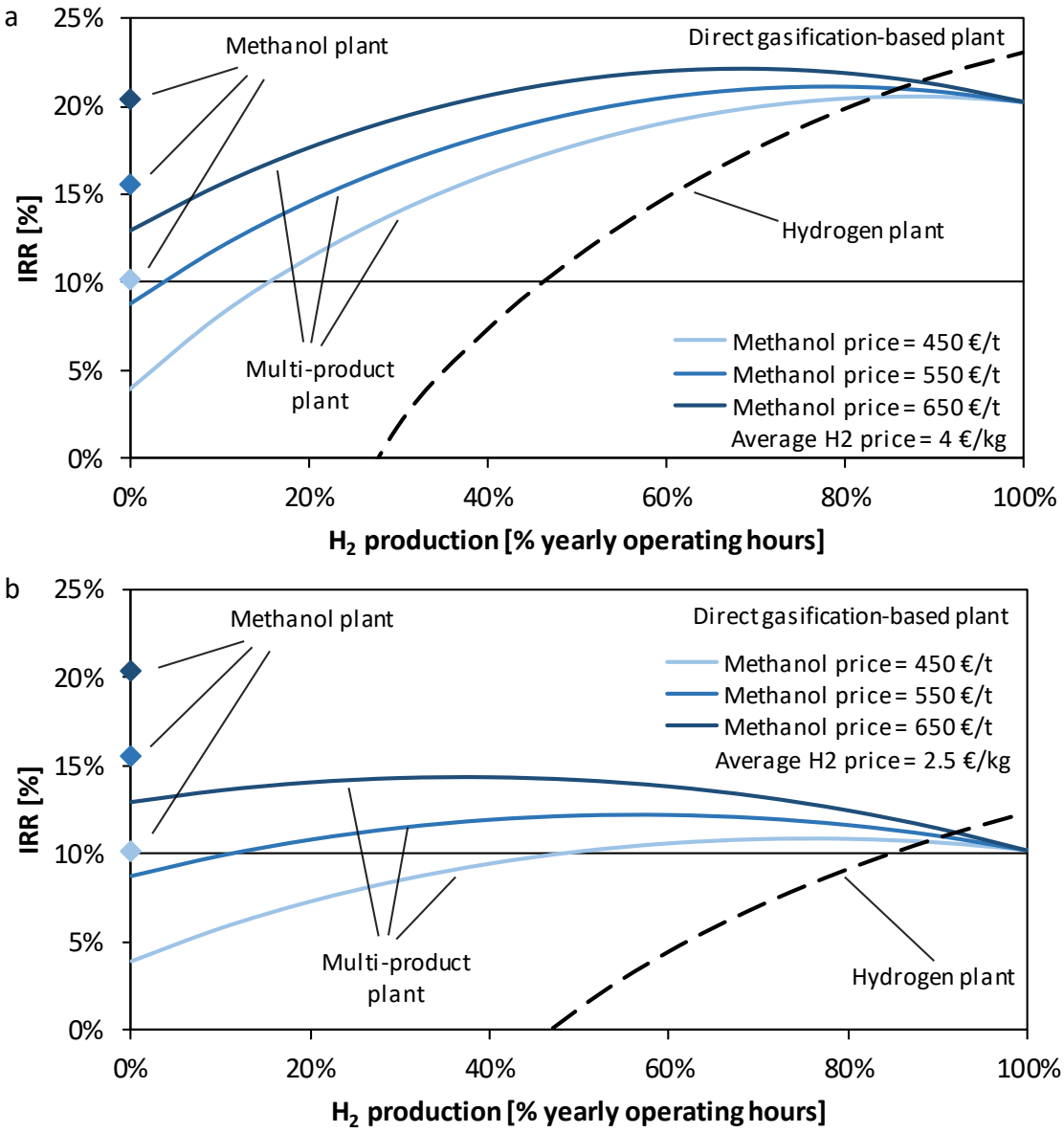

Figure 4-8 – IRR vs. yearly operating hours in hydrogen production mode: (a) yearly average H_2 price = 4 €/kg, (b) yearly average H_2 price = 2.5 €/kg.

4.10 Conclusions

In this chapter, a techno-economic analysis of biomass-to-methanol and biomass-to-hydrogen plants with CCS has been carried out. Each plant is studied including either oxygen-blown direct gasification (DG) or air-blown dual fluidized bed indirect gasification (IG). MDEA and MEA-based solvent scrubbing are considered as CO_2 removal technologies from syngas and flue gas respectively. This solutions have been compared in term of fuel efficiency and carbon recovery potential. The economic impact of adding CCS and of increasing the amount of CO_2 which is captured within the plants is investigated together with the impact of CO_2 credits on the overall economics of the plants.

A third solution involving multi-product bioenergy plants able to flexibly produce methanol or hydrogen depending on the relative selling price are hence introduced in the analysis.

The main conclusions can be summarised as follows:

- in DG-based plants, most of the CO_2 is captured from syngas with MDEA solvent (50% and 86% of the inlet carbon for methanol and hydrogen production, respectively) and a much lower amount of CO_2 is captured from flue gas with MEA (2% and 9% for methanol and hydrogen production, respectively). Conversely, in IG-based plants, MEA is necessary to achieve high CO_2 capture efficiency, as 27% of the total inlet carbon is captured from the IG combustor and between 2% and 7% of the CO_2 is separated from the flue gas of the tail gas boiler. Because of the high heat demand for CO_2 separation in IG cases, plants have been designed without a heat recovery steam cycle. In this way the heat available for solvent regeneration is maximized, penalizing the electricity balance.
- The maximum CO_2 capture rate achieved is 55-57% in methanol production plants and 98-99% in hydrogen production plants. Capture rate in methanol plants is lower than in hydrogen plants, as part of the inlet carbon is stored in the product. In all the assessed cases, less than 2% of the inlet carbon is vented to the atmosphere as CO_2.
- The overall fuel efficiencies are slightly higher in the hydrogen plants (67.6-68.5%) than in the methanol plants (65.1-65.8%), with minor dependency on the gasification technology. The obtained values are in the high range of the fuel efficiency intervals reported in the literature.
- Methanol production plants are characterized by lower LCOF (referred to the LHV energy output) than hydrogen plants: 32.6-34.2 €/GJ (or 649-680 €/t) vs. 36.1-37.5 €/GJ (or 4.3-4.5€/kg), with zero revenues from CO_2 storage. This is mainly due to the higher cost for CO_2 capture in hydrogen plants, where higher amounts of CO_2 are separated and compressed. By considering the same final product, the DG-based plants show slightly lower LCOF (32.6-36.1 €/GJ vs. 34.2-37.1 €/GJ), mainly thanks to the lower CO_2 separation cost.
- In methanol production plants, a CO_2 capture rate up to 55 and 26% can be reached at marginal costs of 41 and 46 €/t_{CO2} for DG- and IG-based plants respectively (including 13.4 €/t_{CO2} for CO_2 transport and storage). Such relatively low costs are associated to the compression (27-32 €/t_{CO2}) and transport and storage (13.4 €/t_{CO2}) costs, as CO_2 separation from syngas is anyway needed to produce syngas tailored for methanol synthesis. By adding MEA-based post-combustion capture and increasing the size of the CO_2 compression unit, the CO_2 capture rate is increased by 2%$_{pt}$ and 29%$_{pt}$ at a marginal cost of 205 and 105 €/t_{CO2} for DG- and IG-based plants respectively. A similar figure is obtained in the hydrogen plants, where the addition of MDEA-based CO_2 separation (not needed in plants without CCS) allows achieving a CO_2 capture rate of 90% and 64% at a cost of 52 and 56 €/t_{CO2} for DG- and IG-based plants respectively. By adding post-combustion capture units and increasing the CO_2 compression unit size, the CO_2 capture rate can

be increased up to 99 and 98% at a marginal cost of 135 and 98 €/t_{CO2} for DG- and IG-based plants respectively.

- When credits for CO_2 storage are included, breakeven price of 47-77 €/t_{CO2} make the plants with maximum CO_2 capture rate competitive with the corresponding plants without CCS. CO_2 credits of 148-158 €/t_{CO2} allow achieving methanol production cost of around 400 €/t and credits of 131-138 €/t_{CO2} allow achieving H_2 production costs of 2 €/kg. Because of the higher amount of captured CO_2 per unit of product output, H_2 production plants obtain higher economic benefits from higher CO_2 storage credits.
- Multi-product plants producing flexibly methanol and hydrogen results in the highest capital costs (+9-14% than the corresponding H_2 production plant) and the highest LCOF. However, with the assumptions adopted in this analysis (fixed methanol selling price varied between 450 and 650 €/t and time dependent H_2 selling price between 1 and 4 or 7 €/kg), the internal rate of return of the flexible methanol+H_2 plants results slightly higher or slightly lower than the corresponding single-product plant with highest revenues. On the other hand, multi-product flexible plants are never the worst case scenario despite the highest investment costs, thus offering a potential advantage from the financial risk perspective thanks to lower exposure to market price volatility.

Chapter 5
Conclusions and outlook

This work aimed at assessing the energy, environmental and economic performance of flexible biomass-to-X plants, based on biomass gasification. Two main pathways are investigated:

- power and biomass-to-X plants, where the bioenergy plant is integrated with a water electrolyzer which generates hydrogen to be combined with the syngas from biomass gasification. Such a plant design allows to increase the carbon utilization and product yield when the electrolysis unit is in operation (i.e. during low electricity price periods);
- biomass-to-X plant with CCS, where the bioenergy plant includes the capture of the excess CO_2 generated in the conversion of the biomass into the final product(s). If the captured CO_2 is permanently stored underground, such plants can produce negative emissions.

The thesis investigates different types of gasification technologies (direct, indirect and sorption-enhanced gasification) and different final products (methanol and hydrogen). The research work is based on modelling and development of techno-economic analysis of different plant configurations. The main conclusions are listed below:

- in power and biomass-to-X plants, the fuel synthesis and purification unit should be sized to achieve high power-to-methanol conversion efficiencies when electrolysis hydrogen is fed to the process. This involves an oversizing of the process units with respect to the baseline operating conditions without hydrogen addition. This is due to the high cost of hydrogen from electrolysis compared to the cost of oversizing the synthesis unit;
- because of the high capital cost of electrolysis systems, high capacity factors of the electrolyser are needed to provide cost competitive e-methanol to the market and to pay back the capital cost of the electrolysis unit;
- since the investment in an electrolysis system for a power and biomass-to methanol plant is profitable for high capacity factors (higher than ~80%), the operational flexibility should be exploited by avoiding the consumption of high-price electricity rather than in the use low-price “excess” electricity that can only be available for a limited number of hours;
- the attractiveness of operating power and biomass-to-X plants in a flexible way may increase significantly in future scenarios with very high penetration of intermittent renewables, leading to low average electricity prices but also longer periods of high peak prices. Conversely, current electricity price curves

with limited number of very high price hours during the year would not justify plants conceived to operate flexibly;

- relatively low credits (i.e. lower than 80 €/t_{CO2}) for CO_2 storage are needed to make biomass-to-X plants with CCS competitive with the corresponding plants without CCS. CO_2 credits of 130-160 €/t_{CO2} allow achieving competitive methanol and hydrogen production costs of 400 €/t and 2 €/kg respectively;
- in the future carbon-constrained world, the best bioenergy conversion pathway (electricity, H_2, methanol, etc.) with/without CCS will depend on the relative value/price of the products and of CO_2, that vary over time with different time scales. In this context, multi-product plants can operate flexibly to produce the good with the highest added value;
- with the assumption of this work, multi-product flexible plants result to be never the worst case scenario compared to similar mono-product plants despite the highest investment costs, thus offering a potential advantage from the financial risk perspective.

This work assessed several case studies and proposed a methodological basis for the analysis of flexible biomass conversion plants. From this basis, future investigations may develop in the following areas:

- the analysis conducted in this thesis provides directions for possible future studies on different processes that integrate different technologies (e.g. high temperature electrolysers, electrified gasifiers etc.) or that consider the production of other goods besides methanol and hydrogen considered in this work (e.g. jet fuels, biochar, electricity);
- the analysis developed in this study provides data that may be used to understand the role that biomass conversion processes may have in the decarbonisation of the global economy. Such process models can be integrated into hourly simulation models of the electricity grid and the broader energy system to assess the environmental and economic impact of flexible biomass conversion plants;
- to evaluate the sustainability of the assessed processes, the results obtained in this study must be supplemented with a comprehensive environmental analysis based on Life-Cycle Assessment, which quantifies the different impacts taking into account the type of biomass feedstock and its supply chain, the avoided emissions with the production of the different bio-products, and the alternative uses of electricity that are largely site specific;
- the capability of modulating electricity consumption will be crucial in the next decades, when the electric grid will have to manage increasing amounts of intermittent renewables. The economic attractiveness of flexible PBtX plants will largely rely on electric market that valorise flexibility, for instance via demand response mechanisms;
- the results of this study might be complemented in future works with dynamic analyses and by experimental validation to investigate the capability of the plant to react to load variations.

Nomenclature

Acronyms

ASU	Air separation unit
ATR	Autothermal reformer
BECCS	Bioenergy with carbon capture and storage
BFB	Bubbling fluidized bed
BO	Baseline operation
BtH_2	Biomass-to-hydrogen
BtM	Biomass-to-Methanol
$BtMH_2$	Biomass-to-methanol and hydrogen
BtX	Biomass-to-X
BWR	Boiling water reactor
CCS	Carbon capture and storage
CFB	Circulating fluidized bed
CZA	Methanol synthesis catalyst $Cu/ZnO/Al_2O_3$
DG	Direct gasification
DGns	Direct gasification no storage
DME	Dimethyl ether
EO	Enhanced operation
GHSV	Gas hourly space velocity
HEN	Heat exchanger network
HP	High pressure level
HRSC	Heat recovery steam cycle
ICE	Internal combustion engine
IG	Indirect gasification
IRR	Internal rate of return
KPI	Key performance indicator
LHV	Lower heating value
LP	Low-pressure level
M	Methanol
MINLP	Mixed integer nonlinear programming
MP	Medium-pressure level
NPV	Net present value
PBtM	Power & Biomass-to-Methanol
PBtX	Power & Biomass-to-X
PtX	Power-to-X
RR	Recycle ratio
SEG	Sorption-enhanced gasification
WGS	Water gas shift

Symbols

$C_{feedstock}$	Cost of feedstock
$C_{fixed\ O\&M}$	Fixed O&M cost
C_{ut}	Utilities cost
C_{tot}	Total cost
CE	Carbon efficiency
CF_{el}	Electrolyser capacity factor
CCF	Capital charge factor
E	Delivered-equipment cost
$F_{C,biom}$	Carbon molar flow rate in the inlet biomass
$F_{C,stored}$	Carbon molar flow rate for storage
$F_{fuel,max,i}$	Maximum fuel production
F_i	Component – i molar flow rate
f_i	Multiplying factors for estimating the total capital investment
F_M	Methanol molar flow rate
F_M	Methanol molar flow rate
FCI	Fixed-capital investment
G_S	Solid mass flow per cross-section unit
h_{eq}	Equivalent yearly operating hours
IRR	Internal rate of return
L	ICE thermal input power (load)
$LCOF$	Levelized cost of fuel
LT	Plant lifetime
$\dot{m}_i$	Component $-i$ mass flow rate
M_{tot}	Amount of fuel
P_{el}	Net electric output
P_{th}	Thermal output
PCE	Potential carbon efficiency
S	ICE size
TCI	Total capital investment cost
ν_i	Stoichiometric coefficient – i
WC	Working capital
WTP_{ST}	Short-term willingness to pay
α	Discount rate
$\eta_{el,ref}$	Reference steam cycle electric efficiency
$\eta_{F,dry}$	Dryer fuel efficiency
$\eta_{F,SEG}$	SEG fuel efficiency
$\eta_{F,ref}$	Reformer fuel efficiency
$\eta_{F,pur}$	Purification fuel efficiency
η_{F,M_syn}	Methanol synthesis fuel efficiency
η_{F,M_pur}	Methanol purification fuel efficiency
$\eta_{F,global}$	Global fuel efficiency

$\eta_{F,i}^{u}$	Useful fuel efficiency of the $-i$ unit
$\eta_{F,eq}$	Equivalent fuel efficiency
η_{HtF}	Hydrogen-to-fuel efficiency
η_{PtF}	Power-to-fuel efficiency
χ_C	Number of carbon atoms in the product molecule

Bibliography

Afman, M., Hers, S., and Scholten, T. (2017). Energy and electricity price scenarios 2020-2023-2030. Input to Power to Ammonia value chains and business cases.

Alamia, A., Òsk Gardarsdòttir, S., Larsson, A., Normann, F., and Thunman, H. (2017). Efficiency Comparison of Large-Scale Standalone, Centralized, and Distributed Thermochemical Biorefineries. *Energy Technol.* 5, 1435–1448. doi:10.1002/ente.201600719.

Albrecht, F. G., König, D. H., Baucks, N., and Dietrich, R.-U. (2017). A standardized methodology for the techno-economic evaluation of alternative fuels – A case study. *Fuel* 194, 511–526. doi:10.1016/j.fuel.2016.12.003.

Amos, W. A. (1998). Report on Biomass Drying Technology Report on Biomass Drying Technology. doi:NREL/TP-570-25885.

Antonini, C., Treyer, K., Moioli, E., Bauer, C., Schildhauer, T. J., and Mazzotti, M. (2021). Hydrogen from wood gasification with CCS – a techno-environmental analysis of production and use as transport fuel. *Sustain. Energy Fuels* 5, 2602–2621. doi:10.1039/D0SE01637C.

Armbrust, N., Schweitzer, D., Gredinger, A., Beirow, M., Poboss, T. B. N., Hawthorne, C., et al. (2014). Gasification of Biomass with In-Situ CO2 Capture and Separation in a 200 kWth Pilot Plant Fluidized bed gasification infrastructure. in *Gasification Technologies* (Washington D.C.).

Arnaiz del Pozo, C., Cloete, S., and Jiménez Álvaro, Á. (2021). Carbon-negative hydrogen: Exploring the techno-economic potential of biomass co-gasification with CO2 capture. *Energy Convers. Manag.* 247, 114712. doi:10.1016/j.enconman.2021.114712.

Aspentech (2018). Aspen Plus Methanol Synthesis Model.

Baker, S. E., Stolaroff, J. K., Peridas, G., Pang, S. H., Goldstein, H. M., Lucci, F. R., et al. (2020). Getting to Neutral: Options for Negative Carbon Emissions in California. Available at: https://www.climateworks.org/programs/carbon-dioxide-removal/getting-to-neutral/.

Bertuccioli, L., Chan, A., Hart, D., Lehner, F., Madden, B., and Standen, E. (2014). Development of water electrolysis in the European Union - Final report. FCH-JU.

Blanco, H., Nijs, W., Ruf, J., and Faaij, A. (2018). Potential for hydrogen and Power-to-Liquid in a low-carbon EU energy system using cost optimization. *Appl. Energy* 232, 617–639. doi:10.1016/j.apenergy.2018.09.216.

Brandl, P., Bui, M., Hallett, J. P., and Mac Dowell, N. (2021). Beyond 90% capture: Possible, but at what cost? *Int. J. Greenh. Gas Control* 105, 103239. doi:10.1016/j.ijggc.2020.103239.

Brown, A., Waldheim, L., Landälv, I., Saddler, J., Ebadian, M., McMillan, J. D., et al. (2020). Advanced Biofuels – Potential for Cost Reduction.

Bui, M., Fajardy, M., Zhang, D., and Mac Dowell, N. (2020). Delivering negative emissions from biomass derived hydrogen. 1–81.

Bussche, K. M. V., and Froment, G. F. (1996). A Steady-State Kinetic Model for Methanol Synthesis and the Water Gas Shift Reaction on a Commercial Cu/ZnO/Al2O3Catalyst. *J. Catal.* 161, 1–10. doi:10.1006/jcat.1996.0156.

Butera, G., Højgaard Jensen, S., Østergaard Gadsbøll, R., Ahrenfeldt, J., and Røngaard Clausen, L. (2020). Flexible biomass conversion to methanol integrating solid oxide cells and TwoStage gasifier. *Fuel* 271, 117654. doi:10.1016/j.fuel.2020.117654.

Butera, G., Jensen, S. H., Ahrenfeldt, J., and Clausen, L. R. (2021). Techno-economic analysis of methanol production units coupling solid oxide cells and thermochemical biomass conversion via the TwoStage gasifier. *Fuel Process. Technol.* 215, 106718. doi:10.1016/j.fuproc.2020.106718.

Camia, A., Rober, N., Jonsson, R., Pilli, R., Garcia-Condado, S., Lopez-Lozano, R., et al. (2018). *Biomass production, supply, uses and flows in the European Union. First results from an integrated assessment*. doi:10.2760/181536.

Echt, B., Leppin, D., Mamrosh, D., Mirdadian, D., Seeger, D., and Warren, B. (2017). Fundamentals of Low-Tonnage Sulfur Removal and Recovery.

Elsido, C., Martelli, E., and Grossmann, I. E. (2020). Simultaneous Multiperiod Optimization of Rankine Cycles and Heat Exchanger Networks. *Comput. Aided Chem. Eng.* 48, 1495–1500.

Elsido, C., Martelli, E., and Grossmann, I. E. (2021). Multiperiod optimization of heat exchanger networks with integrated thermodynamic cycles and thermal storages. *Comput. Chem. Eng.* 149, 107293. doi:10.1016/j.compchemeng.2021.107293.

Elsido, C., Mian, A., and Martelli, E. (2017). A systematic methodology for the techno-economic optimization of Organic Rankine Cycles. *Energy Procedia* 129, 26–33. doi:10.1016/j.egypro.2017.09.171.

ENTSO-E Transparency Platform (2020). *Accessed 2020*. Available at: https://transparency.entsoe.eu/.

European Commission (2021). Directive of the European parliament and of the council as regards the promotion of energy from renewable sources. Available at: https://eur-lex.europa.eu/legal-content/EN/TXT/?uri=CELEX:52021PC0557.

European Commission (2022). REPowerEU Plan. Available at: https://ec.europa.eu/commission/presscorner/detail/es/ip_22_3131.

Fagernäs, L., Brammer, J., Wilén, C., Lauer, M., and Verhoeff, F. (2010). Drying of biomass for second generation synfuel production. *Biomass and Bioenergy* 34, 1267–1277. doi:10.1016/j.biombioe.2010.04.005.

Fajardy, M., Morris, J., Gurgel, A., Herzog, H., Mac Dowell, N., and Paltsev, S. (2021). The economics of bioenergy with carbon capture and storage (BECCS) deployment in a 1.5 °C or 2 °C world. *Glob. Environ. Chang.* 68, 102262. doi:10.1016/j.gloenvcha.2021.102262.

Fuchs, J., Schmid, J. C., Müller, S., Mauerhofer, A. M., Benedikt, F., and Hofbauer, H. (2020). The impact of gasification temperature on the process characteristics of sorption enhanced reforming of biomass. *Biomass Convers. Biorefinery* 10, 925–936. doi:10.1007/s13399-019-00439-9.

Gabrielli, P., Gazzani, M., and Mazzotti, M. (2020). The Role of Carbon Capture and Utilization, Carbon Capture and Storage, and Biomass to Enable a Net-Zero-CO 2 Emissions Chemical Industry. *Ind. Eng. Chem. Res.* 59, 7033–7045. doi:10.1021/acs.iecr.9b06579.

Gale, J. (2017). IEAGHG Technical Review August 2017 Understanding the Cost of Retrofitting CO 2 capture in an Integrated Oil Refinery.

Giuffrida, A., Romano, M. C., and Lozza, G. G. (2010). Thermodynamic assessment of IGCC power plants with hot fuel gas desulfurization. *Appl. Energy* 87, 3374–3383. doi:10.1016/j.apenergy.2010.05.020.

Grabke, H. J. (1995). Metal Dusting of Low- and High-Alloy Steels. *Biomass and Bioenergy* 51, 711–720.

Grasa, G. S., and Abanades, J. C. (2006). CO2 Capture Capacity of CaO in Long Series of Carbonation/Calcination Cycles. *Ind. Eng. Chem. Res.* 45, 8846–8851. doi:10.1021/ie0606946.

Hafner, S., Armbrust, N., and Spörl, R. (2017). Production of tailored syngas for Dimethyl Ether synthesis by sorption enhanced gasification.

Hafner, S., and Schmid, M. (2020). WP 3 – Deliverable D3.4: Final experimental results on SEG process experiments at pilot (TRL5) scale for stationary and flexible operating regimes.

Hafner, S., Schmid, M., and Scheffknecht, G. (2021). Parametric Study on the Adjustability of the Syngas Composition by Sorption-Enhanced Gasification in a Dual-Fluidized Bed Pilot Plant. *Energies* 14, 399. doi:10.3390/en14020399.

Hafner, S., Schmid, M., Spörl, R., and Scheffknecht, G. Experimental Investigation of the Sorption Enhanced Gasification of Biomass in a Dual Fluidized Bed Pilot Plant. in *Proceedings of the 27th European Biomass Conference (EUBCE)* (Lisbon (Portugal)), 2019.

Hafner, S., Spörl, R., and Scheffknecht, G. (2018). Sorption Enhanced Gasification: Process validation and investigations on the syngas composition in a 200 kWth dual fluidized bed facility. in *Conference Proceedings: 23rd International Conference on FBC* (Seoul, South Korea), 826–832.

Hannula, I. (2015). Co-production of synthetic fuels and district heat from biomass residues, carbon dioxide and electricity: Performance and cost analysis. *Biomass and Bioenergy* 74, 26–46. doi:10.1016/j.biombioe.2015.01.006.

Hannula, I. (2016). Hydrogen enhancement potential of synthetic biofuels manufacture in the European context: A techno-economic assessment. *Energy* 104, 199–212.

Hannula, I., and Kurkela, E. (2013). Liquid transportation fuels via large-scale fluidised bed gasification of lignocellulosic biomass.

Hannula, I., and Melin, K. (2021). Biorefineries with CCS. *IEAGHG Tech. Rep.*

Hannula, I., and Reiner, D. M. (2019). Near-Term Potential of Biofuels, Electrofuels, and Battery Electric Vehicles in Decarbonizing Road Transport. *Joule* 3, 2390–2402. doi:10.1016/j.joule.2019.08.013.

Hawthorne, C., Poboss, N., Dieter, H., Gredinger, A., Zieba, M., and Scheffknecht, G. (2012). Operation and results of a 200-kWth dual fluidized bed pilot plant gasifier with adsorption-enhanced reforming. *Biomass Convers. Biorefinery* 2, 217–227.

doi:10.1007/s13399-012-0053-3.

Hillestad, M., Ostadi, M., Alamo Serrano, G. D., Rytter, E., Austbø, B., Pharoah, J. G., et al. (2018). Improving carbon efficiency and profitability of the biomass to liquid process with hydrogen from renewable power. *Fuel* 234, 1431–1451. doi:10.1016/j.fuel.2018.08.004.

IEA (2017). Technology Roadmap - Delivering Sustainable Bioenergy. 1–94.

IEA (2020). Energy Technology Perspectives 2020 - Special Report on Carbon Capture Utilisation and Storage. doi:10.1787/208b66f4-en.

IEAGHG (2017a). Techno-economic evaluation of SMR based standalone (merchant) plant with CCS, 2017/02.

IEAGHG (2017b). Techno - Economic Evaluation of SMR Based Standalone (Merchant) Hydrogen Plant with CCS. *Tech. Rev. 2017-02*, 286.

Ingham, A. (2017). Reducing the Carbon Intensity of Methanol for Use as a Transport Fuel. *Johnson Matthey Technol. Rev.* 61, 297–307. doi:10.1595/205651317X696216.

International Energy Agency (2017). Energy Technology Perspectives (OECD).

International Energy Agency (2019). The Future of Hydrogen - Seizing today's opportunities - Report prepared for the G20, Japan.

Kazemi, A., Malayeri, M., Gharibi kharaji, A., and Shariati, A. (2014). Feasibility study, simulation and economical evaluation of natural gas sweetening processes - Part 1: A case study on a low capacity plant in iran. *J. Nat. Gas Sci. Eng.* 20, 16–22. doi:10.1016/j.jngse.2014.06.001.

Koponen, K., and Hannula, I. (2017). GHG emission balances and prospects of hydrogen enhanced synthetic biofuels from solid biomass in the European context. *Appl. Energy* 200, 106–118. doi:10.1016/j.apenergy.2017.05.014.

Koppatz, S., Pfeifer, C., Rauch, R., Hofbauer, H., Marquard-Moellenstedt, T., and Specht, M. (2009). H2 rich product gas by steam gasification of biomass with in situ CO2 absorption in a dual fluidized bed system of 8 MW fuel input. *Fuel Process. Technol.* 90, 914–921. doi:10.1016/j.fuproc.2009.03.016.

Koytsoumpa, E. I., Karellas, S., and Kakaras, E. (2020). Modelling of methanol production via combined gasification and power to fuel. *Renew. Energy* 158, 598–611. doi:10.1016/j.renene.2020.05.169.

Kreutz, T., Williams, R., Consonni, S., and Chiesa, P. (2005). Co-production of hydrogen, electricity and CO from coal with commercially ready technology. Part B: Economic analysis. *Int. J. Hydrogen Energy* 30, 769–784. doi:10.1016/j.ijhydene.2004.08.001.

Kurkela, E., Kurkela, M., Frilund, C., Hiltunen, I., Rollins, B., and Steele, A. (2021). Flexible Hybrid Process for Combined Production of Heat, Power and Renewable Feedstock for Refineries: Managing seasonal energy supply and demand for heat and power in Europe. *Johnson Matthey Technol. Rev.* 65, 346–348. doi:10.1595/205651321X16158839334031.

Kurkela, E., Kurkela, M., and Hiltunen, I. (2016). Steam-oxygen gasification of forest residues and bark followed by hot gas filtration and catalytic reforming of tars: Results of an extended time test. *Fuel Process. Technol.* 141, 148–158. doi:10.1016/j.fuproc.2015.06.005.

Larson, E. D., Jin, H., and Celik, F. E. (2009). Large-scale gasification-based coproduction

of fuels and electricity from switchgrass. *Biofuels, Bioprod. Biorefining* 3, 174–194. doi:10.1002/bbb.137.

Lee, D.-W., Lee, M. S., Lee, J. Y., Kim, S., Eom, H.-J., Moon, D. J., et al. (2013). The review of Cr-free Fe-based catalysts for high-temperature water-gas shift reactions. *Catal. Today* 210, 2–9. doi:10.1016/j.cattod.2012.12.012.

Löffler, G., Kaiser, S., Bosch, K., and Hofbauer, H. (2003). Hydrodynamics of a dual fluidized-bed gasifier—Part I: simulation of a riser with gas injection and diffuser. *Chem. Eng. Sci.* 58, 4197–4213. doi:10.1016/S0009-2509(03)00232-X.

Martelli, E., Elsido, C., Mian, A., and Marechal, F. (2017). MINLP model and two-stage algorithm for the simultaneous synthesis of heat exchanger networks, utility systems and heat recovery cycles. *Comput. Chem. Eng.* 106, 663–689. doi:10.1016/j.compchemeng.2017.01.043.

Martínez, A., Pröll, T., and Romeo, L. M. (2012). Lime enhanced biomass gasification. Energy penalty reduction by solids preheating in the calciner. *Int. J. Hydrogen Energy* 37, 15086–15095. doi:10.1016/j.ijhydene.2012.08.002.

Martínez, I., and Romano, M. C. (2016). Flexible sorption enhanced gasification (SEG) of biomass for the production of synthetic natural gas (SNG) and liquid biofuels: Process assessment of stand-alone and power-to-gas plant schemes for SNG production. *Energy* 113, 615–630. doi:10.1016/j.energy.2016.07.026.

McDonagh, S., Wall, D. M., Deane, P., and Murphy, J. D. (2019). The effect of electricity markets, and renewable electricity penetration, on the levelised cost of energy of an advanced electro-fuel system incorporating carbon capture and utilisation. *Renew. Energy* 131, 364–371. doi:10.1016/j.renene.2018.07.058.

Meissner, III, R. E., and Wagner, U. (1983). Low-energy process recovers CO2. *Oil Gas J.* 81:5, 55–58.

Moioli, S., Giuffrida, A., Romano, M. C., Pellegrini, L. A., and Lozza, G. (2016). Assessment of MDEA absorption process for sequential H2S removal and CO2 capture in air-blown IGCC plants. *Appl. Energy* 183, 1452–1470. doi:10.1016/j.apenergy.2016.08.155.

Moioli, S., Pellegrini, L. A., Romano, M. C., and Giuffrida, A. (2017). Pre-combustion CO2 Removal in IGCC Plant by MDEA Scrubbing: Modifications to the Process Flowsheet for Energy Saving. *Energy Procedia* 114, 2136–2145. doi:10.1016/j.egypro.2017.03.1349.

Montebelli, A., Visconti, C. G., Groppi, G., Tronconi, E., Ferreira, C., and Kohler, S. (2013). Enabling small-scale methanol synthesis reactors through the adoption of highly conductive structured catalysts. *Catal. Today* 215, 176–185. doi:10.1016/j.cattod.2013.02.020.

Nielsen, A. S., Ostadi, M., Austbø, B., Hillestad, M., del Alamo, G., and Burheim, O. (2022). Enhancing the Efficiency of Power- and Biomass-to-Liquid Fuel Processes Using Fuel-Assisted Solid Oxide Electrolysis Cells. *Fuel* 321, 123987. doi:10.2139/ssrn.4040992.

Palonen, J. (2012). Gasified Biomass for Biofuels Production : Foster Wheeler's Technology Developments for Large Scale Applications.

Palonen, J., Huttenhuis, P., Rexwinkel, G., Astolfi, M., and Elsido, C. (2017). FLEDGED

Deliverable D5.1: Economic framework and simplified model for capital cost estimation.

Patrizio, P., Fajardy, M., Bui, M., and Dowell, N. Mac (2021). CO2 mitigation or removal, the optimal uses of biomass in energy systems decarbonization. *iScience* 24, 102765. doi:10.1016/j.isci.2021.102765.

Pfeifer, C., Puchner, B., and Hofbauer, H. (2009). Comparison of dual fluidized bed steam gasification of biomass with and without selective transport of CO2. *Chem. Eng. Sci.* 64, 5073–5083. doi:10.1016/j.ces.2009.08.014.

Pitkäoja, A., Ritvanen, J., Hafner, S., Hyppänen, T., and Scheffknecht, G. (2020). Simulation of a sorbent enhanced gasification pilot reactor and validation of reactor model. *Energy Convers. Manag.* 204, 112318. doi:10.1016/j.enconman.2019.112318.

Pitkäoja, A., Ritvanen, J., Hafner, S., Hyppänen, T., and Scheffknecht, G. (2021). Numerical modelling of sorption-enhanced gasification: Development of a fuel decomposition model. *Fuel* 289, 119868. doi:10.1016/j.fuel.2020.119868.

Poboß, N. (2016). Experimentelle Untersuchung der sorptionsunterstützten Reformierung.

Poluzzi, A., Guandalini, G., D'Amore, F., and Romano, M. C. (2021). The Potential of Power and Biomass-to-X Systems in the Decarbonization Challenge: a Critical Review. *Curr. Sustain. Energy Reports*. doi:10.1007/s40518-021-00191-7.

Poluzzi, A., Guandalini, G., Guffanti, S., Elsido, C., Moioli, S., Huttenhuis, P., et al. (2022a). Flexible Power & Biomass-to-Methanol plants: Design optimization and economic viability of the electrolysis integration. *Fuel* 310, 122113. doi:10.1016/j.fuel.2021.122113.

Poluzzi, A., Guandalini, G., Guffanti, S., Martinelli, M., Moioli, S., Huttenhuis, P., et al. (2022b). Flexible Power and Biomass-To-Methanol Plants With Different Gasification Technologies. *Front. Energy Res.* 9. doi:10.3389/fenrg.2021.795673.

Poluzzi, A., Guandalini, G., and Romano, M. C. (2020). "Potential carbon efficiency" as a new index to track the performance of biofuels production processes. *Biomass and Bioenergy* 142, 105618. doi:10.1016/j.biombioe.2020.105618.

Poluzzi, A., Guandalini, G., and Romano, M. C. (2022c). Flexible methanol and hydrogen production from biomass gasification with negative emissions. *Sustain. Energy Fuels* 6, 3830–3851. doi:10.1039/D2SE00661H.

Pröll, T., and Hofbauer, H. (2008a). Development and Application of a Simulation Tool for Biomass Gasification Based Processes. *Int. J. Chem. React. Eng.* 6, A89.

Pröll, T., and Hofbauer, H. (2008b). H2 rich syngas by selective CO2 removal from biomass gasification in a dual fluidized bed system — Process modelling approach. *Fuel Process. Technol.* 89, 1207–1217. doi:10.1016/j.fuproc.2008.05.020.

Putta, K. R., Pandey, U., Gavrilovic, L., Rout, K. R., Rytter, E., Blekkan, E. A., et al. (2022). Optimal Renewable Energy Distribution Between Gasifier and Electrolyzer for Syngas Generation in a Power and Biomass-to-Liquid Fuel Process. *Front. Energy Res.* 9, 1–14. doi:10.3389/fenrg.2021.758149.

Queneau, P. E., and Marcuson, S. W. (1996). Oxygen pyrometallurgy at copper cliff—A half century of progress. *JOM* 48, 14–21. doi:10.1007/BF03221355.

Renon, H., and Prausnitz, J. M. (1968). Local compositions in thermodynamic excess functions for liquid mixtures. *AIChE J.* 14, 135–144.

Riva, L., Martínez, I., Martini, M., Gallucci, F., van Sint Annaland, M., and Romano, M. C. (2018). Techno-economic analysis of the Ca-Cu process integrated in hydrogen plants with CO 2 capture. *Int. J. Hydrogen Energy* 43, 15720–15738. doi:10.1016/j.ijhydene.2018.07.002.

Ruhnau, O. (2020). Market-based renewables: How flexible hydrogen electrolyzers stabilize wind and solar market values.

Salkuyeh, Y. K., Saville, B. A., and MacLean, H. L. (2018). Techno-economic analysis and life cycle assessment of hydrogen production from different biomass gasification processes. *Int. J. Hydrogen Energy* 43, 9514–9528. doi:10.1016/j.ijhydene.2018.04.024.

Schmid, J. C., Fuchs, J., Benedikt, F., Mauerhofer, A. M., Müller, S., Hofbauer, H., et al. (2017). Sorption Enhanced Reforming with the novel dual fludized bed test plant at TU Wien. in *EUBCE* (Stockholm).

Schmidt, O., Gambhir, A., Staffell, I., Hawkes, A., Nelson, J., and Few, S. (2017). Future cost and performance of water electrolysis: An expert elicitation study. *Int. J. Hydrogen Energy* 42, 30470–30492. doi:10.1016/j.ijhydene.2017.10.045.

Seel, J., Mills, A., Wiser, R., Deb, S., Asokkumar, A., Hassanzadeh, M., et al. (2018). Impacts of High Variable Renewable Energy Futures on Wholesale Electricity Prices , and on Electric-Sector Decision Making.

Sorknæs, P., Lund, H., Skov, I. R., Djørup, S., Skytte, K., Morthorst, P. E., et al. (2020). Smart Energy Markets - Future electricity, gas and heating markets. *Renew. Sustain. Energy Rev.* 119, 109655. doi:10.1016/j.rser.2019.109655.

STELA drying technology (2019). Brochure on Low-temperature belt dryer.

Stöcker, J., Whysall, M., and Miller, G. Q. (1998). 30 Years of PSA Technology for Hydrogen Purification. 1–25.

Tan, E. C., Talmadge, M., Dutta, A., Hensley, J., Snowden-Swan, L. J., Humbird, D., et al. (2016). Conceptual process design and economics for the production of high-octane gasoline blendstock via indirect liquefaction of biomass through methanol/dimethyl ether intermediates. *Biofuels, Bioprod. Biorefining* 10, 17–35. doi:10.1002/bbb.1611.

TenWolde, A., McNatt, J. D., and Krahn, L. (1998). Thermal properties of wood and wood panel products for use in buildings. Martin Marietta Energy Systems / US DOE.

Thunman, H., Seemann, M., Berdugo Vilches, T., Maric, J., Pallares, D., Ström, H., et al. (2018). Advanced biofuel production via gasification - lessons learned from 200 man-years of research activity with Chalmers' research gasifier and the GoBiGas demonstration plant. *Energy Sci. Eng.* 6, 6–34. doi:10.1002/ese3.188.

Twigg, M. V., and Spencer, M. S. (2001). Deactivation of supported copper metal catalysts for hydrogenation reactions. *Appl. Catal. A Gen.* 212, 161–174. doi:10.1016/S0926-860X(00)00854-1.

Ullmann's encyclopedia (2005). Gas Production. *Ullmann's Encycl. Ind. Chem.*

van Leeuwen, C., and Mulder, M. (2018). Power-to-gas in electricity markets dominated by renewables. *Appl. Energy* 232, 258–272. doi:10.1016/j.apenergy.2018.09.217.

Vanden Bussche, K. M., and Froment, G. F. (1996). A Steady-State Kinetic Model for Methanol Synthesis and the Water Gas Shift Reaction on a Commercial Cu/ZnO/Al2O3 Catalyst. *J. Catal.* 161, 1–10. doi:10.1006/jcat.1996.0156.

Yee, T., and Grossmann, I. (1990). Simultaneous optimization models for heat integration—II. Heat exchanger network synthesis. *Comput. Chem. Eng.* 14(10), 1165–1184.

Zatti, M., Gabba, M., Rossi, M., Morini, M., Gambarotta, A., and Martelli, E. (2018). Towards the optimal design and operation of multi-energy systems: the "efficity" project. *Environ. Eng. Manag. J.* 17, 2409–2419. doi:10.30638/eemj.2018.239.

Zhang, H., Wang, L., Van herle, J., Maréchal, F., and Desideri, U. (2020). Techno-economic evaluation of biomass-to-fuels with solid-oxide electrolyzer. *Appl. Energy* 270, 115113. doi:10.1016/j.apenergy.2020.115113.

Appendix A

Appendix A includes the following:

- process modelling assumptions.
- ERD and BRD configurations SEG-based power & biomass-to-methanol plants: tables with properties of the main streams of the two assessed plants.
- Power & biomass-to-methanol plants different gasification technologies comparison: tables with properties of the main streams of the six assessed plants.
- Power & biomass-to-methanol plants capital costs: breakdown of capital costs.

Table A 1 – Process modelling assumptions.

Assumptions	**DG based plant**	**IG based plant**	**SEG based plant**
Input biomass (as received)			
LHV, MJ/kg_{AR}	9.74		
Moisture, $\%_{wt}$	45		
Proximate analysis, $\%_{wt,dry}$			
Fixed Carbon	18.84		
Volatile matter	80.0		
Ash	1.16		
Ultimate analysis, $\%_{wt,dry}$			
Carbon	51.19		
Hydrogen	6.08		
Nitrogen	0.2		
Chlorine	0.05		
Sulfur	0.02		
Oxygen	41.3		
Ash	1.16		
Biomass pre-treatment			
Biomass moisture at dryer outlet, $\%_{wt}$	15		
Biomass temperature at dryer outlet, °C	80		
Specific heat consumption, MWh/t_{H2O}	1		
Specific power consumption $kWh/t_{bio,dry}$	32		
Gasification			
Gasifier outlet temperature, °C	870	815	-
Gasifier and combustor pressure, bar	4.00	1.43	1.43

Assumptions	DG based plant	IG based plant	SEG based plant
S/C at gasifier inlet[1]	*1.02*[2]	*1.12*[2]	1.50
Methane content in the syngas, $kg_{CH4}/kg_{bio,dry}$	0.07	0.10	0.07
Higher hydrocarbon content in the syngas, $kmol_{C2H4}/kmol_{CH4}$	0.45	0.27	0.25
Char conversion in the gasifier, % of inlet C	95.5	83.0	*68.1/72.8*[3]
Fluidizing steam input temperature in enhanced operation, °C	172	400	400
Fluidizing steam input temperature in baseline operation, °C	172	400	182
Gas injection for sealing and filters, $kg/kg_{bio,dry}$	H_2O=0.12 Air = 0.03	H_2O=0.12 Air = 0.03	H_2O=0.12 Air = 0.03
Combustor exit temperature, °C	-	910	910
Gas superficial velocity at combustor outlet in baseline operation, m/s	-	5.0	5.0
Oxygen concentration in combustor flue gases, $\%_{mol}$	-	3.0	3.0
Combustor air temperature in baseline operation, °C	-	270	270
Overall pressure drop from combustor to stack, % of gas pressure at valve outlet	-	4.5	4.5
Total solid purge, % of inlet biomass	-	1.0	1.0
Combustor air fan isentropic/mech.-el efficiency, %	-	80/94	80/94
Loss of solids from the BFB gasifier, % of the circulating solids	-	0.01	0.01
Combustor cyclone separation efficiency, %	-	Solids: 99.9; Ash:99	Ca: 99.9; Ash:99
Gasifier/combustor thermal losses, % of total thermal input	1.0	1.0/1.0	1.0/1.0
Syngas purification, conditioning and compression			
Reformer exit temperature, °C	915	800	800
CH_4 conversion in the reformer, %	90	90	90
Oxygen input temperature, °C	25	25	25
Oxygen purity, %	100	100	100
S/C at reformer inlet	1.0	1.0	*2.73/1.63*[4]
Syngas temperature at water scrubber inlet, °C	220	220	220
Scrubber pump hydraulic/mech.-el efficiency, %	75/90	75/90	75/90
Electric consumption of the desulfurization unit, $kWh/kg_{H2S,removed}$	1.35	1.35	1.35
Syngas compressor 1 stages	4	6	7
Syngas compressor 1 outlet pressure, bar	30	30	92
Syngas compressor 2 stages	2	2	-
Syngas compressor 2 outlet pressure, bar	92	92	-
Hydrogen compressor stages	-	-	2
Hydrogen compressor outlet pressure, bar	-	-	92
Intercoolers outlet temperature, °C	40	40	40
Syngas compressors isentropic/mech.-el efficiency, %	72/92	72/92	72/92
WGS reactor inlet temperature, °C	300	-	-
WGS reactor pressure, bar	3.5	-	-

Assumptions	DG based plant	IG based plant	SEG based plant
CO_2 absorber pressure, bar	30	30	-
CO_2 separation efficiency, % of inlet CO_2	90	90	
MDEA regenerator thermal duty , $MJ/kg_{CO2,removed}$	1.0	1.0	-
Electrolysis efficiency, MW_{LHV}/MW_{el}	0.69	0.69	0.69
Electrolyser size, MW	129.04	67.46	63.29
Electrolysis pressure, bar	30	30	30
Methanol synthesis			
Reactor pressure, bar	90.0		
Tube length, m	6.0		
Tube diameter, mm	40.0		
Boiling water temperature, °C	238		
Catalyst density, kg/m^3	1712		
Catalyst diameter (cylinder), mm	6.0		
Catalyst height (cylinder), mm	3.5		
Bed voidage degree	0.39		
Flash unit temperature, °C	40		
GHSV in enhanced operation, h^{-1}	5000		
RR in enhanced operation, molar basis	5.0		
Syngas recycle compressor isentropic/mech.-el efficiency, %	80/94		
Methanol purification			
Stabilizing column pressure, bar	1.3	1.3	1.3
Stabilizing column number of stages	23	23	23
Stabilizing column diameter	0.90	0.75	0.66
Concentration column pressure, bar	1.0	1.0	1.0
Concentration column number of stages	48	48	48
Concentration column diameter	2.50	2.10	2.00
Final product methanol purity, $\%_{wt}$	99.85	99.85	99.85

[1] The calculation of the S/C includes the fluidization steam, the steam for sealing and cleaning purposes and the moisture of the biomass.
[2] S/C in direct and indirect gasifiers is tuned to achieve S/C=1 at the reformer inlet.
[3] The char conversion in SEG depends on the gasification temperature and it is calculated with the expression described in Poluzzi et al. (2022). The first value refers to baseline operation, while the second one refers to enhanced operation.
[4] S/C at the reformer inlet in SEG plant derive from the assumption of S/C=1.5 in the gasifier. The first value refers to baseline operation, while the second one refers to enhanced operation.

ERD and BRD configurations SEG-based power & biomass-to-methanol plants

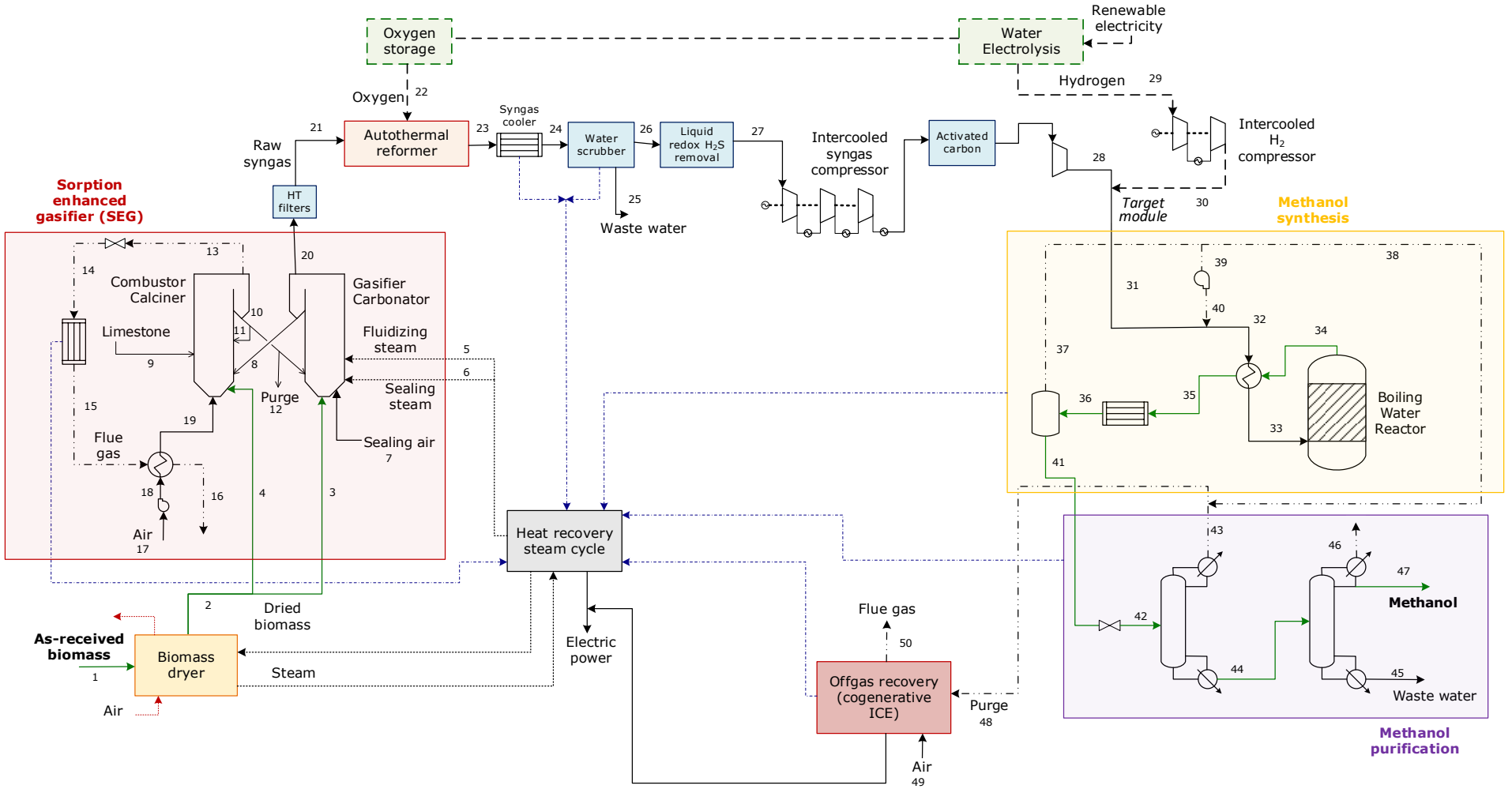

Figure A 1 – Flowsheet of the SEG-based power & biomass-to-methanol plant

Table A 2 – Stream properties of the SEG island of ERD and BRD cases in baseline operation (1)

Stream #	**Units**	**1**	**2**	**3**	**4**	**5**	**6**	**7**	**8**	**9**	**10**
Stream type		As-received biomass	Dried biomass	Biomass to gasifier	Biomass to combustor	Fluidizing steam	Sealing steam	Sealing air	Solids	Make-up	Solids
Temperature	°C	25.00	80.00	80.00	80.00	182.00	182.00	25.00	714.01	25.00	910.00
Pressure	bar	1.01	1.01	1.01	1.01	2.00	2.00	1.60	1.43	1.01	1.43
Total mass flow rate	kg/s	10.27	6.64	6.64	0.01	4.70	0.80	0.21	42.95	0.48	211.04
Gas/liq mass flow rate	kg/s					4.70	0.80	0.21			
Molar flow rate	kmol/h	-	-	-	-	939.75	159.73	25.83	-	-	-
Vapor fraction	-					1.00	1.00	1.00			
Gas composition	$\%_{mol}$										
H_2O						100	100	-			
O_2						-	-	20.48			
N_2						-	-	79.52			
Solid flow rate	kg/s	10.27	6.64	6.64	0.01	-	-	-	42.95	0.48	211.04
Solid composition	$\%_w$										
Biomass		100	100	100	100	-	-	-	-	-	-
Ash		-	-	-	-	-	-	-	2.86	-	2.97
C		-	-	-	-	-	-	-	2.15	-	-
$CaCO_3$		-	-	-	-	-	-	-	14.18	100	-
CaO		-	-	-	-	-	-	-	80.80	-	97.03
LHV	MJ/kg	9.74	16.37	16.37	16.37	-	-	-			
Power	MW_{LHV}	100.00	108.76	108.65	0.11	-	-	-	-	-	-
Moisture	$\%_w$	45.00	15.00								

Table A 3 - Stream properties of the SEG island of ERD and BRD cases in baseline operation (2)

Stream #	**Units**	**11**	**12**	**13**	**14**	**15**	**16**	**17**	**18**	**19**	**20**
Stream type		Solids	Purge	Flue gas	Flue gas	Flue gas	Flue gas	Air	Air	Air	Syngas
Temperature	°C	910.00	910.00	910.00	910.02	300.00	156.12	25.00	79.04	270.00	714.07
Pressure	bar	1.43	1.43	1.43	1.10	1.08	1.05	1.01	1.63	1.60	1.43
Total mass flow rate	kg/s	171.69	0.07	16.97	16.97	16.97	16.97	12.88	12.88	12.88	8.68
Gas/liq mass flow rate	kg/s			16.70	16.70	16.70	16.70	12.88	12.88	12.88	8.68
Molar flow rate	kmol/h	-	-	1843.68	1843.68	1843.68	1843.68	1606.44	1606.44	1606.52	2059.43
Vapor fraction	-			1.00	1.00	1.00	1.00	1.00	1.00	1.00	1.00
Gas composition	$\%_{mol}$										
H_2O				0.91	0.91	0.91	0.91	1.00	1.00	1.00	49.11
H_2				-	-	-	-	-	-	-	32.91
CO_2				27.89	27.89	27.89	27.89	0.03	0.03	0.03	7.12
CO				-	-	-	-	-	-	-	4.39
CH_4				-	-	-	-	-	-	-	4.30
O_2				2.99	2.99	2.99	2.99	20.70	20.70	20.70	-
C_xH_y				-	-	-	-	-	-	-	1.08
Ar				0.85	0.85	0.85	0.85	0.97	0.97	0.97	-
N_2				67.36	67.36	67.36	67.36	77.30	77.30	77.30	1.07
Solid flow rate	kg/s	171.69	0.07	0.27	0.27	0.27	0.27	-	-	-	0.00
Solid composition	$\%_w$										
Biomass		-	-	-	-	-	-	-	-	-	-
Ash		2.97	2.97	23.58	23.58	23.58	23.58	-	-	-	59.60
C		-	-	-	-	-	-	-	-	-	0.89
$CaCO_3$		-	-	-	-	-	-	-	-	-	5.90
CaO		97.03	97.03	76.42	76.42	76.42	76.42	-	-	-	33.61
LHV	MJ/kg	-	-	-	-	-	-	-	-	-	9.28
Power	MW_{LHV}	-	-	-	-	-	-	-	-	-	80.57

Table A 4 - Stream properties of the SEG island of ERD and BRD cases in enhanced operation (1)

Stream #	**Units**	**1**	**2**	**3**	**4**	**5**	**6**	**7**	**8**	**9**	**10**
Stream type		As-received biomass	Dried biomass	Biomass to gasifier	Biomass to combustor	Fluidizing steam	Sealing steam	Sealing air	Solids	Make-up	Solids
Temperature	°C	25.00	80.00	80.00	80.00	400.00	182.00	25.00	771.70	25.00	910.00
Pressure	bar	1.01	1.01	1.01	1.01	1.96	2.00	1.60	1.43	1.01	1.43
Total mass flow rate	kg/s	10.27	6.64	6.27	0.38	4.44	0.75	0.20	137.96	0.42	178.92
Gas/liq mass flow rate	kg/s					4.44	0.75	0.20			
Molar flow rate	kmol/h	-	-	-	-	887.47	150.85	24.40	-	-	-
Vapor fraction						1.00	1.00	1.00			
Gas composition	$\%_{mol}$										
H_2O						100	100	-			
O_2						-	-	20.48			
N_2						-	-	79.52			
Solid flow rate	kg/s	10.27	6.64	6.27	0.38	-	-	-	137.96	0.42	178.92
Solid composition	$\%_w$										
Biomass		100	100	100	100	-	-	-	-	-	-
Ash		-	-	-	-	-	-	-	3.41	-	3.39
C		-	-	-	-	-	-	-	0.54	-	-
$CaCO_3$		-	-	-	-	-	-	-	-	100	-
CaO		-	-	-	-	-	-	-	96.05	-	96.61
LHV	MJ/kg	9.74	16.37	16.37	16.37	-	-	-			
Power	MW_{LHV}	100.00	108.76	102.61	6.15	-	-	-	-	-	-
Moisture	$\%_w$	45.00	15.00								

Table A 5 - Stream properties of the SEG island of ERD and BRD cases in enhanced operation (2)

Stream #	**Units**	**11**	**12**	**13**	**14**	**15**	**16**	**17**	**18**	**19**	**20**
Stream type		Solids	Purge	Flue gas	Flue gas	Flue gas	Flue gas	Air	Air	Air	Syngas
Temperature	°C	910.00	910.00	910.00	910.02	300.00	143.95	25.00	79.04	258.67	771.80
Pressure	bar	1.43	1.43	1.43	1.10	1.08	1.05	1.01	1.63	1.60	1.43
Total mass flow rate	kg/s	41.70	0.06	14.01	14.01	14.01	14.01	12.48	12.48	12.48	10.86
Gas/liq mass flow rate	kg/s			13.78	13.78	13.78	13.78	12.48	12.48	12.48	10.86
Molar flow rate	kmol/h	-	-	1615.16	1615.16	1615.16	1615.16	1556.53	1556.53	1556.55	2190.61
Vapor fraction				1.00	1.00	1.00	1.00	1.00	1.00	1.00	1.00
Gas composition	$\%_{mol}$										
H_2O				3.81	3.81	3.81	3.81	1.00	1.00	1.00	44.41
H_2				-	-	-	-	-	-	-	28.41
CO_2				17.76	17.76	17.76	17.76	0.03	0.03	0.03	13.19
CO				-	-	-	-	-	-	-	8.25
CH_4				-	-	-	-	-	-	-	3.82
O_2				3.00	3.00	3.00	3.00	20.70	20.70	20.70	-
C_xH_y				-	-	-	-	-	-	-	0.96
Ar				0.93	0.93	0.93	0.93	0.97	0.97	0.97	-
N_2				74.50	74.50	74.50	74.50	77.30	77.30	77.30	0.95
Solid flow rate	kg/s	41.70	0.06	0.23	0.23	0.23	0.23	-	-	-	0.00
Solid composition	$\%_w$										
Biomass		-	-	-	-	-	-	-	-	-	-
Ash		3.39	3.39	26.14	26.14	26.14	26.14	-	-	-	63.86
C		-	-	-	-	-	-	-	-	-	0.20
$CaCO_3$		-	-	-	-	-	-	-	-	-	-
CaO		96.61	96.61	73.86	73.86	73.86	73.86	-	-	-	35.94
LHV	MJ/kg	-	-	-	-	-	-	-	-	-	7.59
Power	MW_{LHV}	-	-	-	-	-	-	-	-	-	82.42

Table A 6 - Stream properties of the syngas purification, conditioning and compression island of ERD and BRD cases in baseline operation

Stream #	**Units**	**21**	**22**	**23**	**24**	**25**	**26**	**27**
Stream type		Syngas	Oxygen	Syngas	Syngas	Waste water	Syngas	Syngas
Temperature	°C	714.07	25.00	800.00	220.00	82.14	40.03	30.00
Pressure	bar	1.23	30.00	1.10	1.08	1.08	1.08	1.05
Total mass flow rate	kg/s	8.68	0.54	9.22	9.22	4.36	4.86	4.58
Gas/liq mass flow rate	kg/s	8.68	0.54	9.22	9.22	4.36	4.86	4.58
Molar flow rate	kmol/h	2059.43	61.26	2285.44	2285.44	869.81	1415.62	1359.95
Vapor fraction	-	1.00	1.00	1.00	1.00	-	1.00	1.00
Gas composition	$\%_{mol}$							
H_2O		49.11	-	42.25	42.25	99.85	6.86	3.08
H_2		32.91	-	40.58	40.58	-	65.51	68.19
CO_2		7.12	-	8.35	8.35	0.14	13.39	13.94
CO		4.39	-	7.45	7.45	-	12.03	12.52
CH_4		4.30	-	0.39	0.39	-	0.62	0.65
O_2		-	100	-	-	-	-	-
C_xH_y		1.08	-	-	-	-	-	-
Ar		-	-	-	-	-	-	-
N_2		1.07	-	0.96	0.96	-	1.55	1.62
LHV	MJ/kg	9.28	-	8.42	8.42		15.97	16.95
Power	MW_{LHV}	80.56	-	77.68	77.68	-	77.67	77.65

Table A 7 - Stream properties of the syngas purification, conditioning and compression island of ERD and BRD cases in enhanced operation

Stream #	**Units**	**21**	**22**	**23**	**24**	**25**	**26**	**27**	**28**	**29**	**30**
Stream type		Syngas	Oxygen	Syngas	Syngas	Waste water	Syngas	Syngas	Syngas	Hydrogen	Hydrogen
Temperature	°C	771.80	25.00	800.00	220.00	80.46	40.03	30.00	120.52	25.00	116.30
Pressure	bar	1.23	30.00	1.10	1.08	1.08	1.08	1.05	92.00	30.00	92.00
Total mass flow rate	kg/s	10.86	0.44	11.30	11.30	4.13	7.17	6.86	6.63	0.37	0.37
Gas/liq mass flow rate	kg/s	10.86	0.44	11.30	11.30	4.13	7.17	6.86	6.63	0.37	0.37
Molar flow rate	kmol/h	2190.61	50.05	2404.05	2404.05	822.51	1581.55	1519.57	1472.78	654.12	654.12
Vapor fraction		1.00	1.00	1.00	1.00	-	1.00	1.00	1.00	1.00	1.00
Gas composition	$\%_{mol}$										
H_2O		44.41	-	38.64	38.64	99.76	6.85	3.08	-	-	-
H_2		28.41	-	35.72	35.72	-	54.30	56.51	58.31	100	100
CO_2		13.19	-	13.13	13.13	0.23	19.84	20.65	21.31	-	-
CO		8.25	-	11.28	11.28	0.01	17.14	17.84	18.41	-	-
CH_4		3.82	-	0.35	0.35	-	0.53	0.55	0.57	-	-
O_2		-	100	-	-	-	-	-	-	-	-
C_xH_y		0.96	-	-	-	-	-	-	-	-	-
Ar		-	-	-	-	-	-	-	-	-	-
N_2		0.95	-	0.86	0.86	-	1.31	1.37	1.41	-	-
LHV	MJ/kg	7.59	-	7.16	7.16		11.28	11.79	12.20	119.96	119.96
Power	MW_{LHV}	82.39	-	80.89	80.89	-	80.88	80.86	80.86	43.94	43.94

Table A 8 - Stream properties of the methanol synthesis island of ERD case in baseline operation

Stream #	**Units**	**31**	**32**	**33**	**34**	**35**	**36**	**37**	**38**	**39**	**40**
Stream type		Syngas	Syngas	Syngas	Raw methanol	Raw methanol	Raw methanol	Total recycle	Purge	Recycle	Recycle
Temperature	°C	122.68	55.06	183.35	238.31	107.50	40.00	40.00	40.00	40.00	46.82
Pressure	bar	92.00	92.00	90.16	89.99	88.19	86.43	86.43	86.43	86.43	92.00
Total mass flow rate	kg/s	4.37	42.71	42.71	42.71	42.71	42.71	38.59	0.25	38.34	38.34
Gas/liq mass flow rate	kg/s	4.37	42.71	42.71	42.71	42.71	42.71	38.59	0.25	38.34	38.34
Molar flow rate	kmol/h	1318.11	11943.24	11943.24	11237.54	11237.54	11237.54	10694.31	69.18	10625.14	10625.13
Vapor fraction	-	1.00	1.00	1.00	1.00	1.00	0.95	1.00	1.00	1.00	1.00
Gas composition	$\%_{mol}$										
DME		-	-	-	-	-	-	-	-	-	-
H_2O		-	0.08	0.08	1.72	1.72	1.72	0.09	0.09	0.09	0.09
H_2		70.36	56.18	56.18	51.80	51.80	51.80	54.43	54.43	54.43	54.43
CO_2		14.39	3.96	3.96	2.57	2.57	2.57	2.66	2.66	2.66	2.66
CO		12.92	2.12	2.12	0.74	0.74	0.74	0.78	0.78	0.78	0.78
Methanol		-	0.40	0.40	3.56	3.56	3.56	0.45	0.45	0.45	0.45
CH_4		0.67	9.80	9.80	10.42	10.42	10.42	10.93	10.93	10.93	10.93
O_2		-	-	-	-	-	-	-	-	-	-
C_xH_y		-	-	-	-	-	-	-	-	-	-
Ar		-	-	-	-	-	-	-	-	-	-
N_2		1.67	27.45	27.45	29.18	29.18	29.18	30.65	30.65	30.65	30.65
Ethanol		-	-	-	-	-	-	-	-	-	-
LHV	MJ/kg	17.76	17.33	17.33	17.09	17.09	17.09	17.28	17.28	17.28	17.28
Power	MW_{LHV}	77.65	740.21	740.21	729.74	729.74	729.74	666.87	4.31	662.56	662.56

Table A 9 - Stream properties of the methanol synthesis island of ERD case in enhanced operation

Stream #	**Units**	**31**	**32**	**33**	**34**	**35**	**36**	**37**	**38**	**39**	**40**
Stream type		Syngas	Syngas	Syngas	Raw methanol	Raw methanol	Raw methanol	Total recycle	Purge	Recycle	Recycle
Temperature	°C	118.51	58.84	172.34	238.79	121.44	40.00	40.00	40.00	40.00	46.85
Pressure	bar	92.00	92.00	90.16	90.02	88.22	86.46	86.46	86.46	86.46	92.00
Total mass flow rate	kg/s	6.99	35.05	35.05	35.05	35.05	35.05	28.38	0.32	28.05	28.05
Gas/liq mass flow rate	kg/s	6.99	35.05	35.05	35.05	35.05	35.05	28.38	0.32	28.05	28.05
Molar flow rate	kmol/h	2126.90	12752.04	12752.04	11623.48	11623.48	11623.48	10748.19	123.05	10625.14	10625.14
Vapor fraction		1.00	1.00	1.00	1.00	1.00	0.92	1.00	1.00	1.00	1.00
Gas composition	$\%_{mol}$										
DME		-	-	-	-	-	-	-	-	-	-
H_2O		-	0.07	0.07	2.62	2.62	2.62	0.09	0.09	0.09	0.09
H_2		71.13	71.37	71.37	66.05	66.05	66.05	71.41	71.41	71.41	71.41
CO_2		14.75	6.39	6.39	4.47	4.47	4.47	4.71	4.71	4.71	4.71
CO		12.75	3.12	3.12	1.10	1.10	1.10	1.19	1.19	1.19	1.19
Methanol		-	0.34	0.34	5.22	5.22	5.22	0.40	0.40	0.40	0.40
CH_4		0.39	4.96	4.96	5.45	5.45	5.45	5.88	5.88	5.88	5.88
O_2		-	-	-	-	-	-	-	-	-	-
C_xH_y		-	-	-	-	-	-	-	-	-	-
Ar		-	-	-	-	-	-	-	-	-	-
N_2		0.98	13.75	13.75	15.09	15.09	15.09	16.31	16.31	16.31	16.31
Ethanol		-	-	-	-	-	-	-	-	-	-
LHV	MJ/kg	17.85	22.58	22.58	22.10	22.10	22.10	23.76	23.76	23.76	23.76
Power	MW_{LHV}	124.80	791.42	791.42	774.65	774.65	774.65	674.34	7.72	666.62	666.62

Table A 10 - Stream properties of the methanol synthesis island of BRD case in baseline operation

Stream #	**Units**	**31**	**32**	**33**	**34**	**35**	**36**	**37**	**38**	**39**	**40**
Stream type		Syngas	Syngas	Syngas	Raw methanol	Raw methanol	Raw methanol	Total recycle	Purge	Recycle	Recycle
Temperature	°C	122.68	59.36	175.08	238.71	119.42	40.00	40.00	40.00	40.00	46.82
Pressure	bar	92.00	92.00	90.16	89.99	88.19	86.43	86.43	86.43	86.43	92.00
Total mass flow rate	kg/s	4.37	25.40	25.40	25.40	25.40	25.40	21.34	0.32	21.03	21.03
Gas/liq mass flow rate	kg/s	4.37	25.40	25.40	25.40	25.40	25.40	21.34	0.32	21.03	21.03
Molar flow rate	kmol/h	1318.10	7912.78	7912.78	7224.48	7224.48	7224.48	6694.06	99.38	6594.68	6594.68
Vapor fraction	-	1.00	1.00	1.00	1.00	1.00	0.93	1.00	1.00	1.00	1.00
Gas composition	$\%_{mol}$										
DME		-	-	-	-	-	-	-	-	-	-
H_2O		-	0.08	0.08	2.51	2.51	2.51	0.09	0.09	0.09	0.09
H_2		70.35	64.47	64.47	58.67	58.67	58.67	63.30	63.30	63.30	63.30
CO_2		14.39	6.89	6.89	5.12	5.12	5.12	5.39	5.39	5.39	5.39
CO		12.92	3.20	3.20	1.16	1.16	1.16	1.26	1.26	1.26	1.26
Methanol		-	0.36	0.36	5.15	5.15	5.15	0.43	0.43	0.43	0.43
CH_4		0.67	6.72	6.72	7.37	7.37	7.37	7.93	7.93	7.93	7.93
O_2		-	-	-	-	-	-	-	-	-	-
C_xH_y		-	-	-	-	-	-	-	-	-	-
Ar		-	-	-	-	-	-	-	-	-	-
N_2		1.67	18.28	18.28	20.02	20.02	20.02	21.60	21.60	21.60	21.60
Ethanol		-	-	-	-	-	-	-	-	-	-
LHV	MJ/kg	17.75	19.15	19.15	18.74	18.74	18.74	19.43	19.43	19.43	19.43
Power	MW_{LHV}	77.65	486.29	486.29	476.01	476.01	476.01	414.80	6.16	408.64	408.64

Table A 11 - Stream properties of the methanol synthesis island of BRD case in enhanced operation

Stream #	**Units**	**31**	**32**	**33**	**34**	**35**	**36**	**37**	**38**	**39**	**40**
Stream type		Syngas	Syngas	Syngas	Raw methanol	Raw methanol	Raw methanol	Total recycle	Purge	Recycle	Recycle
Temperature	°C	118.51	64.21	167.85	239.24	130.95	40.00	40.00	40.00	40.00	46.82
Pressure	bar	92.00	92.00	90.16	89.99	88.19	86.43	86.43	86.43	86.43	92.00
Total mass flow rate	kg/s	6.99	24.18	24.18	24.18	24.18	24.18	17.89	0.71	17.18	17.18
Gas/liq mass flow rate	kg/s	6.99	24.18	24.18	24.18	24.18	24.18	17.89	0.71	17.18	17.18
Molar flow rate	kmol/h	2126.79	8721.79	8721.79	7676.59	7676.59	7676.59	6866.53	271.84	6594.68	6595.00
Vapor fraction		1.00	1.00	1.00	1.00	1.00	0.89	1.00	1.00	1.00	1.00
Gas composition	$\%_{mol}$										
DME		-	-	-	-	-	-	-	-	-	-
H_2O		-	0.07	0.07	3.43	3.43	3.43	0.09	0.09	0.09	0.09
H_2		71.13	75.35	75.35	68.64	68.64	68.64	76.71	76.71	76.71	76.71
CO_2		14.75	11.37	11.37	9.57	9.57	9.57	10.28	10.28	10.28	10.28
CO		12.75	4.70	4.70	1.89	1.89	1.89	2.11	2.11	2.11	2.11
Methanol		-	0.30	0.30	7.14	7.14	7.14	0.40	0.40	0.40	0.40
CH_4		0.39	2.26	2.26	2.57	2.57	2.57	2.87	2.87	2.87	2.87
O_2		-	-	-	-	-	-	-	-	-	-
C_xH_y		-	-	-	-	-	-	-	-	-	-
Ar		-	-	-	-	-	-	-	-	-	-
N_2		0.98	5.94	5.94	6.75	6.75	6.75	7.55	7.55	7.55	7.55
Ethanol		-	-	-	-	-	-	-	-	-	-
LHV	MJ/kg	17.85	21.61	21.61	20.96	20.96	20.96	23.14	23.14	23.14	23.14
Power	MW_{LHV}	124.79	522.38	522.38	506.67	506.67	506.67	413.96	16.39	397.57	397.59

Table A 12 - Stream properties of the methanol purification island of ERD case in baseline operation

Stream #	**Units**	**41**	**42**	**43**	**44**	**45**	**46**	**47**	**48**	**49**	**50**
Stream type		Raw methanol	Raw methanol	Off-gas	Raw methanol	Waste water	Incondensable	Methanol	Purge (ICE)	Air (ICE)	Flue gas (ICE)
Temperature	°C	40.00	41.65	38.63	83.54	106.87	64.12	64.12	35.94	25.00	1200.00
Pressure	bar	86.43	2.00	1.36	1.71	1.36	1.01	1.01	1.36	1.01	1.01
Total mass flow rate	kg/s	4.12	4.12	0.08	4.04	0.92	0.00	3.12	0.33	2.38	2.71
Gas/liq mass flow rate	kg/s	4.12	4.12	0.08	4.04	0.92	0.00	3.12	0.33	2.38	2.71
Molar flow rate	kmol/h	543.22	543.22	9.07	534.15	183.84	0.00	350.31	78.25	296.64	356.34
Vapor fraction	-	-	0.01	1.00	0.89	0.03	-	-	1.00	1.00	1.00
Gas composition	$\%_{mol}$										
DME		-	-	0.22	-	-	-	-	0.03	-	-
H_2O		33.76	33.76	1.82	34.30	99.30	0.07	0.19	0.29	1.00	17.75
H_2		0.16	0.16	9.48	-	-	-	-	49.22	-	-
CO_2		0.82	0.82	49.14	-	-	-	-	8.05	0.03	4.98
CO		-	-	0.21	-	-	-	-	0.71	-	-
Methanol		64.88	64.88	17.81	65.68	0.70	89.71	99.78	2.46	-	-
CH_4		0.23	0.23	13.76	-	-	-	-	11.26	-	-
O_2		-	-	-	-	-	-	-	-	20.70	5.98
C_xH_y		-	-	-	-	-	-	-	-	-	-
Ar		-	-	-	-	-	-	-	-	0.97	0.81
N_2		0.13	0.13	7.56	-	-	-	-	27.97	77.30	70.49
Ethanol		0.02	0.02	0.01	0.02	-	10.22	0.03	-	-	-
LHV	MJ/kg	15.25	15.25	7.75	15.40	0.25	20.88	19.90	14.94	-	-
Power	MW_{LHV}	62.86	62.86	0.63	62.23	0.23	0.00	62.00	4.94	-	-

Table A 13 - Stream properties of the methanol purification island of ERD case in enhanced operation

Stream #	**Units**	**41**	**42**	**43**	**44**	**45**	**46**	**47**	**48**	**49**	**50**
Stream type		Raw methanol	Raw methanol	Off-gas	Raw methanol	Waste water	Incondensable	Methanol	Purge (ICE)	Air (ICE)	Flue gas (ICE)
Temperature	°C	40.00	40.90	32.83	83.57	106.88	64.11	64.11	32.52	25.00	360.00
Pressure	bar	86.46	2.00	1.36	1.71	1.36	1.01	1.01	1.36	1.01	1.01
Total mass flow rate	kg/s	6.67	6.67	0.20	6.46	1.49	0.00	4.97	0.53	4.04	4.57
Gas/liq mass flow rate	kg/s	6.67	6.67	0.20	6.46	1.49	0.00	4.97	0.53	4.04	4.57
Molar flow rate	kmol/h	875.27	875.27	20.57	854.70	295.64	0.00	559.06	143.62	503.55	603.44
Vapor fraction		-	0.02	0.97	0.89	0.03	-	-	1.00	1.00	1.00
Gas composition	$\%_{mol}$										
DME		-	-	0.12	-	-	-	-	0.02	-	-
H_2O		33.69	33.69	2.34	34.45	99.31	0.05	0.15	0.41	1.00	19.80
H_2		0.21	0.21	8.85	-	-	-	-	62.45	-	-
CO_2		1.52	1.52	64.57	-	-	-	-	13.28	0.03	5.44
CO		0.01	0.01	0.23	-	-	-	-	1.06	-	-
Methanol		64.35	64.35	15.54	65.52	0.69	85.25	99.81	2.57	-	-
CH_4		0.13	0.13	5.43	-	-	-	-	5.81	-	-
O_2		-	-	-	-	-	-	-	-	20.70	6.02
C_xH_y		-	-	-	-	-	-	-	-	-	-
Ar		-	-	-	-	-	-	-	-	0.97	0.81
N_2		0.07	0.07	2.92	-	-	-	-	14.39	77.30	67.93
Ethanol		0.03	0.03	0.01	0.03	-	14.70	0.05	-	-	-
LHV	MJ/kg	15.05	15.05	4.65	15.38	0.24	21.28	19.91	16.38	-	-
Power	MW_{LHV}	100.32	100.32	0.95	99.37	0.36	0.00	99.01	8.67	-	-

Table A 14 - Stream properties of the methanol purification island of BRD case in baseline operation

Stream #	**Units**	**41**	**42**	**43**	**44**	**45**	**46**	**47**	**48**	**49**	**50**
Stream type		Raw methanol	Raw methanol	Off-gas	Raw methanol	Waste water	Incondensable	Methanol	Purge (ICE)	Air (ICE)	Flue gas (ICE)
Temperature	°C	40.00	40.62	32.39	83.46	107.16	64.11	64.11	31.70	25.00	360.00
Pressure	bar	86.43	2.00	1.36	1.71	1.36	1.01	1.01	1.36	1.01	1.01
Total mass flow rate	kg/s	4.06	4.06	0.14	3.91	0.88	0.00	3.03	0.46	3.25	3.71
Gas/liq mass flow rate	kg/s	4.06	4.06	0.14	3.91	0.88	0.00	3.03	0.46	3.25	3.71
Molar flow rate	kmol/h	530.38	530.38	14.13	516.25	175.27	0.00	340.97	113.51	405.21	487.44
Vapor fraction	-	-	0.02	0.97	0.89	0.02	-	-	1.00	1.00	1.00
Gas composition	$\%_{mol}$										
DME		-	-	0.10	-	-	-	-	0.02	-	-
H_2O		33.03	33.03	2.22	33.87	99.46	0.06	0.16	0.36	1.00	18.72
H_2		0.19	0.19	7.13	-	-	-	-	56.31	-	-
CO_2		1.73	1.73	64.87	-	-	-	-	12.79	0.03	5.61
CO		0.01	0.01	0.22	-	-	-	-	1.13	-	-
Methanol		64.75	64.75	15.38	66.10	0.54	90.13	99.80	2.29	-	-
CH_4		0.17	0.17	6.56	-	-	-	-	7.76	-	-
O_2		-	-	-	-	-	-	-	-	20.70	6.09
C_xH_y		-	-	-	-	-	-	-	-	-	-
Ar		-	-	-	-	-	-	-	-	0.97	0.81
N_2		0.09	0.09	3.50	-	-	-	-	19.34	77.30	68.76
Ethanol		0.03	0.03	-	0.03	-	9.80	0.04	-	-	-
LHV	MJ/kg	15.09	15.09	4.70	15.47	0.19	20.84	19.90	14.88	-	-
Power	MW_{LHV}	61.21	61.21	0.67	60.54	0.17	0.00	60.37	6.83	-	-

Table A 15 - Stream properties of the methanol purification island of BRD case in enhanced operation

Stream #	**Units**	**41**	**42**	**43**	**44**	**45**	**46**	**47**	**48**	**49**	**50**
Stream type		Raw methanol	Raw methanol	Off-gas	Raw methanol	Waste water	Incondensable	Methanol	Purge (ICE)	Air (ICE)	Flue gas (ICE)
Temperature	°C	40.00	38.41	24.03	83.34	107.33	64.11	64.11	35.91	25.00	360.00
Pressure	bar	86.43	2.00	1.36	1.71	1.36	1.01	1.01	1.36	1.01	1.01
Total mass flow rate	kg/s	6.28	6.28	0.38	5.90	1.30	0.00	4.61	1.09	7.76	8.85
Gas/liq mass flow rate	kg/s	6.28	6.28	0.38	5.90	1.30	0.00	4.61	1.09	7.76	8.85
Molar flow rate	kmol/h	810.07	810.07	34.13	775.94	258.03	0.00	517.90	305.97	968.27	1167.99
Vapor fraction		-	0.04	1.00	0.85	0.02	-	-	1.00	1.00	1.00
Gas composition	$\%_{mol}$										
DME		-	-	0.05	-	-	-	-	0.01	-	-
H_2O		31.78	31.78	-	33.18	99.54	-	0.12	0.08	1.00	20.96
H_2		0.24	0.24	5.80	-	-	-	-	68.80	-	-
CO_2		3.52	3.52	83.51	-	-	-	-	18.45	0.03	6.40
CO		0.01	0.01	0.26	-	-	-	-	1.90	-	-
Methanol		64.30	64.30	7.90	66.78	0.46	88.78	99.83	1.24	-	-
CH_4		0.07	0.07	1.63	-	-	-	-	2.73	-	-
O_2		-	-	-	-	-	-	-	-	20.70	5.98
C_xH_y		-	-	-	-	-	-	-	-	-	-
Ar		-	-	-	-	-	-	-	-	0.97	0.80
N_2		0.04	0.04	0.84	-	-	-	-	6.80	77.30	65.86
Ethanol		0.04	0.04	-	0.04	-	11.22	0.06	-	-	-
LHV	MJ/kg	14.76	14.76	1.97		0.16	20.98	19.91	15.76	-	-
Power	MW_{LHV}	92.72	92.72	0.75	-	0.21	0.00	91.76	17.14	-	-

Power & biomass-to-methanol plants different gasification technologies comparison

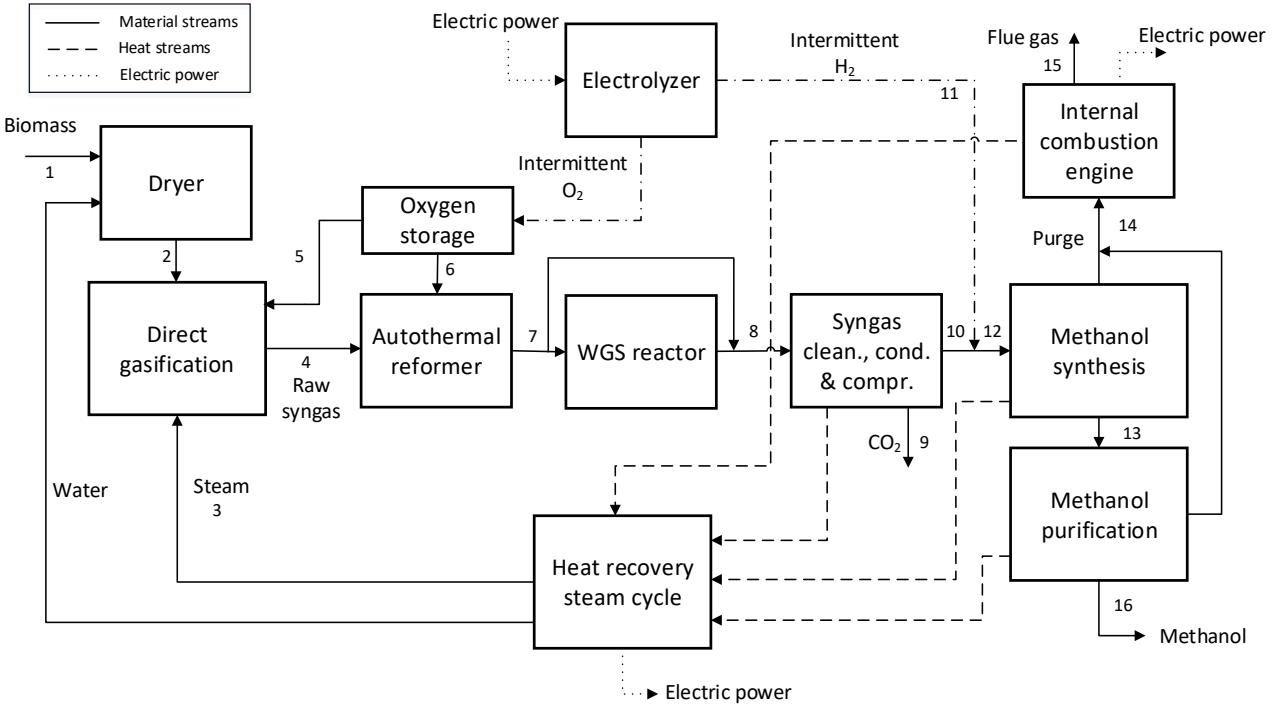

Figure A 2 - Block diagram of the DG-based power & biomass-to-methanol plant

Table A 16 - Plant stream properties DG-based plant baseline operation.

Stream #	**1**	**2**	**3**	**4**	**5**	**6**	**7**	**8**	**9**	**10=12**[1]	**13**	**14**	**15**	**16**
Stream description	As-received biomass	Dried biomass	Fluidizing steam	Raw syngas	Oxygen to gasifier	Oxygen to reformer	Reformed syngas	Shifted syngas	CO_2	Syngas to synthesis	Methanol to purification	Purge to ICE	Flue gas from ICE	Methanol
Temperature, °C	25.00	80.00	171.60	870.00	25.00	25.00	915.00	355.99	40.00	114.49	41.88	29.04	360.00	64.12
Pressure, bar	1.01	1.01	6.50	3.80	30.00	30.00	3.60	3.30	30.00	92.00	2.00	1.36	1.01	1.01
Mass flow rate, kg/s	10.27	6.64	2.64	11.94	1.84	0.60	12.54	12.54	5.34	3.81	3.59	0.28	2.39	3.29
Mole flow rate, kmol/h	-	-	528	2044	207	67.8	2331	2331	437	1225	425	63.8	314	370
Composition, $\%_{mol}$	-	-												
H_2O	-	-	100	40.48	-	-	33.53	28.45	-	-	10.87	0.17	16.88	0.17
H_2	-	-	-	19.95	-	-	30.01	35.10	-	66.81	0.25	43.16	-	-
CO_2	-	-	-	17.40	-	-	15.99	21.07	100	3.96	0.46	3.90	4.62	-
CO	-	-	-	14.61	-	-	19.12	14.03	-	26.70	0.01	0.85	-	-
Methanol	-	-	-	-	-	-	-	-	-	-	87.54	3.35	-	99.83
CH_4	-	-	-	4.46	-	-	0.39	0.39	-	0.74	0.51	14.39	-	-
C_xH_y	-	-	-	2.01	-	-	-	-	-	-	-	-	-	-
O_2	-	-	-	-	100	100	-	-	-	-	-	-	5.98	-
Ar	-	-	-	-	-	-	-	-	-	-	-	-	0.81	-
N_2	-	-	-	1.08	-	-	0.94	0.94	-	1.80	0.32	34.13	71.71	-
Ethanol	-	-	-	-	-	-	-	-	-	-	0.03	-	-	-
DME	-	-	-	-	-	-	-	-	-	-	0.01	0.05	-	-
LHV, MJ/kg	9.74	16.37	-	7.23	-	-	6.70	6.60	-	21.72	18.55	15.44	-	19.90
Power, MW_{LHV}	100.0	108.76	-	86.31	-	-	84.09	82.74	-	82.70	66.53	4.33	-	65.48

[1] In baseline operation, stream 10 coincides with stream 12 and hydrogen addition (i.e. stream 11) is not present

Table A 17 - Plant stream properties DG-based plant enhanced operation.

Stream #	**1**	**2**	**3**	**4**	**5**	**6**	**7=8**[1]	**10**	**11**	**12**	**13**	**14**	**15**	**16**
Stream description	As-received biomass	Dried biomass	Fluidizing steam	Raw syngas	Oxygen to gasifier	Oxygen to reformer	Reformed syngas	Syngas before enriching	Hydrogen	Syngas to synthesis	Methanol to purification	Purge to ICE	Flue gas from ICE	Methanol
Temperature, °C	25.00	80.00	171.60	870.00	25.00	25.00	915.00	40.00	25.00	112.30	41.29	37.41	360.00	64.11
Pressure, bar	1.01	1.01	6.50	3.80	30.00	30.00	3.60	30.00	30.00	92.00	2.00	1.36	1.01	1.01
Mass flow rate, kg/s	10.27	6.64	2.64	11.94	1.84	0.60	12.54	8.58	0.75	9.31	8.98	0.54	4.95	6.99
Mole flow rate, kmol/h	-	-	528	2044	207	67.8	2331	1547	1334	2877	1160	155	656	785
Composition, $\%_{mol}$	-	-												
H_2O	-	-	100	40.48	-	-	33.53	0.23	-	-	30.08	0.21	20.12	0.15
H_2	-	-	-	19.95	-	-	30.01	45.23	100	70.67	0.24	64.28	-	-
CO_2	-	-	-	17.40	-	-	15.99	23.74	-	12.77	1.21	12.01	5.10	-
CO	-	-	-	14.61	-	-	19.12	28.79	-	15.48	0.01	0.92	-	-
Methanol	-	-	-	-	-	-	-	-	-	-	68.22	2.67	-	99.80
CH_4	-	-	-	4.46	-	-	0.39	0.59	-	0.32	0.14	5.84	-	-
C_xH_y	-	-	-	2.01	-	-	-	-	-	-	-	-	-	-
O_2	-	-	-	-	100	100	-	-	-	-	-	-	5.91	-
Ar	-	-	-	-	-	-	-	-	-	-	-	-	0.81	-
N_2	-	-	-	1.08	-	-	0.94	1.42	-	0.76	0.08	14.07	68.06	-
Ethanol	-	-	-	-	-	-	-	-	-	-	0.03	-	-	0.04
DME	-	-	-	-	-	-	-	-	-	-	-	0.03	-	-
LHV, MJ/kg	9.74	16.37	-	7.23	-	-	6.70	9.80	119.96	18.66	15.69	17.61	-	19.90
Power, MW_{LHV}	100.0	108.76	-	86.31	-	-	84.09	84.05	89.58	173.62	140.96	9.57	-	139.07

[1] In enhanced operation, stream 7 coincides with stream 8 since the WGS is bypassed. Moreover, steam 9 is not present since no CO_2 is removed from the syngas stream.

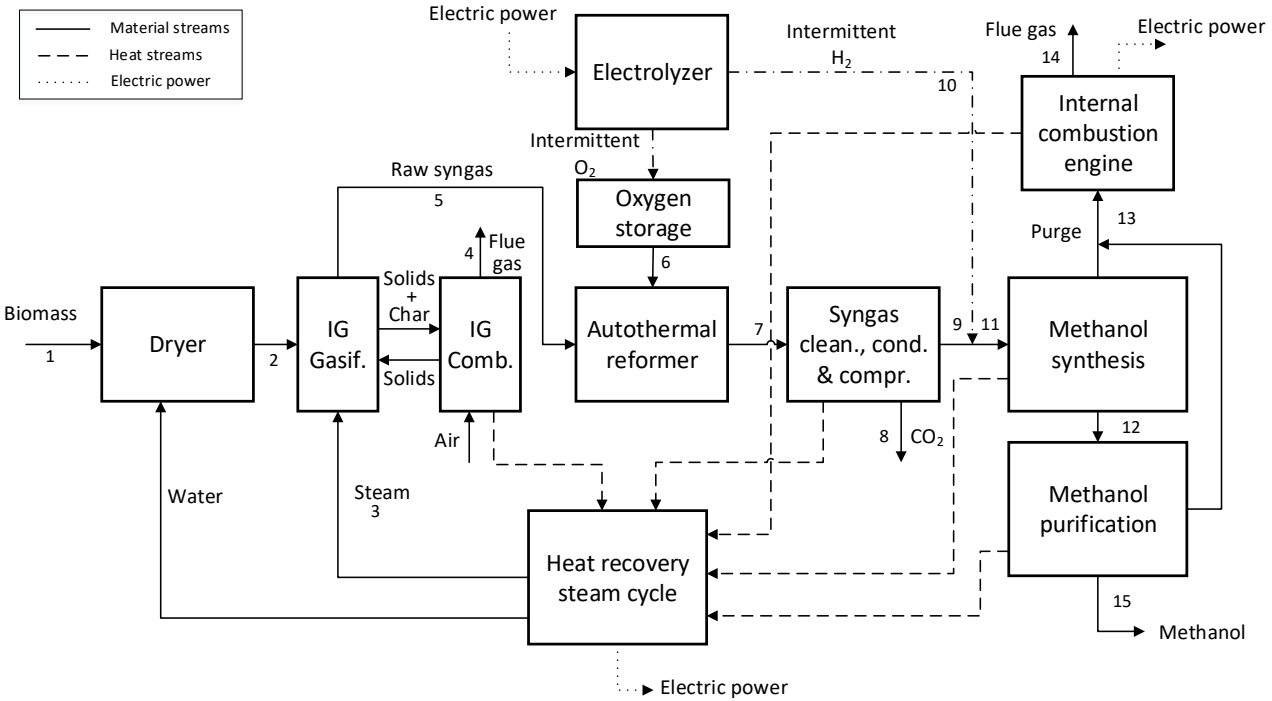

Figure A 3 - Block diagram of the IG-based power & biomass-to-methanol plant

Table A 18 - Plant stream properties IG-based plant baseline operation.

Stream #	**1**	**2**	**3**	**4**	**5**	**6**	**7**	**8**	**9=11[1]**	**12**	**13**	**14**	**15**
Stream description	As-received biomass	Dried biomass	Fluidizing steam	Flue gas from combustor	Raw syngas	Oxygen to reformer	Reformed syngas	CO_2	Syngas to synthesis	Methanol to purification	Purge to ICE	Flue gas from ICE	Methanol
Temperature, °C	25.00	80.00	400.00	139.97	815.00	25.00	800.00	40.00	114.98	41.77	30.27	360.00	64.11
Pressure, bar	1.01	1.01	1.96	1.05	1.23	30.00	1.10	30.00	92.00	2.00	1.36	1.01	1.01
Mass flow rate, kg/s	10.27	6.64	2.62	13.19	8.73	0.47	9.21	2.79	3.71	3.51	0.27	2.53	3.33
Mole flow rate, kmol/h	-	-	523	1551	1710	53.2	1980	229	1213	406	62.9	332	374
Composition, $\%_{mol}$	-	-											
H_2O	-	-	100	8.16	36.24	-	27.10	-	-	5.65	0.06	16.95	0.15
H_2	-	-	-	-	27.99	-	40.61	-	66.27	0.29	44.28	-	-
CO_2	-	-	-	15.92	12.48	-	12.87	100	2.08	0.48	3.97	4.86	-
CO	-	-	-	-	14.48	-	17.92	-	29.23	0.01	1.18	-	-
Methanol	-	-	-	-	-	-	-	-	-	92.52	3.77	-	99.85
CH_4	-	-	-	-	6.07	-	0.52	-	0.85	0.65	16.48	-	-
C_xH_y	-	-	-	-	1.61	-	-	-	-	-	-	-	-
O_2	-	-	-	2.99	-	100	-	-	-	-	-	5.95	-
Ar	-	-	-	0.90	-	-	-	-	-	-	-	0.82	-
N_2	-	-	-	72.02	1.11	-	0.96	-	1.56	0.33	30.20	71.42	-
Ethanol	-	-	-	-	-	-	-	-	-	0.04	-	-	-
DME	-	-	-	-	-	-	-	-	-	0.01	0.05	-	-
LHV, MJ/kg	9.74	16.37	-	-	9.72	-	9.15	-	22.68	19.19	17.46	-	19.90
Power, MW_{LHV}	100.0	108.76	-	-	84.88	-	84.21	-	84.18	67.38	4.67	-	66.23

[1] In baseline operation, stream 9 coincides with stream 11 and hydrogen addition (i.e. stream 10) is not present.

Table A 19 - Plant stream properties IG-based plant enhanced operation.

Stream #	**1**	**2**	**3**	**4**	**5**	**6**	**7**	**9[1]**	**10**	**11**	**12**	**13**	**14**	**15**
Stream description	As-received biomass	Dried biomass	Fluidizing steam	Flue gas from combustor	Raw syngas	Oxygen to reformer	Reformed syngas	Syngas before enriching	Hydrogen	Syngas to synthesis	Methanol to purification	Purge to ICE	Flue gas from ICE	Methanol
Temperature, °C	25.00	80.00	400.00	139.97	815.00	25.00	800.00	40.00	25.00	112.48	41.25	37.63	360.00	64.11
Pressure, bar	1.01	1.01	1.96	1.05	1.23	30.00	1.10	30.00	30.00	92.00	2.00	1.36	1.01	1.01
Mass flow rate, kg/s	10.27	6.64	2.62	13.19	8.73	0.47	9.21	6.52	0.39	6.90	6.62	0.45	4.23	5.23
Mole flow rate, kmol/h	-	-	523	1551	1710	53.2	1980	1445	697	2139	848	123	559	588
Composition, $\%_{mol}$	-	-												
H_2O	-	-	100	8.16	36.24	-	27.10	0.23	-	-	28.33	0.24	19.30	0.16
H_2	-	-	-	-	27.99	-	40.61	55.64	100	70.18	0.24	60.45	-	-
CO_2	-	-	-	15.92	12.48	-	12.87	17.57	-	11.87	1.22	11.27	5.27	-
CO	-	-	-	-	14.48	-	17.92	24.54	-	16.58	0.01	0.91	-	-
Methanol	-	-	-	-	-	-	-	-	-	-	69.88	3.22	-	99.80
CH_4	-	-	-	-	6.07	-	0.52	0.72	-	0.48	0.21	8.44	-	-
C_xH_y	-	-	-	-	1.61	-	-	-	-	-	-	-	-	-
O_2	-	-	-	2.99	-	100	-	-	-	-	-	-	5.96	-
Ar	-	-	-	0.90	-	-	-	-	-	-	-	-	0.82	-
N_2	-	-	-	72.02	1.11	-	0.96	1.31	-	0.89	0.09	15.44	68.65	-
Ethanol	-	-	-	-	-	-	-	-	-	-	0.03	-	-	0.04
DME	-	-	-	-	-	-	-	-	-	-	-	0.02	-	-
LHV, MJ/kg	9.74	16.37	-	-	9.72	-	9.15	12.91	119.96	19.00	15.96	17.98	-	19.90
Power, MW_{LHV}	100.0	108.76	-	-	84.88	-	84.21	84.18	46.83	131.00	105.66	8.09	-	104.19

[1] In enhanced operation, stream 8 is not present since no CO_2 is removed from the syngas stream.

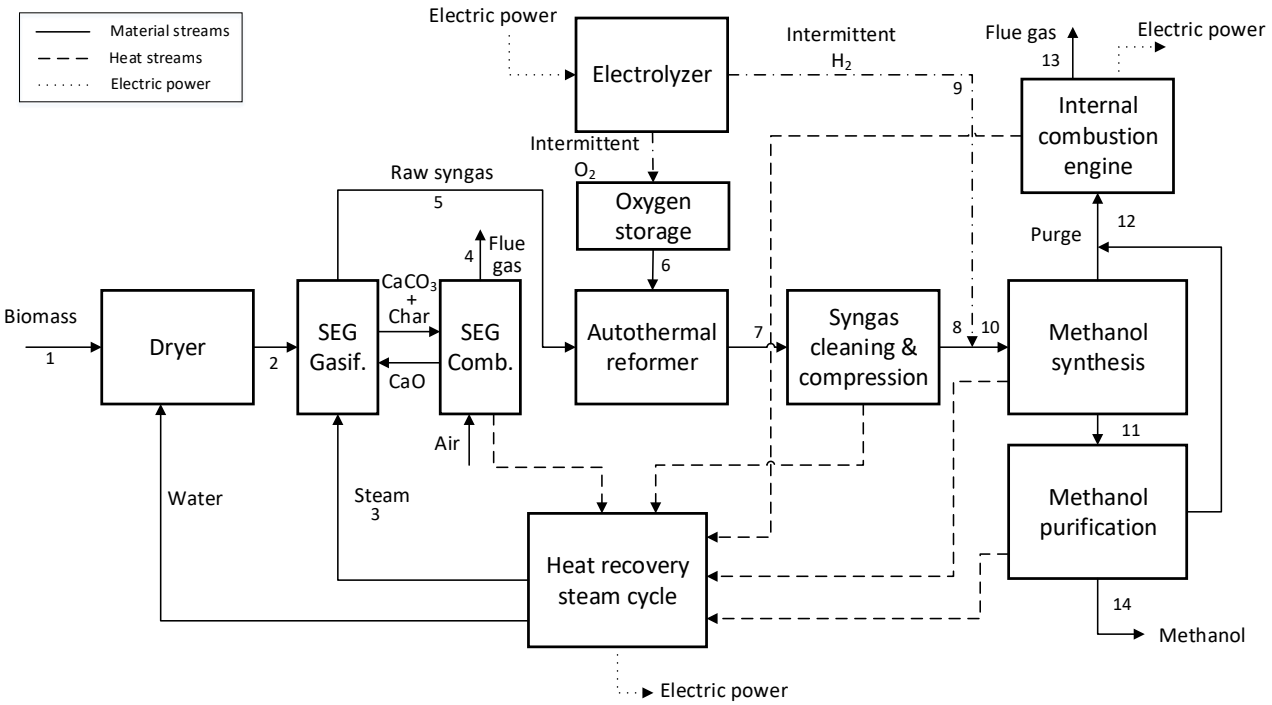

Figure A 4 - Block diagram of the SEG-based power & biomass-to-methanol plant

Table A 20 – Plant stream properties SEG-based plant baseline operation.

Stream #	**1**	**2**	**3**	**4**	**5**	**6**	**7**	**8=10[1]**	**11**	**12**	**13**	**14**
Stream description	As-received biomass	Dried biomass	Fluidizing steam	Flue gas from combustor	Raw syngas	Oxygen to reformer	Reformed syngas	Syngas to synthesis	Methanol to purification	Purge to ICE	Flue gas from ICE	Methanol
Temperature, °C	25.00	80.00	182.00	156.12	714.07	25.00	800.00	122.68	41.65	35.94	360.00	64.12
Pressure, bar	1.01	1.01	2.00	1.05	1.23	30.00	1.10	92.00	2.00	1.36	1.01	1.01
Mass flow rate, kg/s	10.27	6.64	4.70	16.97	8.68	0.54	9.22	4.37	4.12	0.33	2.71	3.12
Mole flow rate, kmol/h	-	-	940	1844	2059.43	61.3	2285	1318	543	78.3	356	350
Composition, $\%_{mol}$	-	-	-	-	-	-	-	-	-	-	-	-
H_2O	-	-	100	0.91	49.11	-	42.25	-	33.76	0.29	17.75	0.19
H_2	-	-	-	-	32.91	-	40.58	70.36	0.16	49.22	-	-
CO_2	-	-	-	27.89	7.12	-	8.35	14.39	0.82	8.05	4.98	-
CO	-	-	-	-	4.39	-	7.45	12.92	-	0.71	-	-
Methanol	-	-	-	-	-	-	-	-	64.88	2.46	-	99.78
CH_4	-	-	-	-	4.30	-	0.39	0.67	0.23	11.26	-	-
C_xH_y	-	-	-	-	1.08	-	-	-	-	-	-	-
O_2	-	-	-	2.99	-	100	-	-	-	-	5.98	-
Ar	-	-	-	0.85	-	-	-	-	-	-	0.81	-
N_2	-	-	-	67.36	1.07	-	0.96	1.67	0.13	27.97	70.49	-
Ethanol	-	-	-	-	-	-	-	-	0.02	-	-	0.03
DME	-	-	-	-	-	-	-	-	-	0.03	-	-
LHV, MJ/kg	9.74	16.37	-	-	9.28	-	8.42	17.76	15.25	14.94	-	19.90
Power, MW_{LHV}	100.0	108.76	-	-	80.56	-	77.68	77.65	62.86	4.94	-	62.00

[1] In baseline operation, stream 8 coincides with stream 10 and hydrogen addition (i.e. stream 9) is not present.

Table A 21 - Plant stream properties SEG-based plant enhanced operation.

Stream #	**1**	**2**	**3**	**4**	**5**	**6**	**7**	**8**	**9**	**10**	**11**	**12**	**13**	**14**
Stream description	As-received biomass	Dried biomass	Fluidizing steam	Flue gas from combustor	Raw syngas	Oxygen to reformer	Reformed syngas	Syngas before enriching	Hydrogen	Syngas to synthesis	Methanol to purification	Purge to ICE	Flue gas from ICE	Methanol
Temperature, °C	25.00	80.00	400.00	143.95	771.80	25.00	800.00	120.52	25.00	118.51	40.90	32.52	360.00	64.11
Pressure, bar	1.01	1.01	1.96	1.05	1.23	30.00	1.10	92.00	30.00	92.00	2.00	1.36	1.01	1.01
Mass flow rate, kg/s	10.27	6.64	4.44	14.01	10.86	0.44	11.30	6.63	0.37	6.99	6.67	0.53	4.57	4.97
Mole flow rate, kmol/h	-	-	887	1615	2191	50.1	2404	1473	654	2127	875	144	603	559
Composition, $\%_{mol}$	-	-	-	-	-	-	-	-	-	-	-	-	-	-
H_2O	-	-	100	3.81	44.41	-	38.64	-	-	-	33.69	0.41	19.80	0.15
H_2	-	-	-	-	28.41	-	35.72	58.31	100	71.13	0.21	62.45	-	-
CO_2	-	-	-	17.76	13.19	-	13.13	21.31	-	14.75	1.52	13.28	5.44	-
CO	-	-	-	-	8.25	-	11.28	18.41	-	12.75	0.01	1.06	-	-
Methanol	-	-	-	-	-	-	-	-	-	-	64.35	2.57	-	99.81
CH_4	-	-	-	-	3.82	-	0.35	0.57	-	0.39	0.13	5.81	-	-
C_xH_y	-	-	-	-	0.96	-	-	-	-	-	-	-	-	-
O_2	-	-	-	3.00	-	100.00%	-	-	-	-	-	-	6.02	-
Ar	-	-	-	0.93	-	-	-	-	-	-	-	-	0.81	-
N_2	-	-	-	74.50	0.95	-	0.86	1.41	-	0.98	0.07	14.39	67.93	-
Ethanol	-	-	-	-	-	-	-	-	-	-	0.03	-	-	0.05
DME	-	-	-	-	-	-	-	-	-	-	-	0.02	-	-
LHV, MJ/kg	9.74	16.37	-	-	7.59	-	7.16	12.20	119.96	17.85	15.05	16.38	-	19.91
Power, MW_{LHV}	100.0	108.76	-	-	82.39	-	80.89	80.86	43.94	124.80	100.32	8.67	-	99.01

Power & biomass-to-methanol plants capital costs

Table A 22 – DG-based plant capital costs.

Capital costs	Cost scaling parameter	Reference capacity	Scaling exponent	Reference purchase equipment delivered, M€	Plant capacity	Lang factor	Reference	Fixed capital investment M€
Biomass-to-syngas island								***90.02***
Oxygen storage	Storage volume, m^3	1.00	1.00	0.006	670.06	5.04	In-house estimate	20.26
Feedstock handling [1]	Feed, MWth	157.00	0.31	6.94	100.00	1.48	(Hannula, 2016)	8.91
Belt dryer [1]	Water evap., kg/s	0.34	0.28	2.49	3.62	1.48	(Hannula, 2016)	7.11
Pressurized O2 CFB gasifier [1]	Dry biom., kg/s	17.80	0.75	49.38	5.65	1.42	(Hannula, 2016)	29.58
Ceramic hot-gas filter [1]	Syngas, kmol/s	1.47	0.67	8.91	0.57	1.48	(Hannula, 2016)	6.96
Catalytic reformer [1]	Syngas, kmol/s	2.04	0.67	28.55	0.57	1.42	(Hannula, 2016)	17.19
Cleaning and conditioning island								***53.47***
Scrubber	Syngas at cleaning inlet, kmol/s	0.64	0.67	0.27	0.65	5.04	(Palonen et al., 2017)	1.38
Liquid redox	Syngas at cleaning inlet, kmol/s	0.64	0.67	0.57	0.65	5.04	(Palonen et al., 2017)	2.88
Syngas compressor 1	Compressor work, MWel	7.01	0.67	7.50	4.51	5.04	(Palonen et al., 2017)	14.60
Syngas compressor 2	Compressor work, MWel	7.01	0.67	7.50	3.85	5.04	(Palonen et al., 2017)	13.14
Activated carbon	Syngas at cleaning inlet, kmol/s	0.64	0.67	0.09	0.65	3.97	(Palonen et al., 2017)	0.37
Waste water treatment	Waste water, m^3/h	22.56	0.67	0.45	20.72	5.04	(Palonen et al., 2017)	2.16
WGS reactor	-	-	-	1.60	-	4.28	In-house estimate	6.85
CO_2 removal (MDEA)	-	-	-	-	-	1.00	In-house estimate	12.10
Syngas-to-methanol island								***22.99***
Methanol synthesis BWR	-	-	-	3.74	-	4.28	In-house estimate	16.00
Recycle compressor	-	-	-	0.78	-	5.04	In-house estimate	3.95
Stabilizing column	-	-	-	0.12	-	5.04	In-house estimate	0.58
Concentration column	-	-	-	0.49	-	5.04	In-house estimate	2.46

Capital costs	Cost scaling parameter	Reference capacity	Scaling exponent	Reference purchase equipment delivered, M€	Plant capacity	Lang factor	Reference	Fixed capital investment M€
Power island								***27.99***
CHP internal combustion engine [1]	Fuel input, kWth	13783	0.95	*2.48*	9568	1.40	(Zatti et al., 2018)	2.45
Power cycle	-	-	-	7.60	-	3.36	In-house estimate	25.54
Electricity-to-hydrogen island								***90.32***
Electrolyser	Electrolyser size, MWel	1.00	1.00	0.70	129.04	1.00	In-house estimate	90.32
Fixed capital investment								**284.80**
Working capital								50.07
Total capital investment								**334.87**

[1] The cost reported in the column “reference equipment delivered" is a direct cost which includes installation and BOP. The corresponding Lang factors have been modified accordingly.

Table A 23 – DGns-based plant capital costs.

Capital costs	Cost scaling parameter	Reference capacity	Scaling exponent	Reference purchase equipment delivered, M€	Plant capacity	Lang factor	Reference	Fixed capital investment M€
Biomass-to-syngas island								***69.76***
Feedstock handling [1]	Feed, MWth	157.00	0.31	6.94	100.00	1.48	(Hannula, 2016)	8.91
Belt dryer [1]	Water evap., kg/s	0.34	0.28	2.49	3.62	1.48	(Hannula, 2016)	7.11
Pressurized O_2 CFB gasifier [1]	Dry biom., kg/s	17.80	0.75	49.38	5.65	1.42	(Hannula, 2016)	29.58
Ceramic hot-gas filter [1]	Syngas, kmol/s	1.47	0.67	8.91	0.57	1.48	(Hannula, 2016)	6.96
Catalytic reformer [1]	Syngas, kmol/s	2.04	0.67	28.55	0.57	1.42	(Hannula, 2016)	17.19
Cleaning and conditioning island								***42.35***
Scrubber	Syngas @cleaning inlet, kmol/s	0.64	0.67	0.27	0.65	5.04	(Palonen et al., 2017)	1.38
Liquid redox	Syngas @cleaning inlet, kmol/s	0.64	0.67	0.57	0.65	5.04	(Palonen et al., 2017)	2.88
Syngas compressor 1	Compressor work, MWel	7.01	0.67	7.50	4.20	5.04	(Palonen et al., 2017)	13.92
Syngas compressor 2	Compressor work, MWel	7.01	0.67	7.50	3.85	5.04	(Palonen et al., 2017)	13.14
Activated carbon	Syngas @cleaning inlet, kmol/s	0.64	0.67	0.09	0.65	3.97	(Palonen et al., 2017)	0.37
Waste water treatment	Waste water, m^3/h	22.56	0.67	0.45	20.72	5.04	(Palonen et al., 2017)	2.16
CO_2 removal (MDEA)	CO_2 captured, kg/s	5.34	0.67	-	3.16	-	In-house estimate	8.51
Syngas-to-methanol island								***22.99***
Methanol synthesis BWR	-	-	-	3.74	-	4.28	In-house estimate	16.00
Recycle compressor	-	-	-	0.78	-	5.04	In-house estimate	3.95
Stabilizing column	-	-	-	0.12	-	5.04	In-house estimate	0.58
Concentration column	-	-	-	0.49	-	5.04	In-house estimate	2.46
Power island								***27.99***
CHP internal combustion engine [1]	Fuel input, kWth	13783	0.95	*2.48*	9568.02	1.40	(Zatti et al., 2018)	2.45
Power cycle				7.60	-	3.36	In-house estimate	25.54
Electricity-to-hydrogen island								***90.32***

Capital costs	Cost scaling parameter	Reference capacity	Scaling exponent	Reference purchase equipment delivered, M€	Plant capacity	Lang factor	Reference	Fixed capital investment M€
Electrolyser	Electrolyser size, MWel	1.00	1.00	0.70	129.04	1.00	In-house estimate	90.32
Fixed capital investment								**253.42**
Working capital								44.54
Total capital investment								**297.96**

[1] The cost reported in the column “reference equipment delivered" is a direct cost which includes installation and BOP. The corresponding Lang factors have been modified accordingly.

Table A 24 – IG-based plant capital costs.

Capital costs	Cost scaling parameter	Reference capacity	Scaling exponent	Reference purchase equipment delivered, M€	Plant capacity	Lang factor	Reference	Fixed capital investment M€
Biomass-to-syngas island								***85.40***
Oxygen storage	Storage volume, m^3	1.00	1.00	0.006	129.53	5.04	In-house estimate	3.92
Feedstock handling [1]	Feed, MWth	157.00	0.31	6.94	100.00	1.48	(Hannula, 2016)	8.91
Belt dryer [1]	Water evap., kg/s	0.34	0.28	2.49	3.62	1.48	(Hannula, 2016)	7.11
Atm steam CFB gasifier [1]	Dry biom., kg/s	17.80	0.75	24.75	4.87	1.42	(Hannula, 2016)	13.27
Combustor with fluegas treatment [1]	Fuel input, MWth	5.90	0.65	7.73	28.90	1.42	(Hannula, 2016)	30.76
Ceramic hot-gas filter [1]	Syngas, kmol/s	1.47	0.67	8.91	0.48	1.48	(Hannula, 2016)	6.18
Catalytic reformer [1]	Syngas, kmol/s	2.04	0.67	28.55	0.48	1.42	(Hannula, 2016)	15.26
Cleaning and conditioning island								***41.35***
Scrubber	Syngas @cleaning inlet, kmol/s	0.64	0.67	0.27	0.55	5.04	(Palonen et al., 2017)	1.23
Liquid redox	Syngas @cleaning inlet, kmol/s	0.64	0.67	0.57	0.55	5.04	(Palonen et al., 2017)	2.58
Syngas compressor 1	Compressor work, MWel	7.01	0.67	7.50	5.77	5.04	(Palonen et al., 2017)	17.23
Syngas compressor 2	Compressor work, MWel	7.01	0.67	7.50	2.88	5.04	(Palonen et al., 2017)	10.81
Activated carbon	Syngas @cleaning inlet, kmol/s	0.64	0.67	0.09	0.55	3.97	(Palonen et al., 2017)	0.33
Waste water treatment	Waste water, m^3/h	22.56	0.67	0.45	14.07	5.04	(Palonen et al., 2017)	1.66
CO_2 removal (MDEA)	-	-	-	-	-	-	In-house estimate	7.50
Syngas-to-methanol island								***17.59***
Methanol synthesis BWR	-	-	-	2.80	-	4.28	In-house estimate	11.96
Recycle compressor	-	-	-	0.63	-	5.04	In-house estimate	3.17
Stabilizing column	-	-	-	0.10	-	5.04	In-house estimate	0.49

Capital costs	Cost scaling parameter	Reference capacity	Scaling exponent	Reference purchase equipment delivered, M€	Plant capacity	Lang factor	Reference	Fixed capital investment M€
Concentration column	-	-	-	0.39	-	5.04	In-house estimate	1.98
Power island								***28.70***
CHP internal combustion engine [1]	Fuel input, kWth	13783	0.95	*2.48*	8087.44	1.40	(Zatti et al., 2018)	2.09
Power cycle				7.92	-	3.36	In-house estimate	26.61
Electricity-to-hydrogen island								***47.22***
Electrolyser	Electrolyser size, MWel	1.00	1.00	0.70	67.46	1.00	In-house estimate	47.22
Fixed capital investment								**220.26**
Working capital								38.73
Total capital investment								**258.99**

[1] The cost reported in the column “reference equipment delivered" is a direct cost which includes installation and BOP. The corresponding Lang factors have been modified accordingly.

Table A 25 – SEG-based plant capital costs.

Capital costs	Cost scaling parameter	Reference capacity	Scaling exponent	Reference purchase equipment delivered, M€	Plant capacity	Lang factor	Reference	Fixed capital investment M€
Biomass-to-syngas island								***92.42***
Oxygen storage	Storage volume, m^3	1.00	1.00	0.006	149.10	5.04	In-house estimate	4.51
Feedstock handling [1]	Feed, MWth	157.00	0.31	6.94	100.00	1.48	(Hannula, 2016)	8.91
Belt dryer [1]	Water evap., kg/s	0.34	0.28	2.49	3.62	1.48	(Hannula, 2016)	7.11
Atm steam CFB gasifier [1]	Dry biom., kg/s	17.80	0.75	24.75	5.64	1.42	(Hannula, 2016)	14.82
Combustor with fluegas treatment [1]	Fuel input, MWth	5.90	0.65	7.73	30.36	1.42	(Hannula, 2016)	31.76
Ceramic hot-gas filter [1]	Syngas, kmol/s	1.47	0.67	8.91	0.61	1.48	(Hannula, 2016)	7.29
Catalytic reformer [1]	Syngas, kmol/s	2.04	0.67	28.55	0.61	1.42	(Hannula, 2016)	18.01
Cleaning and conditioning island								***28.34***
Scrubber	Syngas @cleaning inlet, kmol/s	0.64	0.67	0.27	0.67	5.04	(Palonen et al., 2017)	1.41
Liquid redox	Syngas @cleaning inlet, kmol/s	0.64	0.67	0.57	0.67	5.04	(Palonen et al., 2017)	2.94
Glycol drying (TEG)	Removed water, mol/s	0.47	0.67	0.32	0.00	5.04	(Palonen et al., 2017)	0.00
Syngas compressor	Compressor work, MWel	7.01	0.67	7.50	7.95	5.04	(Palonen et al., 2017)	21.35
Activated carbon	Syngas @cleaning inlet, kmol/s	0.64	0.67	0.09	0.67	3.97	(Palonen et al., 2017)	0.38
Waste water treatment	Waste water, m^3/h	22.56	0.67	0.45	22.17	5.04	(Palonen et al., 2017)	2.26
Syngas-to-methanol island								***17.36***
Methanol synthesis BWR	-	-	-	2.77	-	4.28	In-house estimate	11.86
Recycle compressor	-	-	-	0.63	-	5.04	In-house estimate	3.15
Stabilizing column	-	-	-	0.10	-	5.04	In-house estimate	0.49
Concentration column	-	-	-	0.37	-	5.04	In-house estimate	1.86

Capital costs	Cost scaling parameter	Reference capacity	Scaling exponent	Reference purchase equipment delivered, M€	Plant capacity	Lang factor	Reference	Fixed capital investment M€
Power island								***28.36***
CHP internal combustion engine [1]	Fuel input, kWth	1328	0.95	*0.27*	8671.23	1.40	(Zatti et al., 2018)	2.23
Power cycle				7.78	-	3.36	In-house estimate	26.13
Electricity-to-hydrogen island								***48.97***
Electrolyser	Electrolyser size, MWel	1.00	1.00	0.70	63.29	1.00	In-house estimate	44.31
H2 compressor	Compressor work, MWel	0.64	0.67	0.75	0.88	5.04	In-house estimate	4.66
Fixed capital investment								**215.44**
Working capital								37.87
Total capital investment								**253.32**

[1] The cost reported in the column “reference equipment delivered" is a direct cost which includes installation and BOP. The corresponding Lang factors have been modified accordingly.

Appendix B

Appendix B includes the following:

- process modelling assumptions and TQ diagrams.
- Biomass-to-methanol and hydrogen plants with CCS: tables with properties of the main streams of the four assessed plants.
- Biomass-to-methanol and hydrogen plants with CCS capital costs: breakdown of capital costs.

Table B 1 – Process modelling assumptions.

Assumptions	**BtM DG**	**BtM IG**	**BtH_2 DG**	**BtH_2 IG**
Input biomass (As received)				
LHV, MJ/kg_{AR}	9.74			
Moisture, $\%_{wt}$	45			
Proximate analysis, $\%_{wt,dry}$				
Fixed Carbon	18.84			
Volatile matter	80.0			
Ash	1.16			
Ultimate analysis, $\%_{wt,dry}$				
Carbon	51.19			
Hydrogen	6.08			
Nitrogen	0.2			
Chlorine	0.05			
Sulfur	0.02			
Oxygen	41.3			
Ash	1.16			
Biomass pre-treatment				
Biomass moisture at dryer outlet, $\%_{wt}$	15			
Biomass temperature at dryer outlet, °C	80			
Specific heat consumption, MWh/t_{H2O}	1.0			
Specific power consumption $kWh/t_{bio,dry}$	32			
Gasification				
Gasifier outlet temperature, °C	870	815	870	815
Gasifier and combustor pressure, bar	4.00	1.43	4.00	1.43
Char conversion in the gasifier, % of inlet C	95.50	83.00	95.50	83.00
Fluidizing steam input temperature, °C	200	400	200	400
Gas injection for sealing and filters, $kg/kg_{bio,dry}$	H_2O=0.12 Air = 0.03	H_2O=0.12 Air = 0.03	H_2O=0.12 Air = 0.03	H_2O=0.12 Air = 0.03

Assumptions	**BtM DG**	**BtM IG**	**BtH_2 DG**	**BtH_2 IG**
Combustor exit temperature, °C	-	910	-	910
Oxygen concentration in combustor flue gases, $\%_{mol}$	-	3.0	-	3.0
Combustor air temperature, °C	-	270	-	270
Overall pressure drop from combustor to stack, % of gas pressure at valve outlet	-	4.5	-	4.5
Total solid purge, % of inlet biomass	-	1.0	-	1.0
Combustor air fan isentropic/mech.-el efficiency, %	-	80/94	-	80/94
Gasifier/reformer oxygen compressor isentropic/mech.-el efficiency, %	80/94	-	80/94	-
Loss of solids from the BFB gasifier, % of the circulating solids	-	0.01	-	0.01
Combustor cyclone separation efficiency, %	-	Solids: 99.9; Ash:99	-	Solids: 99.9; Ash:99
Gasifier/combustor thermal losses, % of total thermal input	1.0	1.0/1.0	1.0	1.0/1.0
Syngas purification, conditioning and compression				
Reformer exit temperature, °C	915	800	915	800
CH_4 conversion in the reformer, %	90	90	90	90
S/C at reformer inlet	1.0	1.0	1.0	1.0
Oxygen purity, $\%_{mol}$	95	95	95	95
Oxygen temperature at ASU outlet, °C	15	15	15	15
Oxygen pressure at ASU outlet, bar	2.0	2.0	2.0	2.0
Oxygen preheating temperature, °C	- [1]	150	- [1]	150
Minimum syngas temperature upstream water scrubber, °C [2]	220	220	220	220
Scrubber pump hydraulic/mech.-el efficiency, %	75/90	75/90	75/90	75/90
Electric consumption of the desulfurization unit, $kWh/kg_{H2S,removed}$	1.35	1.35	1.35	1.35
Syngas compressor 1 stages	4	6	4	6
Syngas compressor 1 outlet pressure, bar	30.0	30.0	30.2	33.6
Syngas compressor 2 stages	2	2	-	-
Syngas compressor 2 outlet pressure, bar	92	92	-	-
Intercoolers outlet temperature, °C	40	40	40	40
Syngas compressors isentropic/mech.-el efficiency, %	72/92	72/92	72/92	72/92

Assumptions	**BtM DG**	**BtM IG**	**BtH$_2$ DG**	**BtH$_2$ IG**
1st WGS reactor inlet temperature, °C	220	-	220	300
1st WGS reactor pressure, bar	3.5	-	3.5	33.0
2nd WGS reactor inlet temperature, °C	-	-	220	180
2nd WGS reactor pressure, bar	-	-	3.2	31.6
CO_2 absorber pressure, bar	30	30	30	30
CO_2 separation efficiency, % of inlet CO_2	95	90	95	95
Methanol synthesis				
Reactor pressure, bar	90.0		-	
Tube length, m	6.0		-	
Tube diameter, mm	40.0		-	
Boiling water temperature, °C	238		-	
Catalyst density, kg/m^3	1712		-	
Catalyst diameter (cylinder), mm	6.0		-	
Catalyst height (cylinder), mm	3.5		-	
Bed voidage degree	0.39		-	
Flash unit temperature, °C	40		-	
GHSV in enhanced operation, h^{-1}	5000		-	
RR in enhanced operation, molar basis	5.0		-	
Syngas recycle compressor isentropic/mech.-el efficiency, %	80/94		-	
Methanol purification				
Stabilizing column pressure, bar	1.3	1.3	-	
Stabilizing column number of stages	20	20	-	
Concentration column pressure, bar	1.0	1.0	-	
Concentration column number of stages	40	40	-	
Final product methanol purity, %$_{wt}$	99.85	99.85	-	
Hydrogen production				
Hydrogen separation efficiency, %	-		90	
Final product hydrogen purity, %$_{vol}$	-		99.9	

Assumptions	**BtM DG**	**BtM IG**	**BtH$_2$ DG**	**BtH$_2$ IG**
Hydrogen pressure, bar	-		30	
CO_2 separation and compression				
MDEA regeneration thermal duty , MJ/kg$_{CO2,removed}$	1.0			
MEA regeneration thermal duty , MJ/kg$_{CO2,removed}$	3.7			
MDEA electric consumption, kWh/ kg$_{CO2,removed}$	0.012			
MEA electric consumption, kWh/ kg$_{CO2,removed}$	0.025			
CO_2 compressor stages	5			
CO_2 compressor outlet pressure, bar	80			
CO_2 compressors isentropic/mech.-el efficiency, %	80/92			
Intercoolers outlet temperature, °C	40			
Supercritical CO_2 pump hydraulic/mech.-el efficiency, %	75/90			
Supercritical CO_2 pump outlet pressure, bar	150			
Thermal integration				
ICE flue gas outlet temperature,°C	400	-	400	-
ICE flue gas temperature at the stack, °C	100	-	100	-
Boiler flue gas cooler exit temperature, °C	-	160	-	160
Boiler hot side air pre-heater exit temperature, °C	-	80	-	80

[1] The oxygen stream is not preheated, since it reaches 108°C after compression up to the gasification pressure.

[2] Minimum syngas temperature to avoid condensation of residual tars upstream their complete removal within the water scrubber.

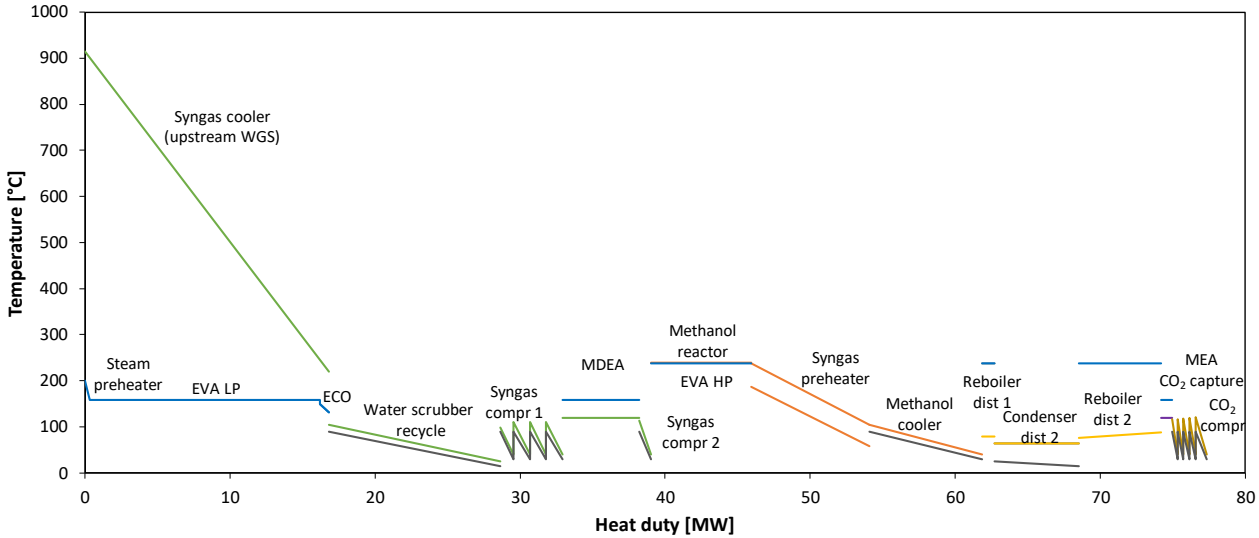

Figure B 1 – TQ diagram of the BtM DG plant (recovering heat from ICE flue gas is not necessary).

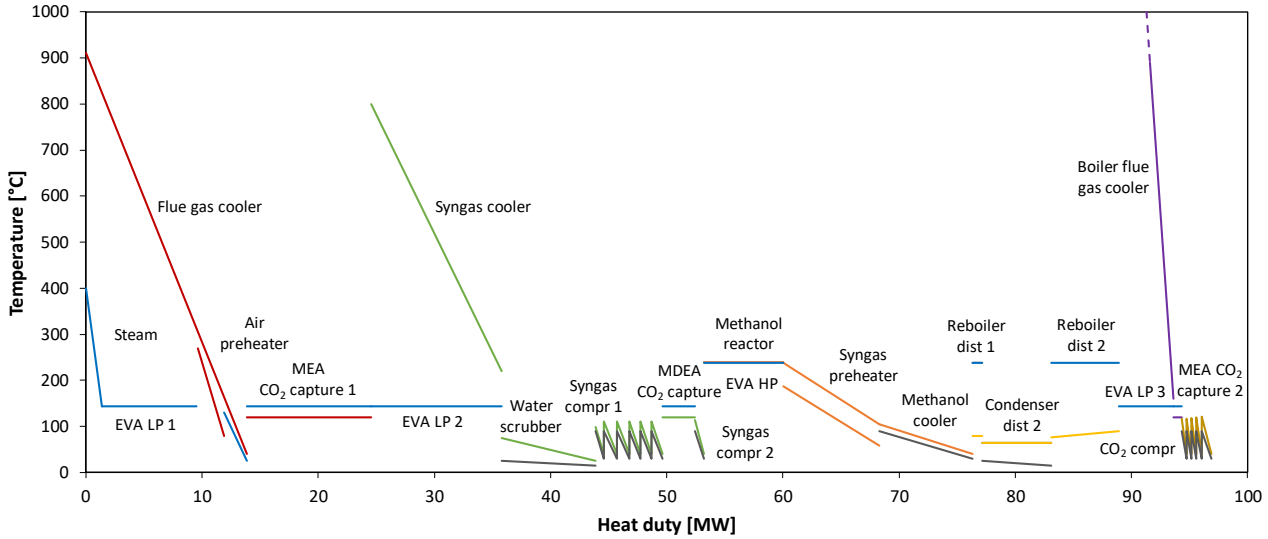

Figure B 2 – TQ diagram of the BtM IG plant (flue gas from boiler available at 1880°C).

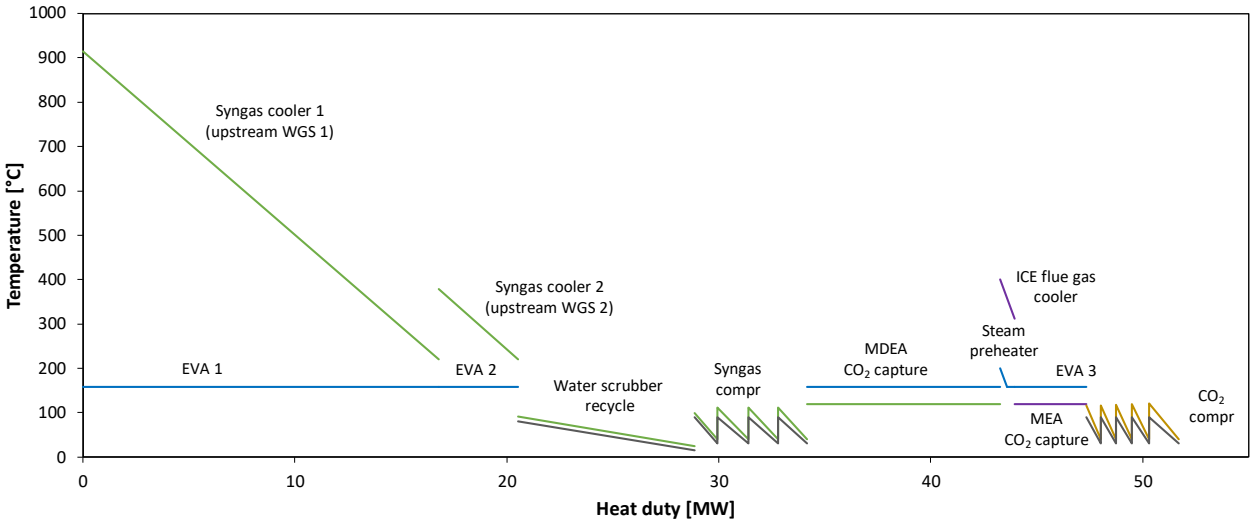

Figure B 3 – TQ diagram of the BtH_2 DG plant.

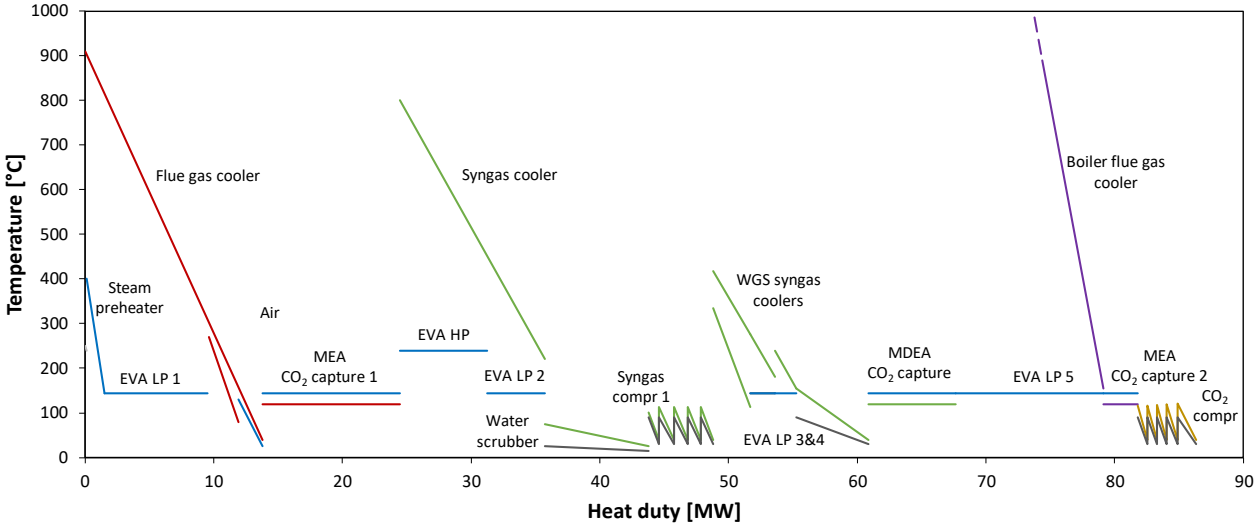

Figure B 4 – TQ diagram of the BtH2 IG plant. (flue gas from boiler available at 1933°C).

Biomass-to-methanol and hydrogen plants with CCS

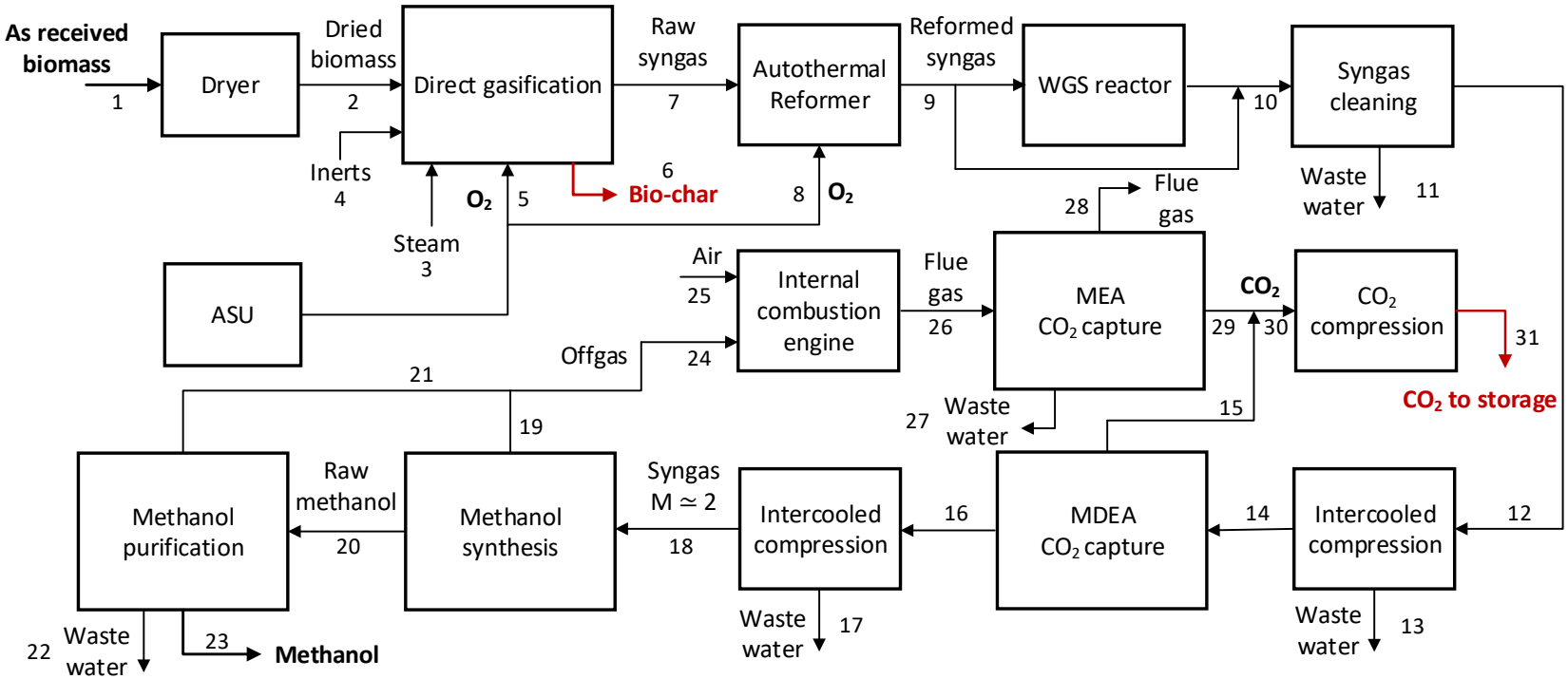

Figure B 5 – Block diagram of the direct gasification-based Biomass-to-Methanol plant.

Table B 2 - Plant stream properties DG-based Biomass-to-Methanol plant..

Stream #	**1**	**2**	**3**		**4**	**5**	**6**	**7**	**8**	**9**	**10**	**11**		**12**	**13**	**14**
Stream description	As-received biomass	Dried biomass	Steam input[1]		Inerts	Oxygen to gasifier	Bio-char[2]	Raw syngas	Oxygen to reformer	Reformed syngas	Shifted syngas	Waste water		Syngas	Waste water	Syngas
Temperature, °C	25.0	80.0	200.0	200.0	25.0	108.4	870.0	870.0	108.4	915.0	265.4	104.1	30.0	30.0	40.1	40.0
Pressure, bar	1.0	1.0	5.9	5.9	4.5	4.5	4.0	3.8	4.5	3.6	3.3	3.2	3.0	3.0	9.5	30.0
Mass flow rate, kg/s	10.27	6.64	2.66	0.80	0.21	1.93	0.19	12.04	0.64	12.68	12.68	3.33	0.10	9.25	0.07	9.17
Mole flow rate, kmol/h	-	-	531	160	26	216	-	2058	71	2349	2349	656	21	1672	14	1657
Composition, $\%_{mol}$	-	-														
H_2O	-	-	100	100	-	-	-	40.23	-	33.28	29.34	99.10	100	1.09	99.99	0.23
H_2	-	-	-	-	-	-	-	19.95	-	29.93	33.87	-	-	47.59	-	48.00
CO_2	-	-	-	-	-	-	-	17.22	-	15.82	19.76	0.87	-	27.42	0.01	27.66
CO	-	-	-	-	-	-	-	14.56	-	19.01	15.08	0.02	-	21.18	-	21.36
Methanol	-	-	-	-	-	-	-	-	-	-	-	-	-	-	-	-
CH_4	-	-	-	-	-	-	-	4.43	-	0.39	0.39	0.01	-	0.54	-	0.55
C_xH_y	-	-	-	-	-	-	-	1.99	-	-	-	-	-	-	-	-
O_2	-	-	-	-	20.48	95.00	-	-	95.00	-	-	-	-	-	-	-
Ar	-	-	-	-	-	3.00	-	0.32	3.00	0.37	0.37	-	-	0.52	-	0.52
N_2	-	-	-	-	79.52	2.00	-	1.28	2.00	1.18	1.18	-	-	1.66	-	1.67
Ethanol	-	-	-	-	-	-	-	-	-	-	-	-	-	-	-	-
DME	-	-	-	-	-	-	-	-	-	-	-	-	-	-	-	-
LHV, MJ/kg	9.74	16.37	-	-	-	-	-	7.19	-	6.66	6.57	-	-	9.01	-	9.08
Power, MW_{LHV}	100.0	108.76	-	-	-	-	-	86.58	-	84.39	83.34	-	-	83.30	-	83.30

[1] The first row corresponds to the fluidization steam. The second row includes steam for sealing and cleaning purposes.

[2] The stream contains 67.42%wt of carbon and 32.58%wt of ashes.

Table B 3 - Plant stream properties DG-based Biomass-to-Methanol plant

Stream #	**15**	**16**	**17**	**18**	**19**	**20**	**21**	**22**	**23**	**24**	**25**	**26**	**27**	**28**	**29**	**30**	**31**
Stream description	CO_2 from MDEA	Syngas	Waste	Syngas to synthesis	Purge from synthesis	Methanol to purification	Purge from purification	Waste water	Methanol	Purge to ICE	Air to ICE	Flue gas from ICE	Waste water	Flue gas from MEA	CO_2 from MEA	CO_2 to compression	Compressed CO_2
Temperature, °C	40.0	40.0	40.0	115.2	33.3	41.5	32.3	88.2	64.5	33.3	25.0	100.0	40.0	40.0	40.0	40.0	89.5
Pressure, bar	1.2	30.0	52.5	92.0	2.0	2.0	1.4	1.0	1.0	1.4	1.0	1.0	1.0	1.0	1.2	1.2	150.0
Mass flow rate, kg/s	5.32	3.85	0.02	3.83	0.37	3.47	0.09	0.11	3.27	0.45	2.39	2.85	0.30	2.35	0.20	5.52	5.52
Mole flow rate, kmol/h	435	1222	4	1218	77	398	10	20	368	88	298	369	60	293	16	452	452
Composition, $\%_{mol}$																	
H_2O	-	0.32	100	-	0.02	4.77	0.04	90.59	0.21	0.02	1.00	16.26	100	-	-	-	-
H_2	-	65.11	-	65.32	42.86	0.26	10.01	-	-	38.98	-	-	-	-	-	-	-
CO_2	100	1.88	-	1.88	1.48	0.73	28.29	-	-	4.65	0.03	4.65	-	0.29	100	100	100
CO	-	28.98	-	29.07	1.88	0.02	0.82	-	-	1.76	-	-	-	-	-	-	-
Methanol	-	-	-	-	0.61	93.07	17.92	9.18	99.77	2.65	-	-	-	-	-	-	-
CH_4	-	0.74	-	0.75	9.51	0.44	16.92	-	-	10.38	-	-	-	-	-	-	-
C_xH_y	-	-	-	-	-	-	-	-	-	-	-	-	-	-	-	-	-
O_2	-	-	-	-	-	-	-	-	-	-	20.70	6.01	-	7.57	-	-	-
Ar	-	0.71	-	0.71	9.52	0.32	12.24	-	-	9.84	0.97	3.12	-	3.93	-	-	-
N_2	-	2.27	-	2.28	34.11	0.35	13.59	-	-	31.68	77.30	69.97	-	88.21	-	-	-
Ethanol	-	-	-	-	-	0.03	-	0.23	0.02	-	-	-	-	-	-	-	-
DME	-	-	-	-	-	-	0.18	-	-	0.02	-	-	-	-	-	-	-
LHV, MJ/kg	-	21.63	-	21.74	11.05	19.11	9.26	-	19.90	10.71	-	-	-	-	-	-	-
Power, MW_{LHV}	-	83.30	-	83.30	4.06	66.21	0.80	-	65.07	4.86	-	-	-	-	-	-	-

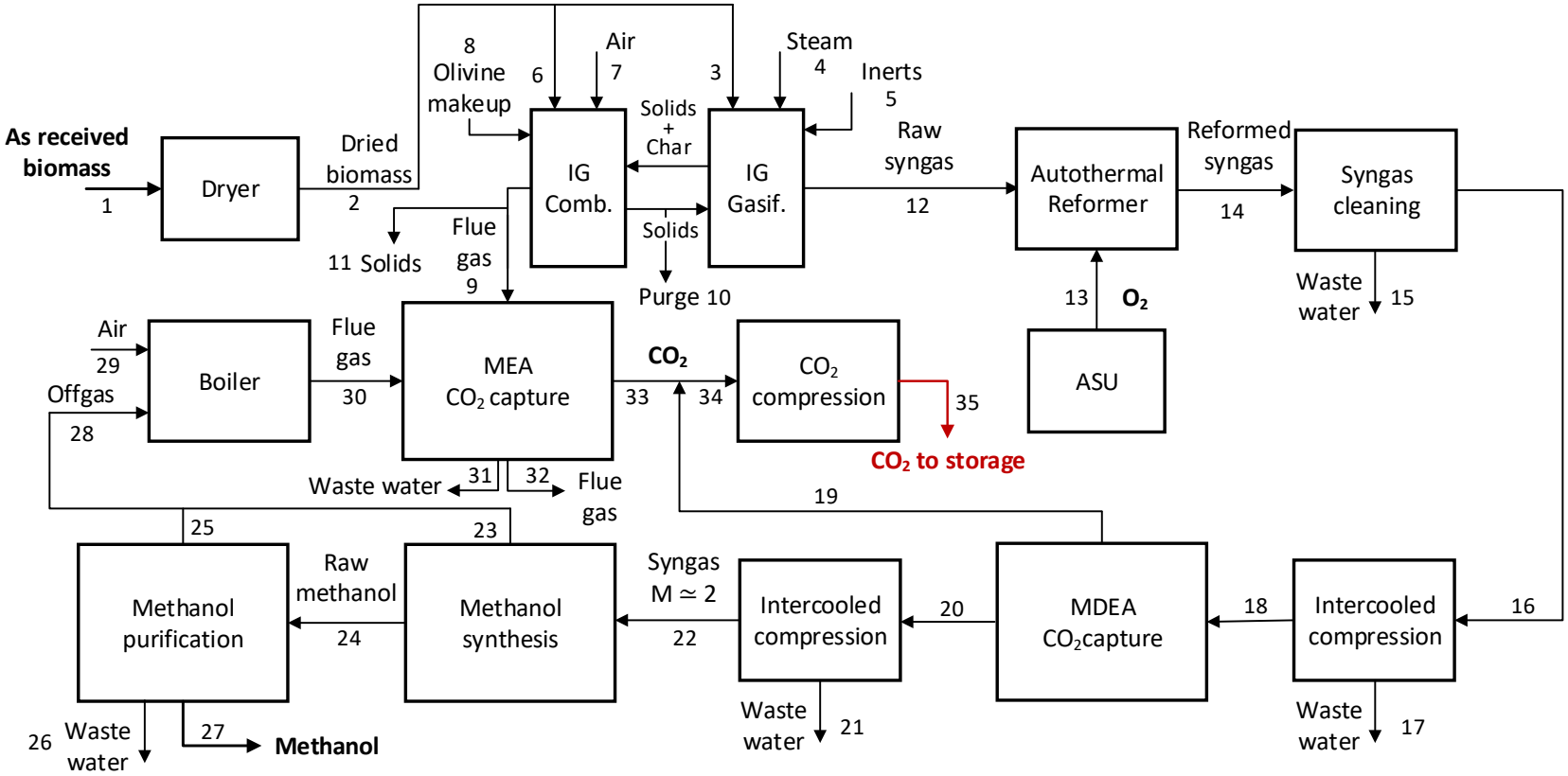

Figure B 6 – Block diagram of the indirect gasification-based Biomass-to-Methanol plant.

Table B 4 - Plant stream properties IG-based Biomass-to-Methanol plant

Stream #	**1**	**2**	**3**	**4**		**5**	**6**	**7**	**8**	**9**	**10**	**11**	**12**	**13**	**14**
Stream description	As-received biomass	Dried biomass	Biomass to gasifier	Steam input[1]		Inerts	Biomass to combustor	Air to combustor	Olivine makeup[2]	Flue gas from combustor	Solid purge[2]	Solids[2]	Raw syngas	Oxygen to reformer	Reformed syngas
Temperature, °C	25.0	80.0	80.0	400.0	180.0	25.0	80.0	270.0	25.0	140.1	910.0	140.1	815.0	150.0	800.0
Pressure, bar	1.0	1.0	1.0	3.9	3.9	1.6	1.0	1.6	1.0	1.1	1.4	1.1	1.2	2.0	1.1
Mass flow rate, kg/s	10.27	6.64	5.71	2.62	0.69	0.18	0.93	11.64	0.28	12.98	0.06	0.28	8.72	0.50	9.21
Mole flow rate, kmol/h	-	-	-	523	138	22	-	1452	-	1560	-	-	1707	56	1978
Composition, $\%_{mol}$															
H_2O	-	-	-	100	100	-	-	1.00	-	8.21	-	-	36.25	-	27.05
H_2	-	-	-	-	-	-	-	-	-	-	-	-	27.99	-	40.57
CO_2	-	-	-	-	-	-	-	0.03	-	15.91	-	-	12.48	-	12.84
CO	-	-	-	-	-	-	-	-	-	-	-	-	14.47	-	17.90
Methanol	-	-	-	-	-	-	-	-	-	-	-	-	-	-	-
CH_4	-	-	-	-	-	-	-	-	-	-	-	-	6.07	-	0.52
C_xH_y	-	-	-	-	-	-	-	-	-	-	-	-	1.61	-	-
O_2	-	-	-	-	-	20.48	-	20.70	-	2.99	-	-	-	95.00	-
Ar	-	-	-	-	-	-	-	0.97	-	0.90	-	-	-	3.00	0.08
N_2	-	-	-	-	-	79.52	-	77.30	-	71.98	-	-	1.11	2.00	1.01
Ethanol	-	-	-	-	-	-	-	-	-	-	-	-	-	-	-
DME	-	-	-	-	-	-	-	-	-	-	-	-	-	-	-
LHV, MJ/kg	9.74	16.37	16.37	-	-	-	16.37	-	-	-	-	-	9.72	-	9.13
Power, MW_{LHV}	100.0	108.76	93.55	-	-	-	15.19	-	-	-	-	-	84.70	-	84.07

[1] The first row corresponds to the fluidization steam. The second row includes steam for sealing and cleaning purposes.

[2] Olivine makeup stream contains 50%wt olivine Fe-based and 50%wt olivine Mg-based. Solid purge stream contains 48.80%wt olivine Fe-based,48.80%wt olivine Mg-based, and 2.40%wt ashes. Solids stream contains 40.06%wt olivine Fe-based,40.06%wt olivine Mg-based, and 19.87%wt ashes.

Table B 5 - Plant stream properties IG-based Biomass-to-Methanol plant

Stream #	**15**		**16**	**17**	**18**	**19**	**20**	**21**	**22**	**23**	**24**	**25**	**26**	**27**
Stream description	Waste water		Syngas	Waste water	Syngas	CO_2 from MDEA	Syngas	Waste water	Syngas to synthesis	Purge from synthesis	Methanol to purification	Purge from purification	Waste water	Methanol
Stream description														
Temperature, °C	74.1	30.0	30.0	40.1	40.0	40.0	40.0	40.0	115.0	34.6	41.7	34.1	89.2	64.5
Pressure, bar	1.1	1.1	1.1	3.2	30.0	1.2	30.0	52.5	92.0	2.0	2.0	1.4	1.0	1.0
Mass flow rate, kg/s	2.16	0.30	6.75	0.21	6.53	2.79	3.75	0.02	3.73	0.23	3.50	0.07	0.12	3.31
Mole flow rate, kmol/h	430	60	1487	43	1445	228	1217	3	1214	59	405	10	23	372
Composition, $\%_{mol}$														
H_2O	99.75	100	3.08	100	0.23	-	0.27	100	-	0.02	5.51	0.06	91.85	0.21
H_2	-	-	53.96	-	55.54	-	65.94	-	66.12	49.07	0.29	12.27	-	-
CO_2	0.23	-	17.01	-	17.52	100	2.07	-	2.08	1.19	0.59	24.76	-	-
CO	0.01	-	23.80	-	24.50	-	29.08	-	29.16	1.47	0.02	0.69	-	-
Methanol	-	-	-	-	-	-	-	-	-	0.59	92.54	19.48	7.95	99.77
CH_4	-	-	0.69	-	0.72	-	0.85	-	0.85	13.40	0.61	25.72	-	-
C_xH_y	-	-	-	-	-	-	-	-	-	-	-	-	-	-
O_2	-	-	-	-	-	-	-	-	-	-	-	-	-	-
Ar	-	-	0.11	-	0.12	-	0.14	-	0.14	2.31	0.08	3.21	-	-
N_2	-	-	1.35	-	1.39	-	1.65	-	1.65	31.94	0.32	13.63	-	-
Ethanol	-	-	-	-	-	-	-	-	-	-	0.03	-	0.20	0.02
DME	-	-	-	-	-	-	-	-	-	-	-	0.19	-	-
LHV, MJ/kg	-	-	12.46	-	12.86	-	22.42	-	22.52	16.56	19.16	13.57	2.77	19.90
Power, MW_{LHV}	-	-	84.04	-	84.04	-	84.04	-	84.04	3.81	67.09	0.97	0.35	65.77

Table B 6 - Plant stream properties IG-based Biomass-to-Methanol plant

Stream #	**28**	**29**	**30**	**31**	**32**	**33**	**34**	**35**
Stream description	Purge to boiler	Air to boiler	Flue gas from boiler	Waste water	Flue gas from MEA	CO_2 from MEA	CO_2 to compression	Compressed CO_2
Temperature, °C	34.6	131.5	80.0	40.0	40.0	40.0	40.0	89.5
Pressure, bar	1.4	1.0	1.0	1.0	1.0	1.2	1.2	150.0
Mass flow rate, kg/s	0.30	1.68	1.98	0.93	10.97	3.08	5.86	5.86
Mole flow rate, kmol/h	68	210	264	185	1387	252	479	479
Composition, $\%_{mol}$								
H_2O	0.03	1.00	21.70	100	-	-	-	-
H_2	43.89	-	-	-	-	-	-	-
CO_2	4.51	0.03	6.32	-	0.95	100	100	100
CO	1.36	-	-	-	-	-	-	-
Methanol	3.25	-	-	-	-	-	-	-
CH_4	15.13	-	-	-	-	-	-	-
C_xH_y	-	-	-	-	-	-	-	-
O_2	-	20.70	1.49	-	3.65	-	-	-
Ar	2.44	0.97	1.40	-	1.28	-	-	-
N_2	29.36	77.30	69.09	-	94.11	-	-	-
Ethanol	-	-	-	-	-	-	-	-
DME	0.03	-	-	-	-	-	-	-
LHV, MJ/kg	15.85	-	-	-	-	-	-	-
Power, MW_{LHV}	4.79	-	-	-	-	-	-	-

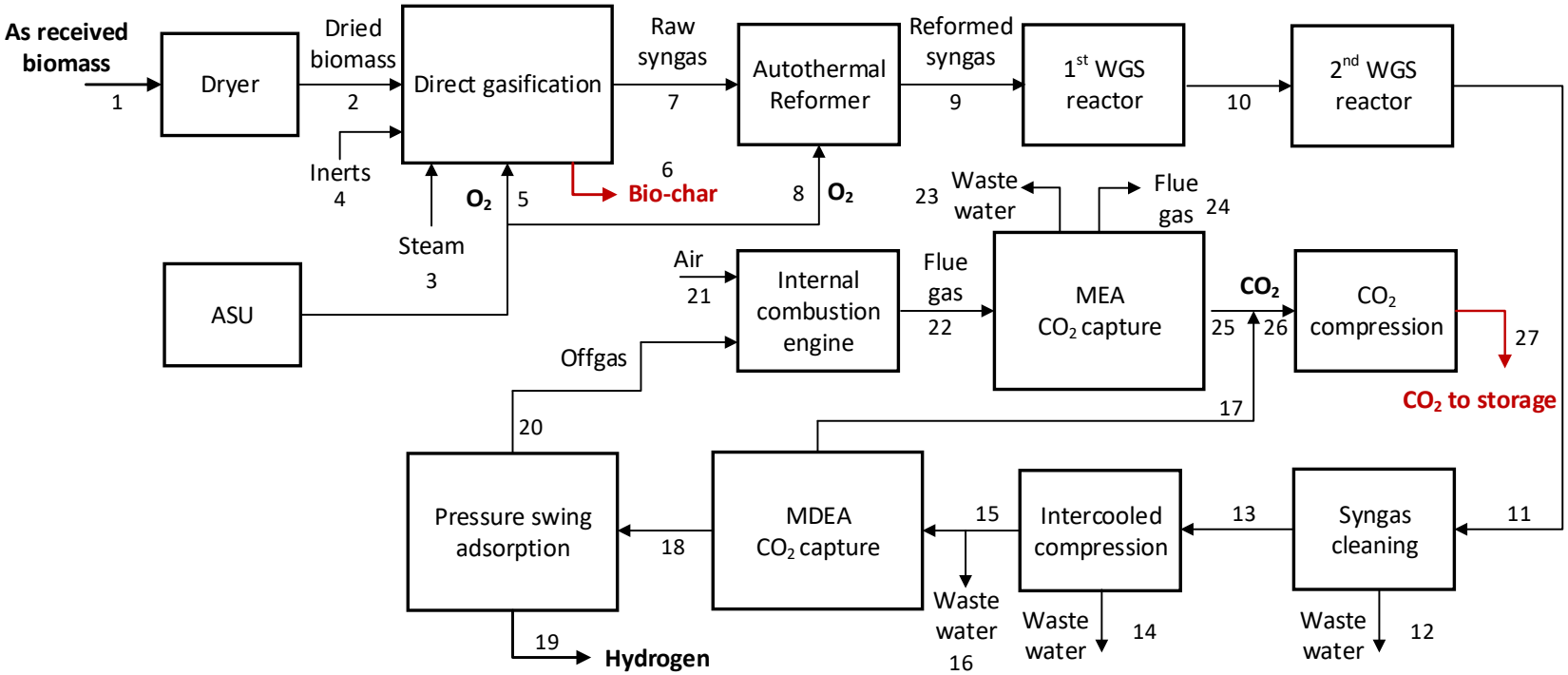

Figure B 7 – Block diagram of the direct gasification-based Biomass-to-Hydrogen plant

Table B 7 - Plant stream properties DG-based Biomass-to-Hydrogen plant

Stream #	**1**	**2**	**3**		**4**	**5**	**6**	**7**	**8**	**9**	**10**	**11**	**12**	
Stream description	As-received biomass	Dried biomass	Steam input[1]		Inerts	Oxygen to gasifier	Bio-char[2]	Raw syngas	Oxygen to reformer	Reformed syngas	Shifted syngas	Shifted syngas	Waste water	
Temperature, °C	25.0	80.0	200.00	200.00	25.00	108.42	870.00	870.00	108.42	915.00	378.71	257.45	91.28	30.00
Pressure, bar	1.0	1.0	5.90	5.90	4.50	4.50	4.00	3.80	4.50	3.60	3.30	3.00	2.95	2.75
Mass flow rate, kg/s	10.27	6.64	2.66	0.80	0.21	1.93	0.19	12.04	0.64	12.68	12.68	12.68	1.64	0.13
Mole flow rate, kmol/h	-	-	531	160	26	216	-	2058	71	2349	2349	2349	320	26
Composition, $\%_{mol}$														
H_2O	-	-	100	100	-	-		40.23	-	33.28	18.92	15.57	98.54	100
H_2	-	-	-	-	-	-		19.95	-	29.93	44.29	47.64	-	-
CO_2	-	-	-	-	-	-		17.22	-	15.82	30.17	33.53	1.45	-
CO	-	-	-	-	-	-		14.56	-	19.01	4.66	1.31	-	-
Methanol	-	-	-	-	-	-		-	-	-	-	-	-	-
CH_4	-	-	-	-	-	-		4.43	-	0.39	0.39	0.39	0.01	-
C_xH_y	-	-	-	-	-	-		1.99	-	-	-	-	-	-
O_2	-	-	-	-	20.48	95.00		-	95.00	-	-	-	-	-
Ar	-	-	-	-	-	3.00		0.32	3.00	0.37	0.37	0.37	-	-
N_2	-	-	-	-	79.52	2.00		1.28	2.00	1.18	1.18	1.18	-	-
Ethanol	-	-	-	-	-	-		-	-	-	-	-	-	-
DME	-	-	-	-	-	-		-	-	-	-	-	-	-
LHV, MJ/kg	9.74	16.37	-	-	-	-		7.19	-	6.66	6.35	6.28	-	-
Power, MW_{LHV}	100.0	108.76	-	-	-	-	-	86.58	-	84.39	80.54	79.64	-	-

[1] The first row corresponds to the fluidization steam. The second row includes steam for sealing and cleaning purposes.

[2] The stream contains 67.42%wt of carbon and 32.58%wt of ashes.

Table B 8 - Plant stream properties DG-based Biomass-to-Hydrogen plant

Stream #	**13**	**14**	**15**	**16**	**17**	**18**	**19**	**20**	**21**	**22**	**23**	**24**	**25**	**26**	**27**
Stream description	Syngas	Waste water	Syngas	Waste water	CO_2 from MDEA	Syngas	Hydrogen	Purge to ICE	Air to ICE	Flue gas from ICE	Waste water	Flue gas from MEA	CO_2 from MEA	CO_2 to compression	Compressed CO_2
Temperature, °C	30.0	40.1	40.0	40.0	40.0	40.0	40.0	40.0	25.0	100.0	40.0	40.0	40.0	40.0	89.5
Pressure, bar	2.8	9.1	30.2	30.2	1.2	30.2	30.0	1.0	1.0	1.0	1.0	1.0	1.2	1.2	150.0
Mass flow rate, kg/s	10.91	0.10	10.81	0.02	9.09	1.70	0.56	1.13	5.41	6.54	0.68	4.94	0.92	10.01	10.01
Mole flow rate, kmol/h	2002	19	1983	5	744	1234	1007	227	675	831	137	619	75	819	819
Composition, $\%_{mol}$															
H_2O	1.19	99.99	0.23	100	-	-	-	-	1.00	16.47	100	-	-	-	-
H_2	55.90	-	56.44	-	-	90.66	100	49.24	-	-	-	-	-	-	-
CO_2	39.11	0.01	39.49	-	100	3.17	-	17.23	0.03	9.53	-	0.64	100	100	100
CO	1.53	-	1.55	-	-	2.49	-	13.52	-	-	-	-	-	-	-
Methanol	-	-	-	-	-	-	-	-	-	-	-	-	-	-	-
CH_4	0.45	-	0.46	-	-	0.74	-	4.01	-	-	-	-	-	-	-
C_xH_y	-	-	-	-	-	-	-	-	-	-	-	-	-	-	-
O_2	-	-	-	-	-	-	-	-	20.70	6.04	-	8.12	-	-	-
Ar	0.43	-	0.43	-	-	0.70	-	3.79	0.97	1.82	-	2.45	-	-	-
N_2	1.39	-	1.40	-	-	2.25	-	12.21	77.30	66.14	-	88.79	-	-	-
Ethanol	-	-	-	-	-	-	-	-	-	-	-	-	-	-	-
DME	-	-	-	-	-	-	-	-	-	-	-	-	-	-	-
LHV, MJ/kg	7.30	-	7.36	-	-	46.93	119.96	10.56	-	-	-	-	-	-	-
Power, MW_{LHV}	79.61	-	79.61	-	-	79.61	67.65	11.96	-	-	-	-	-	-	-

t

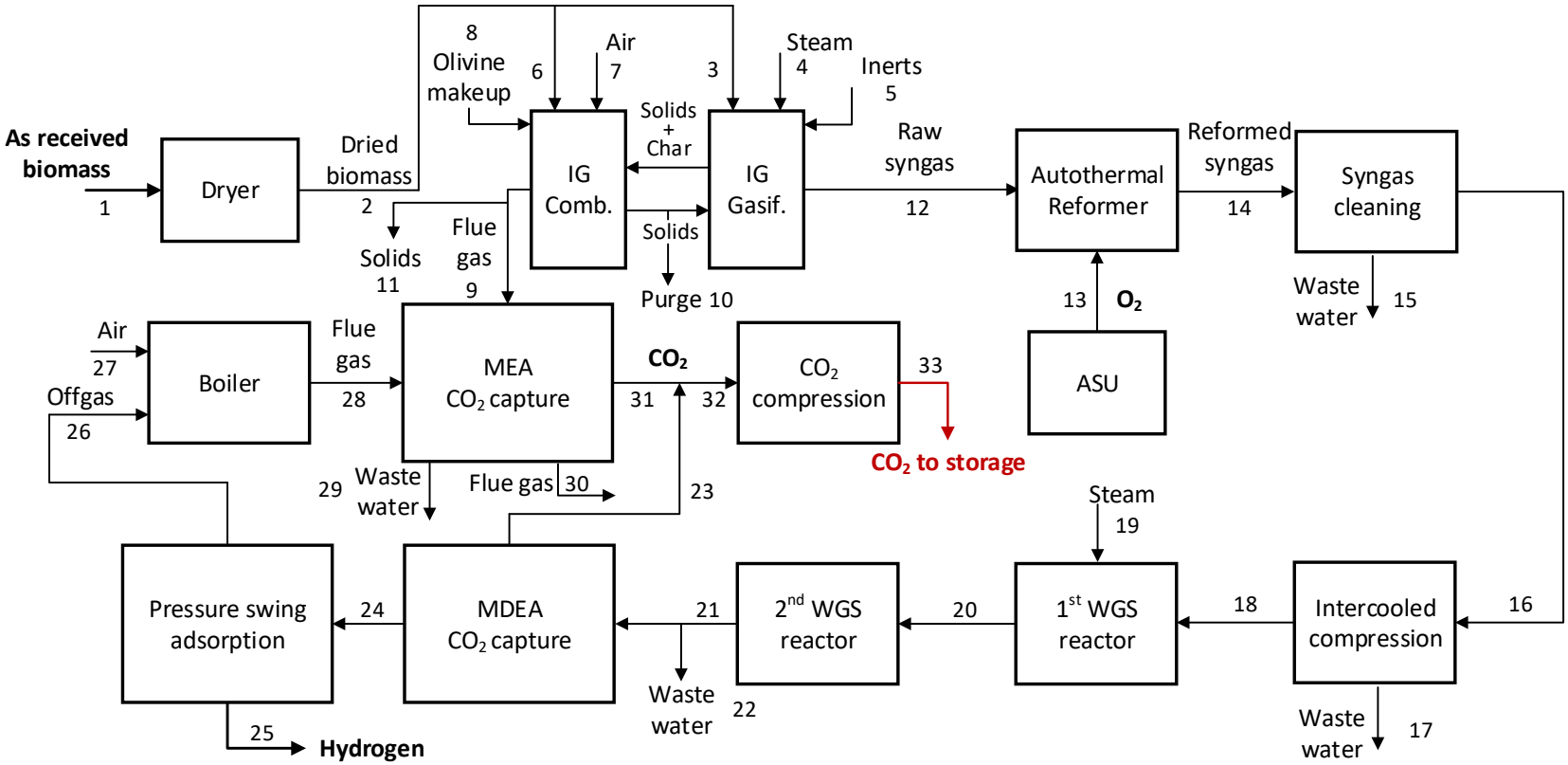

Figure B 8 – Block diagram of the indirect gasification-based Biomass-to-Hydrogen plant

Table B 9 - Plant stream properties IG-based Biomass-to-Hydrogen plant

Stream #	**1**	**2**	**3**	**4**		**5**	**6**	**7**	**8**	**9**	**10**	**11**	**12**	**13**	**14**
Stream description	As-received biomass	Dried biomass	Biomass to gasifier	Steam input[1]		Inerts	Biomass to combustor	Air to combustor	Olivine makeup[2]	Flue gas from combustor	Solid purge[2]	Solids[2]	Raw syngas	Oxygen to reformer	Reformed syngas
Temperature, °C	25.0	80.0	80.0	400.0	180.0	25.0	80.0	270.0	25.0	140.1	910.0	140.1	815.0	150.0	800.0
Pressure, bar	1.0	1.0	1.0	3.9	3.9	1.6	1.0	1.6	1.0	1.0	1.4	1.0	1.2	2.0	1.1
Mass flow rate, kg/s	10.27	6.64	5.71	2.62	0.69	0.18	0.93	11.64	0.28	12.98	0.06	0.28	8.72	0.50	9.21
Mole flow rate, kmol/h	-	-	0	523	138	22	-	1452	-	1560	-	-	1707	56	1978
Composition, $\%_{mol}$															
H_2O	-	-		100	100	-	-	1.00	-	8.21	-	-	36.25	-	27.05
H_2	-	-		-	-	-	-	-	-	-	-	-	27.99	-	40.57
CO_2	-	-		-	-	-	-	0.03	-	15.91	-	-	12.48	-	12.84
CO	-	-		-	-	-	-	-	-	-	-	-	14.47	-	17.90
Methanol	-	-		-	-	-	-	-	-	-	-	-	-	-	-
CH_4	-	-		-	-	-	-	-	-	-	-	-	6.07	-	0.52
C_xH_y	-	-		-	-	-	-	-	-	-	-	-	1.61	-	-
O_2	-	-		-	-	20.48	-	20.70	-	2.99	-	-	-	95.00	-
Ar	-	-		-	-	-	-	0.97	-	0.90	-	-	-	3.00	0.08
N_2	-	-		-	-	79.52	-	77.30	-	71.98	-	-	1.11	2.00	1.01
Ethanol	-	-		-	-	-	-	-	-	-	-	-	-	-	-
DME	-	-		-	-	-	-	-	-	-	-	-	-	-	-
LHV, MJ/kg	9.74	16.37	16.37	-	-	-	16.37	-	-	-	-	-	9.72	-	9.13
Power, MW_{LHV}	100.0	108.76	93.55	-	-	-	15.19	-	-	-	-	-	84.70	-	84.07

[1] The first row corresponds to the fluidization steam. The second row includes steam for sealing and cleaning purposes.

[2] Olivine makeup stream contains 50%wt olivine Fe-based and 50%wt olivine Mg-based. Solid purge stream contains 48.80%wt olivine Fe-based,48.80%wt olivine Mg-based, and 2.40%wt ashes. Solids stream contains 40.06%wt olivine Fe-based,40.06%wt olivine Mg-based, and 19.87%wt ashes.

Table B 10 - Plant stream properties IG-based Biomass-to-Hydrogen plant

Stream #	**15**		**16**	**17**	**18**	**19**	**20**	**21**	**22**	**23**	**24**	**25**
Stream description	Waste water		Syngas	Waste water	Syngas	Steam input	Shifted syngas	Shifted syngas	Waste water	CO_2 from MDEA	Syngas	Hydrogen
Temperature, °C	74.1	30.0	30.0	40.1	334.0	250.0	418.2	238.6	40.0	40.0	40.0	40.0
Pressure, bar	1.1	1.1	1.1	3.3	33.0	33.0	32.8	31.4	30.2	1.2	30.2	30.0
Mass flow rate, kg/s	2.16	0.30	6.75	0.20	6.54	3.00	9.54	9.54	1.37	6.78	1.39	0.57
Mole flow rate, kmol/h	430	60	1487	41	1447	599	2046	2046	273	555	1218	1020
Composition, $\%_{mol}$												
H_2O	99.75	100	3.08	100	0.34	100	18.55	13.34	100	-	-	-
H_2	-	-	53.96	-	55.48	-	50.20	55.41	-	-	93.08	100
CO_2	0.23	-	17.01	-	17.50	-	23.34	28.55	-	100	2.40	-
CO	0.01	-	23.80	-	24.47	-	6.34	1.13	-	-	1.89	-
Methanol	-	-	-	-	-	-	-	-	-	-	-	-
CH_4	-	-	0.69	-	0.71	-	0.51	0.51	-	-	0.85	-
C_xH_y	-	-	-	-	-	-	-	-	-	-	-	-
O_2	-	-	-	-	-	-	-	-	-	-	-	-
Ar	-	-	0.11	-	0.12	-	0.08	0.08	-	-	0.14	-
N_2	-	-	1.35	-	1.38	-	0.98	0.98	-	-	1.64	-
Ethanol	-	-	-	-	-	-	-	-	-	-	-	-
DME	-	-	-	-	-	-	-	-	-	-	-	-
LHV, MJ/kg	-	-	12.46	-	12.85	-	8.54	8.41	-	-	57.68	119.96
Power, MW_{LHV}	-	-	84.04	-	84.04	-	81.48	80.26	-	-	80.26	68.53

Table B 11 - Plant stream properties IG-based Biomass-to-Hydrogen plant

Stream #	**26**	**27**	**28**	**29**	**30**	**31**	**32**	**33**
Stream description	Purge to boiler	Air to boiler	Flue gas from boiler	Waste water	Flue gas from MEA	CO_2 from MEA	CO_2 to compression	Compressed CO_2
Temperature, °C	40.0	128.0	80.0	40.0	40.0	40.0	40.0	89.5
Pressure, bar	1.0	1.0	1.0	1.0	1.0	1.2	1.2	150.0
Mass flow rate, kg/s	0.82	3.79	4.61	1.33	12.65	3.61	10.39	10.39
Mole flow rate, kmol/h	198	473	602	267	1600	295	850	850
Composition, $\%_{mol}$								
H_2O	-	1.00	23.03	100	-	-	-	-
H_2	57.36	-	-	-	-	-	-	-
CO_2	14.78	0.03	10.41	-	0.97	100	100	100
CO	11.66	-	-	-	-	-	-	-
Methanol	-	-	-	-	-	-	-	-
CH_4	5.23	-	-	-	-	-	-	-
C_xH_y	-	-	-	-	-	-	-	-
O_2	-	20.70	1.50	-	3.48	-	-	-
Ar	0.84	0.97	1.04	-	1.27	-	-	-
N_2	10.14	77.30	64.02	-	94.27	-	-	-
Ethanol	-	-	-	-	-	-	-	-
DME	-	-	-	-	-	-	-	-
LHV, MJ/kg	14.30	-	-	-	-	-	-	-
Power, MW_{LHV}	11.73	-	-	-	-	-	-	-

Biomass-to-methanol and hydrogen plants with CCS capital costs

Table B 12 – BtM DG plant capital costs detail.

Capital costs	Cost scaling parameter	Reference capacity	Scaling exponent	Reference purchase equipment delivered, M€	Plant capacity	Lang factor	Reference	Fixed capital investment, M€
Biomass-to-syngas island								***95.54***
Feedstock handling [1]	Feed, MWth	157	0.31	*6.94*	100	1.48	(Hannula, 2016)	8.91
Belt dryer [1]	Water evap., kg/s	0.342	0.28	*2.49*	3.62	1.48	(Hannula, 2016)	7.11
ASU (O_2 at 1.05 bar) (air compr. included) [1]	Pure oxygen, t/d	1839.00	0.5	*47.96*	221.79	1.40	(Kreutz et al., 2005)	23.32
Oxygen compressor (from 1.05 bar)	Compressor work, MWel	0.41	0.67	0.44	0.46	5.04	(Poluzzi et al., 2022a, 2022b)	2.35
Pressurized O_2 CFB gasifier [1]	Dry biom., kg/s	17.80	0.75	*49.38*	5.65	1.42	(Hannula, 2016)	29.58
Ceramic hot-gas filter [1]	Syngas, kmol/s	1.47	0.67	*8.91*	0.57	1.48	(Hannula, 2016)	6.99
Catalytic reformer [1]	Syngas, kmol/s	2.037	0.67	*28.55*	0.57	1.42	(Hannula, 2016)	17.27
Cleaning and conditioning island								***50.71***
Scrubber	Syngas at cleaning inlet, kmol/s	0.64	0.67	0.270	0.65	5.04	(Poluzzi et al., 2022a, 2022b)	1.38
Liquid redox	Syngas at cleaning inlet, kmol/s	0.64	0.67	0.565	0.65	5.04	(Poluzzi et al., 2022a, 2022b)	2.90
Syngas compressor 1	Compressor work, MWel	7.01	0.67	7.501	4.49	5.04	(Poluzzi et al., 2022a, 2022b)	14.56
Syngas compressor 2	Compressor work, MWel	7.01	0.67	7.501	1.66	5.04	(Poluzzi et al., 2022a, 2022b)	7.49
Activated carbon	Syngas at cleaning inlet, kmol/s	0.64	0.67	0.092	0.65	3.97	(Poluzzi et al., 2022a, 2022b)	0.37

Capital costs	Cost scaling parameter	Reference capacity	Scaling exponent	Reference purchase equipment delivered, M€	Plant capacity	Lang factor	Reference	Fixed capital investment, M€
Waste water treatment	Waste water, m^3/h	22.56	0.67	0.453	12.45	5.04	(Poluzzi et al., 2022a, 2022b)	1.53
WGS reactor	Syngas , kmol/s	0.263	0.67	1.60	0.18	4.28	(Poluzzi et al., 2022a, 2022b)	5.30
CO_2 removal pre-combustion (MDEA) [1]	CO_2 captured, kg/h	46600	0.67	*16.69*	19168	1.40	(IEAGHG, 2017b)	12.89
CO_2 removal post-combustion (MEA) [1]	CO_2 captured, kg/h	80048	0.67	*72.17*	717	1.40	(IEAGHG, 2017b)	4.29
Syngas-to-methanol island								***10.99***
Methanol synthesis BWR	Syngas molar flow, kmol/s	2.20	0.67	1.72	2.0	4.28	(Poluzzi et al., 2022a, 2022b)	6.97
Recycle compressor	Compressor work, MWel	0.41	0.67	0.44	0.385	5.04	(Poluzzi et al., 2022a, 2022b)	2.10
Stabilizing column	Raw methanol, kmol/s	0.15	0.67	0.10	0.11	5.04	(Poluzzi et al., 2022a, 2022b)	0.41
Concentration column	Raw methanol, kmol/s	0.14	0.67	0.36	0.11	5.04	(Poluzzi et al., 2022a, 2022b)	1.52
Heat recovery island								***2.97***
CHP internal combustion engine [1]	Fuel input, kWth	13783	0.95	*2.480*	4861	1.40	(Zatti et al., 2018)	1.29
ECO (WGS)	Area, m^2	10000	0.68	0.957	107	5.04	(Elsido et al., 2021)	0.22
EVA (WGS)	Area, m^2	5000	0.79	1.164	839	5.04	(Elsido et al., 2021)	1.44
SH (WGS)	Area, m^2	505	0.74	0.127	8	5.04	(Elsido et al., 2021)	0.03
CO_2 compression island								***14.40***
CO_2 compression and dehydration unit [1]	Compressor work, MWel	3.005	0.67	*12.97*	2.1	1.40	(IEAGHG, 2017b)	14.40
Fixed capital investment								174.60
Working capital								30.75

Capital costs	Cost scaling parameter	Reference capacity	Scaling exponent	Reference purchase equipment delivered, M€	Plant capacity	Lang factor	Reference	Fixed capital investment, M€
Total capital investment								205.35

[1] The cost reported in the column “reference equipment delivered" is a direct cost which includes installation and BOP. The corresponding Lang factors have been modified accordingly.

Table B 13 – BtM IG plant capital costs detail.

Capital costs	Cost scaling parameter	Reference capacity	Scaling exponent	Reference purchase equipment delivered, M€	Plant capacity	Lang factor	Reference	Fixed capital investment, M€
Biomass-to-syngas island								***92.22***
Feedstock handling [1]	Feed, MWth	157	0.31	*6.94*	100	1.48	(Hannula, 2016)	8.91
Belt dryer [1]	Water evap., kg/s	0.342	0.28	*2.49*	3.62	1.48	(Hannula, 2016)	7.11
ASU (O_2 at 1.05 bar (air compr. included) [1]	Pure oxygen, t/d	1839.00	0.5	*47.96*	42.86	1.40	(Kreutz et al., 2005)	10.25
Oxygen compressor	Compressor work, MWel	0.41	0.67	0.44	0.04	5.04	(Poluzzi et al., 2022a, 2022b)	0.43
Atm steam CFB gasifier [1]	Dry biom., kg/s	17.80	0.75	*24.75*	4.86	1.42	(Hannula, 2016)	13.25
Combustor with fluegas treatment [1]	Fuel input, MWth	5.9	0.65	*7.727*	29.06	1.42	(Hannula, 2016)	30.87
Ceramic hot-gas filter [1]	Syngas, kmol/s	1.47	0.67	*8.91*	0.47	1.48	(Hannula, 2016)	6.17
Catalytic reformer [1]	Syngas, kmol/s	2.037	0.67	*28.55*	0.47	1.42	(Hannula, 2016)	15.24
Cleaning and conditioning island								***65.39***
Scrubber	Syngas at cleaning inlet, kmol/s	0.64	0.67	0.270	0.55	5.04	(Poluzzi et al., 2022a, 2022b)	1.23
Liquid redox	Syngas at cleaning inlet, kmol/s	0.64	0.67	0.565	0.55	5.04	(Poluzzi et al., 2022a, 2022b)	2.58
Syngas compressor 1	Compressor work, MWel	7.01	0.67	7.501	5.77	5.04	(Poluzzi et al., 2022a, 2022b)	17.23
Syngas compressor 2	Compressor work, MWel	7.01	0.67	7.501	1.66	5.04	(Poluzzi et al., 2022a, 2022b)	7.48
Activated carbon	Syngas at cleaning inlet, kmol/s	0.64	0.67	0.092	0.55	3.97	(Poluzzi et al., 2022a, 2022b)	0.33
Waste water treatment	Waste water, m^3/h	22.56	0.67	0.453	10.14	5.04	(Poluzzi et al., 2022a, 2022b)	1.34

Capital costs	Cost scaling parameter	Reference capacity	Scaling exponent	Reference purchase equipment delivered, M€	Plant capacity	Lang factor	Reference	Fixed capital investment, M€
CO_2 removal pre-combustion (MDEA) [1]	CO_2 captured, kg/s	46600	0.67	*16.69*	10027	1.40	(IEAGHG, 2017b)	8.35
CO_2 removal post-combustion (MEA) [1]	CO_2 captured, kg/s	80048	0.67	*72.17*	11073	1.40	(IEAGHG, 2017b)	26.85
Syngas-to-methanol island								***10.98***
Methanol synthesis BWR	Syngas molar flow, kmol/s	2.20	0.67	1.72	2.0	4.28	(Poluzzi et al., 2022a, 2022b)	6.95
Recycle compressor	Compressor work, MWel	0.41	0.67	0.44	0.381	5.04	(Poluzzi et al., 2022a, 2022b)	2.09
Stabilizing column	Raw methanol, kmol/s	0.15	0.67	0.10	0.11	5.04	(Poluzzi et al., 2022a, 2022b)	0.41
Concentration column	Raw methanol, kmol/s	0.14	0.67	0.36	0.11	5.04	(Poluzzi et al., 2022a, 2022b)	1.53
Heat recovery island								***2.52***
Boiler [1]	Fuel input, kWth	10000	0.92	*0.598*	4789	1.40	(Zatti et al., 2018)	0.43
EVA 1 (syngas cooler)	Area, m^2	5000	0.79	1.164	682	5.04	(Elsido et al., 2021)	1.22
EVA2 (flue gas cooler)	Area, m^2	5000	0.79	1.164	376	5.04	(Elsido et al., 2021)	0.76
SH (GAS 1) (flue gas cooler)	Area, m^2	505	0.74	0.127	40	5.04	(Elsido et al., 2021)	0.10
SH (GAS 2) (flue gas cooler)	Area, m^3	505	0.74	0.127	1	5.04	(Elsido et al., 2021)	0.01
CO_2 compression island								***14.98***
CO_2 compression and dehydration unit [1]	Compressor work, MWel	3.005	0.67	*12.97*	2.3	1.40	(IEAGHG, 2017b)	14.98
Fixed capital investment								186.09
Working capital								32.77
Total capital investment								218.86

[1] The cost reported in the column “reference equipment delivered" is a direct cost which includes installation and BOP. The corresponding Lang factors have been modified accordingly.

Table B 14 – BtH_2 DG plant capital costs detail.

Capital costs	Cost scaling parameter	Reference capacity	Scaling exponent	Reference purchase equipment delivered, M€	Plant capacity	Lang factor	Reference	Fixed capital investment, M€
Biomass-to-syngas island								***95.54***
Feedstock handling [1]	Feed, MWth	157	0.31	*6.94*	100	1.48	(Hannula, 2016)	8.91
Belt dryer [1]	Water evap., kg/s	0.342	0.28	*2.49*	3.62	1.48	(Hannula, 2016)	7.11
ASU (O_2 at 1.05 bar) (air compr. included) [1]	Pure oxygen, t/d	1839.00	0.5	*47.96*	221.79	1.40	(Kreutz et al., 2005)	23.32
Oxygen compressor (from 1.05 bar)	Compressor work, MWel	0.41	0.67	0.44	0.46	5.04	(Poluzzi et al., 2022a, 2022b)	2.35
Pressurized O_2 CFB gasifier [1]	Dry biom., kg/s	17.80	0.75	*49.38*	5.65	1.42	(Hannula, 2016)	29.58
Ceramic hot-gas filter [1]	Syngas, kmol/s	1.47	0.67	*8.91*	0.57	1.48	(Hannula, 2016)	6.99
Catalytic reformer [1]	Syngas, kmol/s	2.037	0.67	*28.55*	0.57	1.42	(Hannula, 2016)	17.27
Cleaning and conditioning island								***84.40***
Scrubber	Syngas at cleaning inlet, kmol/s	0.64	0.67	0.270	0.65	5.04	(Poluzzi et al., 2022a, 2022b)	1.38
Liquid redox	Syngas at cleaning inlet, kmol/s	0.64	0.67	0.565	0.65	5.04	(Poluzzi et al., 2022a, 2022b)	2.90
Syngas compressor	Compressor work, MWel	7.01	0.67	7.501	5.58	5.04	(Poluzzi et al., 2022a, 2022b)	16.84
Activated carbon	Syngas at cleaning inlet, kmol/s	0.64	0.67	0.092	0.65	3.97	(Poluzzi et al., 2022a, 2022b)	0.37
Waste water treatment	Waste water, m^3/h	22.56	0.67	0.453	6.79	5.04	(Poluzzi et al., 2022a, 2022b)	1.02
WGS reactors [2]	Syngas , kmol/s	0.263	0.67	4.00	0.65	4.28	(Poluzzi et al., 2022a, 2022b)	31.48
CO_2 removal pre-combustion (MDEA) [1]	CO_2 captured, kg/s	46600	0.67	*16.69*	32732	1.40	(IEAGHG, 2017b)	18.44

Capital costs	Cost scaling parameter	Reference capacity	Scaling exponent	Reference purchase equipment delivered, M€	Plant capacity	Lang factor	Reference	Fixed capital investment, M€
CO_2 removal post-combustion (MEA) [1]	CO_2 captured, kg/s	80048	0.67	*72.17*	3310	1.40	(IEAGHG, 2017b)	11.96
Syngas-to-hydrogen island								***3.63***
PSA [1]	Syngas, m^3/s	4.63	1.00	*39.49*	0.30	1.42	(Riva et al., 2018)	3.63
Heat recovery island								***5.55***
CHP internal combustion engine [1]	Fuel input, kWth	13783	0.95	*2.480*	11962	1.40	(Zatti et al., 2018)	3.03
EVA 1 (WGS 1st reactor)	Area, m^2	5000	0.79	1.164	945	5.04	(Elsido et al., 2021)	1.58
EVA2 (WGS 2nd reactor)	Area, m^2	5000	0.79	1.164	489	5.04	(Elsido et al., 2021)	0.94
CO_2 compression island								***21.44***
CO_2 compression and dehydration unit [1]	Compressor work, MWel	3.005	0.67	*12.97*	3.9	1.40	(IEAGHG, 2017b)	21.44
Fixed capital investment								210.56
Working capital								37.07
Total capital investment								247.63

[1] The cost reported in the column “reference equipment delivered" is a direct cost which includes installation and BOP. The corresponding Lang factors have been modified accordingly.

[2] The cost of the reference purchase equipment delivered has been modified in such a way that the cost for single-stage system is 40% of the cost of the two-stage system as indicated in (Larson et al., 2009).

Table B 15 – BtH_2 IG plant capital costs detail.

Capital costs	Cost scaling parameter	Reference capacity	Scaling exponent	Reference purchase equipment delivered, M€	Plant capacity	Lang factor	Reference	Fixed capital investment, M€
Biomass-to-syngas island								***92.22***
Feedstock handling [1]	Feed, MWth	157	0.31	*6.94*	100	1.48	(Hannula, 2016)	8.91
Belt dryer [1]	Water evap., kg/s	0.342	0.28	*2.49*	3.62	1.48	(Hannula, 2016)	7.11
ASU (O_2 at 1.05 bar (air compr. included) [1]	Pure oxygen, t/d	1839.00	0.5	*47.96*	42.86	1.40	(Kreutz et al., 2005)	10.25
Oxygen compressor	Compressor work, MWel	0.41	0.67	0.44	0.04	5.04	(Poluzzi et al., 2022a, 2022b)	0.43
Atm steam CFB gasifier [1]	Dry biom., kg/s	17.80	0.75	*24.75*	4.86	1.42	(Hannula, 2016)	13.25
Combustor with fluegas treatment [1]	Fuel input, MWth	5.9	0.65	*7.727*	29.06	1.42	(Hannula, 2016)	30.87
Ceramic hot-gas filter [1]	Syngas, kmol/s	1.47	0.67	*8.91*	0.47	1.48	(Hannula, 2016)	6.17
Catalytic reformer [1]	Syngas, kmol/s	2.037	0.67	*28.55*	0.47	1.42	(Hannula, 2016)	15.24
Cleaning and conditioning island								***97.24***
Scrubber	Syngas at cleaning inlet, kmol/s	0.64	0.67	0.270	0.55	5.04	(Poluzzi et al., 2022a, 2022b)	1.23
Liquid redox	Syngas at cleaning inlet, kmol/s	0.64	0.67	0.565	0.55	5.04	(Poluzzi et al., 2022a, 2022b)	2.58
Syngas compressor	Compressor work, MWel	7.01	0.67	7.501	5.98	5.04	(Poluzzi et al., 2022a, 2022b)	17.65
Activated carbon	Syngas at cleaning inlet, kmol/s	0.64	0.67	0.092	0.55	3.97	(Poluzzi et al., 2022a, 2022b)	0.33
Waste water treatment	Waste water, m^3/h	22.56	0.67	0.453	14.51	5.04	(Poluzzi et al., 2022a, 2022b)	1.70
WGS reactors [2]	Syngas , kmol/s	0.263	0.67	4.000	0.57	4.28	(Poluzzi et al., 2022a, 2022b)	28.70

Capital costs	Cost scaling parameter	Reference capacity	Scaling exponent	Reference purchase equipment delivered, M€	Plant capacity	Lang factor	Reference	Fixed capital investment, M€
CO_2 removal pre-combustion (MDEA) [1]	CO_2 captured, kg/s	46600	0.67	*16.69*	24417.52	1.40	(IEAGHG, 2017b)	15.16
CO_2 removal post-combustion (MEA) [1]	CO_2 captured, kg/s	80048	0.67	*72.17*	12998.62	1.40	(IEAGHG, 2017b)	29.89
Syngas-to-hydrogen island								***3.59***
PSA [1]	Syngas, m^3/s	4.63	1.00	*39.49*	0.30	1.42	(Riva et al., 2018)	3.59
Heat recovery island								***3.72***
Boiler [1]	Fuel input, kWth	10000	0.92	*0.598*	11729.537	1.40	(Zatti et al., 2018)	0.97
EVA 1 (syngas cooler)	Area, m^2	5000	0.79	1.164	440	5.04	(Elsido et al., 2021)	0.86
EVA2 (flue gas cooler)	Area, m^2	5000	0.79	1.164	373	5.04	(Elsido et al., 2021)	0.76
EVA 3 (WGS 1st-2nd reactor)	Area, m^2	5000	0.79	1.164	51	5.04	(Elsido et al., 2021)	0.16
EVA 5 (WGS 2nd reactor)	Area, m^2	5000	0.79	1.164	83	5.04	(Elsido et al., 2021)	0.23
EVA HP (syngas cooler)	Area, m^2	5000	0.79	1.164	290	5.04	(Elsido et al., 2021)	0.62
SH (GAS 1) (flue gas cooler)	Area, m^2	505	0.74	0.127	40	5.04	(Elsido et al., 2021)	0.10
SH (GAS 2) (flue gas cooler)	Area, m^2	505	0.74	0.127	1	5.04	(Elsido et al., 2021)	0.01
SH (WGS) (flue gas cooler)	Area, m^3	505	0.74	0.127	3	5.04	(Elsido et al., 2021)	0.01
CO_2 compression island								***21.99***
CO_2 compression and dehydration unit [1]	Compressor work, MWel	3.005	0.67	*12.97*	4.0	1.40	(IEAGHG, 2017b)	21.99
Fixed capital investment								218.77
Working capital								38.50

Capital costs	Cost scaling parameter	Reference capacity	Scaling exponent	Reference purchase equipment delivered, M€	Plant capacity	Lang factor	Reference	Fixed capital investment, M€
Total capital investment								257.27

[1] The cost reported in the column “reference equipment delivered" is a direct cost which includes installation and BOP. The corresponding Lang factors have been modified accordingly.

[2] The cost of the reference purchase equipment delivered has been modified in such a way that the cost for single-stage system is 40% of the cost of the two-stage system as indicated in (Larson et al., 2009).

Table B 16 – $BtMH_2$ DG plant capital costs detail.

Capital costs	Cost scaling parameter	Reference capacity	Scaling exponent	Reference purchase equipment delivered, M€	Plant capacity	Lang factor	Reference	Fixed capital investment, M€
Biomass-to-syngas island								***95.54***
Feedstock handling [1]	Feed, MWth	157	0.31	*6.94*	100	1.48	(Hannula, 2016)	8.91
Belt dryer [1]	Water evap., kg/s	0.342	0.28	*2.49*	3.62	1.48	(Hannula, 2016)	7.11
ASU (O_2 at 1.05 bar) (air compr. included) [1]	Pure oxygen, t/d	1839.00	0.5	*47.96*	221.79	1.40	(Kreutz et al., 2005)	23.32
Oxygen compressor (from 1.05 bar)	Compressor work, MWel	0.41	0.67	0.44	0.46	5.04	(Poluzzi et al., 2022a, 2022b)	2.35
Pressurized O_2 CFB gasifier [1]	Dry biom., kg/s	17.80	0.75	*49.38*	5.65	1.42	(Hannula, 2016)	29.58
Ceramic hot-gas filter [1]	Syngas, kmol/s	1.47	0.67	*8.91*	0.57	1.48	(Hannula, 2016)	6.99
Catalytic reformer [1]	Syngas, kmol/s	2.037	0.67	*28.55*	0.57	1.42	(Hannula, 2016)	17.27
Cleaning and conditioning island								***92.40***
Scrubber	Syngas at cleaning inlet, kmol/s	0.64	0.67	0.270	0.65	5.04	(Poluzzi et al., 2022a, 2022b)	1.38
Liquid redox	Syngas at cleaning inlet, kmol/s	0.64	0.67	0.565	0.65	5.04	(Poluzzi et al., 2022a, 2022b)	2.90
Syngas compressor 1	Compressor work, MWel	7.01	0.67	7.501	5.58	5.04	(Poluzzi et al., 2022a, 2022b)	16.84
Syngas compressor 2	Compressor work, MWel	7.01	0.67	7.501	1.66	5.04	(Poluzzi et al., 2022a, 2022b)	7.49
Activated carbon	Syngas at cleaning inlet, kmol/s	0.64	0.67	0.092	0.65	3.97	(Poluzzi et al., 2022a, 2022b)	0.37
Waste water treatment	Waste water, m^3/h	22.56	0.67	0.453	12.45	5.04	(Poluzzi et al., 2022a, 2022b)	1.53
WGS reactors [2]	Syngas , kmol/s	0.263	0.67	4.00	0.65	4.28	(Poluzzi et al., 2022a, 2022b)	31.48

Capital costs	Cost scaling parameter	Reference capacity	Scaling exponent	Reference purchase equipment delivered, M€	Plant capacity	Lang factor	Reference	Fixed capital investment, M€
CO_2 removal pre-combustion (MDEA) [1]	CO_2 captured, kg/s	46600	0.67	*16.69*	32732	1.40	(IEAGHG, 2017b)	18.44
CO_2 removal post-combustion (MEA) [1]	CO_2 captured, kg/s	80048	0.67	*72.17*	3310	1.40	(IEAGHG, 2017b)	11.96
Syngas-to-methanol & hydrogen island								***14.62***
Methanol synthesis BWR	Syngas molar flow, kmol/s	2.20	0.67	1.72	2.03	4.28	(Poluzzi et al., 2022a, 2022b)	6.97
Recycle compressor	Compressor work, MWel	0.41	0.67	0.44	0.39	5.04	(Poluzzi et al., 2022a, 2022b)	2.10
Stabilizing column	Raw methanol, kmol/s	0.15	0.67	0.10	0.11	5.04	(Poluzzi et al., 2022a, 2022b)	0.41
Concentration column	Raw methanol, kmol/s	0.14	0.67	0.36	0.11	5.04	(Poluzzi et al., 2022a, 2022b)	1.52
PSA [1]	Syngas, m^3/s	4.63	1.00	*39.49*	0.30	1.42	(Riva et al., 2018)	3.63
Heat recovery island								***5.77***
CHP internal combustion engine [1]	Fuel input, kWth	13783	0.95	*2.480*	11962	1.40	(Zatti et al., 2018)	3.03
ECO (WGS)	Area, m^2	10000	0.68	0.957	107	5.04	(Elsido et al., 2021)	0.22
EVA 1 (WGS 1st reactor)	Area, m^2	5000	0.79	1.164	945	5.04	(Elsido et al., 2021)	1.58
EVA2 (WGS 2nd reactor)	Area, m^2	5000	0.79	1.164	489	5.04	(Elsido et al., 2021)	0.94
CO_2 compression island								***21.44***
CO_2 compression and dehydration unit [1]	Compressor work, MWel	3.005	0.67	*12.97*	3.9	1.40	(IEAGHG, 2017b)	21.44
Fixed capital investment								229.77
Working capital								40.45
Total capital investment								270.22

[1] The cost reported in the column “reference equipment delivered" is a direct cost which includes installation and BOP. The corresponding Lang factors have been modified accordingly.
[2] The cost of the reference purchase equipment delivered has been modified in such a way that the cost for single-stage system is 40% of the cost of the two-stage system as indicated in (Larson et al., 2009).

Table B 17 – $BtMH_2$ IG plant capital costs detail.

Capital costs	Cost scaling parameter	Reference capacity	Scaling exponent	Reference purchase equipment delivered, M€	Plant capacity	Lang factor	Reference	Fixed capital investment, M€
Biomass-to-syngas island								***92.22***
Feedstock handling [1]	Feed, MWth	157	0.31	*6.94*	100	1.48	(Hannula, 2016)	8.91
Belt dryer [1]	Water evap., kg/s	0.342	0.28	*2.49*	3.62	1.48	(Hannula, 2016)	7.11
ASU (O_2 at 1.05 bar (air compr. included) [1]	Pure oxygen, t/d	1839.00	0.5	*47.96*	42.86	1.40	(Kreutz et al., 2005)	10.25
Oxygen compressor	Compressor work, MWel	0.41	0.67	0.44	0.04	5.04	(Poluzzi et al., 2022a, 2022b)	0.43
Atm steam CFB gasifier [1]	Dry biom., kg/s	17.80	0.75	*24.75*	4.86	1.42	(Hannula, 2016)	13.25
Combustor with fluegas treatment [1]	Fuel input, MWth	5.9	0.65	*7.727*	29.06	1.42	(Hannula, 2016)	30.87
Ceramic hot-gas filter [1]	Syngas, kmol/s	1.47	0.67	*8.91*	0.47	1.48	(Hannula, 2016)	6.17
Catalytic reformer [1]	Syngas, kmol/s	2.037	0.67	*28.55*	0.47	1.42	(Hannula, 2016)	15.24
Cleaning and conditioning island								***104.72***
Scrubber	Syngas at cleaning inlet, kmol/s	0.64	0.67	0.270	0.55	5.04	(Poluzzi et al., 2022a, 2022b)	1.23
Liquid redox	Syngas at cleaning inlet, kmol/s	0.64	0.67	0.565	0.55	5.04	(Poluzzi et al., 2022a, 2022b)	2.58
Syngas compressor 1	Compressor work, MWel	7.01	0.67	7.501	5.98	5.04	(Poluzzi et al., 2022a, 2022b)	17.65
Syngas compressor 2	Compressor work, MWel	7.01	0.67	7.501	1.66	5.04	(Poluzzi et al., 2022a, 2022b)	7.48
Activated carbon	Syngas at cleaning inlet, kmol/s	0.64	0.67	0.092	0.55	3.97	(Poluzzi et al., 2022a, 2022b)	0.33
Waste water treatment	Waste water, m^3/h	22.56	0.67	0.453	14.51	5.04	(Poluzzi et al., 2022a, 2022b)	1.70

Capital costs	Cost scaling parameter	Reference capacity	Scaling exponent	Reference purchase equipment delivered, M€	Plant capacity	Lang factor	Reference	Fixed capital investment, M€
WGS reactors [2]	Syngas , kmol/s	0.263	0.67	4.000	0.57	4.28	(Poluzzi et al., 2022a, 2022b)	28.70
CO_2 removal pre-combustion (MDEA) [1]	CO_2 captured, kg/s	46600	0.67	*16.69*	24417.52	1.40	(IEAGHG, 2017b)	15.16
CO_2 removal post-combustion (MEA) [1]	CO_2 captured, kg/s	80048	0.67	*72.17*	12998.62	1.40	(IEAGHG, 2017b)	29.89
Syngas-to-methanol & hydrogen island								***14.57***
Methanol synthesis BWR	Syngas molar flow, kmol/s	2.20	0.67	1.72	2.02	4.28	(Poluzzi et al., 2022a, 2022b)	6.95
Recycle compressor	Compressor work, MWel	0.41	0.67	0.44	0.38	5.04	(Poluzzi et al., 2022a, 2022b)	2.09
Stabilizing column	Raw methanol, kmol/s	0.15	0.67	0.10	0.11	5.04	(Poluzzi et al., 2022a, 2022b)	0.41
Concentration column	Raw methanol, kmol/s	0.14	0.67	0.36	0.11	5.04	(Poluzzi et al., 2022a, 2022b)	1.53
PSA [1]	Syngas, m^3/s	4.63	1.00	*39.49*	0.30	1.42	(Riva et al., 2018)	3.59
Heat recovery island								***4.09***
Boiler [1]	Fuel input, kWth	10000	0.92	*0.598*	11729.537	1.40	(Zatti et al., 2018)	0.97
EVA 1 (syngas cooler)	Area, m^2	5000	0.79	1.164	682	5.04	(Elsido et al., 2021)	1.22
EVA2 (flue gas cooler)	Area, m^2	5000	0.79	1.164	376	5.04	(Elsido et al., 2021)	0.76
EVA 3 (WGS 1st-2nd reactor)	Area, m^2	5000	0.79	1.164	51	5.04	(Elsido et al., 2021)	0.16
EVA 5 (WGS 2nd reactor)	Area, m^2	5000	0.79	1.164	83	5.04	(Elsido et al., 2021)	0.23
EVA HP (syngas cooler)	Area, m^2	5000	0.79	1.164	290	5.04	(Elsido et al., 2021)	0.62
SH (GAS 1) (flue gas cooler)	Area, m^2	505	0.74	0.127	40	5.04	(Elsido et al., 2021)	0.10

Capital costs	Cost scaling parameter	Reference capacity	Scaling exponent	Reference purchase equipment delivered, M€	Plant capacity	Lang factor	Reference	Fixed capital investment, M€
SH (GAS 2) (flue gas cooler)	Area, m^2	505	0.74	0.127	1	5.04	(Elsido et al., 2021)	0.01
SH (WGS) (flue gas cooler)	Area, m^3	505	0.74	0.127	3	5.04	(Elsido et al., 2021)	0.01
CO_2 compression island								***21.99***
CO_2 compression and dehydration unit [1]	Compressor work, MWel	3.005	0.67	*12.97*	4.0	1.40	(IEAGHG, 2017b)	21.99
Fixed capital investment								237.59
Working capital								41.82
Total capital investment								279.40

[1] The cost reported in the column “reference equipment delivered" is a direct cost which includes installation and BOP. The corresponding Lang factors have been modified accordingly.

Acknowledgement

The part of this work on the study of flexible biomass and power-to-X plants was performed within the framework of FLEDGED H2020 Project, that received funding from the European Union's Horizon 2020 Research and Innovation Programme under Grant Agreement no. 727600.

List of publications

(Poluzzi et al., 2020): Poluzzi, A., Guandalini, G., and Romano, M. C. (2020). “Potential carbon efficiency” as a new index to track the performance of biofuels production processes. *Biomass and Bioenergy* 142, 105618. doi:10.1016/j.biombioe.2020.105618.

(Poluzzi et al., 2021): Poluzzi, A., Guandalini, G., D’Amore, F., and Romano, M. C. (2021). The Potential of Power and Biomass-to-X Systems in the Decarbonization Challenge: a Critical Review. *Curr. Sustain. Energy Reports*. doi:10.1007/s40518-021-00191-7.

(Poluzzi et al., 2022a): Poluzzi, A., Guandalini, G., Guffanti, S., Elsido, C., Moioli, S., Huttenhuis, P., Rexwinkel, G., Martelli, E., Groppi, G., Romano, M. C. (2022). Flexible Power & Biomass-to-Methanol plants: Design optimization and economic viability of the electrolysis integration. *Fuel* 310, 122113. doi:10.1016/j.fuel.2021.122113.

(Poluzzi et al., 2022b): Poluzzi, A., Guandalini, G., Guffanti, S., Martinelli, M., Moioli, S., Huttenhuis, P., Rexwinkel, G., Palonen, J., Martelli, E., Groppi, G., Romano, M. C. (2022). Flexible Power and Biomass-To-Methanol Plants With Different Gasification Technologies. *Front. Energy Res.* 9. doi:10.3389/fenrg.2021.795673.

(Poluzzi et al., 2022c): Poluzzi, A., Guandalini, G., and Romano, M. C. (2023). Flexible methanol and hydrogen production from biomass gasification with negative emissions. *Sustain. Energy Fuels* 6, 3830–3851. doi:10.1039/D2SE00661H.